

NEO- AND SEISMO-TECTONIC CHARACTERISTICS OF THE
YENİGEDİZ (KÜTAHYA) AREA

A THESIS SUBMITTED TO
THE GRADUATE SCHOOL OF NATURAL AND APPLIED SCIENCES
OF
MIDDLE EAST TECHNICAL UNIVERSITY

BY

ŞULE GÜRBOĞA

IN PARTIAL FULFILLMENT OF THE REQUIREMENTS
FOR
THE DEGREE OF DOCTOR OF PHILOSOPHY
IN
GEOLOGICAL ENGINEERING

NOVEMBER 2011

Approval of the thesis

**NEO- AND SEISMO-TECTONIC CHARACTERISTICS OF THE
YENİGEDİZ (KÜTAHYA) AREA**

submitted by **ŞULE GÜRBOĞA** in partial fulfillment of the requirements
for the degree of **Doctor of Philosophy in Geological Engineering**
Department, Middle East Technical University by,

Prof. Dr. Canan Özgen
Dean, Graduate School of **Natural and Applied Sciences** _____

Prof. Dr. Erdin Bozkurt
Head of Department, **Geological Engineering** _____

Prof. Dr. Ali Koçyiğit
Supervisor, **Geological Engineering Dept., METU** _____

Examining Committee Members:

Prof. Dr. Ergun Gökten
Geological Engineering Dept., Ankara University _____

Prof. Dr. Ali Koçyiğit
Geological Engineering Dept., METU _____

Prof. Dr. Reşat Ulusay
Geological Engineering Dept., Hacettepe University _____

Prof. Dr. Kadir Dirik
Geological Engineering Dept., Hacettepe University _____

Prof. Dr. Erdin Bozkurt
Geological Engineering Dept., METU _____

Date: November 14, 2011

I hereby declare that all information in this document has been obtained and presented in accordance with academic rules and ethical conduct. I also declare that, as required by these rules and conduct, I have fully cited and referenced all material and results that are not original to this work.

Name, Last name: Şule GÜRBOĞA

Signature:

ABSTRACT

NEO- AND SEISMO-TECTONIC CHARACTERISTICS OF THE YENİGEDİZ (KÜTAHYA) AREA

Gürboğa, Şule

Ph.D., Department of Geological Engineering

Supervisor: Prof. Dr. Ali Koçyiğit

November 2011, 272 pages

Erdoğmuş-Yenigediz graben is one of the major structural elements of Akşehir-Simav Fault System (ASFS), which is a major extensional structure in the southwestern Anatolian extensional neotectonic province (SWAEP). It is about 6-10-km-wide, 15-km-long and approximately ENE-trending and is actively growing structure as indicated by the 1970.03.28 ($M_w=7.2$) Gediz earthquake.

The graben is characterized by two distinct units, separated by an angular unconformity: (i) Miocene-middle Pliocene Arica formation and (ii) Plio–Quaternary Erdoğmuş formation. The former unit commences with a basal conglomerate above the basement rocks and is composed mainly of coal-bearing continental and lacustrine sediments with lava flows and pyroclastics, particularly common in the middle parts of the sequence. The volcanics are dated at 18.4 ± 0.1 Ma (Ar-Ar mica ages). They record evidence for two deformation phases as suggested by two

sets of overprinting slickenlines, intense folding, thrust and strike-slip faulting. The Erdoğmuş formation commences with terrace conglomerates and is composed mainly of travertines, older and younger alluvial deposits, fan-apron sediments and the recent axial graben floor sediments.

Kinematic analysis of the graben-bounding normal faults, growth faults within the graben-infill and those deforming the sediments are consistent with three distinct phases of deformation: (i) Miocene–middle Pliocene extensional phase, (ii) intervening NE–SW contractional phase and (iii) Plio-Quaternary extensional phase. The data also suggests a distributed stress field and a multi-directional recent extension in predominantly NNE–SSW, E–W and NE–SW directions. This is also consistent with available focal mechanism solutions for the region.

The graben therefore has an episodic evolutionary history with two extensional phases and an intervening short-term contraction, as described in many different parts of the SWAEP. The latter phase of extension is considered as the part of Neotectonic regime, which therefore commenced by the Late Pliocene.

Keywords: Erdoğmuş-Gediz graben, episodic evolution, normal fault, phases of deformation, neotectonics, and seismotectonics.

ÖZ

YENİGEDİZ (KÜTAHYA) BÖLGESİNİN NEOTEKTONİK ve SİSMOTEKTONİK ÖZELLİKLERİ

Gürboğa, Şule

Doktora, Jeoloji Mühendisliği Bölümü

Tez Yöneticisi: Prof. Dr. Ali Koçyiğit

Kasım 2011, 272 sayfa

Erdoğmuş-Yenigediz grabeni GB Anadolu genişlemeli neotektonik bölgesindeki başlıca genişleme yapısı olan Akşehir-Simav Fay Sistemi'nin ana yapısal unsurlarından biridir. Bu graben yaklaşık 6-10 km genişlikte, 15 km uzunlukta ve DKD gidişlidir. 1970.03.28 $M_w=7.2$ Gediz depreminin de gösterdiği gibi oluşumu aktif olarak devam eden bir yapıdır.

Bu graben birbirinden açılı uyumsuzlukla ayrılan iki farklı birim ile temsil edilir: (i) Miyosen-orta Pliyosen yaşlı Arıca formasyonu ve (ii) Pliyo-Kuvaterner yaşlı Erdoğmuş formasyonu. Arıca formasyonu temel kayalar üzerine gelen taban konglomeraları ile başlar ve orta seviyelerde gözlenen başlıca lav akıntısı ve piroklastikler içeren kömürlü kıtasal ve gölsel sedimanlardan oluşur. Volkanik kayaların yaşı 18.4 ± 0.1 My olarak tarihlendirilmiştir (Ar-Ar mika yaşı). Bu formasyon iki farklı

deformasyon fazının verisini kaydetmiştir. Bunlar üst üste gelişmiş kayma çizikleri, çalışma alanında yaygın olarak gözlenen kıvrımlanma, ters ve doğrultu atımlı faylanmalardır. Erdoğmuş formasyonu ise taraça konglomeraları ile başlar, traverten, yaşlı ve genç alüvyon çökelleri, yelpaze-önlük sedimanları ve güncel grabenin taban çökellerinden oluşur.

Grabeni sınırlayan normal faylardan, graben dolgusu içinde bulunan büyüme faylarından ve bunların deforme ettiği sedimanlardan alınan kayma verilerinin kinematic analizi üç farklı deformasyon evresinin varlığıyla uyumludur: (i) Miyosen-orta Pliyosen yaşlı genişleme rejimi, (ii) KD-GB yönlü sıkışma rejimi ve (iii) Pliyo-Kuvaterner yaşlı genişleme rejimi. Bu veriler aynı zamanda KKD-GGB, D-B ve KD-GB olmak üzere çok yönlü bir genişleme rejimi sunar. Bölgede ki odak mekanizma sonuçları da elde edilen genişleme yönüyle uyumludur.

Erdoğmuş-Yenigediz grabeni iki genişleme evresi ve bunların arasında yeralan kısa bir sıkışma evresini içeren episodic bir gelişime sahiptir. Son genişleme evresi neotektonik dönemin bir parçasıdır ve bu dönemin başlama yaşı geç Pliyosen'dir.

Anahtar Sözcükler: Erdoğmuş-Gediz grabeni, episodik evrim, normal fay, deformasyon fazları, neotektonik ve sismotektonik.

To my husband and daughter...

ACKNOWLEDGEMENTS

It is a highly rewarding experience gained by working under the supervision of Prof. Dr. Ali Koçyiğit, to whom I am greatly indebted for his generosity in sharing his knowledge, guidance, continuous encouragement and interest, constructive discussions, critically reviewing and editing of the manuscript, and supervision throughout every stage of this study. Without him, this thesis could have never been completed.

Thanks are greatly expanded to Prof. Dr. Erdin Bozkurt for his critical point of view during the thesis progress. He helped me to gain an insight on bringing solutions to some problems while working at a different scale, from a different perspective.

Thanks are also due to Prof. Dr. Reşat Ulusay for providing valuable feedback about seismic hazard investigation and contributions during the thesis progress committee meetings.

Funding for this study was provided by BAP Project Code: BAP-0811-DPT2002K120510. DPT's support under the Scientific HR Development Program is gratefully acknowledged.

I would like to thanks to Gilles Ruffet from University of Rennes for performing the Ar/Ar dating results and his comments, Prof. Dr. James Jackson for his generosity in sharing earthquake photos, Fatma Geneli for her contributions on comments about geochemical analyses and Gülcan Sarp for her recommendations on ArcGIS applications.

I would also like to give my special thanks to my sister, Zehra Deveci, elder brother, Mehmet Deveci, and my father, Memiř Deveci for their valuable encouragement and support during the everlasting field studies. I ought to thank mother-in-law Durdu Grboęa. Without her care on Bilge, the thesis cannot be completed.

I would like to thank to all my friends, especially Ayře Atakul zdemir and Ceren iek for their encouragement and people in and around Gediz for their hospitality, spech about the 1970 Gediz earthquake and offers.

Last, but not the least, I offer my grateful thanks to my husband, Cořgun Grboęa for his unlimited patience, unwavering support and encouragement in all steps of the thesis. Without the love and support he has given to me; this work would be simply impossible, and would lack the strongest cause as well.

TABLE OF CONTENTS

ABSTRACT	iv
ÖZ	vi
ACKNOWLEDGEMENTS	ix
TABLE OF CONTENTS	xi
LIST OF TABLES	xv
LIST OF FIGURES.....	xvi
CHAPTERS.....	1
1. INTRODUCTION.....	1
1.1. Preamble	1
1.2. Aims of This Research.....	2
1.3. Study Area	4
1.4. Methodology	5
1.5. Regional Tectonic Settings	7
1.6. Previous Studies.....	17
2. STRATIGRAPHIC OUTLINE OF THE STUDY AREA.....	20
2.1. Introduction.....	20
2.2. Stratigraphic Outline of the Graben Deposits	21
2.2.1. Pre-Modern Graben Infill (Arıca formation)	23
2.2.2. Modern Graben Infill (Erdoğmuş formation)	37
3. GEOCHEMICAL CHARACTERISTICS OF VOLCANICS IN PRE- MODERN GRABEN INFILL	44
3.1. Introduction.....	44
3.2. Dating Results	44
3.3. Geochemistry	47
4. STRUCTURAL GEOLOGY	55
4.1. Introduction.....	55
4.2. Lineament Analysis from Aerial Photos	57

4.3. Geological Structures	61
4.3.1. Latest Palaeotectonic Structures.....	63
4.3.1.1. Contractional Structures (1 st Phase of Contraction)	63
4.3.1.1.1. Beds.....	64
4.3.1.1.2. Unconformities	66
4.3.1.1.3. Folds	67
4.3.1.1.4. Reverse Faulting.....	71
4.3.2. Neotectonic Structures.....	72
4.3.2.1. Beds	75
4.3.2.2. Faults.....	77
4.3.2.2.1. MURATDAĞI FAULT ZONE	77
4.3.2.2.1.1. Muratdağı Fault	80
4.3.2.2.1.2. Fırdan Fault.....	81
4.3.2.2.1.3. Erdoğan Fault	82
4.3.2.2.1.4. Kızılçayer Fault.....	89
4.3.2.2.1.5. Canbulat Fault	89
4.3.2.2.1.6. Gümele Fault.....	92
4.3.2.2.1.7. Çomaklar Fault	93
4.3.2.2.1.8. Binbatçayırı Fault.....	95
4.3.2.2.1.9. Koç Fault	97
4.3.2.2.1.10. Altıntaş Fault	97
4.3.2.2.1.11. Kuyucak Fault.....	99
4.3.2.2.1.12. Gediz Fault	99
4.3.2.2.1.13. Yenigediz Fault.....	100
4.3.2.2.1.14. Bahçeler Faults	105
4.3.2.2.1.15. Dörtdeğirmen Fault.....	105
4.3.2.2.1.16. Gümüşlü Fault	108
4.3.2.2.2. SIMAV FAULT ZONE.....	109
4.3.2.2.2.1. Abide Fault	111
4.3.2.2.2.2. Gedik Fault	112
4.3.2.2.2.3. Kagnı Fault	113

4.3.2.2.2.4. Aksaklar Fault.....	114
3.3.2.2.2.5. Kurupınar Fault.....	116
4.3.2.2.2.6. Arıca Fault.....	116
4.3.2.2.2.7. Tültepe Fault.....	117
4.3.2.2.3. ŞAPHANE FAULT ZONE.....	118
4.3.2.2.3.1. Şaphane Fault.....	120
4.3.2.2.3.2. Gürlek Fault.....	122
4.3.2.2.3.3. Eskigediz Fault.....	124
4.3.2.2.3.4. Çeltikçi Fault.....	126
4.3.2.2.3.5. Background on Relay Ramp.....	128
4.3.2.2.3.6. Şaphane Relay Ramp.....	131
4.3.2.2.4. YEŞİLOVA FAULT ZONE.....	137
4.3.2.2.4.1. Yeşilova Fault.....	140
4.3.2.2.4.2. Akkaya Fault.....	142
4.3.2.2.4.3. Güzüngülü Fault.....	144
4.3.2.2.4.4. Akçaalan Fault.....	146
4.3.2.2.4.5. Aşıkpaşa Fault.....	151
4.3.2.2.4.6. Sazak Fault.....	153
4.3.2.2.5. INDIVIDUAL FAULTS.....	154
4.3.2.3. Fault Patterns of the Erdoğan-Yenigediz Graben....	157
4.3.2.4. Deformation Patterns of Graben Infill.....	163
4.4. The Computed Stress Field.....	165
4.4.1. Stress Field of Faulting in pre-modern Graben Infill.....	166
4.4.2. Stress Field of Faulting in Modern Graben Deposits.....	170
4.5. Conclusion.....	173
5. PALAEOSEISMOLOGY.....	174
5.1. Introduction.....	174
5.2. Pre-trenching Survey.....	175
5.3. Trench Site Selection.....	178
5.4. Trench Descriptions.....	183
5.4.1. Trench – 1 (EF-1).....	184

5.4.2. Trench – 2 (EF-2).....	192
6. DETERMINISTIC SEISMIC HAZARD ASSESSMENT.....	195
6.1. Introduction.....	195
6.2. Approaches for the Preparation of Seismic Hazard Maps	196
6.2.1. Deterministic Seismic Hazard Analysis	198
6.2.2. Probabilistic Seismic Hazard Analysis	200
6.2.3. Comparison between DSHA and PSHA.....	202
6.3. Input Data	204
6.3.1. Fault Zones (as line sources).....	204
6.3.1.1. Muratdağı, Simav, Şaphane and Yeşilova Fault Zones	205
6.3.1.2. Estimation in Magnitudes of Scenario Earthquakes	205
6.3.1.3. Determination of PGA Values	210
6.3.2. Previous Earthquake Information (as a point source)	213
6.4. Flow Chart of the Deterministic Seismic Hazard Mapping	213
6.4.1. Results of the DSHA for Line Sources	214
7. DISCUSSION AND EVOLUTIONARY HISTORY OF THE AREA..	224
8. CONCLUSIONS.....	234
REFERENCES.....	238
APPENDIX.....	267
A. GEOLOGICAL MAP OF THE STUDY AREA.....	267
CURRICULUM VITAE.....	268

LIST OF TABLES

TABLES

Table 3.1. $^{40}\text{Ar}/^{39}\text{Ar}$ analytical data. $^{40}\text{Ar}_{\text{atm}}$ = atmospheric ^{40}Ar . $^{40}\text{Ar}^*$ = radiogenic ^{40}Ar . Ca = produced by Ca-neutron interferences. K = produced by K-neutron interferences. Age (Ma) = the date is calculated using the decay constants recommended by Steiger and Jäger (1977). The errors are at the 1σ level and do not include the error in the value of the J parameter. Correction factors for interfering isotopes produced by neutron irradiation in the McMaster reactor were $(^{39}\text{Ar}/^{37}\text{Ar})_{\text{Ca}} = 7.06 \times 10^{-4}$, $(^{36}\text{Ar}/^{37}\text{Ar})_{\text{Ca}} = 2.79 \times 10^{-4}$, $(^{40}\text{Ar}/^{39}\text{Ar})_{\text{K}} = 2.97 \times 10^{-2}$ 45

Table 3.2. Major and trace element contents of the volcanic rocks in the Erdoğmuş-Yenigediz graben. 49

LIST OF FIGURES

FIGURES

Figure 1.1. (a) Simplified map showing the major active fault systems in Turkey and adjacent areas (ASFS: Akşehir-Simav Fault System; DSFS: Dead Sea Fault System; EAFS: East Anatolian Fault System; NAFS: North Anatolian Fault System; SACA: South Aegean Cyprus Arc) (b) simplified map showing the Yenigediz-Erdoğmuş Graben and its vicinities.....	6
Figure 1.2. Map showing location of the study area and major active fault systems governing neotectonics of Turkey, and neotectonic provinces in Turkey and surrounding areas (Color codes and specific numbers illustrate major neotectonic provinces each of which is characterized by unique deformation style and sedimentary basin formation) (DFZ: Doğanbey fault zone; BFZ: Başkale fault zone; YFZ: Yüksekova fault zone) (courtesy of Prof. Dr. Ali Koçyiğit).....	8
Figure 1.3. Simplified tectonic map of western Turkey showing the major blocks in Turkey (Okan and Tüysüz, 1999).	10
Figure 1.4. Current models for the formation of Mediterranean basin (www.es.ucl.ac.uk).....	12
Figure 2.1. Generalized columnar section of the study area (See text for detailed explanation) (not to scale).....	22
Figure 2.2. General view of the angular unconformity (AU) between the Plio-Quaternary modern graben infill (Erdoğmuş formation, TQe) above and metamorphic rocks (Tb) below (~ 5 km SE of Gümele village, view to E).	23

Figure 2.3. Measured stratigraphic column of the Arica formation (lower detrital part of the sedimentary package).	24
Figure 2.4. Measured stratigraphic column of the Arica formation (central part of the sedimentary package).	25
Figure 2.5. Measured stratigraphic column of the Arica Formation (uppermost part of the sedimentary package).	26
Figure 2.6. Correlation chart for the stratigraphic units between previous studies and recent study (not to scale).	28
Figure 2.7. General view of the volcano-sedimentary package around Eskigediz county (Ta. Arica formation; TQe. Erdoğan formation; view to NNW).	29
Figure 2.8. Close-up view of the basal conglomerates (~3 km NE of Arica village).	29
Figure 2.9. Basaltic dyke cutting across the limestone beds (Yellow arrow locates baked zone).	30
Figure 2.10. General view of the columnar basalt in Yaylaköy village.	31
Figure 2.11. Close-up view of the slump folds (near E of Deliağatarlası).	32
Figure 2.12.a) General view of the reverse faulted pre-modern graben infill (Location: near NE of Eskigediz county, view to NW), b) sketched pattern of field photograph.	33
Figure 2.13. General view of the uppermost part of volcano-sedimentary package (Location: Akçaalan village).	36
Figure 2.14. Angular unconformity (AU) between the nearly flat-lying Plio-Quaternary modern graben infill (TQe) and the deformed (tilted, folded and reverse-faulted) lacustrine marl-shale-limestone alternation of the lower Miocene-Lower Pliocene pre-modern graben infill (Ta) (Location: crossroads of Çeltikçi village).	38
Figure 2.15. Angular unconformity (AU) between the Plio-Quaternary modern graben infill (TQe) and the deformed	

lacustrine marl-shale-limestone alternation of the Miocene-Lower Pliocene pre-modern graben infill (Ta) (Location: entrance of Erdoğmuş village).	39
Figure 2.16. Close-up view of a normal growth fault (GRF) in red fluvial conglomerate-mudstone alternation (Location: near S of Abide village).....	40
Figure 2.17. General view of the travertine deposits, near west of Yeşilova village (view to N).	41
Figure 2.18. General view of the alluvial fan deposits around Gümüşlü village.....	42
Figure 3.1. ^{39}Ar - ^{40}Ar age spectra of 4 samples of volcanic rocks from Erdoğmuş-Yenigediz graben. The age error bars for each temperature steps are at the 1σ level and do not include errors in the J-values. The errors in the J-values are included in the plateau age calculations.	47
Figure 3.2. Thin section view from the volcanic rocks containing plagioclase (Plg) and pyroxene (Px).	51
Figure 3.3. Classification of the 12 samples in Winchester and Floyd (1977) diagram.	51
Figure 3.4.a) The chondrite normalized (McDonough and Sun 1995) REE patterns of the studied rocks, b) The primitive mantle-normalized (McDonough and Sun 1995) trace-element patterns of the volcanic rocks.....	53
Figure 3.5. Tectonic discrimination diagram, Zr vs Zr/Y (Pearce and Norry, 1979).	54
Figure 4.1. Lineaments extracted from 109 stereographic aerial photographs by using manual approach and corresponding trend weighted rose diagram. According to the diagram,	60
Figure 4.2. Simplified map showing the outline of the Erdoğmuş-Yenigediz graben and major margin-boundary fault zones. a. pre-Miocene rocks, b. Miocene-Quaternary graben infill, GSR. ground	

surface rupture of the 1970.03.28 $M_w=7.2$ Gediz earthquake, and Ts. thermal spring.	61
Figure 4.3. Well-developed bedding planes of marl-limestone alternation in the Arica formation.	65
Figure 4.4. a) and b) Views from variable thick bedding planes in the Arica formation.	65
Figure 4.5. Histogram showing predominant dip amounts of bedding planes in the Arica formation.	66
Figure 4.6. Angular unconformity (AU) between the nearly flat-lying Plio-Quaternary Erdoğmuş formation (TQe) and the tilted lacustrine marl-shale-limestone alternation of the Miocene-Lower Pliocene Arica formation (Ta).	67
Figure 4.7. Geological map of the type area included in the Erdoğmuş-Yenigediz graben.	69
Figure 4.8. Poles to bedding on the Schmidt's lower hemisphere net. Large arrows show the shortening direction of the contractional phase that deformed the Arica formation at the end of Middle Pliocene (the last phase of paleotectonic period).	70
Figure 4.9. Close-up view of the angular unconformity (AU) between the Plio-Quaternary Erdoğmuş formation (TQe) and the reverse faulted Miocene-Lower Pliocene Arica formation (Ta).	71
Figure 4.10. a) Field photograph of the strike-slip faulting-induced slickenside recorded in pre-modern graben infill (see SS3 and SS4 in Figure 4.7 for location). b) and c) stereographic plots of slip- plane data measured at stations SS3 and SS4 on the Schmidt's lower hemisphere net. Large converging arrows show localized shortening direction of the contractional phase that deformed the pre-modern graben infill at the end of Middle Pliocene (the last phase of paleotectonic period).	72
Figure 4.11. a) Field photograp showing close-up view of extensional slip-plane data recorded within the Arica formation. b)	

and c) Stereographic plot of slip-plane data on the Schmidt's lower hemisphere net. Slip-plane data were measured at stations SS.2 (b) and SS.3 (c) (in Figure 4.7 for location of slip-data) within the pre-modern graben infill. Large arrows show localized extension direction during the sedimentation of pre-modern graben infill.....	73
Figure 4.12. a) Stereographic plot of slip-plane data on the Schmidt's lower hemisphere net. Large arrows indicate neotectonic extension along the Abide fault, b) Stereographic plot of slip-plane data on the Schmidt's lower hemisphere net. Large arrows indicate localized extension along the Erdoğmuş fault during neotectonic period (see SS.4 in Figure 4.7 for location of slip-plane data).....	73
Figure 4.13. a), b) and c) Stereographic plots of slip-plane data measured at stations 3 and 4 (see SS.3 and SS.4 in Figure 4.7 for location) on the Schmidt's lower hemisphere net. Large arrows show localized extension direction in Plio-Quaternary neotectonic period (2 nd phase of extension); d) focal mechanism solution diagram, in which large arrows show the recent extension direction, of the 1970.03.28, Mw=7.2 Gediz Earthquake (Eyidoğan and Jackson, 1985).....	75
Figure 4.14. Close-up view of a poorly sorted and weakly lithified terrace deposits.....	76
Figure 4.15. Travertine deposits in Yeşilova village (view to NW). Yellow arrows indicate the margin-boundary faults (Yeşilova Fault Zone).....	76
Figure 4.16. General view of the Muratdağı Fault Zone (different colored arrows indicate traces of different faults comprising the Muratdağı Fault Zone on the surface) (view to SE).....	79
Figure 4.17. General view of the Muratdağı fault (view to SSE). Vertical white arrows indicate trace of the fault.	80

Figure 4.18. Stereographic plot of slip-plane data from Muratdağı fault on the Schmidt's lower hemisphere net, S.1 in Appendix – A.	81
Figure 4.19. General view of the Firdan fault (view to S). Vertical red arrows point to trace of the fault.	82
Figure 4.20. Close up view of the Firdan fault which is the boundary between Arica formation (Ta) (middle Miocene – early Pliocene) and Erdoğmuş fault (TQe) (Middle Pliocene) along its western part.	82
Figure 4.21. General view of the Erdoğmuş fault scarp and trace. Vertical white arrows indicate trace of the fault (view to S).	84
Figure 4.22. Close-up view of the ground surface rupture of the 1970.03.28, $M_w=7,2$ Gediz earthquake in the west of Erdoğmuş town (courtesy of Prof. Dr. James Jackson).	85
Figure 4.23. Recent view of the ground surface rupture of the 1970.03.28, $M_w=7.2$ Gediz earthquake in the west of Erdoğmuş town. Dash line indicates surface rupture of the earthquake (view to east).	85
Figure 4.24. Ground surface rupture of the 1970.03.28 $M_w=7.2$ Gediz earthquake around Sazköy village (view to east).	86
Figure 4.25. Field photograph illustrating the Erdoğmuş fault slickenside with two overprinted sets of slip-lines (in the Erdoğmuş-Sandıklı road, Appendix – A).	86
Figure 4.26. Stereographic plot of slip-plane data from Erdoğmuş fault on the Schmidt's lower hemisphere net, S.2 in Appendix – A.	87
Figure 4.27. Stereographic plot of contractional slip-plane data on the Schmidt's lower hemisphere net, S.2 in Appendix – A.	87
Figure 4.28. Close-up view of extensional slickenside on the pre-modern graben infill deformed by the Erdoğmuş fault.	88
Figure 4.29. Stereographic plot of slip-plane data on the Schmidt's lower hemisphere net, S.3 in Appendix – A.	88

Figure 4.30. Stereographic plot of slip-plane data on the Schmidt's lower hemisphere net, S.4 in Appendix – A.....	89
Figure 4.31. General view of the Canbulat fault (location: 5 km south of Gümele village; view to NW). Vertical white arrows point to trace of the fault.	90
Figure 4.32. Field photograph indicating the Arıca formation (near west of Gümele dam site).....	91
Figure 4.33. Stereographic plot of slip-plane data from Canbulat fault on the Schmidt's lower hemisphere net, S.5 in Appendix – A.	91
Figure 4.34. General view of the Gümele fault (location: 4 km SE of Gümele village; view to NW). Vertical purple arrows show trace of the fault.	92
Figure 4.35. Stereographic plot of slip-plane data from Gümele fault on the Schmidt's lower hemisphere net, S.6 in Appendix – A.	93
Figure 4.36. General view of the Çomaklar fault (location: 3 km SSW of Gümüşlü village; view to ENE). Vertical white arrows point to trace of the Çomaklar fault.	94
Figure 4.37. Stereographic plot of slip-plane data on the Schmidt's lower hemisphere net, S.7 in Appendix – A.....	94
Figure 4.38. General view of the Binbatçayırı fault (view to NNW). Vertical white arrows point to trace of the fault.....	95
Figure 4.39. Close up view of a slickenside in Arıca formation deformed by the Binbatçayırı fault.....	96
Figure 4.40. Stereographic plot of slip-plane data from Binbatçayırı fault on the Schmidt's lower hemisphere net, S.8 in Appendix – A.	96
Figure 4.41. General view of the Koç fault (view to NE). Vertical white arrows show trace of the fault.	97
Figure 4.42. General view of the Altıntaş fault (view to NW). Vertical red arrows indicate trace of the fault.	98
Figure 4.43. Geological cross-section along the line AS-AS'. 1. Miocene-Middle Pliocene pre-modern graben infill, 2. angular	

unconformity, 3. terrace conglomerate, 4. angular unconformity, 5. Quaternary deposits, and 6. normal fault (see AS-AS' in Appendix – A for location).	98
Figure 4.44. General view of the Kuyucak fault (view to NE). Vertical red arrows point to trace of the fault.	99
Figure 4.45. General view of the Gediz fault (view to SE). Vertical yellow arrows point to trace of the fault.	100
Figure 4.46. Cross-sectional view of the Yenigediz fault (view to SSW). Dash line points to the Yenigediz fault.	101
Figure 4.47. a. General view of the Yenigediz fault plane (view to NW), b. Close-up view of the slickenside. Black arrow points to the motion direction of hanging-wall block.	102
Figure 4.48. Sketched cross-section along the road cut in the near west of Hacibaba village. a. pinkish, highly crushed marl, b. dark black colored marl, c. highly crushed grey colored marl, d. highly crushed, dark grey colored marl, e. sandy channel fill.	102
Figure 4.49. Close-up view of the Yenigediz fault slickenside (see S.9 in Appendix – A for location).	103
Figure 4.50. Stereographic plot of contractional slip-plane data, which was recorded during the last palaeotectonic period on the Schmidt's lower hemisphere net, S.9 in Appendix – A.	103
Figure 4.51. Stereographic plot of extensional slip-plane data from Yenigediz fault on the Schmidt's lower hemisphere net, S.10 in Appendix – A.	104
Figure 4.52. Stereographic plot of extensional slip-plane data on the Schmidt's lower hemisphere net, S.11 in Appendix – A.	104
Figure 4.53. General view of the Bahçeler fault (view to E). Vertical yellow arrows point to trace of the easterly dipping fault.	105
Figure 4.54. General view of the Dörtdeğirmen fault (view to WSW). Vertical yellow arrows point to trace of the fault.	106

Figure 4.55. Close-up view of the Dörtdeğirmen fault slickenside. The slip-plane data have been recorded on the Plio-Quaternary deposits.....	107
Figure 4.56. Stereographic plot of extensional slip-plane data from Dörtdeğirmen fault on the Schmidt's lower hemisphere net, S.12 in Appendix – A.....	107
Figure 4.57. General view of the Gümüşlü fault in the Plio-Quaternary deposits (view to NW, location: near southwest of Gümüşlü village). Dash line shows the fault.....	108
Figure 4.58. General view of the Ilica-Abide section of the Simav Fault Zone (red arrows indicate trace of the master fault) (Abide town in foreground, view to SSE).	110
Figure 4.59. General view of the Abide fault (view to SE). Vertical black arrows point to trace of the fault.....	111
Figure 4.60. General view of the Abide fault scarp (view to SE). Vertical yellow arrows indicate trace of the fault.....	112
Figure 4.61. Stereographic plot of extensional slip-plane data from Abide fault on the Schmidt's lower hemisphere net, S.13 in Appendix – A.....	112
Figure 4.62. General view of the Gedik fault (view to S). Vertical white arrows point to trace of the fault.....	113
Figure 4.63. General view of the Kagnı fault (view to S). Vertical yellow arrows point to trace of the fault.	114
Figure 4.64. General view of the Aksaklar (yellow arrows), and Kagnı (white arrows) fault scarps (view to S).	115
Figure 4.65. General view of the Kurupınar fault (view to S). Vertical black arrows point to trace of the fault.....	116
Figure 4.66. General view of the Arıca fault (view to S). Vertical yellow arrows point to trace of the fault.	117
Figure 4.67. General view of the Şaphane Fault Zone and its scarp (view to NW).....	119

Figure 4.68. General view of the Şaphane fault slickenside (view to NW) (location: 1 km west of Gürlek village).....	120
Figure 4.69. Close-up view of the Şaphane fault slickenside.	121
Figure 4.70. Stereographic plot of slip-plane data from Şaphane fault on the Schmidt's lower hemisphere net at, S.14 in Appendix – A.....	121
Figure 4.71. General view of the Gürlek fault scarp and slickenside (view to NW) (S.15 in Appendix – A).....	122
Figure 4.72. Close-up view of the Gürlek fault slickenside (S.15 in Appendix – A).....	123
Figure 4.73. Stereographic plot of extensional slip-plane data from Gürlek fault on the Schmidt's lower hemisphere net, S.15 in Appendix – A.....	123
Figure 4.74. General view of the Eskigediz fault (view to NNW). Vertical red arrows poin to trace of the fault.	124
Figure 4.75. General view of the Eskigediz fault scarp cutting across the volcano-sedimentary sequence of Late Miocene age (settlement in foreground is Eskigediz county, view to NE).....	125
Figure 4.76. Landslides developed along the Eskigediz fault. In this locality, Eskigediz fault defines the boundary between volcano-sedimentary units (Ta) and Plio-Quaternary deposits (TQe) (yellow arrows indicate trace of the Eskigediz fault).....	125
Figure 4.77. Stereographic plot of extensional slip-plane data from Eskigediz fault on the Schmidt's lower hemisphere, net S.16 in Appendix – A.....	126
Figure 4.78. General view of the Çeltikçi fault scarp (view to N). Vertical red arrows point to fault trace.	127
Figure 4.79. Stereographic plot of contractional slip-plane data from Çeltikçi fault on the Schmidt's lower hemisphere net S.17 in Appendix – A.....	127

Figure 4.80. Stereographic plot of normal motion along Çeltikçi fault on the Schmidt's lower hemisphere net, S.18 in Appendix – A.....	128
Figure 4.81. Block diagram of two overstepping normal fault segments dipping in the same direction. Displacement among the fault segments is transferred by formation of a relay ramp (Bozkurt and Çiftçi, 2007).....	129
Figure 4.82. Schematic diagram to show the evolutionary stages of a relay ramp. (A) There is no interact between faults; (B) The faults have started to interact and a relay ramp developed to transfer the displacement among the segments; (C) The initiation of fracturing resulted from accumulated strain between faults; (D)The relay ramp is broken by a breaching fault to form a single fault zone with strike irregularity; (E) Upper bench is abandoned and two segments joined through breaching of lower ramp that form an along strike bend on the course of the main fault (Çiftçi and Bozkurt, 2007).....	130
Figure 4.83. Geological map of the area around Şaphane relay ramp.....	131
Figure 4.84. Field photograph showing the first breaching fault (view to N).....	132
Figure 4.85. a) Field photograph showing the second breaching fault (view to S), b) Close-up view of the slickenside (purple line indicate the strike of fault plane).....	133
Figure 4.86. Stereoplots illustrating fault slip-data from Şaphane and Gürlek faults. Regional extension direction is NNE-SSW.....	134
Figure 4.87. Stereoplots illustrating fault slip-data from breaching fault to show the local stress anomalies.....	134
Figure 4.88. Formation stages of Şaphane relay ramp and related stress orientations.(A) There is no interaction between fault segments and stereographic plot of slip-plane data from Şaphane	

fault indicates regional stress direction at station 1 (St.1); (B) The faults have started to interact and two relay ramps developed to transfer the displacement among the segments and stereographic plot of slip-plane data from Gürlek fault indicates regional stress direction at station 2 (St.2); (C) The initiation of fracturing resulted from accumulated strain between fault segments; (D)The relay ramps are broken to form a single fault zone with strike irregularity...	136
Figure 4. 89. Two different slip motion along the breaching fault; a) older extensional motion, and b) younger strike-slip motion at St. 4 in Figure 4.88 (C) and (D), respectively.....	137
Figure 4.90. General view of the Yeşilova fault zone (view to N). Vertical red arrows point to trace of the master fault (Ta: Arıca formation; TQe: Erdoğmuş formation).	139
Figure 4.91. General view of the Yeşilova fault scarp. The vertical arrows indicate trace of master fault, along which older rocks were tectonically juxtaposed with the nearly flat-lying Plio-Quaternary travertine (TQe) (NNE of Yeşilova settlement, view to E).	141
Figure 4.92. General view of the Akkaya fault zone (view to NE). Vertical red arrows point to trace of the fault.	142
Figure 4.93. Close-up view of the Akkaya fault slickenside (see S.19 in Appendix – A for location).	143
Figure 4.94. Stereographic plot of slip-plane data from Akkaya fault on the Schmidt's lower hemisphere net, S.19 in Appendix – A.....	143
Figure 4.95. General view of the Güzüngülü fault zone (view to NE). Vertical yellow arrows point to trace of the fault.	144
Figure 4.96. The Güzüngülü fault forms the boundary between volcanics (basalt) and lacustrine (marl-limestone) deposits (location: ~1 km SW of Yaylaköy village on the Kütahya-Uşak highway). Yellow dash line indicates the site of Güzüngülü fault.	145

Figure 4.97. Close-up view of the Güzüngülü fault slickenside (see S.20 in Appendix – A for location).	145
Figure 4.98. Stereographic plot of extensional slip-plane data from Güzüngülü fault on the Schmidt's lower hemisphere net, S.20 in Appendix – A.	146
Figure 4.99. General view of the Akçaalan fault scarp and trace (view to SW). Vertical yellow arrows point to trace of the fault. The settlement in background is Akçaalan village. The Akçaalan fault defines the boundary between pre-modern (Ta) and modern graben infill (TQe).	148
Figure 4.100. Stereographic plot of 1 st phase of extensional slip-plane data on the Schmidt's lower hemisphere net, S.21 in Appendix – A.	149
Figure 4.101. Stereographic plot of extensional slip-plane data on the Schmidt's lower hemisphere net, S.22 in Appendix – A.	149
Figure 4.102. Stereographic plot of contractional slip-plane data on the Schmidt's lower hemisphere net, S.23 in Appendix – A. Large black arrows indicate palaeotectonic contraction direction along the Akçaalan fault.	150
Figure 4.103. Stereographic plot of extensional (2 nd phase) slip-plane data on the Schmidt's lower hemisphere net, S.24 in Appendix – A. Large black arrows indicate neotectonic extension (2 nd phase of extension) direction along the Akçaalan fault.	150
Figure 4.104. Close-up view of ground surface rupture (~ 2 m vertical displacement) of the 1970.03.28, M _w =7.2 Gediz earthquake in the far northwest of Akçaalan village (courtesy of Prof. Dr. James Jackson).	151
Figure 4.105. General view of the Aşıkpaşa fault scarp and trace (view to SW). Vertical yellow arrows point to trace of the fault.	152
Figure 4.106. Close-up view of the ground surface rupture along the Aşıkpaşa fault moved by the 1970.03.28, M _w =7.2 Gediz	

earthquake in the far west of Aşıkpaşa village (courtesy of Prof. Dr. James Jackson, 2010).....	152
Figure 4.107. General view of the Sazak fault scarp and trace (view to SW). Vertical yellow arrows point to trace of the fault.	153
Figure 4.108. Stereographic plot of extensional slip-plane data on the Schmidt's lower hemisphere net, S.25 in Appendix – A. Large black arrows indicates neotectonic extension direction along the Sazak fault.	154
Figure 4.109. General view of the Eskimuhpler fault scarp and trace (view to SW). Vertical yellow arrows point to trace of the fault.	155
Figure 4.110. General view of the Üçbaş fault cutting across the Plio-Quaternary terrace conglomerate (view to S, location: 1.3 km south of Üçbaş village).....	156
Figure 4.111. General view of the Dörtdeğirmen fault (F1), the Kışla fault (F2), the Çeltikçi fault (F3) and the Şaphane fault zone (F4) (view to N).	157
Figure 4.112. Fault data (N=50) of the near NE of Erdoğan village. Plot showing the fault dips versus rake of the slickenside lineations.	158
Figure 4.113. A field photograph (A) and its sketched pattern (B) in the near north of the Erdoğan village. Master fault (F1) cut and displaced the sedimentary deposits. A series of antithetic and synthetic faults have also deformed the modern graben infill.....	160
Figure 4.114. Field photograph (A) and its sketched (B), near NE of Eskigediz County. Antithetic and synthetic normal faults developed in the area between pre- and modern graben infill along the northern outline of the Erdoğan-Yenigediz graben.	161
Figure 4.115. Two sets of conjugate faults measured near NE of Eskigediz County. Pentagon shows the average position of the line of intersection of the two sets (β -axis).	162

Figure 4.116. Cross-sections along the lines A-A', B-B', C-C', D-D' and E-E' in Appendix – A.	164
Figure 4.117. Stress analyses obtained the pre-modern graben infill. Stereographic plots illustrate slip-plane data measured on the fault slickenside and in the deformed sediments, and the operation direction of principle stress axes. All analyses have also Φ ratio and ANG value.	169
Figure 4.118. Stress analyses obtained from the pre-modern graben infill. Stereographic plots illustrate slip-plane data from fault slickenside to deformed sediments, and the positions of principle stress axes. All analyses have also Φ ratio and ANG value.	170
Figure 4.119. Stress analyses obtained from the modern graben infill. Stereographic plots illustrate slip-plane data from the slickenside and deformed sediments, and the position of principle stress axes.	172
Figure 5.1. Aerial photograph of the Şaphane and Gürlek faults.	176
Figure 5.2. Close-up view of the Şaphane active fault slickenside and the colluvial wedge (debris slope) accumulated on the hanging block (view to NNW).	177
Figure 5.3. Field photograph showing the ground surface rupture of the 1970.03.28 Gediz earthquake on the western side of Erdoğan village (view to ESE).	178
Figure 5.4. Microtopographic map of the target area showing the location of trenches (1 and 2), surface rupture of the 1970.03.28 Gediz earthquake and geologic cross-sections (A-A' and B-B') along the Erdoğan fault.	180
Figure 5.5. Geological cross-sections across the ground surface rupture of 1970.03.28 Gediz earthquake. A maximum and minimum displacement is plotted on each cross-section (see Figure 5.4. for location).	180

Figure 5.6. Digital elevation model of Erdoğmuş village and its vicinity based on elevations.....	181
Figure 5.7. Digital elevation model of Erdoğmuş village and its vicinity based on topographic map.	182
Figure 5.8. Digital elevation model of Erdoğmuş village and its close vicinity based on topographic map. a) close up view of trench sites.....	182
Figure 5.9. Field photograph showing the ground surface rupture of 1970.03.28 Gediz earthquake; where people are aligned on the rupture (view to NNW).....	183
Figure 5.10. Panoramic view of the eastern wall of EF-1.	186
Figure 5.11. EF-1 trench log of eastern wall (see text for more explanation). a. Dark to light grey highly deformed marl. Dark brown sand to pebble size polygenetic unsorted conglomerates having irregular boundary between c1 unit, c1. Light brown colored, coarse grained sandy gravel lenses, c2. Light yellow to dark yellow, fine to coarse grained sandy gravels, massive containing uneven lenses with larger grain size of sand, highly deformed by faults and fractures, d. Light brown-yellow sandy gravel to gravelly sand imbricated pebbles massive layer polygenetic, unsorted well-rounded, moderately lithified, e1 and e2. Brown to yellow-brown soil level made up of boulder to pebble clasts polygenetic, unsorted and angular to semi rounded with granular matrix contains stumps abundantly (Horizon A).....	187
Figure 5.12. Close up view of the deformed marl (unit a) exposed on the eastern wall of EF-1.	188
Figure 5.13. Close up view of the faulted unit c1.....	188
Figure 5.14. Close-up view of the slickenside on the ground surface rupture of the 1970 earthquake (Fault no: 9 in Figure 5.11).....	189
Figure 5.15. Photo from western wall of the EF-2.	193

Figure 5.16. EF-2 trench log of western wall.....	194
Figure 6.1. Earthquake hazard map of Turkey. Rectangle shows the study area (After Ministry of Public Works and Settlement of Turkey, 1996).....	197
Figure 6.2. Four main steps of a deterministic seismic hazard analysis (Kramer 1996).....	199
Figure 6.3. Four main steps of a deterministic seismic hazard analysis (Kramer, 1996).....	201
Figure 6.4. Correlations between M_w and M_s , M_b , M_d and M_L values for Turkish earthquakes (r : correlation coefficient; S.D: standart deviation) (Ulusay <i>et al.</i> , 2004).....	209
Figure 6.5. Relation between surface magnitude (M_s) and surface rupture length (L) based on the Turkish earthquakes (Aydan <i>et al.</i> , 2002).....	210
Figure 6.6. Close up view of the basement (a) and volcanic rocks (b) ($S_A = S_B = 0$).....	211
Figure 6.7. General view of the tilted Miocene beds ($S_A = 1$ and $S_B = 0$).....	212
Figure 6.8. Close up view of the Plio-Quaternary (a) and alluvial deposits (b) ($S_A = 0$ and $S_B = 1$).	212
Figure 6.9. Assigned point locations of the study area as base map for deterministic hazard analyse.....	215
Figure 6.10. The locations of Muratdağı (blue line), Simav (black line), Şaphane (red line) and Yeşilova (purple line) fault zones (purple dots are showing the settlements).....	216
Figure 6.11. Deterministic seismic hazard map showing ground motions (PGA) expected from M_w 6.7 scenario earthquake sourced from Muratdağı fault zone.....	218
Figure 6.12. Deterministic seismic hazard map showing ground motions (PGA) expected from a M 6.6 scenario earthquake sourced from Simav fault zone.....	219

Figure 6.13. Deterministic seismic hazard map showing ground motions (PGA) expected from a M_w 6.6 scenario earthquake sourced from Şaphane fault zone.	220
Figure 6.14. Deterministic seismic hazard map showing ground motions (PGA) expected from a M_w 6.5 scenario earthquake sourced from Yeşilova fault zone.	221
Figure 6.15. Deterministic seismic hazard map showing ground motions (PGA) expected from M_w 7.2 1970 Gediz earthquake (red star is the epicenter of the earthquake).	222
Figure 6.16. Izoseist map of the 1970 Gediz earthquake (Abdüsselamoğlu, 1970).	223
Figure 7. 1. Sketched cross-sections and block diagrams illustrating episodic two-stage evolution of the Erdoğmuş-Yenigediz graben.	233

CHAPTER 1

INTRODUCTION

1.1.Preamble

Intracontinental basins form in an extensive diversity of tectonic settings, from pure extensional to pure contractional in nature. The driving forces of these tectonic settings and the resulting structures display various relationships. The Erdoğmuş-Yenigediz graben is issued in the thesis. It is a key basin to get more understanding about the mechanisms of formation and description of tectonic settings in an extensional area in western Turkey. This thesis presents an integrated study in relation to the Miocene–Quaternary tectono-stratigraphic evolution of the Erdoğmuş-Yenigediz graben by means of the detailed documentation of stratigraphy, structural geology, paleostress analysis, paleoseismic study and seismic hazard assessment for earthquake vulnerability.

Stratigraphic studies concern detailed research of the lateral and vertical changes in the sequence. It includes characteristics of units, their deformation patterns and relations among the tectonic settings in the study area. Geologically, the most significant clue for the evolution of an area is deformation pattern of sedimentary sequence. In this case, if the deformation patterns and sufficient data about the succession can be obtained, it will be easy to construct the geologic history. Therefore, slip data which are attained from the basin infill and basin margin bounding faults' slickensides can be analyzed by the method of

stereographic plot (Angelier, 1979). Additionally, paleoseismic study is applied to get 3D survey by using the trenching process and radiometric dating (C^{14} -dating) to determine historical seismic events on the faults. Moreover, the thesis reports the result of deterministic seismic hazard map of the territory of study area. This chapter contains introductory information about the frames of the work, literature survey, problematic issues and location of the study area.

1.2. Aims of This Research

The present study intends to improve; (i) the geological understanding of the structural evolution of an intraplate basin located along the Akşehir-Simav Fault System (ASFS) and (ii) to assess the seismic hazard which is sourced from an earthquake. It is performed by studying a specific region of graben formation in a young and active tectonic context which is the Erdoğmuş-Yenigediz graben. Although, the graben is relatively smaller compared to the other grabens in western Anatolia, it contains considerable amount of structural and stratigraphical data which are enough to discuss its evolution as a model for the extensional evolution in western Anatolia. Over the last two decades, many researchers carried out detailed investigations about the geological evolution of the western Anatolia. However, there is still no consensus, and there are many controversial issues remain to be addressed. The initiation time of extension and its evolution (whether episodic or continuous) form the subject of major discussion. Based on this study, a new approach has been developed by considering the detailed geological mapping, the detailed stratigraphy of both the last palaeotectonic unit (stratigraphy of the Miocene rocks) and the neotectonic units, and the deformation phases recorded in both graben infill and on margin-boundary faults of the Erdoğmuş-Yenigediz graben. The term neotectonic is used to describe the tectonic period that has started at any time in the geologic past and is still continuing today.

Moreover, palaeotectonic period is the tectonic period that had started at any time in the geologic past and has terminated at any time in the geologic past. Based on the descriptions, neotectonic and palaeotectonic division has been done in this research.

Briefly, how did the studied region structurally develop in the current tectonic regime? And how can we explain and relate both the contractional and extensional features observed in the Erdoğmuş-Yenigediz graben?

Another aim is to investigate the historical events sourced from faults in the study area, i.e. palaeoseismological application. Palaeoseismology has an increasing trend during the last two decades all around the world in the investigation of active faults. The activity of faults before instrumental time in seismology is a very important issue. Magnitude and recurrence interval of historical events and seismic capacity of faults are used in palaeoseismology in order to shed light on the seismic hazard and risk assessment studies. Thus, at two locations along the ground surface rupture of the 1970.03.28, $M_w=7.2$ Gediz earthquake, trenching operations were carried out.

Finally, deterministic seismic hazard maps were prepared by using the scenario earthquakes. It is a kind of vulnerability assessment that evaluates the community's susceptibility to a specific hazard. Therefore, it estimates the impact and describes the effect of hazard on the community. There are many factors affecting the vulnerability of community. In this study, it is preferred to use fault parameters and geological units in the preparation of hazard maps for scenario earthquakes on the active faults.

1.3. Study Area

In the world, one of the well-known area of current intra-plate continental extension is the Southwestern Anatolian Extensional Province (SWAEP) (Arpat and Bingöl 1969; Ambraseys and Tchalenko 1972; McKenzie 1972, 1978; Koçyiğit, 1984; Eyidoğan and Jackson 1985; Şengör 1987; Westaway, 1990; Paton 1992; Seyitoğlu *et al.*, 1992; Taymaz and Price 1992; Zanchi and Angelier 1993; Price and Scott 1994; Cohen *et al.*, 1995; Hetzel *et al.*, 1995; Yusufoglu, 1998; Koçyiğit *et al.*, 1999; Koçyiğit *et al.*, 2000; Bozkurt 2000, 2001; Yılmaz *et al.*, 2000; Koçyiğit and Özacar 2003; Bozkurt and Sözbilir 2004; Koçyiğit and Deveci, 2005). It is characterized by a series of actively growing grabens, horst and their margin-boundary normal faults. One of the major extensional structures is the Akşehir-Simav Fault System (ASFS) (Koçyiğit and Özacar 2003; Koçyiğit and Deveci 2005). It is 500-kmlong, 10-30-km wide and NW-SE-trending discontinuous zone of deformation characterized by oblique-slip normal faulting. Along these faults many destructive events took place during the last century such as the 1921 September 26 ($M_s = 5.4$) Argıthanı-Akşehir, 1944 June 24 ($M_s = 6.0$) Abide, the 1946 February 21 ($M_s = 5.5$) Argıthanı-İlgın, 1969 March 25 ($M_s = 6.5$) Demirci, 1970 March 28 ($M_w = 7.2$) Eskigediz, the 2000 December 15 ($M_w = 6.0$) Sultandağı and the 2002 February 3 ($M_w = 6.5$) Çay earthquakes (Ambraseys and Tchalenko 1972; Soysal *et al.*, 1981; Eyidoğan and Jackson 1985; Eyidoğan *et al.*, 1991; Ambraseys and Finkel 1995; Ambraseys and Jackson 1998; Ambraseys, 2001; Koçyiğit *et al.*, 2000; Taymaz *et al.*, 2002; Koçyiğit and Özacar 2003). The 1970 $M_w = 7.2$ Gediz earthquake affected the study area severely and it has moved most of the graben margin-boundary faults which are Şaphane, Erdoğmuş (with a vertical displacement of maximum 2.2 m (Ambraseys and Tchalenko, 1972)), Muhipler, Eskimuhipler faults. The presence of several settlements along the active faults increases the

significance of this fault system. From this point of view, ASFS deserves the investigation of its various characteristics at several localities. One of them is the Erdoğmuş-Yenigediz graben located in the western half of the ASFS. The Erdoğmuş-Yenigediz graben is 6-10-km wide, 15-km-long and ~ENE-WSW-trending active basin (Figure 1.1). Morphotectonically, the graben has two different configurations. These are the wider and uplifted marginal configuration and the relatively narrower central configuration. The marginal configuration is bounded by the Şaphane Fault along the northwestern margin (Şaphane Mountain, 2120 m) and by Arıca Fault along the southern margin (western shoulder of Muratdağı, 2309 m). Central configuration is a newly forming active graben. Former and latter configurations of the graben are occupied by older and younger (modern) basin infill, respectively.

1.4. Methodology

There are two main stages of this study. (1) Field work during the summer times of the years 2005 – 2010 period and (2) data processes and laboratory works. Field works mainly contain preparation of geological map including;

- (i) boundary relationships among various units,
- (ii) their deformation patterns,
- (iii) determination of active faults used to set up the deterministic seismic hazard assessment,
- (iv) mapping of folds at a scale of 1/25.000,
- (v) fault-slip data acquisition for the construction of palaeostress directions (obtained from margin-boundary faults and lithofacies within the basin),
- (vi) measured and sketched cross-sections to identify the deformation types and structures on the basin infill (older and younger) and
- (vi) trenching for the palaeoseismological study.

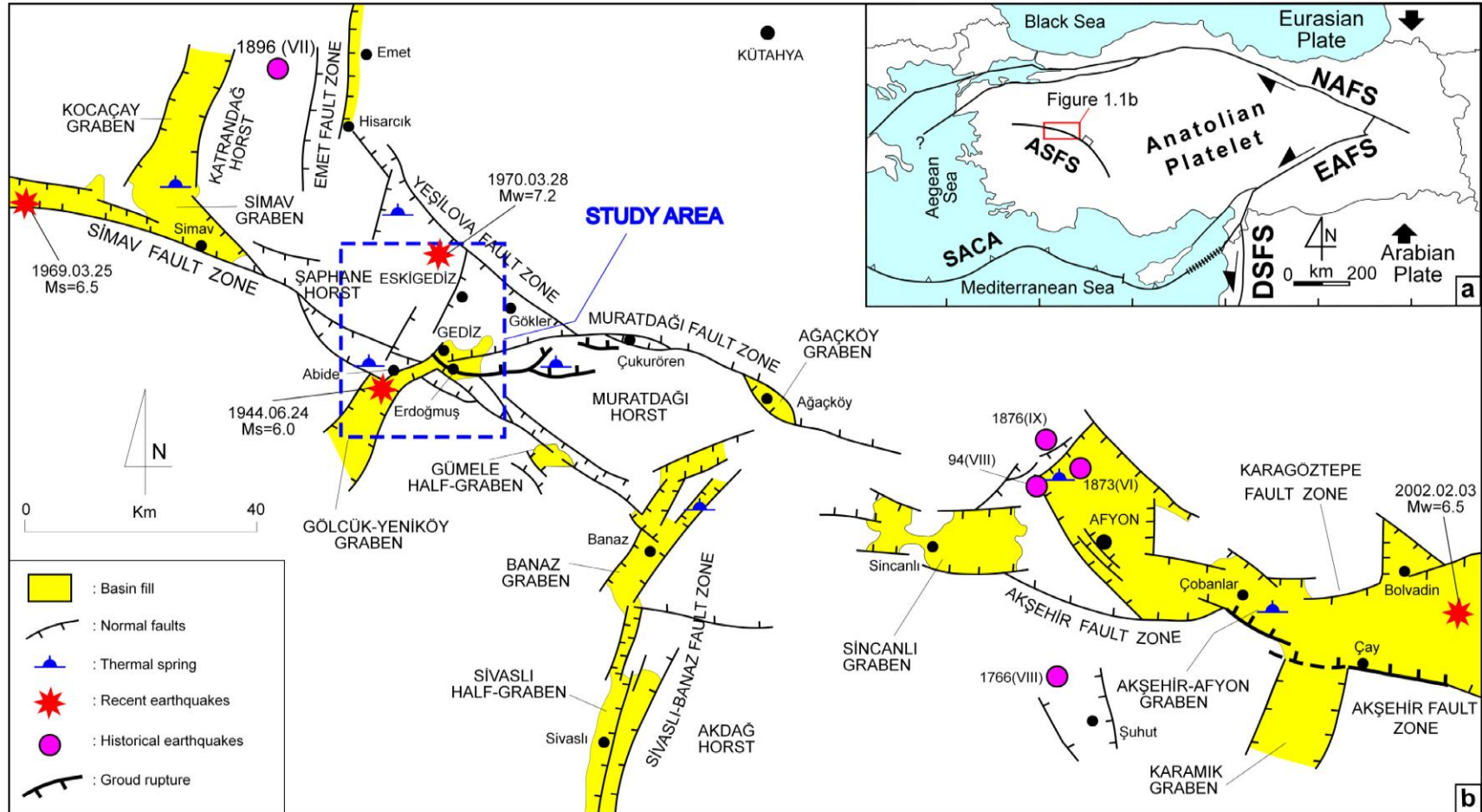


Figure 1.1. (a) Simplified map showing the major active fault systems in Turkey and adjacent areas (ASFS: Akşehir-Simav Fault System; DSFS: Dead Sea Fault System; EAFS: East Anatolian Fault System; NAFS: North Anatolian Fault System; SACA: South Aegean Cyprus Arc) (b) simplified map showing the Yenigediz-Erdoğmuş Graben and its vicinities.

At the further step, these field data were evaluated by using the computer programs (Angelier, 1979; Arcview etc.). There are two important variables in the method. They are Φ and ANG values. The value Φ is the orientation of principal stress axes and ANG is misfit angle between the actual slip vector measured on the fault plane and computed resolved shear stress. They are presented for each slip-plane analyses. Finally, the results and the end products are all interpreted to understand of geological, geometrical and structural patterns of the Erdoğmuş-Yenigediz graben.

1.5. Regional Tectonic Settings

The Alpine – Himalayan belt is one of the most interesting mountain range in the world. Turkey is located in the western end of the belt where a complicated convergence among Arabian, African and Eurasian plates is taking place; this has led to various deformation patterns (Şengör, 1979; Dewey, 1988). These remarkable and peculiar motions are the main reason of major structures governing the neotectonics of Turkey and its neighbourhood (Figure 1.2.).

The Aegean-Cyprian subduction zone represents the plate boundary between African at the southern side and Eurasian to the north. In this part of the subduction zone, the African plate has been subducting towards the north and beneath the Anatolian platelet. Two intraplate transform fault systems, the dextral North Anatolian Fault System (NAFS) and the sinistral East Anatolian Fault System (EAFS), outline the Anatolian platelet and govern its west-southwestward movement from the continental collision between the Arabian and Eurasian plates along the Bitlis-Zagros suture zone in the east to the South Aegean-west Cyprian arc in the west (Şengör, 1979; Dewey and Şengör, 1979; Şengör *et al.*, 1985). According to the model of active tectonics proposed by McKenzie (1972), the Anatolian platelet behaves as a rigid

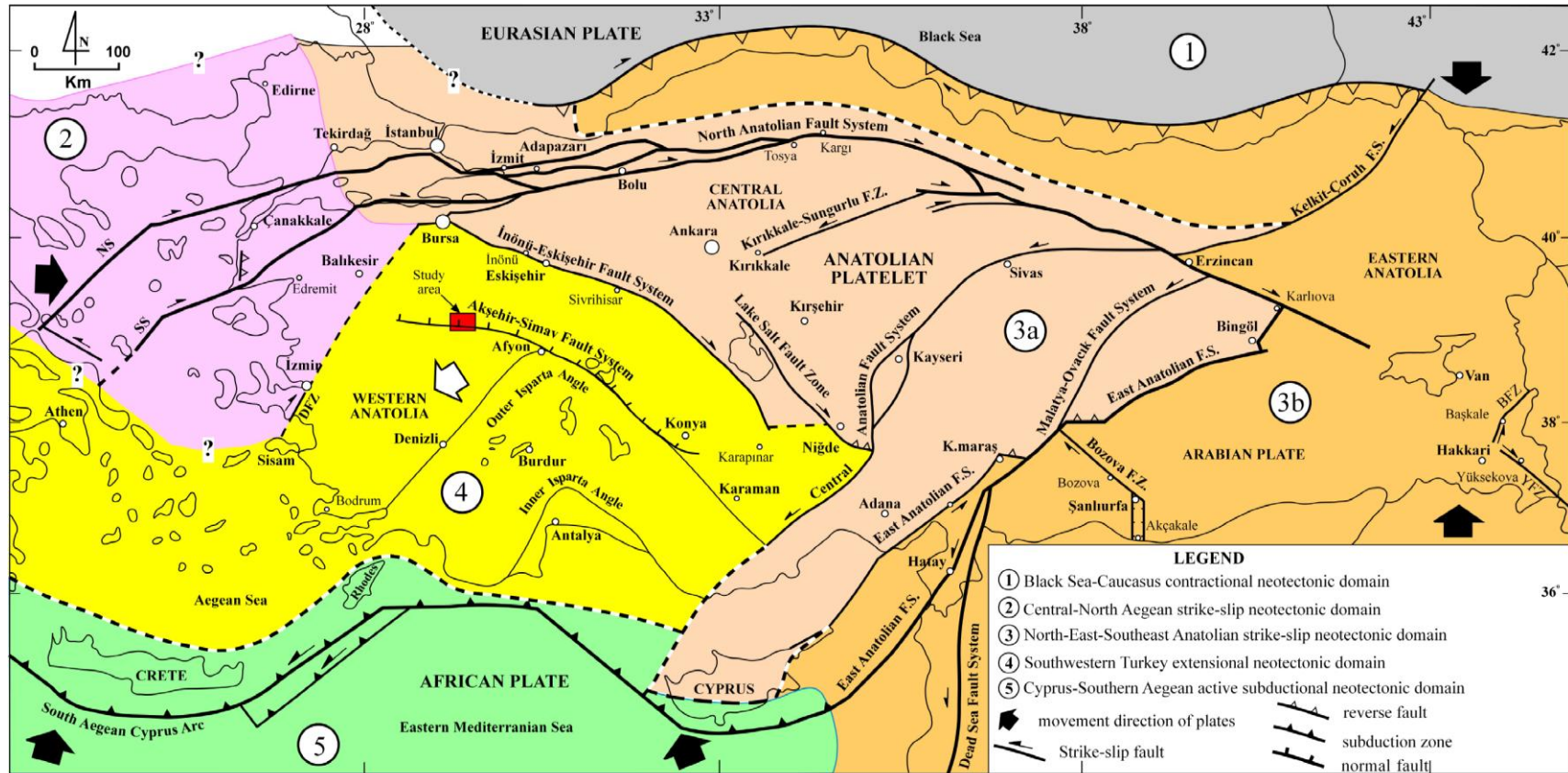


Figure 1.2. Map showing location of the study area and major active fault systems governing neotectonics of Turkey, and neotectonic provinces in Turkey and surrounding areas (Color codes and specific numbers illustrate major neotectonic provinces each of which is characterized by unique deformation style and sedimentary basin formation) (DFZ: Doğanbey fault zone; BFZ: Başkale fault zone; YFZ: Yüksekova fault zone) (courtesy of Prof. Dr. Ali Koçyiğit).

microplate to the forces applied at its boundaries by the larger plates around it. Specifically, because of the interaction between Eurasian and Arabian plates the Anatolian platelet is forced to move, and wedged, towards the west. This motion is compensated by motion along the dextral NAFS and sinistral EAFS. Another significant structure affecting the neotectonic of Turkey is Dead Sea Fault System (DSFS). It compensates the differential north-directed movement between the Arabian and African plates.

Briefly, the main land and near vicinity of Turkey is being shaped by the differential plate motion. Based on the type and nature of the recent tectonic regime, Turkey and its neighborhood can be subdivided into 5 main neotectonic provinces (Figure 1.2., Koçyiğit, 2009) each of which is characterized by unique deformation style and sedimentary basin formation (Koçyiğit, 2009). They are Black Sea-Caucasus contractional neotectonic domain, Central-North Aegean strike-slip neotectonic domain, North-East-Southeast Anatolian strike-slip neotectonic domain, Southwestern Turkey extensional neotectonic domain and Cyprus-South Aegean active subductional neotectonic domain. Our study area is included in southwestern Turkey neotectonic domain characterized by tensional neotectonic and related graben-horst systems bounded by active normal faults. The study area, which is located in southwestern Anatolia and reflects the extensional characteristics of the place known "Southwestern Turkey Extensional Domain".

Southwestern Turkey consists of several continental blocks with characteristic stratigraphy, structures and deformation patterns (Figure 1.3). The boundaries of these continental blocks are defined by major suture zones, namely the Intra-Pontide Suture, the İzmir-Ankara-Erzincan Suture and the Inner-Tauride Suture. They were welded to

each other during the Early Tertiary continent-continent collision across the Neotethys (Okay and Tüysüz, 1999).



Figure 1.3. Simplified tectonic map of western Turkey showing the major blocks in Turkey (Okan and Tüysüz, 1999).

As has been stated before, the commencement age of neotectonic regime and its origin in Turkey and its neighborhood have been the subject of major controversies for many years. Widely excepted idea about the direction and rate of extension suggested by Oral *et al.* (1995) and Le Pichon *et al.* (1995) is that it is N-S and at a rate of 30-40 mm/yr. Indeed, the cause and initiation age of extension in western Anatolia are more complex than that has been envisaged. It may be related to the combined effects of different models suggested by

different authors. There are several ideas about the controversial issues and many studies carried out in western Anatolia to solve the problems. There is no a common agreement on the evolutionary history of the Southwest Anatolian graben-horst system (SWAGHS). This problem is still under debate. In general, there are two different views on this problem:

(1) Latest Oligocene to recent continuous evolutionary model (continuous extension) (Seyitoğlu and Scott 1991; Glodny and Hetzel 2007; Seyitoğlu and Işık 2009; Agostini *et al.*, 2010) and,

(2) Episodic two-stage extensional model (discontinuous extension) (Koçyiğit *et al.*, 1999; Koçyiğit *et al.*, 2000; Ring *et al.*, 1999; Yılmaz *et al.*, 2000; Gürer *et al.*, 2001; Kaya *et al.*, 2004; Bozkurt and Sözbilir 2004; Purvis and Robertson, 2004, 2005; Koçyiğit, 2005; Bozkurt and Rojay 2005; Beccaletto and Steiner 2005; Emre and Sözbilir 2007).

Based on the first idea, the SWAGHS has been evolving without any interruption under the control of the N-S extension since latest Oligocene-Early Miocene (Seyitoğlu and Scott 1991; Glodny and Hetzel 2007; Seyitoğlu and Işık 2009; Agostini *et al.*, 2010).

Whereas, the SWAGHS has been evolving at two extensional phases interrupted by an intervening short-term contractional phase based on the second model (Koçyiğit *et al.*, 1999; Koçyiğit *et al.*, 2000; Ring *et al.*, 1999; Yılmaz *et al.*, 2000; Gürer *et al.*, 2001; Kaya *et al.*, 2004; Bozkurt and Sözbilir 2004; Koçyiğit 2005; Bozkurt and Rojay 2005; Beccaletto and Steiner 2005; Emre and Sözbilir 2007). In addition, according to the first idea, the back-arc spreading is the main mechanism for the evolution of SWAGHS (Figure 1.4). Across Aegean Sea and its onshore section, a back-arc spreading phenomenon is adapted to the

southwestern migration of the western Anatolia by means of subduction along the South Aegean-Cyprian arc where African plate is being consumed at a rate of approximately 1cm/yr beneath the Anatolia (McKenzie, 1978; Le Pichon and Angelier, 1979; Jackson and McKenzie, 1988; Kissel and Laj, 1989; Meulenkamp *et al.*, 1988, 1994; Thompson *et al.*, 1998; Avigad *et al.*, 1997; Jolivet *et al.*, 1998).

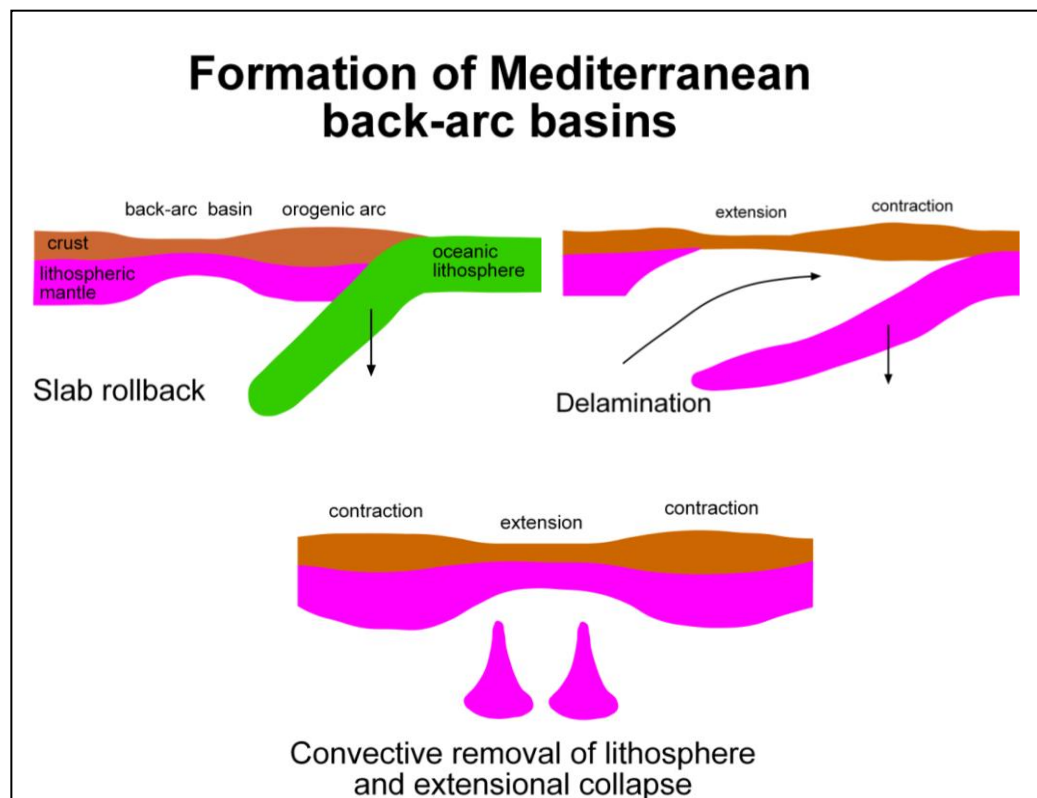


Figure 1.4. Current models for the formation of Mediterranean basin (www.es.ucl.ac.uk).

Some studies carried out in the central Aegean suggested that back arc extension has begun at least in Early Miocene (Seyitoğlu and Scott 1991; Doglioni *et al.*, 1999; Rojay *et al.*, 2005; Glodny and Hetzel 2007; Seyitoğlu and Işık 2009; Agostini *et al.*, 2010). On the other hand, some of other studies argue for large range of initiation time from 5-60 Ma for

the extension (McKenzie, 1978; Mercier, 1981; Le Pichon and Angelier, 1979; Thomson *et al.*, 1998). According to mechanism of the back-arc extension, the roll-back of subducting slab takes place, and then it was followed by the escaping plate. In the numeric model of the Hassani *et al.*, (1997), the sufficient slab length should be at least 300 km to present enough forces to manage the roll-back process and as a progressive manner back-arc extension takes place. Similar progressive processes are suggested by Meulenkamp *et al.*, (1988) who suggested 26 Ma for the initiation of subduction and 12 Ma for the commencement age of extension in the region.

According to Dewey and Şengör (1979), the wedge-shaped Anatolian fragment moved westward between dextral NAFS at the north and sinistral EAFS at the south (Figure 1.2.). In this model, Turkey is being squeezed by northward motion of African plate. For this reason, Turkey moves along the two main fault systems in the westward direction to compensate the force coming from the plate motions. Şengör *et al.* (1985) stated that the plate motion has caused to the E-W shortening. It is now relieved that it occurs in the form of N-S extension due to the lateral spreading of the continental material onto the oceanic lithosphere of the eastern Mediterranean. According to escape model of Dewey and Şengör (1979), the initiation age of the NAFS is Late Miocene (Ketin, 1969) or late Serravallian (~12 Ma) (Barka and Hancock, 1984; Şengör *et al.*, 1985). But recent studies carried out on the NAFS indicated that its age is Pliocene and younger than ~12 Ma (Barka and Kadinsky-Cade, 1988; Koçyiğit, 1988, 1989; Westaway, 1994; Koçyiğit *et al.*, 2000).

Another model suggested for the evolution of SWAGHS is orogenic collapse (called gravitational collapse, extensional collapse etc.) which says that the continental extension over Aegean and western Anatolia

is related to the spreading and thinning of over-thickened crust (Dewey, 1988). As a general description, orogenic or gravitational collapse refers to the gravity-driven flow that reduces lateral contrasts in gravitational potential energy (Rey *et al.*, 2001). It is a process that transfers gravitational potential energy from regions of high potential energy to regions of lower potential energy (Selverstone, 2005). The origin of this potential energy difference has been attributed either to an over-thickened crust only (Molnar and Tapponnier, 1978; Molnar and Lyon-Caen, 1988; Dewey, 1988) or to the over-thickened crust and convective removal of the lower lithospheric mantle (Fleitout and Froideveaux, 1982; England and Houseman, 1989; Platt and England, 1994; Houseman and Molnar, 1997). In this model, orogen starts to collapse under its own weight. For the occurrence of this process, a thick crust is needed. Şengör *et al.* (1985) suggested that following the Paleocene–Eocene collision across the northern branch of Neotethys, a crustal thickness of 65–70 km was probably reached in western Turkey. This crustal configuration could be the potential cause of the extension in the region. Consequently, post orogenic collapse model, encouraged by field evidence in western Anatolia, supported by many researchers following the first proposal by Dewey (1988) (e.g., Seyitoğlu and Scott, 1991; Bozkurt and Park, 1994; Collins and Robertson, 1998; Ring *et al.*, 1999; Koçyiğit *et al.*, 1999a, b; Yılmaz *et al.*, 2000).

Episodic two-stage graben model or discontinuous extension model argues that none of the above mentioned models alone satisfactorily explains the age and origin of crustal extension, and the multi-stage nature of extension (Koçyiğit *et al.*, 1999), because the extension occurs in two distinct structural styles of different timing: (1) an Early-Middle Miocene phase of core-complex formation, and (2) a subsequent modern phase of Plio-Quaternary normal faulting and graben formation, separated by an interval of N-S crustal shortening during Late Miocene-

Early Pliocene times. They claim that the origin of first phase of extension is mostly readily attributed to orogenic collapse model along the İzmir-Ankara-Erzincan suture zone. Later on, it was replaced by a short phase of ~ N-S contraction in Late Miocene to Early Pliocene times. The intervening contractional phase is related to a change in the kinematics of the Eurasian and African plates. In the Late-early Pliocene, sea-floor spreading started along Red Sea (Hempton, 1987), and then the main structures namely dextral NAFS and sinistral EAFS were formed; consequently, the Anatolian platelet has started to move in south-southwestward direction (Koçyiğit *et al.*, 1999). This model is being supported by numerous studies (Bozkurt, 2000, 2001, 2003; Yılmaz *et al.*, 2000; Sözbilir, 2001, 2002; Cihan *et al.*, 2003; Bozkurt and Sözbilir, 2004, 2006; Purvis and Robertson, 2004, 2005; Kaya *et al.*, 2004; Bozkurt and Rojay, 2005; Beccaletto and Stenier, 2005; Westaway *et al.*, 2005; Koçyiğit and Deveci, 2007). Additionally, Yılmaz *et al.* (2000) suggested that the evolution process is slightly different than the episodic evolution model. They concluded that the Early-Middle Miocene time is represented by N-S contractional phase related to the convergence along İzmir-Ankara suture zone. Subsequently, this phase was replaced by a N-S extension which has been caused by the orogenic collapse. The N-S extensional regime was interrupted by Late Miocene–Early Pliocene (?) quiescent period. Then, N-S extensional regime was rejuvenated again by Pliocene to establish the present day neotectonic configuration. Tectonic escape of the Anatolian microplate, which began during Late Miocene–Early Pliocene period may be responsible for the beginning of neotectonic period.

According to another recent model, the current extension in the Aegean province is driven by the differential rate of convergence between the northeastward directed subduction of the African plate and the hanging-wall disrupted Eurasian lithosphere. Considering the African plate is

fixed, the faster southwestward motion of Greece relative to Cyprus-Anatolia determines the Aegean extension (Doglioni *et al.*, 2002). This model depends on the paleomagnetic studies (Gürsoy *et al.*, 2003; Kissel *et al.*, 2003).

Gürer *et al.* (2009) have suggested a new evolutionary history for the E-W trending Büyük Menderes graben. They have claimed that the graben had recorded two successive and independent complex tectonic events. The first event is characterized by an E-W extension caused by the NE-SW contraction during Early-Middle Miocene. There is an unconformity between the Lower-Middle Miocene basin infill and the Plio-Quaternary sequence which implies to folding, uplift and severe erosion caused by NE-SW shortening. The second tectonic event is the change in the sense of extension from E-W to N-S which influenced the formation of the graben by a series of progressive pulses of deformation. These are the exhumation of Menderes Massif, rapid deposition of alluvial deposits, initiation and formation of approximately E-W-trending high-angle normal faults, which bound the graben, and in the last pulse, depocentre of the graben migrated into the present position by the diachronous activity of secondary steeper listric faults. The driving mechanism of the first tectonic event is the back-arc spreading or probably the roll-back of African slab below the south Aegean region. The cause of second and later event is the southwestward escape of the Anatolian block along its boundary faults, that is, the North Anatolian and the East Anatolian Fault Systems.

Consequently, the models suggested explaining origin, initiation age of extension and evolutionary history of the SWAGHS are still under debate. In this context, one of the aims of the current study to present new stratigraphical, structural and palaeoseismic data in order to make a contribution to the solution of above-mentioned problems.

1.6. Previous Studies

The neotectonic characteristics of the Yenigediz-Erdoğmuş graben were poorly studied. It is first named and described as a graben in this study. A number of previous studies were performed after the 1970 Gediz earthquake which is noticed the importance of the Gediz and near sites. The contributions to the geology of Gediz and its vicinities are summarized below.

First scientific study was concentrated with the geology of Paleozoic, Mesozoic and Neogene deposits exposed in the area between Kütahya and Gediz (Akkuş, 1962). The tectonic and stratigraphic characteristics of the area are the main subject of this paper.

Muratdağı and near vicinities are very attractive for the economic geology. Mariko (1970) and Bingöl (1977) focused on the petrographical, petrological and geochemical characteristics of the basement rocks in Muratdağı region.

Gökalp (1970) has prepared an unpublished report in MTA which includes the hydrogeological investigation in Gediz-Abide region. He focused on the thermal spring in Ilica region.

Erinç *et al.* (1970), Ambraseys and Tchalenko (1972), Eyidoğan and Jackson (1985) investigated the Gediz and surrounding areas from the earthquake point of view after 1970 Gediz earthquake. Erinç *et al.* (1970) investigated the geomorphological characteristics of the earthquake. Ambraseys and Tchalenko (1972) evaluated seismotectonic aspects of the earthquake, whereas, Eyidoğan and Jackson (1985) studied the source of the 1970 Gediz earthquake.

Abdüsselamoğlu (1970) studied the geological and tectonic characteristics of the Gediz county and its vicinity. He presented the sedimentary deposits and source of 1970 Gediz earthquake.

Ercan *et al.* (1979) presented petrology of the volcanics around Uşak and its meaning in the aspect of plate tectonic in Aegean region.

Gün *et al.* (1979) studied the geology and age arguments in Neogene basins of Gediz and Emet regions. He investigated the fossil content in Miocene and Quaternary deposits and tried to explain the definite age range of the sedimentary sequences.

Ercan *et al.* (1984) examined the volcanics in Cenozoic ages around the Simav which is located west of the Gediz. Classification of the volcanics and their geochemical characteristics were presented.

In the regional scale, Koçyiğit (1980, 1983 and 1984) have mapped a very broad area of Lakes district comprising the study area. Especially, all the geological structures faults, folds, unconformities, lithological units were investigated particularly.

These studies mentioned above have focused on the Gediz county and it's near vicinity. Furthermore, a number of studies were performed along the ASFS from different aspects such as 2002.02.03 Çay earthquake (Özden *et al.*, 2002 (occurrence process); Kalafat *et al.*, 2002 (focal mechanism solution); Dirik, 2002 (geological observations); Tapırdamaz *et al.*, 2002 (aftershock evaluation); Başokur *et al.*, 2002 (surface rupture); Ulusay *et al.*, 2002 (geotechnical point of view); Dinç, 2003 (3-D wave velocity); Emre *et al.*, 2003 (surface faulting); Gökten *et al.*, 2003 (earthquake mechanism and seismic risk); Koçyiğit and Özacar, 2003 (evolutionary history); and Ergin *et al.*, 2009 (aftershock

study). Additionally, eastern part of the ASFS (Çay and Maltepe section) has been studied for palaeoseismological purpose by Akyüz *et al.* (2006).

CHAPTER 2

STRATIGRAPHIC OUTLINE OF THE STUDY AREA

2.1. Introduction

In this chapter, general stratigraphic frame of the units exposed in and adjacent to the Erdoğmuş-Yenigediz graben was investigated and described in detail. That is the only way to understand the geological development and different variations in the graben during its evolutionary history. In this context, there are two important questions to answer: (1) what are the characteristic features of different units and their stratigraphic relationships? (2) what kind of deformation patterns are observed within the stratigraphic units and what do they mean?

The previous studies about the Neogene stratigraphy of the Erdoğmuş-Yenigediz graben are very limited. Most of them are related to the coal mine (Lebküchner, 1965; Bingöl, 1974), hot springs and geothermal boreholes (Gökalp, 1970) in and around the study area, and the 1970 Gediz earthquake (Arpat and Özgül, 1970). A few studies have focused on the geology of the region and were mainly concentrated with the geologic mapping by the General Directorate of Mineral Research and Exploration (MTA) geologists (Demirsu and Kutlu, 1955; Gün, 1975). So, neither naming nor deformation characteristics of the units have not been described up to present study.

2.2. Stratigraphic Outline of the Graben Deposits

The graben infill is subdivided based on the lithology, age and deformation style, into three categories: (1) pre-Miocene rocks cut by the Paleocene felsic intrusions, (2) Miocene-Middle Pliocene pre-modern graben infill (Arıca formation), and (3) Plio-Quaternary modern graben infill (Erdoğmuş formation) (Figure 2.1).

Pre-Miocene rocks are widely exposed at both the southern and northern margins of the Erdoğmuş-Yenigediz graben. They consist mostly of low- to high-grade metamorphic rocks of the northern Menderes Massif and the Cretaceous ophiolitic mélangé full of carbonatized to silicified magnesite veins. The ophiolitic mélangé overlies tectonically the metamorphic rocks, and both of which are cut across by the felsic intrusions. Ophiolitic rocks are composed of diverse-sized radiolarite, spilite, peridotite, serpentinite and recrystallized limestone blocks set in a scaly sandy matrix rich in ophiolitic clasts. The metamorphic rocks are made up of augen gneiss, mica schist, quartzite, quartz-mica-chlorite schist, marble and calcschist. They are overlain with an angular unconformity by both the pre-modern and modern graben infill (Figure 2.2). Detailed description of older basement rocks is beyond the scope of this thesis. On the other hand, the graben infill is described in more detail below.

AGE	UNITS	THICKNESS	LITHOLOGY	DESCRIPTIONS	TECTONIC PERIOD
Plio-Quaternary	Erdöğmuş formation	~150 m		<p>c. Alluvium : recent flood plain sediments and alluvial fan deposits (unsorted pebble to mud size sediments)</p> <p>b. Travertine: yellow, porous, thick-bedded to massive, range from self-built channel type travertines</p> <p>a. Terrace deposits : alternation of red boulder-block conglomerate, sandstone and mudstone</p> <p><i>angular unconformity</i></p>	NEOTECTONIC PERIOD
late Early Miocene - Early Pliocene	Arıca formation	110 m 100 m 158 m		<p>6. yellow grey coarse-grained to conglomeratic sandstone with limestone and marl-claystone alternation of regressive nature.</p> <p>5. andesitic-basaltic sill, dyke, lava, tuff, tuffite and volcanic breccia</p> <p>4. thin- to thick-bedded lacustrine limestone and green-blue marl-shale alternation (depocentral facies)</p> <p>3. sandstone to conglomeratic sandstone of marginal facies</p> <p>2. well-cemented sandstone and red fluvial conglomerate alternation with coal (lignite) seams</p> <p>1. polygenetic, well-cemented basal conglomerate</p> <p><i>nonconformity</i></p>	PALEOTECTONIC PERIOD
pre - Miocene	Basement	?		<p>Basement rocks:</p> <p>c. Upper Oligocene - Lower Miocene felsic intrusions.</p> <p>b. Ophiolitic mélangé</p> <p>X: tectonic contact</p> <p>a. metamorphic rocks made up of augen gneiss, shist and marble. They belong to the Menderes massif.</p>	

Figure 2.1. Generalized columnar section of the study area (See text for detailed explanation) (not to scale).



Figure 2.2. General view of the angular unconformity (AU) between the Plio-Quaternary modern graben infill (Erdoğmuş formation, TQe) above and metamorphic rocks (Tb) below (~ 5 km SE of Gümele village, view to E).

2.2.1. Pre-Modern Graben Infill (Arıca formation)

The Erdoğmuş-Yenigediz graben has two different graben infill: (1) pre-modern graben infill (Arıca formation) and (2) modern graben infill (Erdoğmuş formation). Pre-modern graben infill consists of three packages in the nature of coarsening upward sequence; these from bottom to top, are (1) lower detrital sedimentary package, (2) central volcano-sedimentary package and (3) uppermost clastic sedimentary package (Figure 2.1).

The lithological characteristics of the formations were documented through 3 measured stratigraphic sections (locations in Appendix – A) (Figures 2.3, 2.4 and 2.5). The section in Figure 2.3 was measured outside the study area, where, the lower package of the Arıca formation is exposed.

Location: Yeşilyurt village/Altıntaş, Kütahya (east of study area)
 Start: 35754960E / 4316581N
 End: 35754722E / 4318311N
 Date: 15.07.2006

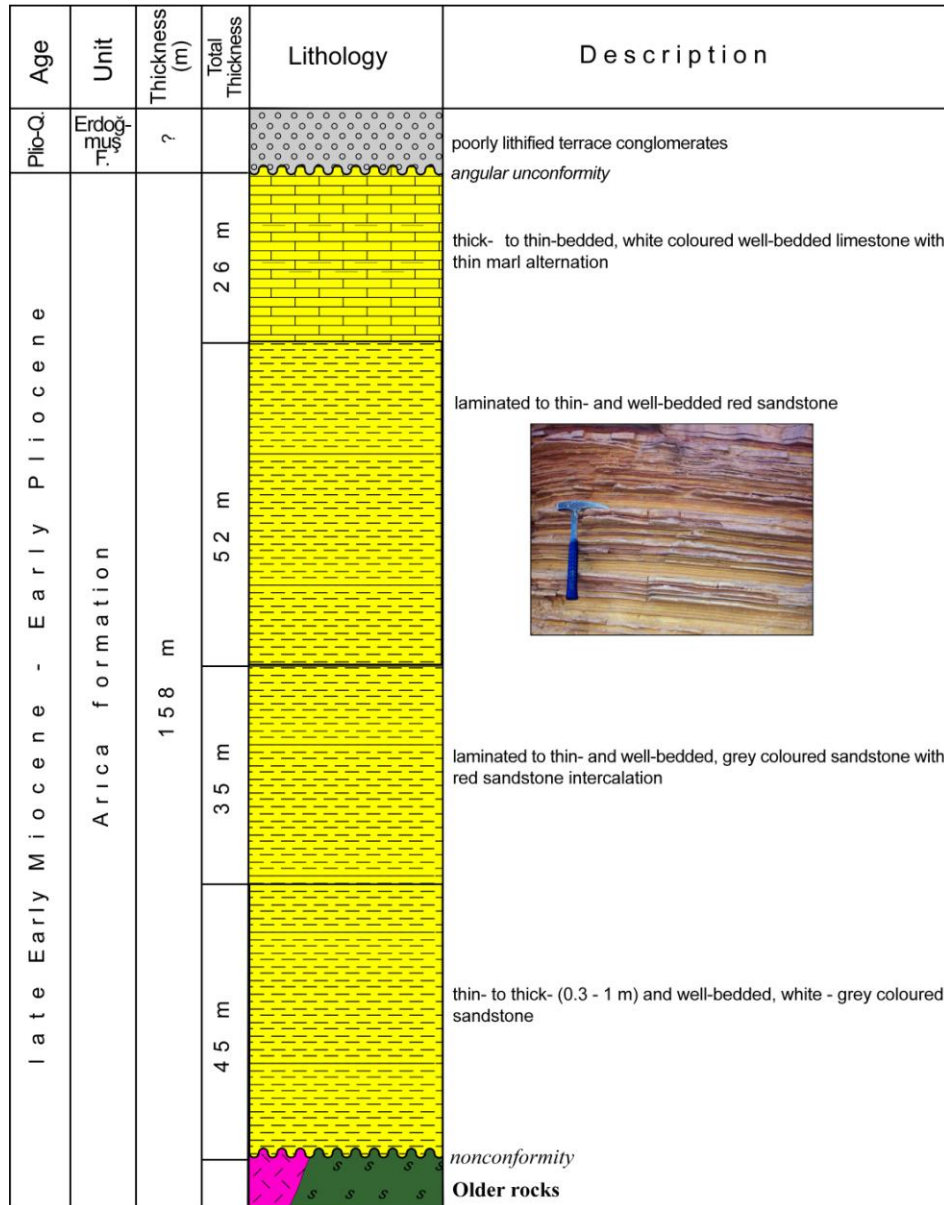


Figure 2.3. Measured stratigraphic column of the Arıca formation (lower detrital part of the sedimentary package).

Location: Gediz, Kütahya
 Start: 35 707540E / 4316581N
 End: 35 707722E / 4318311N
 Date: 30.07.2006

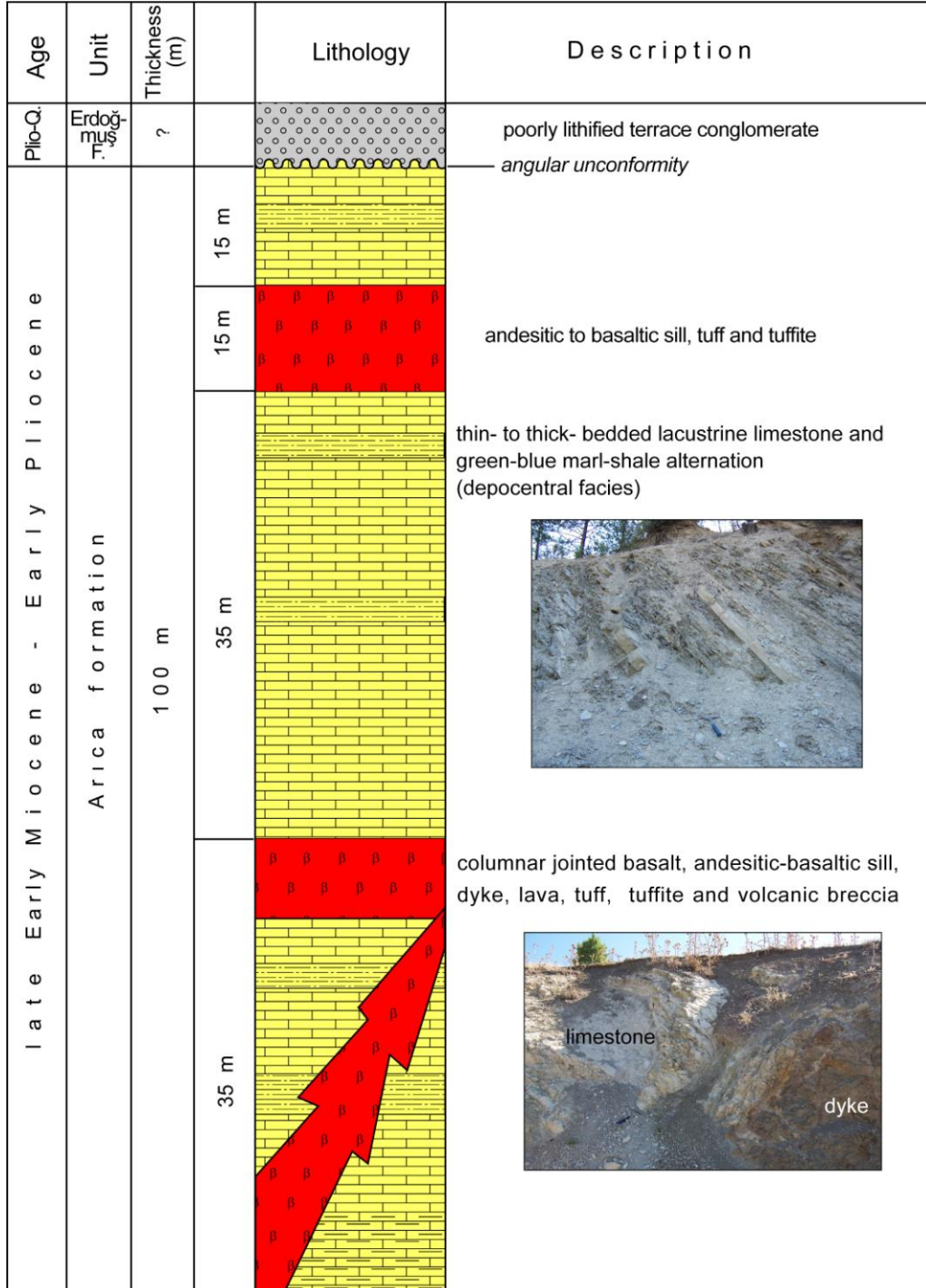


Figure 2.4. Measured stratigraphic column of the Arıca formation (central part of the sedimentary package).

Location: Erdoğmuş village/Gediz, Kütahya
 Start: 35709208E / 4314567N
 End: 35709130E/4315205N
 Date: 22.07.2006

Age	Unit	Total Thickness (m)	Thickness (m)	Lithology	Description
Plio-Q.	Erdoğmuş	?			poorly lithified terrace conglomerates <i>angular unconformity</i>
Late Miocene - Early Pliocene	Arıca Formation	110	5.8		thick- to thin-bedded white limestone
			5.8		thin-bedded, grey marl with clay intercalations
			12.5		thick-bedded pinkish colour red mostly sandstone beds with lesser clay
			22		similar with unit a. Laminated light grey, white marl and limestone alternation
			7.2		similar with unit b. Additionally, grain size is about 15 cm, poorly sorted limestone conglomerate with quartz, basalt, metamorphic clasts.
			13.5		similar with unit a. Laminated light grey, white marl and limestone alternation
			12.5		thin-bedded to laminated white-grey clay, sandstone and marl alternations. Top and bottom boundaries of the units could not be defined exactly, so it was measured as one unit
			5.8		similar with unit b. Additionally, grain size is about 15 cm, poorly sorted limestone conglomerates with quartz, basalt, metamorphic clasts
			3.9		laminated to thin-bedded, grey and greenish marl beds
			2.9		thin-bedded, white calcareous limestone
			3.3		laminated to thin-bedded, grey and greenish marl beds
			2.4		poorly consolidated, thin-bedded, light grey white conglomerate with clay matrix
			8.6		laminated to thin-bedded, light grey, white marl and limestone alternation (attitude of beds: 238°/18°N)

Figure 2.5. Measured stratigraphic column of the Arıca Formation (uppermost part of the sedimentary package).

The name (Arıca formation) of the pre-modern graben infill is first used in the present study. In some previous works different facies of the Arıca formation were named while they did not cover the Arıca formation as a whole (Özpeker, 1969; Gün *et al.*, 1976; Abdülselamoğlu, 1977; Akdeniz and Konak, 1979; Ercan *et al.*, 1979; Akbulut *et al.*, 1984; Yalçın, 1984; Helvacı, 1986) (Figure 2.6). The name of Arıca formation comes from Arıca village. Because, the lower basal clastics and type section of the Arıca formation are well-exposed around Arıca village along the southern margin of the graben. On the other hand, the central volcano-sedimentary package is more widespread around Eskigediz county (Figure 2.7) and its vicinity along the northern margin of the graben. Additionally, the uppermost clastic package is observed around the Erdoğan village. Therefore, the uppermost horizon of the formation is separated by an angular unconformity from the modern graben infill (Erdoğan formation) (Figure 2.1).

The older graben fill starts with a weakly-sorted, and well-rounded polygenetic basal conglomerate (Figure 2.8) above the erosional surface of the basement rocks at the bottom and then continues upward with the alternation of sandstone and conglomerate with intercalations thin coal seam. The basal conglomerate consists of pebble- to cobble-sized clasts of marble, gneiss, schist, quartzite, chert, various ophiolitic rocks and older volcanic rocks set within a matrix of sandy iron-rich siliceous cement.

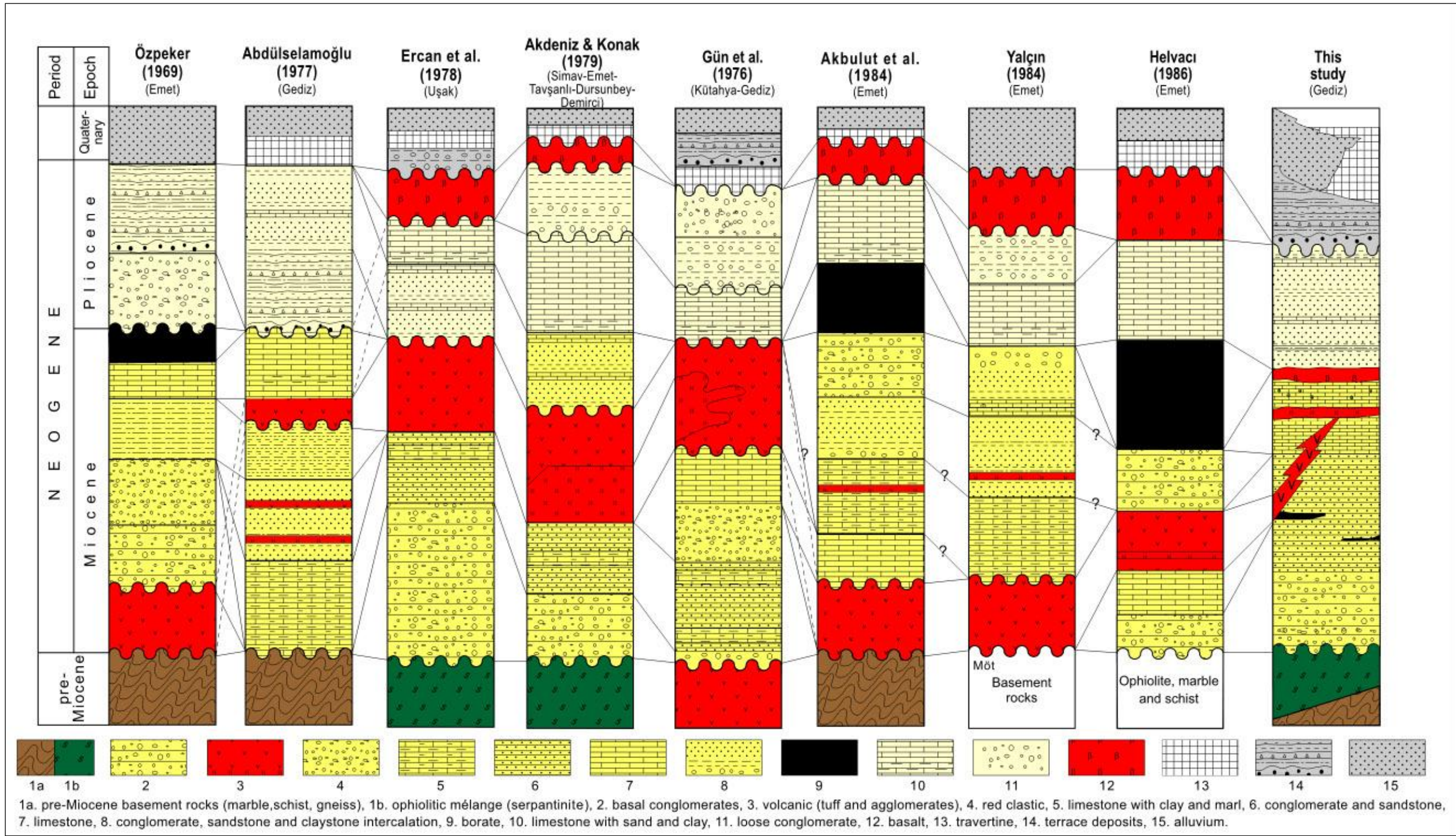


Figure 2.6. Correlation chart for the stratigraphic units between previous studies and recent study (not to scale).



Figure 2.7. General view of the volcano-sedimentary package around Eskigediz county (Ta. Arica formation; TQe. Erdoğan formation; view to NNW).



Figure 2.8. Close-up view of the basal conglomerates (~3 km NE of Arica village).

The basal conglomerate is cut by the basaltic-andesitic dikes in places. The total thickness of this horizon was measured as 158 m (Figure 2.1). Furthermore, the missing overlies part of this package is exposed around Yeşilyurt village (Altıntaş/Kütahya) ~46 km E of Gediz (Figure 2.3). The lower basal clastics are succeeded conformably by a volcano-sedimentary sequence composed of sandstone to conglomeratic sandstone at and near graben margin, which thin- to thick-bedded lacustrine limestone, blue-green marl, shale and turbiditic sandstones alternation occur towards the central part of the graben. Both the marginal and the depo-central facies either alternate with andesitic to basaltic lavas (Figure 2.9), or intruded by dyke and sills of same composition such as tuff, volcanic breccia and tuffite are also common. Besides around Yaylaköy village, columnar jointed basalt is well-exposed (Figure 2.10).



Figure 2.9. Basaltic dyke cutting across the limestone beds (Yellow arrow locates baked zone).



Figure 2.10. General view of the columnar basalt in Yaylaköy village.

The 100m-thick volcano-sedimentary sequence (Figure 2.4) displays syn-depositional features, such as normal growth faults, slump folds (Figure 2.11) and broken formations in the nature of olistostrome, which may imply to a sedimentation under the control of both volcanic eruption and/or active tectonics.

Deformation styles of both pre-modern and modern graben infill reflect morphotectonically the ancient and the modern configurations of the Erdoğmuş-Yenigediz graben. The pre-modern graben infill consists of a deformed (folded and reverse to strike-slip faulted) (Figure 2.12a and b) volcano-sedimentary sequence exposed in uplifted margins of the graben.



Figure 2.11. Close-up view of the slump folds (near E of Deliağatarlası).

Age of the volcano-sedimentary central package of the pre-modern graben infill was previously reported as Late Miocene based on both the micro- and macro fossil content. Abundant plant fossils and samples from lignite levels containing *Taxodium distichum miocenicum* have defined a Miocene age (Gün, 1975). Furthermore, a yellowish clastic level located on Gökler-Sazköy villages has been examined and pores and pollens are described: such as *Inaperturopollenites hiatus*, *Pityosporites microalatus*, *Priatriopollenites rurensis*, *Triatriopollenites bituitus*, *Triatriopollenites coryphaeus*, *Triatriopollenites robustus*, *Subtriporopollenites simplex*, *Polyvestibulopollenites verus*, *Polyporopollenites undulosus*, *Tricolporopollenites microherici*, *Tricolporopollenites megaexactus*, *Tricolporopollenites microreticulatus*, *Tricolporopollenites margaritatus*, *Periporopollenites multiporatus* (Gün, 1975). Accordingly, Middle Miocene age was assigned to the clastic rocks of the Arica formation (Gün, 1975).

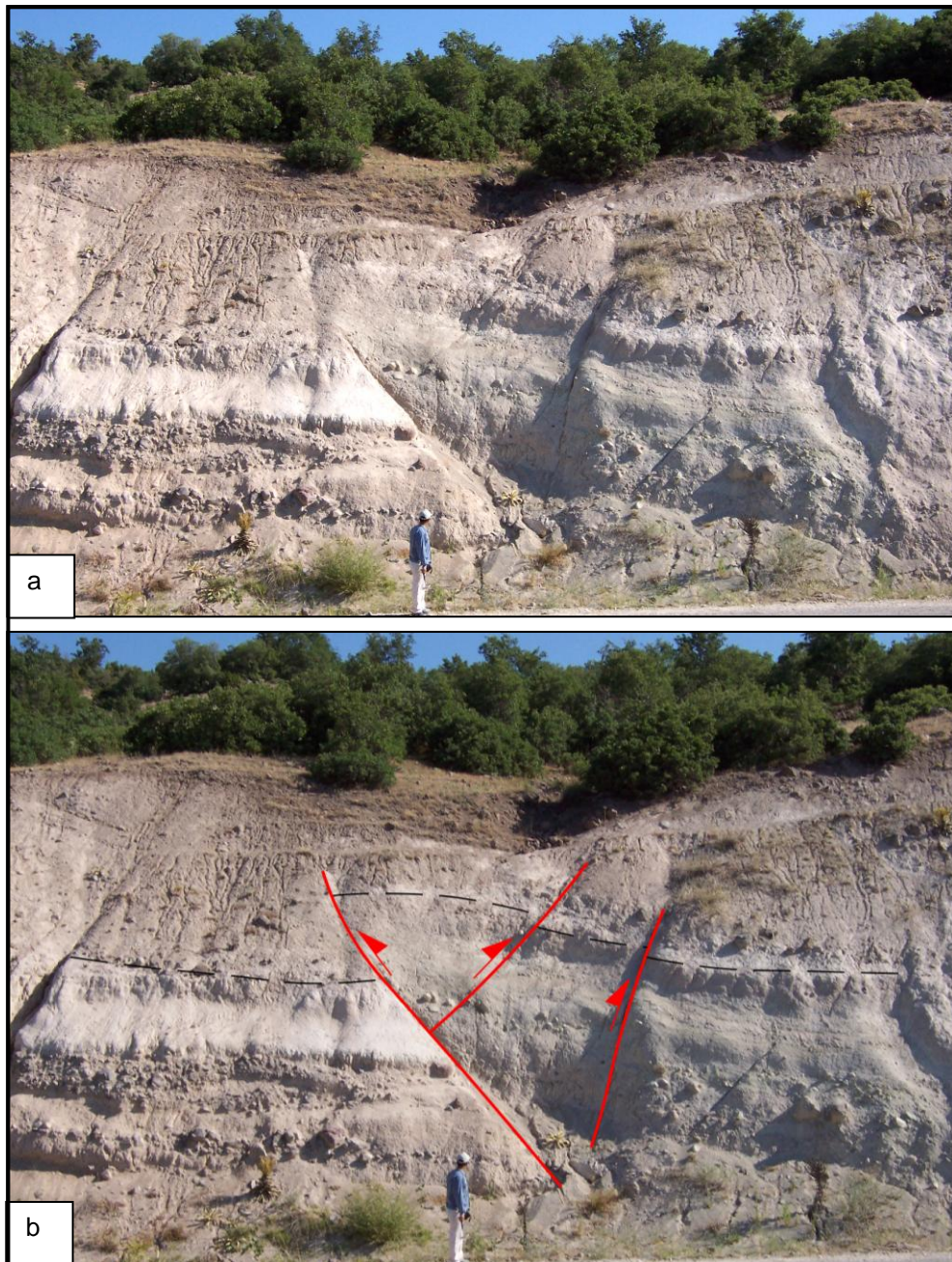


Figure 2.12.a) General view of the reverse faulted pre-modern graben infill (Location: near NE of Eskigediz county, view to NW), b) sketched pattern of field photograph.

Another work (Yalçınlar, 1946) defined very rich vertebrate fossil content in the clay-limestone unit around Balçıklı stream (near west of Şaphane village, out of the study area). The mammalian fossils *Mastadon sp.*, *Aceratherium sp.*, *Rhinoceras sp.*, *Hipparian gracile*, *Suserymantihius*, *Gazella sp.*, *Helicotragus sp.*, *Camelo pardalis attica*, and *Palaeoryx sp.* suggest a Late Miocene age (Yalçınlar, 1946).

East of Akçaalan village on the highway to Emet, plant fossils such as *Theodoxus cf. soceni JEKELIUS*, *Micromelonia ptycophora BRUS*, *Melanopsis sp.*, *Planorbarius thiollierei*, *Planorbarius cf. thiollierei*, *Lymaea indet.*, *Helicidae*, *Planorbidae*, and *Unionidae* are represented (Gün, 1975) in the folded and deformed lacustrine marl and limestone units; Early-Middle Miocene age was assigned. This central volcano-sedimentary package is conformably succeeded by a second and coarsening upward clastic sequence (Figure 2.1). The sequence consists mostly of yellow-grey sandstone and conglomeratic sandstone with marl and limestone intercalations (Figure 2.13). The topmost part of the pre-modern graben infill reflects that some changes in the depositional conditions and an initial uplift in the basin. The total thickness of the regressive sequence was measured as 110 m. Total thickness of the upper regressive part of the Arica formation has been calculated by using the measured section (Figures 2.3, 2.4 and 2.5). Approximately, all beds are conformable to each other as 240°/14°N.

In addition, this sequence contains a rich macrofossils such as *Theodoxus*, *Micromelania*, *Melanopsis*, *Planorbarius thiollierei*, *Lymaea indet.*, *Helicidae*, *Planorbidae*, and *Unionidae* in the east of Akçaalan village (outside of study area) and in the north of Eskigediz County (Gün, 1975). Based on this fossil content, Early Miocene – Early Middle Pliocene age was assigned to the topmost part of the pre-modern graben infill (Gün, 1975). Because, radiometric dating results of this

volcano-sedimentary sequence (Ar/Ar dating) has been obtained as ~18 Ma (see next Chapter). Briefly, based on the age result (Early Miocene according to Stratigraphic Time scale of International Stratigraphy Commission ICS, 2008) in the present study and paleontological ages obtained from fossil content in volcano-sedimentary package, an Early Miocene – Early Pliocene age is assigned.



Figure 2.13. General view of the uppermost part of volcano-sedimentary package (Location: Akçaalan village).

2.2.2. Modern Graben Infill (Erdoğmuş formation)

Erdoğmuş formation is named in the present study. This formation was also named by different researchers, but their works did not include all facies of the Erdoğmuş formation as a whole (Gün *et al.*, 1976; Abdülselamoğlu, 1977; Akdeniz and Konak, 1979; Yalçın, 1984) (Figure 2.6). The formal stratigraphic name (Erdoğmuş formation) of the modern graben infill comes from the Erdoğmuş Town. Because, it's basal and type facies are well-exposed around Erdoğmuş town. The Erdoğmuş formation is exposed most part of the study area. It overlies, with an angular unconformity, different facies of the pre-modern graben infill (Figures 2.14 and 2.15).

This is the nearly flat-lying, undeformed and weakly lithified to loose sedimentary sequence, deposited during the Plio-Quaternary extensional neotectonic period. The modern graben infill consists of three different lithofacies: (a) terrace deposits, (b) travertine, and (c) recent axial plain deposits (Figure 2.1).

The terrace deposits mostly consisting of weakly lithified to loose polygenetic and boulder-block conglomerate form the lowermost and basal facies. They are well-exposed on both sides of Gediz River valley and around Erdoğmuş town. They occur in diverse-sized, isolated and patch-like outcrops (Appendix A). Their relatively older age, uplifted positions and distribution pattern altogether indicate the incipient outline of the modern graben.

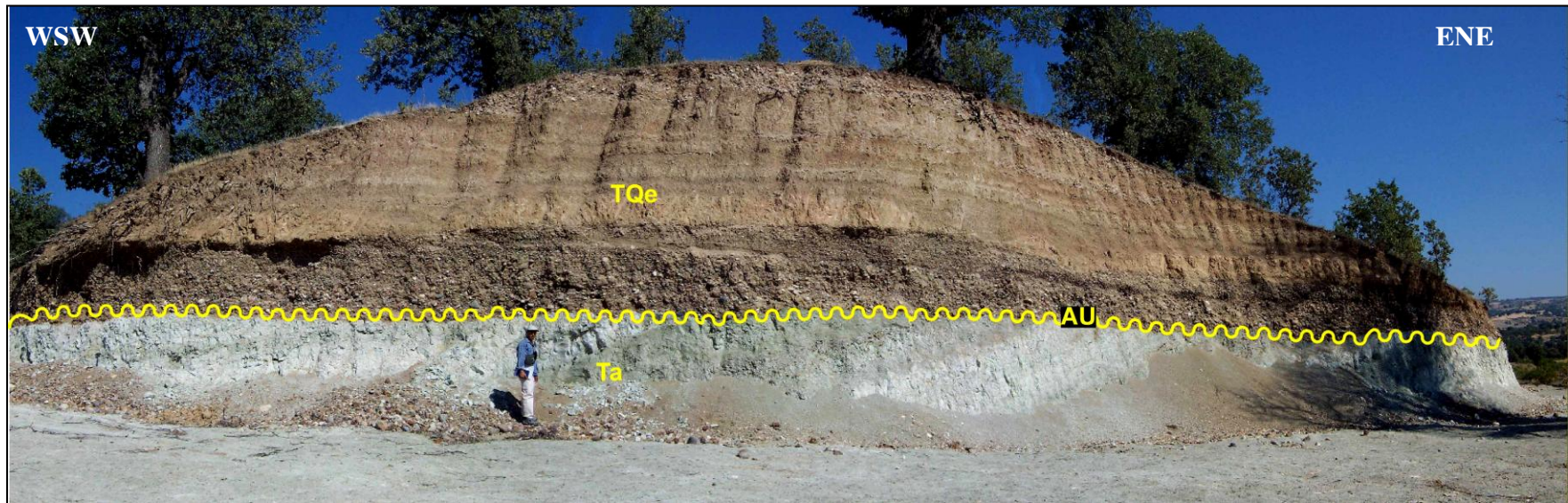


Figure 2.14. Angular unconformity (AU) between the nearly flat-lying Plio-Quaternary modern graben infill (TQe) and the deformed (tilted, folded and reverse-faulted) lacustrine marl-shale-limestone alternation of the lower Miocene-Lower Pliocene pre-modern graben infill (Ta) (Location: crossroads of Çeltikçi village).

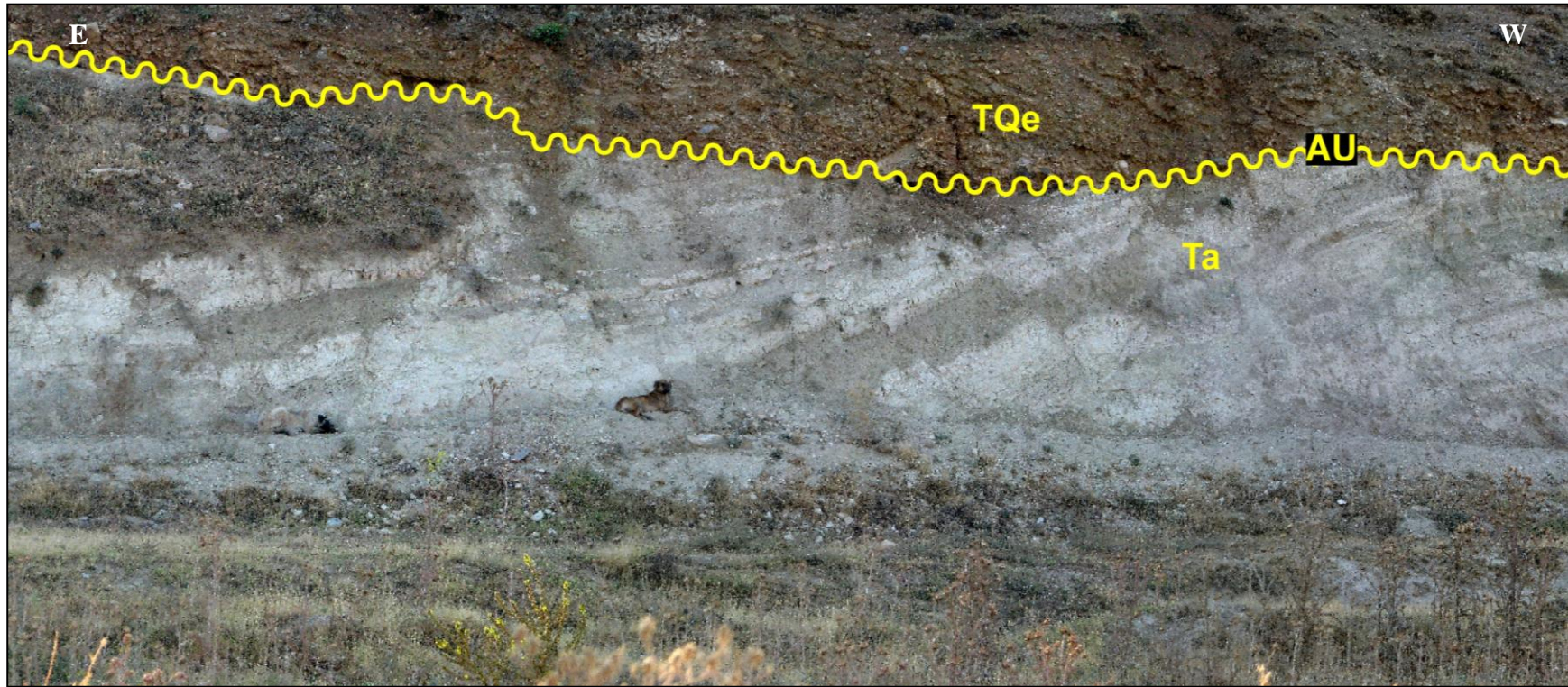


Figure 2.15. Angular unconformity (AU) between the Plio-Quaternary modern graben infill (TQe) and the deformed lacustrine marl-shale-limestone alternation of the Miocene-Lower Pliocene pre-modern graben infill (Ta) (Location: entrance of Erdoğan village).

Red fluvial conglomerate is unsorted and made-up of well-rounded, marble, gneiss, quartzite, quartz, various volcanic rocks, radiolarite, spilite, serpentinite, lacustrine limestone, marl, red sandstone, and granite clasts set within a sandy matrix and iron-rich carbonaceous to siliceous cement. Conglomerates also contain wedge-shaped red sandstone and mudstone intercalations. The widespread occurrence of the normal growth faults, particularly within the red clastics, indicates a tectonically active depositional setting (Figure 2.16).

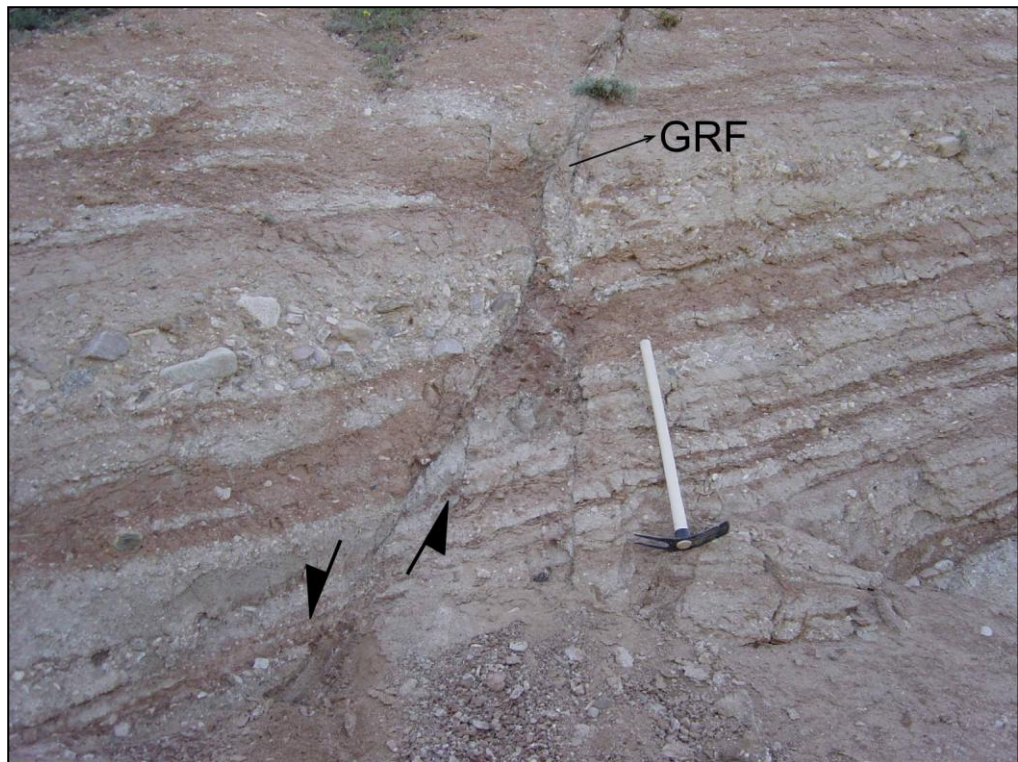


Figure 2.16. Close-up view of a normal growth fault (GRF) in red fluvial conglomerate-mudstone alternation (Location: near S of Abide village).

The travertine occurrences are exposed around Yeşilova village (Figure 2.17) north of the study area. At this locality, they occur in a nearly flat-

lying plateau of travertine at the elevation of 1050 m and cover an area of approximately 2 km². They also overly with an angular unconformity the older rocks. They are fissure-ridge, range-front and self-built channel type travertines deposited under the control of the active faulting. The long axis of actively-growing fissure-ridge travertines indicates a localized tension in the direction of NE-SW.



Figure 2.17. General view of the travertine deposits, near west of Yeşilova village (view to N).

The topmost facies of the modern graben infill are confined to the fault valleys, such as, the Muratdağı and Gediz fault valleys, and consist of recent alluvial deposits of flood plain sediments and alluvial fans (Figure 2.18). Alluvial fan deposits are made up of poorly lithified, unsorted and polygenetic pebble to boulder-sized clasts in their proximal parts, but coarse-grained sand, clay and silt in the distal parts. Older and younger

alluvial fan deposits display lateral to vertical gradations into finer-grained and organic material-rich axial plain deposits, composed of sand, silt and clay across the center of the modern graben. The total thickness of the modern graben infill is about 150 m (measured stratigraphical section and the borehole data by Lebküchner, 1965).

Gün (1975) defined macrofossils and ostracoda types (*Candona sp.*, *Candona cf.*, *neglecta SARS*, *Cyprididae*) around Gediz in recent deposits and a Pliocene age is assigned.



Figure 2.18. General view of the alluvial fan deposits around Gümüşlü village.

The ideal method for determining the onset of active faulting in a basin is to examine the stratigraphy of the footwall and hanging-wall blocks adjacent to the major border-faults to the basin, and establish the earlier time at which stratigraphic expansion occurred across the fault. In this chapter, the rock types and their deformation differences have been

determined clearly. It shows that these two packages in the graben have been deposited and deformed under the control of different mechanisms. The lithological differences by means of their depositional environment, deformation patterns are used for this discrimination.

CHAPTER 3

GEOCHEMICAL CHARACTERISTICS OF VOLCANICS IN PRE-MODERN GRABEN INFILL

3.1. Introduction

In this chapter, Ar/Ar geochronology and geochemical characteristics of the volcanic rocks are presented. 16 representative samples are analyzed. The aim of this chapter is to present the volcanic environment of volcanic rocks by means of their classification and evaluation on the basis of, major, trace and rare earth element (REE) variations.

3.2. Dating Results

Four samples from central volcano-sedimentary package of Arica formation are analyzed (^{39}Ar - ^{40}Ar dating) in Geosciences Rennes (University of Rennes, France). Their locations are shown in Appendix – A.

Based on the $^{40}\text{Ar}/^{39}\text{Ar}$ method, minerals (amphibole, biotite and sanidine) included in samples taken from lavas comprising central volcano-sedimentary package, were analyzed. Four samples (KG-1, KG-2, KG-3 and KG-4) were analyzed with a ^{39}Ar - ^{40}Ar laser probe (CO₂ Synrad®). Analyses were performed on single minerals like sanidine (KG-1), amphibole (KG-2 and KG-4) or biotite (KG-3) (Table 3.1).

Table 3.1. $^{40}\text{Ar}/^{39}\text{Ar}$ analytical data. $^{40}\text{Ar}_{\text{atm}}$ = atmospheric ^{40}Ar . $^{40}\text{Ar}^*$ = radiogenic ^{40}Ar . Ca = produced by Ca-neutron interferences. K = produced by K-neutron interferences. Age (Ma) = the date is calculated using the decay constants recommended by Steiger and Jäger (1977). The errors are at the 1σ level and do not include the error in the value of the J parameter. Correction factors for interfering isotopes produced by neutron irradiation in the McMaster reactor were $(^{39}\text{Ar}/^{37}\text{Ar})_{\text{Ca}} = 7.06 \times 10^{-4}$, $(^{36}\text{Ar}/^{37}\text{Ar})_{\text{Ca}} = 2.79 \times 10^{-4}$, $(^{40}\text{Ar}/^{39}\text{Ar})_{\text{K}} = 2.97 \times 10^{-2}$.

Step	$^{40}\text{Ar}_{\text{Atm.}}$ (%)	$^{39}\text{Ar}_{\text{K}}$ (%)	$^{37}\text{Ar}_{\text{Ca}}/^{39}\text{Ar}_{\text{K}}$	$^{40}\text{Ar}^*/^{39}\text{Ar}_{\text{K}}$			Age (Ma)
KG-1 Sanidine							
1	31.7	1.6	0.1200	1.83	18.50	±	1.25
2	4.1	7.66	0.0200	1.79	18.05	±	0.17
3	2.8	33.81	0.0160	1.81	18.32	±	0.07
4	6.0	6.1	0.0160	1.79	18.05	±	0.26
Fusion	2.0	50.84	0.0310	1.81	18.25	±	0.06
KG-2 Amphibole							
1	87.6	2.01	2.5890	2.74	27.57	±	10.58
2	69.7	2.96	4.5200	1.47	14.89	±	5.88
3	61.8	18.23	4.7340	1.82	18.41	±	0.79
4	26.2	31.82	4.7110	1.87	18.85	±	0.54
Fusion	17.6	44.98	5.0290	1.82	18.42	±	0.35
KG-3 Biotite							
1	100.2	0.23	2.2900	0.00	0.00	±	0.00
2	97.1	0.14	8.6700	0.91	9.22	±	54.79
3	44.4	0.34	3.6020	3.48	34.89	±	20.35
4	45.5	1.13	0.2410	2.47	24.85	±	5.98
5	9.1	2.03	0.3480	2.23	22.51	±	2.74
6	17.7	5.46	0.1210	1.90	19.18	±	1.34
7	18.0	7.95	0.3300	1.84	18.60	±	0.76
8	17.0	5.89	0.0000	1.86	18.75	±	0.73
Fusion	8.2	76.82	0.0270	1.82	18.37	±	0.07
KG-4 Amphibole							
1	94.5	2.6	0.0000	7.93	78.60	±	16.98
2	97.5	0.52	6.4530	2.86	28.73	±	85.97
3	93.0	4.95	1.7240	1.72	17.29	±	8.77
4	89.0	4.6	3.9380	2.14	21.50	±	9.38
Fusion	66.2	87.32	5.1990	1.82	18.36	±	0.58

Minerals were carefully handpicked under a binocular microscope from crushed rocks (0.3-2 mm fraction). The samples were wrapped in A1 foil to form packets (11 mm × 11 mm × 0.5 mm). These packets were stacked up to form a pile, within which packets of flux monitors were inserted every 8 to 10 samples. The stack, put in an irradiation can, was irradiated for 16.7 hours at the McMaster reactor (Hamilton, Canada) with a total flux of 2.1×10^{18} n.cm⁻². The irradiation standard was the sanidine TCR-2 (28.34 Ma according to Renne *et al.*, 1998). The sample arrangement allowed us to monitor the flux gradient with a precision of $\pm 0.2\%$.

The step-heating experimental procedure has been described in detail by Ruffet *et al.*, (1995 and 1997). Blanks are routinely performed each first or third run, and are subtracted from the subsequent sample gas fractions. Analyses are performed on a Map215[®] mass spectrometry.

To define a plateau age (Figure 3.1), a minimum of three consecutive steps are required, corresponding to a minimum of 70% of the total ³⁹Ar_K released, and the individual fraction ages should agree to within 1σ or 2σ with the integrated age of the plateau segment. All discussed ³⁹Ar-⁴⁰Ar results are displayed at the 1σ level.

Based on the ³⁹Ar-⁴⁰Ar age spectra, the ages of these samples are in the range of 18.3±0.1 and 18.6±0.3 Ma. This apparent synchronicity of plateau ages suggests that they characterize concomitant events. It is therefore concluded that their mean age, at 18.4 ± 0.1 Ma, is the best estimate of the emplacement age of these rocks. The age results of the volcano-sedimentary packages are consistent with the proposed, based on fossil content, ages (Gün, 1976).

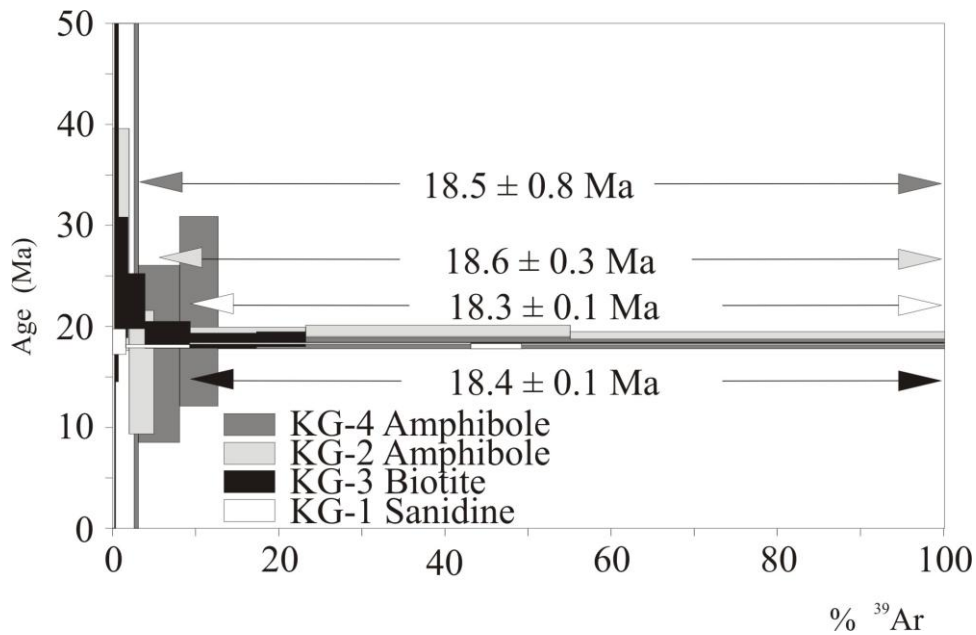


Figure 3.1. ^{39}Ar - ^{40}Ar age spectra of 4 samples of volcanic rocks from Erdoğmuş-Yenigediz graben. The age error bars for each temperature steps are at the 1σ level and do not include errors in the J-values. The errors in the J-values are included in the plateau age calculations.

3.3. Geochemistry

The volcanic rocks occur as lava flows, sill and dykes in the field. They are petrographically classified as basaltic andesites and andesites based on mineralogical content. They are black, dark grey and pinkish in color in hand specimen. Their textures vary from aphanitic to microphaneritic. Mineralogically, they consist of clinopyroxene, orthopyroxene, plagioclase, biotite, sanidine and quartz. Fe-Ti oxides and titanite are found as accessory phases. The groundmass is, in general, hypocrySTALLINE. In some samples, it only consists of glass only. They are characterized by porphyritic to glomeroporphyritic texture define by cluster of pyroxene and plagioclase (Figure 3.2). Vesicular textures are also common and the cavities are often filled with the secondary zeolites. Some of the rocks display various degrees of

alteration (e.g. kaolinite, replacing plagioclase). Evidence of disequilibrium crystallization such as sieve texture plagioclase, poikilitic inclusions, embayed felsic crystals, pyroxene rims on quartz crystals are also common.

For petrographical and geochemical purposes, a total of 12 rock samples (AK-1, DS-1, DS-2, YK-2, KK-1, KK-2, KK-3, SK-1, SK-2, SK-3, CK-1 and CK-2) have been collected from the volcanic rocks in different parts of the study area. Their geochemical analyses were performed at Acme Analytical Laboratories in Canada. Major oxide analyses were carried out by inductively coupled plasma-atomic emission spectrometry (ICP-AES). Trace and rare earth elements (REE) have also been determined by inductively coupled plasma-mass spectrometry (ICP-MS). Detection limits range from 0.01 to 0.1 wt % for major oxides, from 0.1 to 10 ppm for trace elements, and from 0.01 to 0.5 ppm for REE (Table 3.2).

In an attempt to determine geochemical affinity of the samples several diagrams have been employed. Winchester and Floyd (1977) diagram based on the immobile elements has been used to avoid the effects of mobility. On this diagram volcanic rocks plot in the basaltic andesite and andesite field. Whereas, a few samples fall into the trachy-andesite field (Figure 3.3).

The Chondrite normalized (McDonough and Sun 1995) REE patterns are strongly light REE (LREE) enriched relative to heavy ones (Figure 3.4a). They show slight negative Eu anomaly which may indicate plagioclase fractionation phase during crystallization. The flat HREE patterns in chondrite normalized REE diagram rule out garnet as residual phase in the mantle source region. Instead, observed patterns are consistent with the derivation from a shallower depth.

Table 3.2. Major and trace element contents of the volcanic rocks in the Erdoğmuş-Yenigediz graben.

Sample	SK-1	SK-2	SK-3	CK-1	KK-1	KK-2	KK-3	DS-1	DS-2	YK-1	YK-2	AK-1
Major Elements (wt %)												
SiO ₂	63,15	65,37	65,54	55,20	69,13	68,70	65,21	53,86	49,83	57,89	57,85	71,26
Al ₂ O ₃	16,24	15,39	15,30	16,34	15,57	15,54	16,49	17,12	15,91	16,84	17,08	14,54
Fe ₂ O ₃	5,58	4,95	5,36	5,08	2,90	3,47	3,41	7,36	7,64	6,31	6,48	2,42
MgO	1,44	1,11	0,97	2,78	0,46	0,48	0,57	2,61	6,55	2,41	3,55	0,47
CaO	4,62	3,98	4,55	5,43	2,40	2,22	1,89	8,18	8,93	6,36	6,38	1,73
Na ₂ O	3,35	3,08	3,21	2,70	3,92	3,88	3,22	3,09	2,71	3,24	3,12	3,87
K ₂ O	3,36	3,37	3,27	6,00	4,48	4,30	4,20	3,13	3,09	3,00	3,00	4,48
TiO ₂	0,75	0,69	0,72	1,76	0,38	0,38	0,36	0,89	1,13	0,78	0,81	0,32
P ₂ O ₅	0,24	0,14	0,21	0,85	0,12	0,11	0,15	0,26	0,60	0,20	0,19	0,08
MnO	0,06	0,04	0,07	0,05	0,04	0,05	0,02	0,08	0,12	0,14	0,12	0,05
LOI	0,9	1,6	0,5	3,3	0,3	0,6	4,1	3,0	3,0	2,3	1,1	0,5
Total	99,67	99,68	99,69	99,59	99,71	99,72	99,58	99,62	99,56	99,50	99,63	99,69
Trace Element (ppm)												
Ni	20	20	20	138	20	20	20	20	115	20	20	20
Sc	13	12	12	27	4	4	5	17	24	15	16	4
Ba	1440	1425	1391	1047	1555	1592	1511	1531	1121	2746	1347	1672
Co	12,5	8,7	10,3	25,9	3,3	3,7	2,9	16,4	27,8	16,6	17,7	3,2
Cs	3,2	6,2	5,0	7,9	8,9	11,0	7,0	13,8	2,5	7,6	5,4	7,9
Ga	17,7	17,8	17,3	20,0	16,7	15,7	15,8	17,8	16,6	17,3	17,7	15,5
Hf	5,5	4,9	4,9	16,6	5,3	5,3	4,6	5,1	7,1	4,8	4,3	5,6
Nb	12,4	11,8	11,4	30,8	16,6	16,0	15,4	10,6	19,5	11,4	11,7	16,9
Rb	98,7	114,2	104,1	193,5	150,6	147,0	109,3	100,9	99,6	95,4	96,3	147,1
Sr	614,6	577,6	609,2	650,9	417,2	393,3	1610,3	731,5	803,3	658,6	656,3	364,3

Table 3.2. continued.

Th	20,7	19,9	20,7	17,1	31,9	32,2	31,2	16,4	18,5	18,1	17,1	33,5
U	5,4	5,2	5,3	6,0	6,0	6,4	6,9	4,8	5,4	5,3	5,1	7,8
V	126	121	106	240	42	40	48	178	187	151	161	30
Zr	171,1	161,8	161,3	568,6	191,5	174,1	163,7	166,6	259,0	174,0	174,9	190,5
Y	25,7	24,2	23,6	23,6	19,3	18,5	8,3	27,1	28,6	27,1	28,0	28,7
La	43,8	40,9	41,7	58,0	50,2	44,8	49,0	40,7	57,4	39,7	40,0	59,4
Ce	87,2	77,6	81,8	120,2	89,6	81,5	86,9	79,3	119,1	76,5	79,1	109,6
Pr	9,18	8,29	8,64	14,37	8,69	7,82	8,52	8,7	13,29	8,54	8,56	11,68
Nd	35,5	30,6	30,8	55,2	29,2	27,0	27,9	34,2	51,3	32,7	33,5	4,1
Sm	6,08	5,65	6,10	9,01	4,50	4,22	3,87	6,31	8,91	6,08	5,87	7,07
Eu	1,43	1,30	1,35	2,16	0,97	0,91	0,86	1,53	2,17	1,36	1,37	1,36
Gd	5,02	4,61	4,65	6,32	3,57	3,22	2,02	5,24	6,81	4,96	5,12	5,52
Tb	0,82	0,75	0,79	0,94	0,59	0,54	0,33	0,83	1,05	0,83	0,84	0,93
Dy	4,38	4,14	4,19	4,59	3,24	3,08	1,61	4,63	5,23	4,56	4,79	5,05
Ho	0,91	0,84	0,82	0,86	0,66	0,63	0,33	0,93	1,00	0,96	0,99	0,97
Er	2,60	2,42	2,30	2,23	1,85	1,88	0,89	2,77	2,65	2,73	2,76	2,92
Tm	0,40	0,40	0,36	0,32	0,32	0,31	0,16	0,42	0,42	0,43	0,44	0,49
Yb	2,54	2,63	2,27	2,02	2,07	2,00	1,21	2,66	2,59	2,59	2,79	3,07
Lu	0,38	0,38	0,36	0,29	0,33	0,31	0,19	0,41	0,37	0,40	0,40	0,46
Mo	0,4	0,6	0,2	1,1	0,5	0,9	1,3	1,0	0,7	1,6	0,2	0,5
Cu	10,5	10,6	8,1	42,9	3,9	3,2	3,0	9,5	44,2	9,5	17,4	1,9
Pb	6,7	2,2	3,7	2,8	5,3	5,1	15,6	6,0	3,4	5,4	3,1	16,9

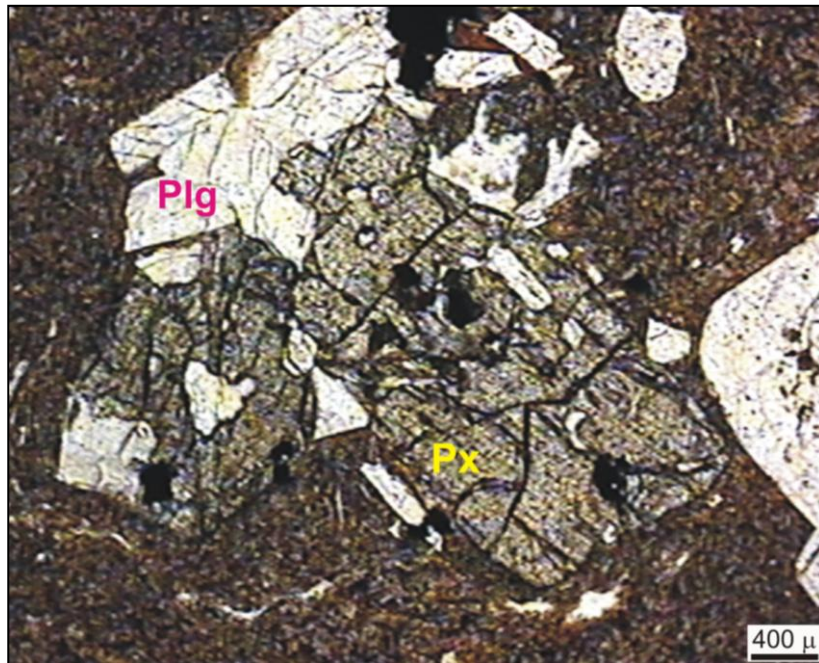


Figure 3.2. Thin section view from the volcanic rocks containing plagioclase (Plg) and pyroxene (Px).

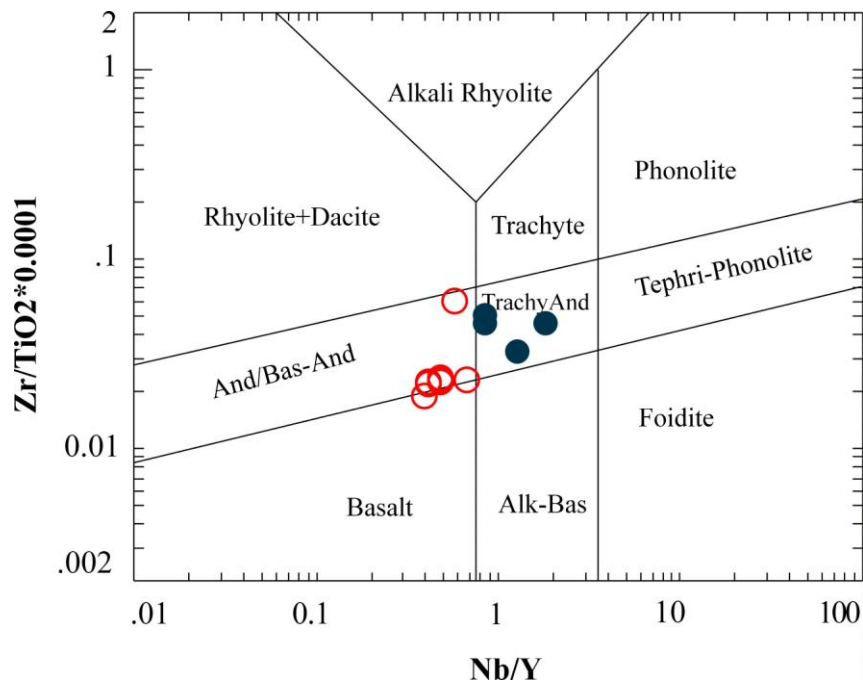


Figure 3.3. Classification of the 12 samples in Winchester and Floyd (1977) diagram.

The primitive mantle-normalized (McDonough and Sun 1995) trace-element patterns are consistent with significant enrichments in large ion lithophile elements (LILE; Rb, Ba, Th, U) and LREE (Figure 3.4b). They have negative Nb and Ta anomaly. Most of the samples display negative Pb spike but a few do not. Nb and Ta depletions become more pronounced in basaltic and andesitic samples. One of alkali samples shows negative Ba anomaly, which can be attributed to the post magmatic alteration. On the whole, all samples display the same pattern. This can be explained by derivation from the same or similar source region.

The Zr–Zr/Y discrimination diagram (Pearce and Norry, 1979; Figure 3.5), the volcanic basaltic andesites-andesites fall into within-plate field while Trachy-andesites seems to lie at the edge of within plate field. This would/may suggest an extensional setting but a special case must be given to significance of geochemistry.

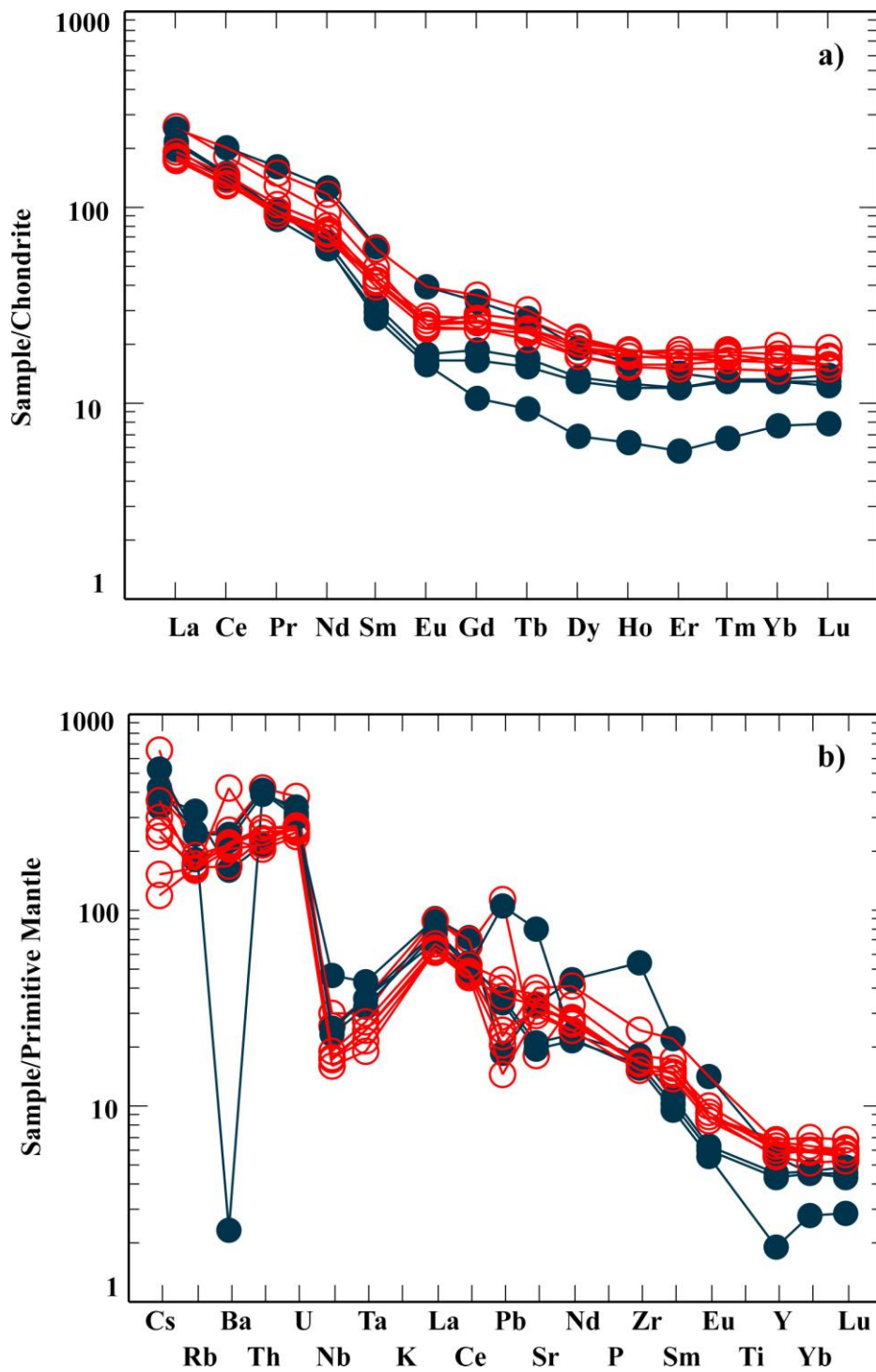


Figure 3.4.a) The chondrite normalized (McDonough and Sun 1995) REE patterns of the studied rocks, b) The primitive mantle-normalized (McDonough and Sun 1995) trace-element patterns of the volcanic rocks.

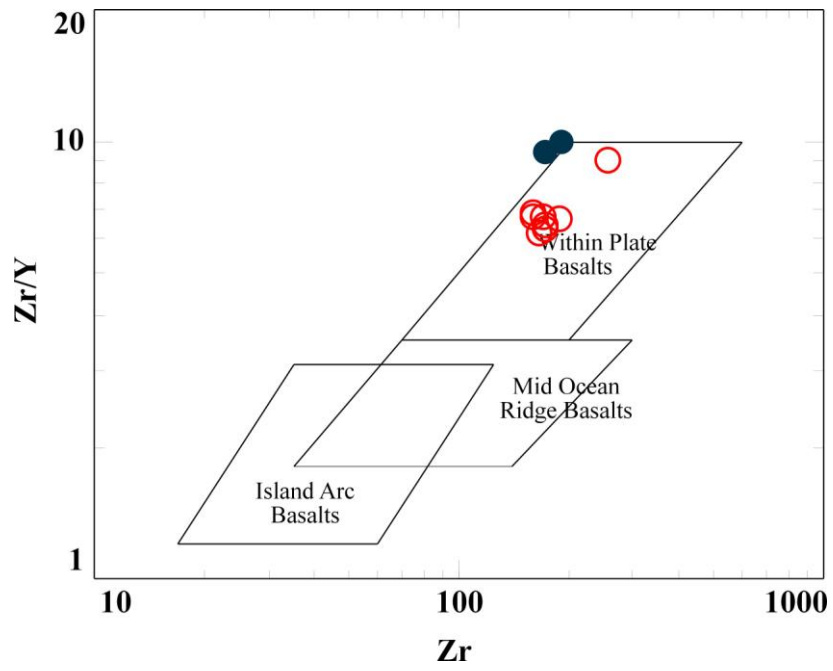


Figure 3.5. Tectonic discrimination diagram, Zr vs Zr/Y (Pearce and Norry, 1979).

CHAPTER 4

STRUCTURAL GEOLOGY

4.1. Introduction

This chapter focuses on the detailed description and analysis of the geological structures. The main targets are;

- (i) to describe the structures formed during different phases and
- (ii) finally to discuss their kinematic and tectonic significance.

The main structures are beds, unconformities, folds and faults. Based on tectonic periods during which the structures formed, they can be subdivided into two major categories: (1) Palaeotectonic structures, (2) Neotectonic structures.

The Erdoğmuş-Yenigediz graben was an ill-defined structure before this study in the Southwestern Anatolian Extensional Province (SWAEP) (Figure 1.2). This region is a representative area of an extensional deformation within the Alpine-Himalayan belt. Because of the characteristics of this area, rate and mechanism of deformation, initiation age of extensional deformation and evolutionary history of grabens as well as the significance of seismic activity in SWAEP were studied by many scientists during the last 20 years (Jackson and McKenzie, 1984; Eyidoğan and Jackson, 1985; Ambrassey, 1988; Taymaz *et al.*, 1991; Seyitoğlu and Scott 1991; Taymaz, 1993; Le

Pichon *et al.*, 1995; Reilinger *et al.*, 1997; Ambrasseys and Jackson, 1998; Altunel, 1999; Koçyiğit *et al.*, 1999; Koçyiğit *et al.*, 2000; Ring *et al.*, 1999; McClusky *et al.*, 2000; Yılmaz *et al.*, 2000; Gürer *et al.*, 2001; Bozkurt, 2001; Bozkurt and Sözbilir 2004; Kaya *et al.*, 2004; Beccaletto and Steiner 2005; Bozkurt and Rojay 2005; Koçyiğit 2005; Emre and Sözbilir 2007 and the references therein). All these studies agree that western Anatolia is currently experiencing an extension. Because of the high extension rate, 30-40 mm/yr (Oral *et al.*, 1995; Westaway, 1994; Le Pichon *et al.*, 1995), numerous well-developed horst and graben structures developed in western Anatolia. One of them is newly defined here, the Erdoğan-Yenigediz graben. There are a number of normal faults and fault zones that manipulate the formation of Erdoğan-Yenigediz graben. Consequently, to shed light on the graben formation and geometry, these parameters should be examined in the aspect of kinematics, geometry and the characteristics of the faults. Additionally, Evolutionary history of the graben can only be manifested by the changes in stress field and structural style. These kinds of changes can create some structural complexities. The complexities of the geology and structures needs to be explained by a detailed geological investigations including structural and stratigraphical framework.

In this frame, the chapter centers to the geometric properties of the structures (beds, folding, faults and unconformities), their relationships and different stress field configurations (structural analysis). Later on, the data were analysed by using the software named Data Base for Tectonic Orientation (Angelier, 1989). Furthermore, one of the main steps for the structural analysis is to detect linear features before going to detailed field work because of the imagination of general picture here.

Lineament analysis of aerial photos, fault pattern geometry, distribution and variation of the lithologies within the pre-modern and modern graben infill, geomorphologic characteristics, and surface distribution of rock units are controlled by these faults.

4.2. Lineament Analysis from Aerial Photos

Lineaments on the aerial photos can be obtained from two main sources; (1) tectonic structures (faults, joints and/or boundaries), and (2) man-made structures, such as, roads, crops field or any kind of variations in used areas. First type lineaments are the main concern of the structural pattern in geology. Rock units and any structural features to predict the stress-strain relation and sub-surface conditions, special surface features and occurrence relationships of rocks are very significant in geology. Scientists dealing with the structural geology have to visualize the three dimensional view to get the mechanism and formation of Earth's deformation. From this point of view, three dimensional view of the Earth's surface and the relations of structures on it have been more significant for them. This is the reason of that why the aerial photos are significant for structural geology to get panoramic continuity.

Any linear feature in the landscape possessing an abnormal degree of regularity is immediately viewed by the interpreter with suspicion. Such lineaments, whether straight or gently curving, are generally believed to be the surface expression of some structural feature in the bedrock. Experience and careful judgment are required, in many cases, to distinguish a diagnostic linear structure from random river stretches, hill, because, man-made and natural structures must be differentiated from each other clearly.

There is a clear difference between the terms lineament and lineation. "Lineation" refers to geological features which are true lines in space, such as elongation of pebbles, the trace of bedding on cleavage surface, or axially orientated crystals. Bedrock linear, on the other hand, represents the surface trace of such geological planar features as faults, contacts (boundaries), joints and bedding planes. Lineament may represent one of several structural features such as fault, bed, joint, or narrow dikes. The main trends and characters of the linear patterns must be shown as well as their relative density. Because of the difference, lineaments are only thing that is deal with in aerial photograph. For example, strike is one of the fundamental concepts of structural geology, but the aerial photo interpreter may easily loose sight of its precise meaning. It is frequently confused with trace or trend. Trace is the intersection of a plane and another surface of reference the Earth's surface. In general, it is not equivalent to strike. Only where the topography is horizontal, all traces are parallel to strike. Therefore, fault interpretation is based on one or more of the following features, in order of increasing reliability; (1) persistent linear usually clear defined, (2) linear scarp usually erosional, but may be on actual fault scarp, (3) persistent linear feature, near and parallel to a proven fault, (4) offsetting of pattern of linear with or without a change in trend, (5) major regional change in lithologies and/or structure, (6) offsetting of bedding linear, outcrop ridges, formations.

In some cases suggestive or indicative lines of faults may be expressed as alignments of vegetation, straight segments of lakes, ponds, and springs; conspicuous changes in photographic tone or drainage and erosional texture on opposite sides of a linear feature resulting from vegetation which may appear dark; alignment of topography, including saddles, knobs, or straight scarps (Lueder, 1959; Lattman, 1965). To identify these features on the aerial photos, there are some basic

elements are used such as tone, texture, pattern, size association and shadow.

Although the usage of aerial photos has some advantages in relation to the aforementioned factors, it has been noticed that they may also cause some problems due to the inevitable distortion of photo or image which is the main problem in the stereoscopic study and defines the geological structures (Lueder, 1959; Lattman, 1965). Although they are out of scope, their names are listed for profitable in this research: (a) aircraft elevation differences, (b) time of year, sun affecting the gray tone interpretation, (c) flight path etc.

Furthermore, geological photo interpretation is not in itself an answer to all geological problems. As, there are some limitations. All data from aerial applications have to be confirmed in the field. Extraction of lineaments by using the 109 aerial photographs has been applied manually. For this extraction process, the morphological signatures such as alluvial fans, displaced linear valleys, stream courses and definite rock units have been used to produce the final lineament map (Figure 4.1).

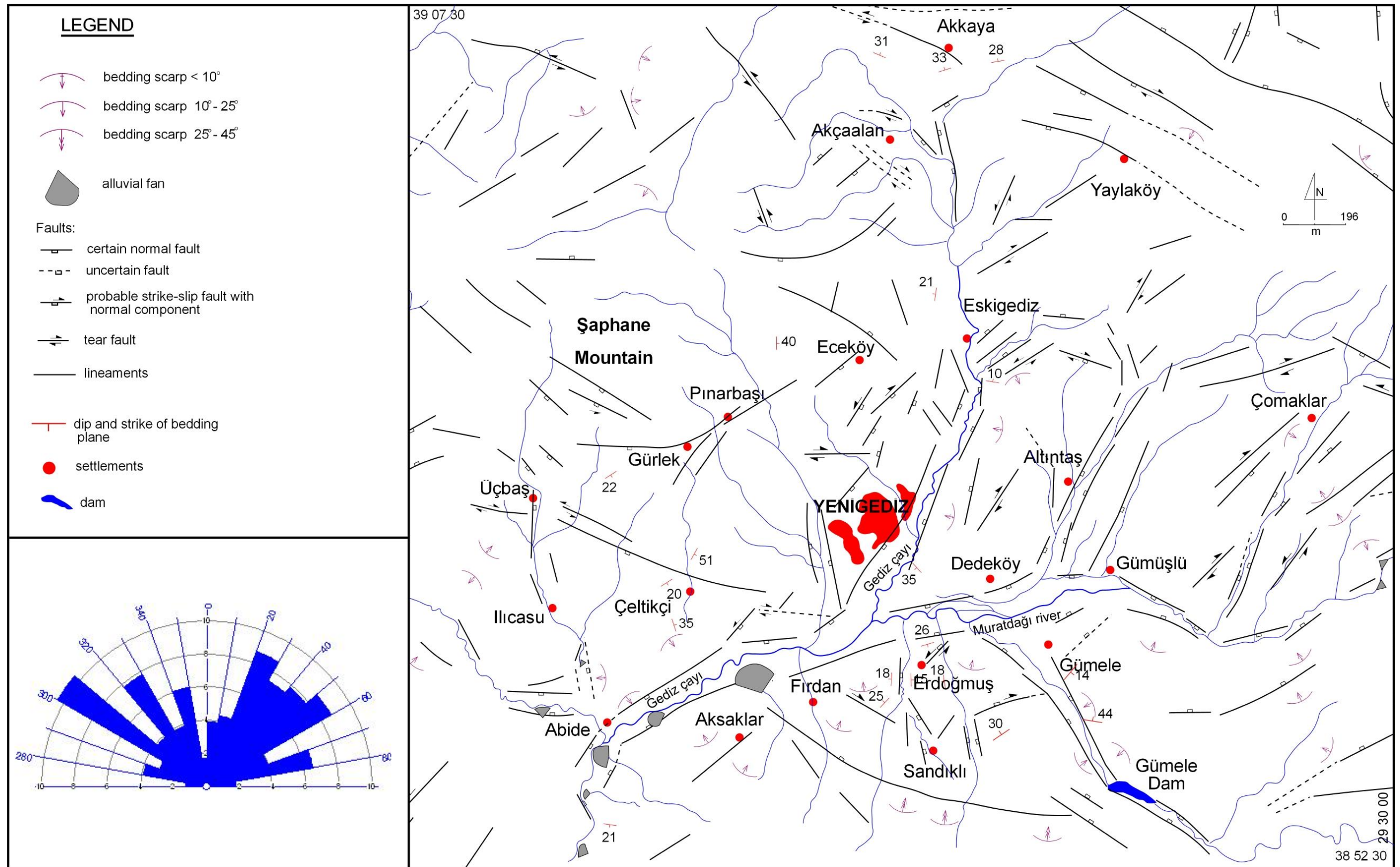


Figure 4.1. Lineaments extracted from 109 stereographic aerial photographs by using manual approach and corresponding trend weighted rose diagram. According to the diagram, there are two dominant directions NE and NW.

4.3. Geological Structures

The Erdoğmuş-Yenigediz graben is a 16-km-wide, 40-km-long, ENE-trending superimposed basin (Koçyiğit, 1996). It branches into two wedges out in east-southeastward. The major bounding structures are the Şaphane horst and its margin-boundary fault (Şaphane fault zone) in the west-northwest, Arpayaylası horst and its margin-boundary fault zone (Yeşilova fault zone) in the north-northeast, the Muratdağı horst and margin-boundary fault zone (Muratdağı fault zone) in the east-southeast and the Deveboynu horst and related margin-boundary fault zone (Simav fault zone) (Figure 4.2).

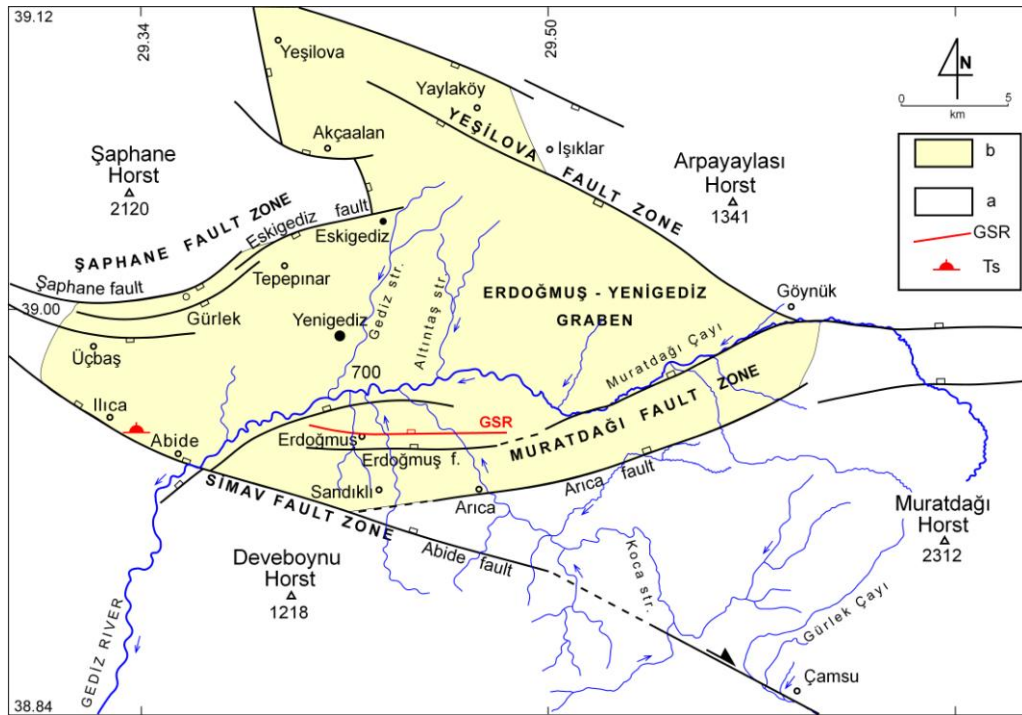


Figure 4.2. Simplified map showing the outline of the Erdoğmuş-Yenigediz graben and major margin-boundary fault zones. a. pre-Miocene rocks, b. Miocene-Quaternary graben infill, GSR. ground surface rupture of the 1970.03.28 $M_w=7.2$ Gediz earthquake, and Ts. thermal spring.

The maximum reliefs among these horsts and the axial floor of the modern graben are 1420 m, 641 m, 1612 m and 518 m, respectively. Morphotectonically, the graben is being drained by a major drainage system, namely the Gediz River and its branches (Figure 4.2).

Two major groups of structures occur along the margins and within the graben. These are the faults and folds. Based on the age, size and nature, the faults are divided into three categories: (1) the mapable normal faults, (2) mesoscopic or outcrop-scale growth faults, and (3) fault arrays or slickensides of dissimilar nature. Mapable faults occur in different trends such as the E-W, NW and NE. They mostly bound the margins of the graben, some cut across the graben infill (Figure 4.2). Major mapable fault zones and segments, which took a key role in the evolutionary history of the Yenigediz-Erdoğmuş graben include the Şaphane fault zone, the Eskigediz fault, the Yeşilova fault zone, the Simav fault zone, the Muratdağı fault zone. In addition, based on the age or tectonic periods during which they formed, above-mentioned structures can also be subdivided into three categories: (a) the first phase of extensional structures, (b) first phase of contractional structures, and (c) the second phase of extensional structures. The earlier two of them characterize last two phases of palaeotectonic period, while the latter represents the neotectonic period. The most of these structures and the related phases of deformation are described and analyzed below.

As stated before, the Erdoğmuş-Yenigediz graben has a number of active normal faults that all are directly governing the formation of this graben in the palaeotectonic and neotectonic period. They are firstly named in this study in various scales from meters to kilometers.

In lineament extraction step, two groups of lineaments were delineated: (i) some of the faults are inherited from the previous style of deformation which is proven by the overprinted motion along the fault and (ii) some others are newly forming faults that have only extensional motion. Not only the fault pattern of any graben but also its deformation pattern and stratigraphic outline have a significant role to investigate the different styles of deformation. This may indicate the existence of multiphase deformation history (different tectonic styles) in the study area. As explained in Chapter 2, there are three different tectonic regimes, two of which are palaeotectonic (1st phase of extensional and the 1st phase of intervening contraction-based) and one of them is neotectonic regime (2nd phase of extension) have influenced the pre-modern graben infill. By using these findings, two main regimes come out with their special structures; palaeotectonic and neotectonic regimes.

4.3.1. Latest Palaeotectonic Structures

Based on the different deformation patterns recorded in sedimentary infill, palaeotectonic structures can be subdivided into two categories: (1) extensional structures formed in the latest palaeotectonic units of graben infill, and (2) contractional structures deforming the latest palaeotectonic units of graben infill. Because of the overprinting relationship between tectonic phases, it is not possible to clearly identify the first phase of extensional structures from the deformation patterns of deposits. On the other hand, contractional structures can be still observed in the pre-modern graben infill.

4.3.1.1. Contractional Structures (1st Phase of Contraction)

Kinematic analysis of the structures recorded within the pre-modern graben infill of the Erdoğmuş-Yenigediz graben (Appendix – A) evidently indicates that they have experienced a contractional phase.

All analyses results are given in each fault parts separately. This phase so called the first phase of contraction represents the palaeotectonic period. They started to occur towards the end of deposition of pre-modern graben infill and deformed it in turn by folding, reverse faulting and strike-slip faulting. Moreover, the deformation was the main cause of regressive sequence for the uppermost package of the pre-modern graben infill.

Generally, the footprints of the contractional phase are determined into four groups: (1) beds, (2) unconformity, (3) folds and (4) reverse faults (mesoscobic).

4.3.1.1.1. Beds

The Arica formation is exposed along the road cuts and sites for construction of water channel and pond) in the study area. At these places, a number of well-developed beds with thicknesses ranging from a few ten millimetres to tens of centimetres and bedding planes can be observed (Figure 4.3).

The attitudes of bedding planes are documented and mapped at 1/25000 scale (Appendix – A). The dip amounts show a very broad range from 10° to 85° (Figures 4.4.a and b). The histogram of dip amounts at the measured places is clearly indicating the broad range of dips as well (Figure 4.5).



Figure 4.3. Well-developed bedding planes of marl-limestone alternation in the Arica formation.



Figure 4.4. a) and b) Views from variable thick bedding planes in the Arica formation.

The differences between dip amounts of the beds in the Arıca formation can not be explained without contractional motion. In some extensional areas, it is possible to observe tilted and folded beds but they are located in the very limited part of study area. Oppositely, tilted and folded beds can be observed in different parts of the western Turkey such as Şuhut graben (Afyon) (Koçyiğit and Devenci, 2007), Orhaneli (Bursa) and Simav (Kütahya).

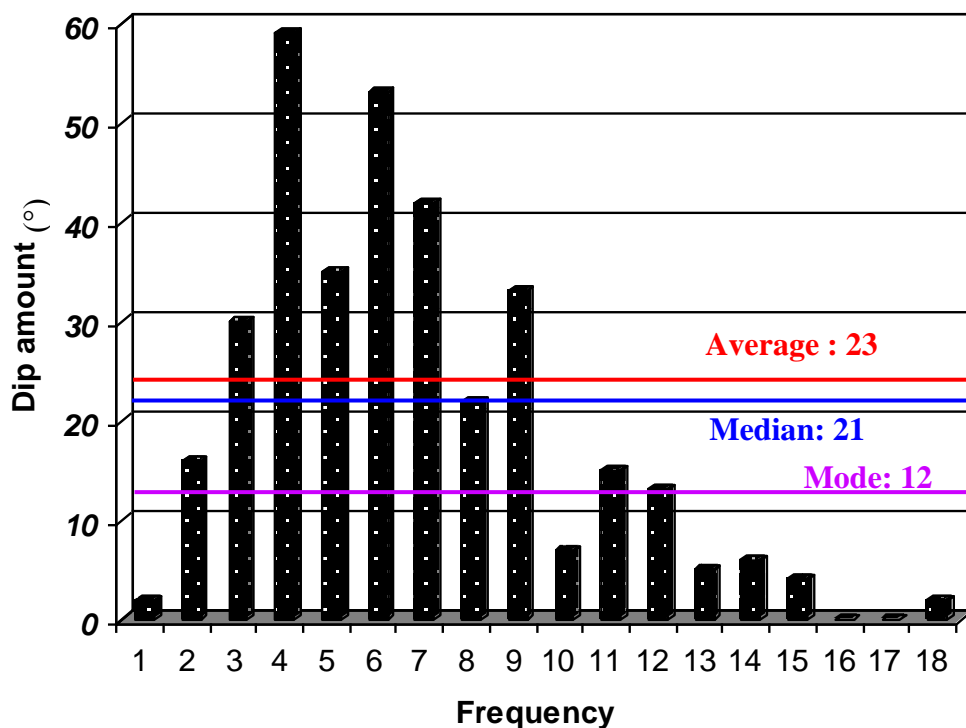


Figure 4.5. Histogram showing predominant dip amounts of bedding planes in the Arıca formation.

4.3.1.1.2. Unconformities

The Neotectonic units (Erdoğmuş formation) overly on the deformed Palaeotectonic pre-modern graben infill (Arıca formation) with an angular unconformity (Figure 4.6). The angular differences between

nearly flat-lying unconformity surface and the underlying dipping Arıca formation range from 10° to 50°.

Second one is the unconformity between pre-Miocene rocks and Arıca formation.



Figure 4.6. Angular unconformity (AU) between the nearly flat-lying Plio-Quaternary Erdoğmuş formation (TQe) and the tilted lacustrine marl-shale-limestone alternation of the Miocene-Lower Pliocene Arıca formation (Ta).

4.3.1.1.3. Folds

The most part of the graben consists of volcano-sedimentary sequence (Upper-lower Miocene – Lower Pliocene Arıca formation) and it displays

well-developed bedding planes. According to field mapping and strike-dip measurements of the beds, a series of syncline and anticline with the NW- and a limited number of NE-trending axes are interpreted; they usually occur in axes close to active faults (Figure 4.7). Their dips vary between 10° and 57°. By using the strike-dip measurement, poles to the bedding planes on the Schmidt lower hemisphere net indicate that the pre-modern graben infill was deformed (first phase of contraction) into a series of anticlines and synclines by a compressive stress in which the principal stress was operating in NE-SW direction during the deposition of sedimentation of pre-modern graben infill (Figure 4.8).

The axes of anticline and syncline display a parallel-subparallel pattern with a NW and NNE direction. The folds become tightly packed resulting in closely spaced fold axes in all parts of the Arica formation. They are also well-observed on the geological map of the area (Figure 4.7, Appendix – A).

Based on the trends of fold axes, it is not possible to define an exact stress direction. This can be results of the local rotation, local variations or multidirectional contraction directions. But if the dominant fold axes have been taken for evaluation of contraction direction, it is reasonable to conclude that main contraction direction is ~ NE – SW.

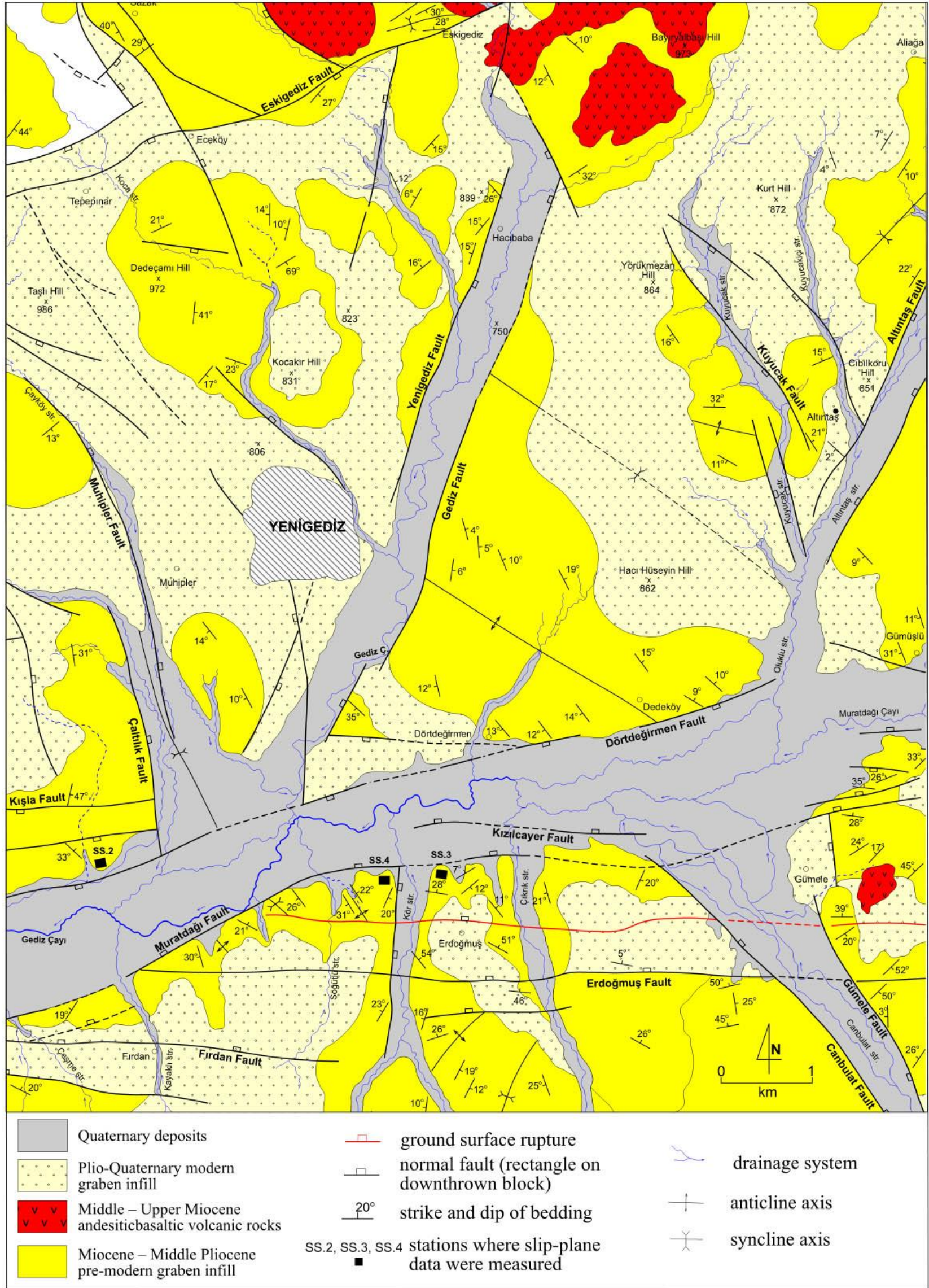


Figure 4.7. Geological map of the type area included in the Erdoğan-Yenigediz graben.

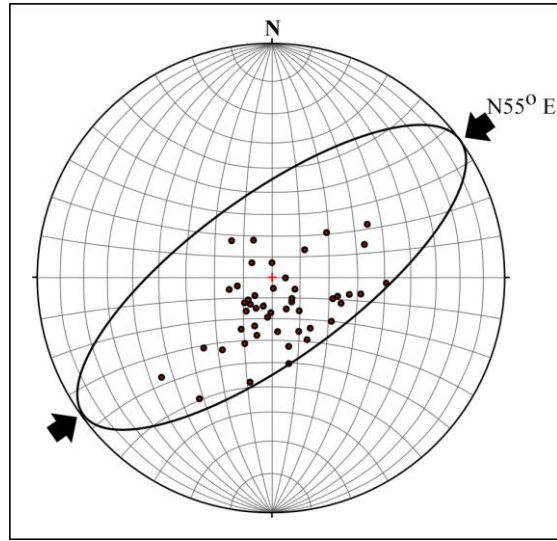


Figure 4.8. Poles to bedding on the Schmidt's lower hemisphere net. Large arrows show the shortening direction of the contractional phase that deformed the Arica formation at the end of Middle Pliocene (the last phase of paleotectonic period).

In the recent literature following to Koçyiğit *et al.*, (1999), many reliable evidences have been presented for the existence of a short term contractional phase during Miocene – Early Pliocene in the western Turkey (Koçyiğit *et al.*, 1999; Ring *et al.*, 1999; Bozkurt, 2000; Koçyiğit *et al.*, 2000; Koçyiğit, 2005; Yılmaz *et al.*, 2000; Gürer *et al.*, 2001; Koçyiğit and Özacar, 2003; Kaya *et al.*, 2004; Bozkurt and Sözbilir, 2004; Bozkurt and Rojay, 2005; Beccalotto and Steiner, 2005; Bozkurt and Sözbilir, 2006; Emre and Sözbilir, 2007; Baccaletto and Steiner, 2005; Kaya *et al.*, 2004, 2007; Rojay *et al.*, 2005; Westaway *et al.*, 2005; Koçyiğit and Deveci 2007). For this study, not only the folded beds but also the reverse faulting in the limited part of the study area may indicate the existence of the contractional phase.

4.3.1.1.4. Reverse Faulting

In the very limited part of the Arica formation, numerous outcrop-scaled reverse faults were observed (Figure 4.9). In the areas, overprinting relationship is used to construct relative age order between motions. On the other hand, the strike-slip faulting-induced slickensides, those are also the results of the contractional motion have been recorded within the Arica formation and have overprinted on the first phase of extensional slickenside (Figure 4.10.a). Stereographic plot of these slip-plane data (Figure 4.10.b and c) on the Schmidt lower hemisphere net indicates that the pre-modern graben infill has also been deformed by the strike-slip faulting, in which the principal stress axis was operating in ENE-WSW direction at late sedimentation of the Arica formation.

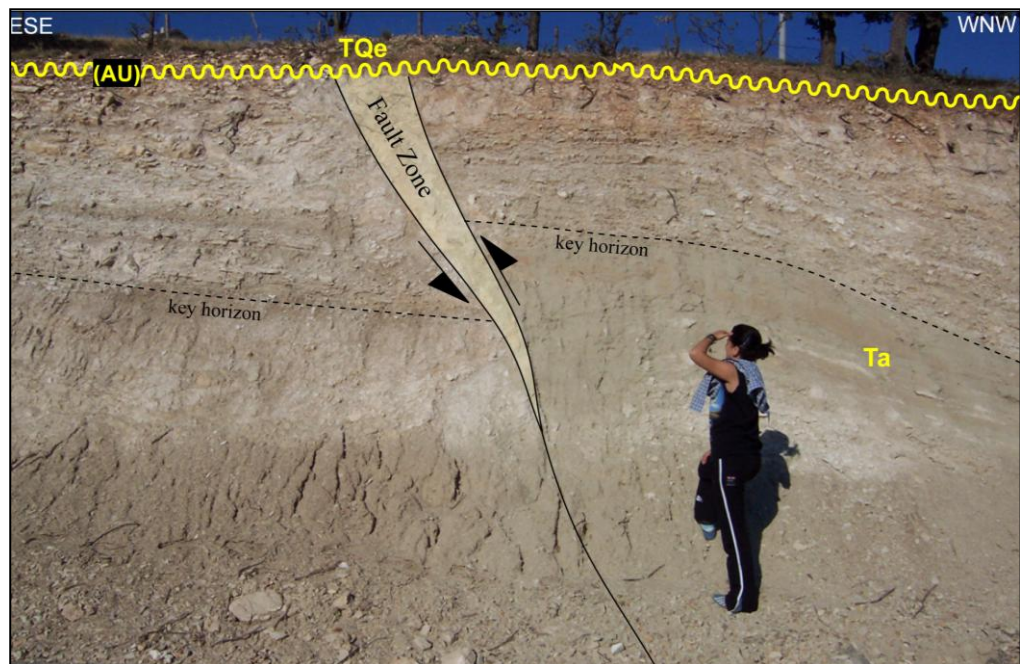


Figure 4.9. Close-up view of the angular unconformity (AU) between the Plio-Quaternary Erdoğmuş formation (TQe) and the reverse faulted Miocene-Lower Pliocene Arica formation (Ta).

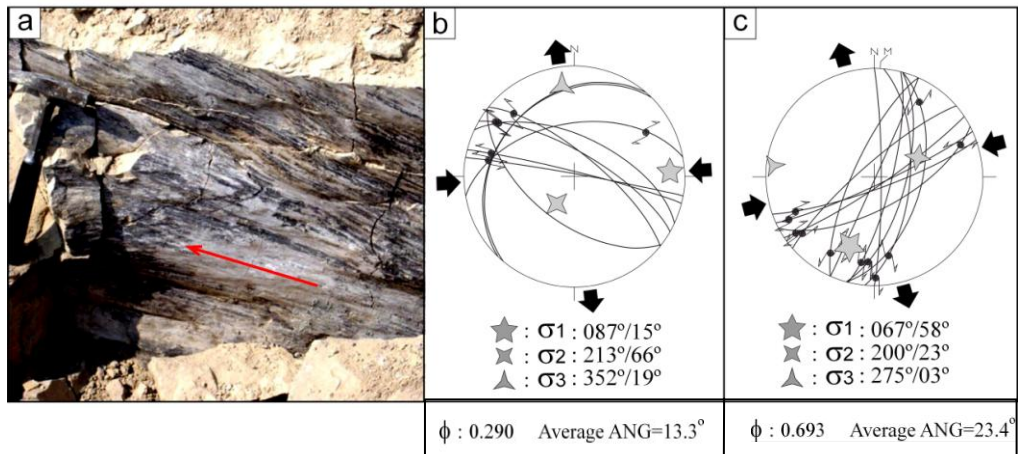


Figure 4.10. a) Field photograph of the strike-slip faulting-induced slickenside recorded in pre-modern graben infill (see SS3 and SS4 in Figure 4.7 for location). b) and c) stereographic plots of slip-plane data measured at stations SS3 and SS4 on the Schmidt's lower hemisphere net. Large converging arrows show localized shortening direction of the contractional phase that deformed the pre-modern graben infill at the end of Middle Pliocene (the last phase of paleotectonic period).

4.3.2. Neotectonic Structures

The analyses of geological structures have enlightened the tectonic history. In this section, characteristics of partly deformed younger infill of the Erdoğmuş-Yenigediz graben including Plio-Quaternary Erdoğmuş formation and Holocene sediments have been examined. Detailed descriptions of all deposits are given in Chapter 2. In this part, source of the deformation, faults, are presented. They are the margin-boundary mapable normal faults, such as the Şaphane, Simav, Muratdağı and Yeşilova fault zones inherited from the early evolutionary stage of pre-modern graben. Most were also reactivated as the oblique-slip normal faults during the Plio-Quaternary neotectonic period. However, the localized extension directions along these fault zones show a range from the NW-SE direction (Figures 4.11a, b and c) in the paleotectonic period. This is obtained from the syn-depositional features. On the other

hand the NE-SW direction (Figures 4.12a and b) are obtained during the neotectonic period.

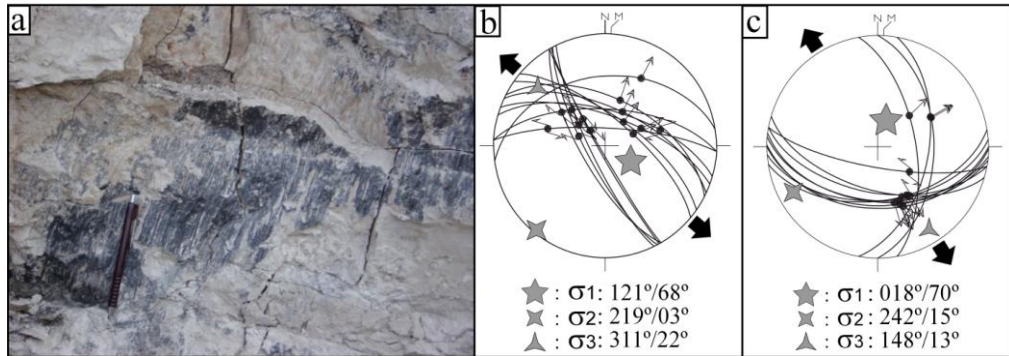


Figure 4.11. a) Field photograph showing close-up view of extensional slip-plane data recorded within the Arica formation. b) and c) Stereographic plot of slip-plane data on the Schmidt's lower hemisphere net. Slip-plane data were measured at stations SS.2 (b) and SS.3 (c) (in Figure 4.7 for location of slip-data) within the pre-modern graben infill. Large arrows show localized extension direction during the sedimentation of pre-modern graben infill.

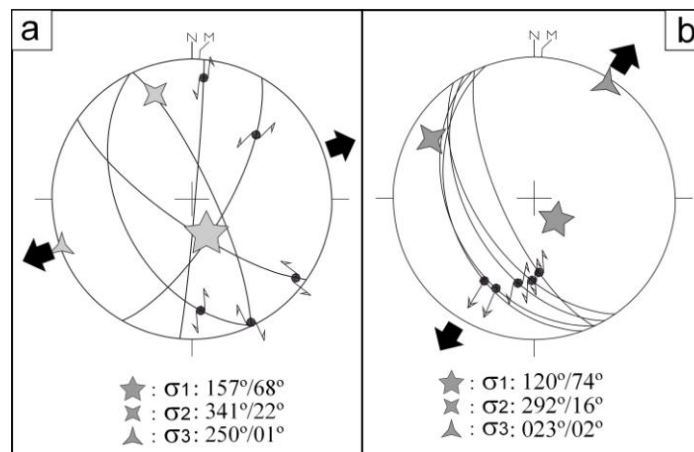


Figure 4.12. a) Stereographic plot of slip-plane data on the Schmidt's lower hemisphere net. Large arrows indicate neotectonic extension along the Abide fault, b) Stereographic plot of slip-plane data on the Schmidt's lower hemisphere net. Large arrows indicate localized extension along the Erdoğan fault during neotectonic period (see SS.4 in Figure 4.7 for location of slip-plane data).

Recent extension direction is proved by a series of evidence: (1) the normal type of growth faults in the Plio-Quaternary fluvial conglomerates (Figure 2.18), (2) the widespread occurrence of overprinted sets of slip-plane data in both the Miocene-Middle Pliocene pre-modern graben and the Plio-Quaternary modern graben infill and their kinematic analyses (Figure 4.13.a, b and c), and (3) focal mechanism solution diagram (Figure 4.19.d) of the 1970.03.28, $M_w=7.2$ Gediz earthquake (Eyidođan and Jackson 1985).

Consequently, the localized extension direction obtained from the stereographic plots of slip-plane data on the Schmidt's lower hemisphere net fits well with the very recent extension direction obtained from the focal mechanism solution of the 1970.03.28, $M_w=7.2$ Gediz earthquake is NE-SW (Figure 4.13).

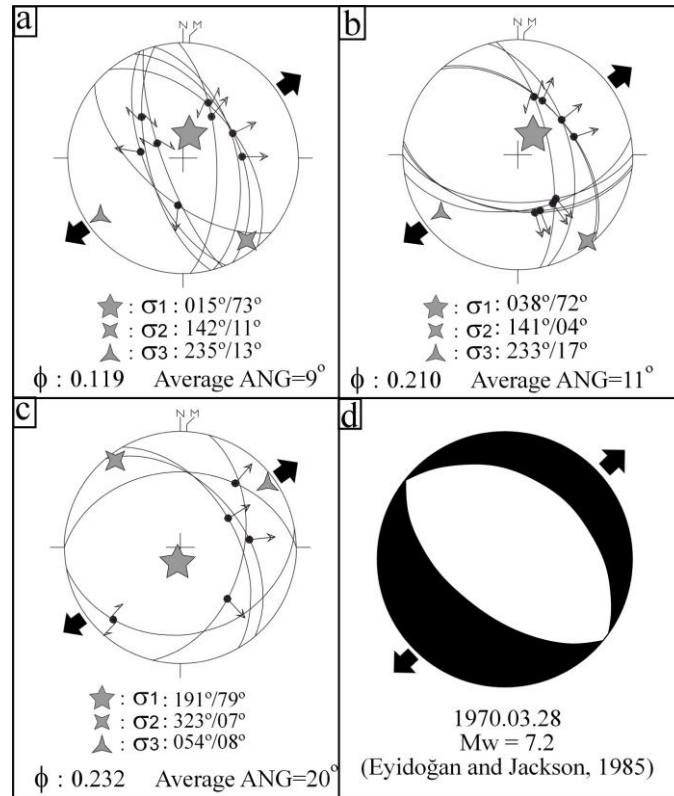


Figure 4.13. a), b) and c) Stereographic plots of slip-plane data measured at stations 3 and 4 (see SS.3 and SS.4 in Figure 4.7 for location) on the Schmidt's lower hemisphere net. Large arrows show localized extension direction in Plio-Quaternary neotectonic period (2nd phase of extension); d) focal mechanism solution diagram, in which large arrows show the recent extension direction, of the 1970.03.28, Mw=7.2 Gediz Earthquake (Eyidoğan and Jackson, 1985).

The neotectonic structures consists of three main parts: (1) Plio-Quaternary deposits; beds, (2) unconformity and (3) margin-boundary faults.

4.3.2.1. Beds

Erdoğmuş formation is the youngest unit in the graben. It is a nearly flat-lying (undeformed) and weakly lithified to loose sedimentary sequence. The formation consists of three different litho-facies: (a)

terrace deposits (Figure 4.14), (b) travertine (Figure 4.15), and (c) recent axial plain deposits (Figure 2.1).



Figure 4.14. Close-up view of a poorly sorted and weakly lithified terrace deposits.



Figure 4.15. Travertine deposits in Yeşilova village (view to NW). Yellow arrows indicate the margin-boundary faults (Yeşilova Fault Zone).

4.3.2.2. Faults

Based on the aerial photograph interpretations, rose diagrams and field mapping, three major trends are defined: (1) ENE-WSW-trending faults, (2) NW-SE-trending faults and (3) NE-SW-trending faults. They are oblique-slip normal faults with minor amount of dextral or sinistral strike-slip components. The Erdoğmuş-Yenigediz graben is bounded by ENE-WSW-trending Muratdağı Fault Zone in the SE, WNW-ESE-trending Simav Fault Zone in the SW, ENE-WSW-trending Şaphane Fault Zone in the NW, and NW-SE-trending Yeşilova Fault Zone in the NE. These fault zones are composed of numerous fault segments. In addition to them, single fault segments like Muhipler, Eskimuhipler, Çaltılık, Üçbaş, Ağıl and Kışla faults are also mapped. Additionally, all fault segments and fault zones are named in this study.

4.3.2.2.1. MURATDAĞI FAULT ZONE

Muratdağı fault zone is an about 2-5 km wide, 32 km long and ENE-trending active normal fault (Appendix – A and Figure 4.16). It is located between Soğanlı town in the east which is outside of the study area, and Abide town in the west (Figure 4.2). Part of the fault zone in the study area controls south-southeastern margin of the Erdoğmuş-Yenigediz graben. It consists of a number of closely- to intermediately spaced (0.1-4 km), diverse-sized (2-18 km) predominant E-W, NW-, NE- and NNE-trending fault segments (Appendix – A). They mostly dip at 50°-70° and display a northerly facing step-like landscape. Some of fault segments cut across both the older basement rocks (various metamorphic rocks and mostly serpentized peridotites) and the younger graben infill (Miocene-Quaternary fluvio-lacustrine sedimentary sequence and volcanic rocks). Fault valleys (e.g., Muratdağı Çayı, Gediz stream and Altıntaş stream), sheared and crushed stripes of rocks, triangular facets, steeply-sloping scarps, sudden break in slope,

diverted to offset drainage systems, uplifted-dissected and fault suspended terrace conglomerates and well-developed slickensides with two sets of overprinting slip-lines are common criteria for the recognition of fault segments.

Stereographic plot of slip-plane data on Schmidt's lower hemisphere net reveals that the Erdoğmuş fault, which is one of fault segment comprising the Muratdağı fault zone, is an oblique-slip normal fault with the localized neotectonic extension in NNE-SSW direction. The Muratdağı fault zone has reactivated and caused to the occurrence of the 1970.03.28, $M_w=7.2$ Gediz earthquake and related ground surface ruptures (GSR in Figure 4.2), i.e. the source of Gediz earthquake is the Erdoğmuş fault. It was first identified and mapped in the frame of the present study. Other fault segments comprising the Muratdağı fault zone are explained to introduce its geometry and kinematic characteristics.

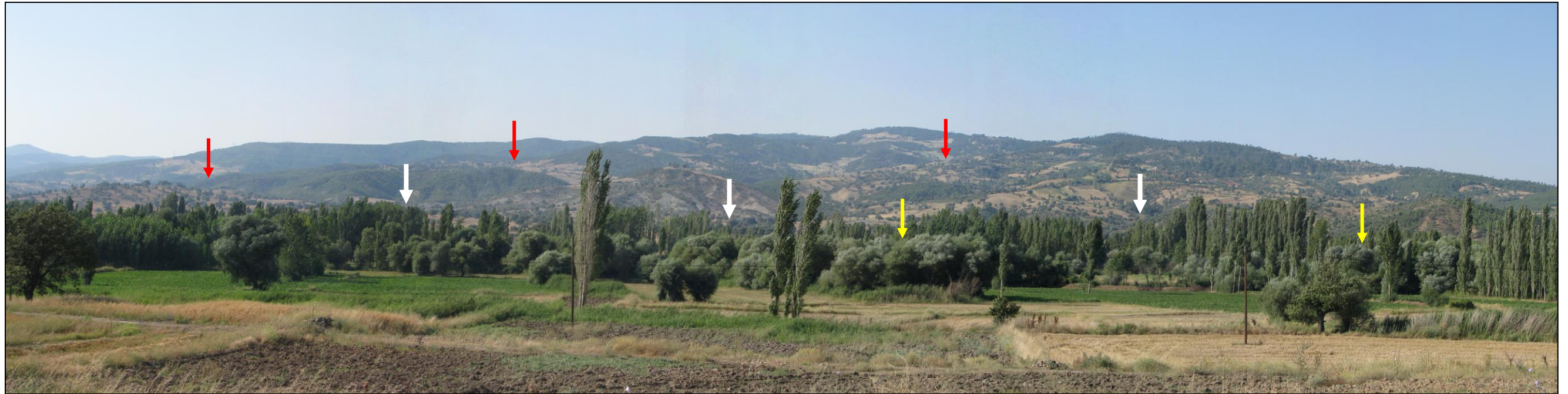


Figure 4.16. General view of the Muratdağı Fault Zone (different colored arrows indicate traces of different faults comprising the Muratdağı Fault Zone on the surface) (view to SE).

4.3.2.2.1.1. Muratdağı Fault

The Muratdağı fault (Figure 4.17) is named in this study. It is an about 15 km long, ~ NE-SW to E-W-trending curvilinear and northerly dipping normal fault with minor sinistral strike-slip component (Appendix – A). It is located in the area between Abide village in the SW and Gümele village in the NE (Appendix – A).

The Muratdağı fault cuts the pre-modern graben infill of Upper Miocene-Lower Pliocene Arica formation and tectonically juxtaposes with the Plio-Quaternary modern graben infill of the Erdoğmuş-Yenigediz graben (Appendix – A). At some localities along the Muratdağı fault, slickenside was observed and some slip plane data measurements have been taken from the sediments against the fault. The slip-plane has been analyzed by Angelier's stress tensor programme (Figure 4.18). Stereographic plot of slip-plane data indicates an oblique-slip normal fault and N-S directed tension (large arrows in Figure 4.18).



Figure 4.17. General view of the Muratdağı fault (view to SSE). Vertical white arrows indicate trace of the fault.

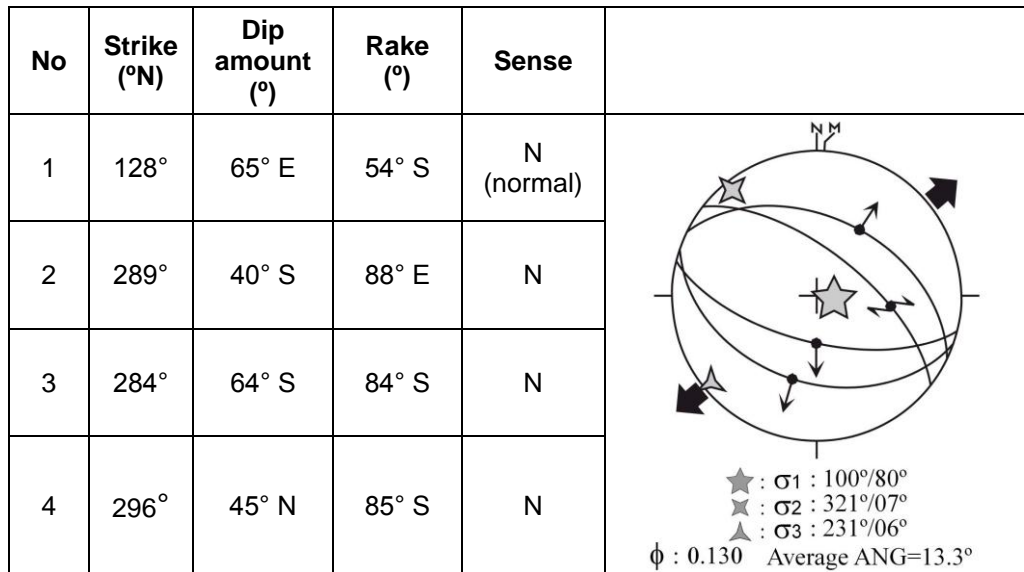


Figure 4.18. Stereographic plot of slip-plane data from Muratdağı fault on the Schmidt's lower hemisphere net, S.1 in Appendix – A.

4.3.2.2.1.2. Firdan Fault

Firdan fault is named in this study. It is a 5 km long, E-W-trending and north-dipping normal fault (Figure 4.19 and Appendix – A), located in the near north of the Firdan village. It bifurcates from the Muratdağı fault in the west, and then continues eastwards through Firdan village. It deforms the terrace conglomerates of Plio-Quaternary age and displaces them in both vertical and lateral direction (Appendix – A).

The Firdan fault displays steep scarp (Figure 4.20). Unfortunately, very limited number of slickensides and striations are observed on the fault scarp. Due to the lack of slickensides to perform kinematic analysis, stereographic plot could not be handled. On the other hand, morphotectonic criteria such as sudden break in slope along the fault (Figure 4.19) and their geometrical relationship with the current direction of principal stress indicate that the fault is a normal fault with minor amount of right-lateral component (Figure 4.20).



Figure 4.19. General view of the Firdan fault (view to S). Vertical red arrows point to trace of the fault.

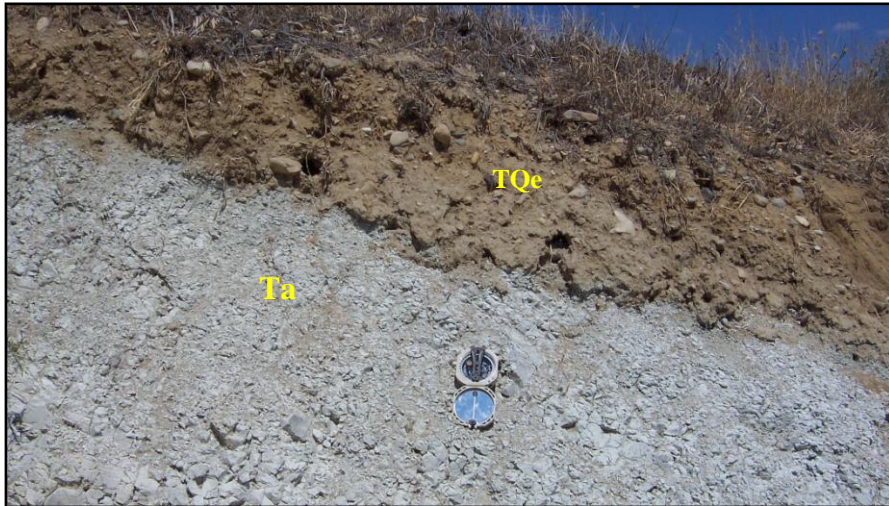


Figure 4.20. Close up view of the Firdan fault which is the boundary between Arica formation (Ta) (middle Miocene – early Pliocene) and Erdoğmuş fault (TQe) (Middle Pliocene) along its western part.

4.3.2.2.1.3. Erdoğmuş Fault

The Erdoğmuş fault is named in this study. It is an about 12 km long, approximately E-W-trending and north-dipping normal fault with minor right-lateral strike-slip component. It also splays off the Muratdağı fault

in the west, and then runs eastwards for 12 km up to near ESE of Gümele village (Appendix – A). The Erdoğmuş fault cuts across both the Arıca and Erdoğmuş formations, displaces them in vertical and lateral directions, and also juxtaposes them tectonically in places (Appendix – A). The sudden break in slope and steeply sloping scarp are two morphotectonic criteria used for the recognition of fault (Figure 4.21).

The Erdoğmuş fault is the most important fault segment in very significant for Gediz area. Since, it is considered as the source of 1970.03.28 Gediz earthquake; a series of ground surface ruptures with vertical displacement of 0.5 m have formed during earthquake (Figure 4.22). These ruptures are still presented at the surface in Erdoğmuş town in the west (Figure 4.23) and in the hillside around the Sazköy in the east (Figure 4.24).

The Erdoğmuş fault displays well-preserved slickenside, in places. Three different sets of superimposed striations occur slip-plane data have been measured. They are interpreted to suggest that the Erdoğmuş fault has experienced at least two different phases of deformation (Figure 4.25) and that the fault is an older structure inherited from the latest palaeotectonic period. Stereographic plot of the slip-plane data on the Schmidt's lower hemisphere net is consistent with a NW-SE-extension (Figure 4.26) and ENE-WSW contraction direction (Figure 4.27). This contraction direction fits well with the contraction direction obtained from the fold analyses (Figure 4.8). The third set of slickenside is also overprinted the first and second sets of slip-lines on the slickensides of various faults (Figure 4.28). Their stereographic plots (Figure 4.29 and 4.30) are clearly showing a NE-SW and ENE-WSW directed extension in the neotectonic period.

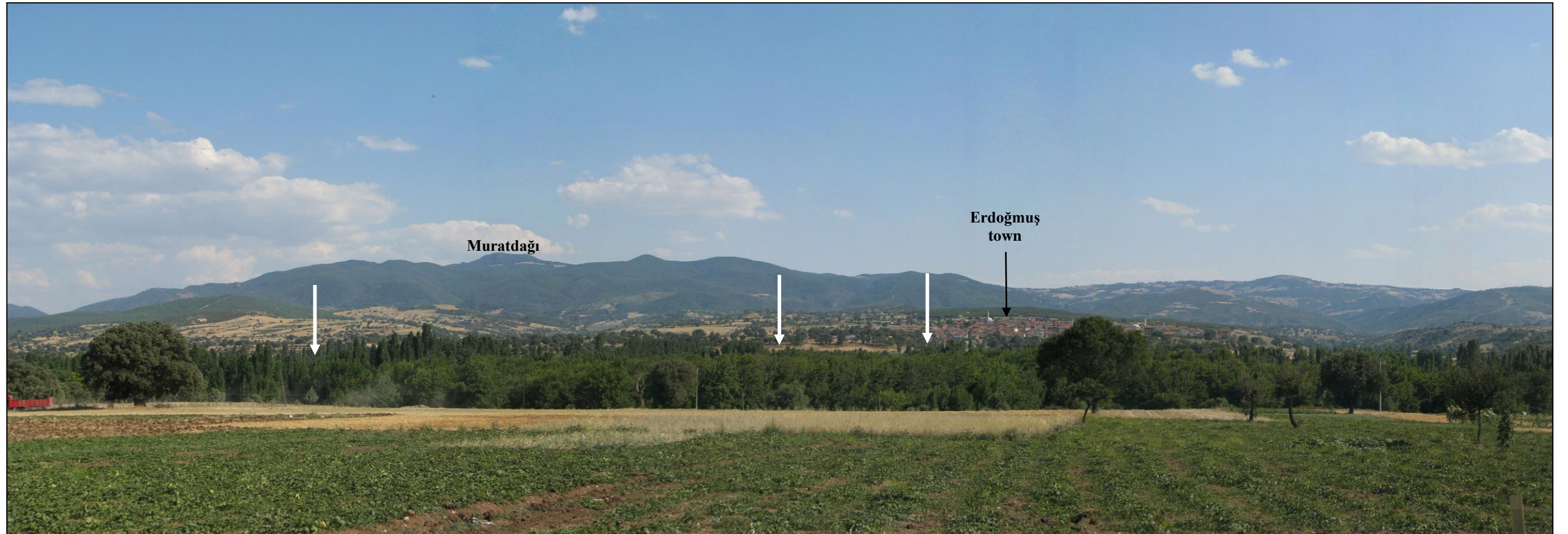


Figure 4.21. General view of the Erdoğmuş fault scarp and trace. Vertical white arrows indicate trace of the fault (view to S).



Figure 4.22. Close-up view of the ground surface rupture of the 1970.03.28, $M_w=7.2$ Gediz earthquake in the west of Erdoğmuş town (courtesy of Prof. Dr. James Jackson).



Figure 4.23. Recent view of the ground surface rupture of the 1970.03.28, $M_w=7.2$ Gediz earthquake in the west of Erdoğmuş town. Dash line indicates surface rupture of the earthquake (view to east).



Figure 4.24. Ground surface rupture of the 1970.03.28 $M_w=7.2$ Gediz earthquake around Sazköy village (view to east).



Figure 4.25. Field photograph illustrating the Erdoğmuş fault slickenside with two overprinted sets of slip-lines (in the Erdoğmuş-Sandıklı road, Appendix – A).

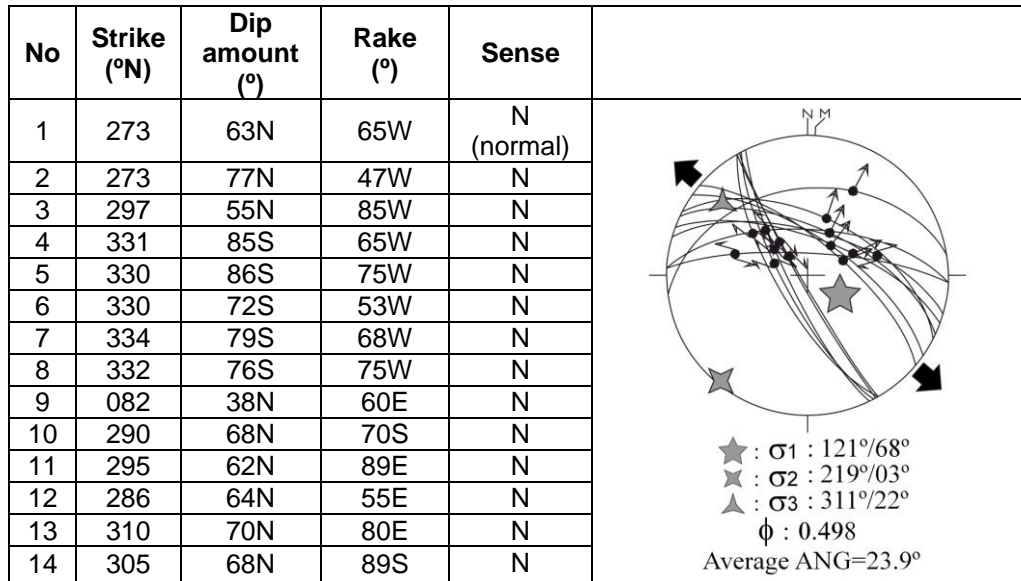


Figure 4.26. Stereographic plot of slip-plane data from Erdoğan fault on the Schmidt's lower hemisphere net, S.2 in Appendix – A.

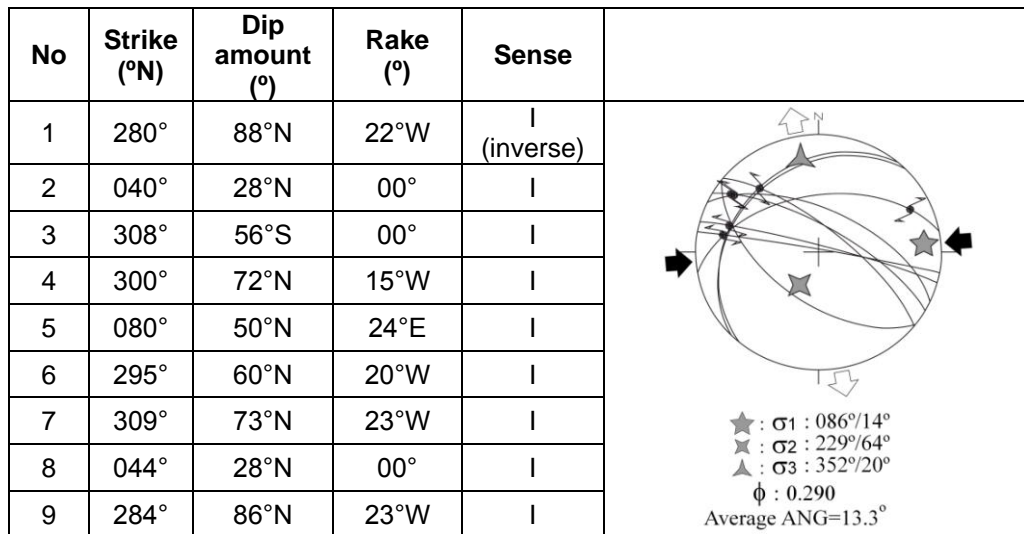


Figure 4.27. Stereographic plot of contractional slip-plane data on the Schmidt's lower hemisphere net, S.2 in Appendix – A.



Figure 4.28. Close-up view of extensional slickenside on the pre-modern graben infill deformed by the Erdoğmuş fault.

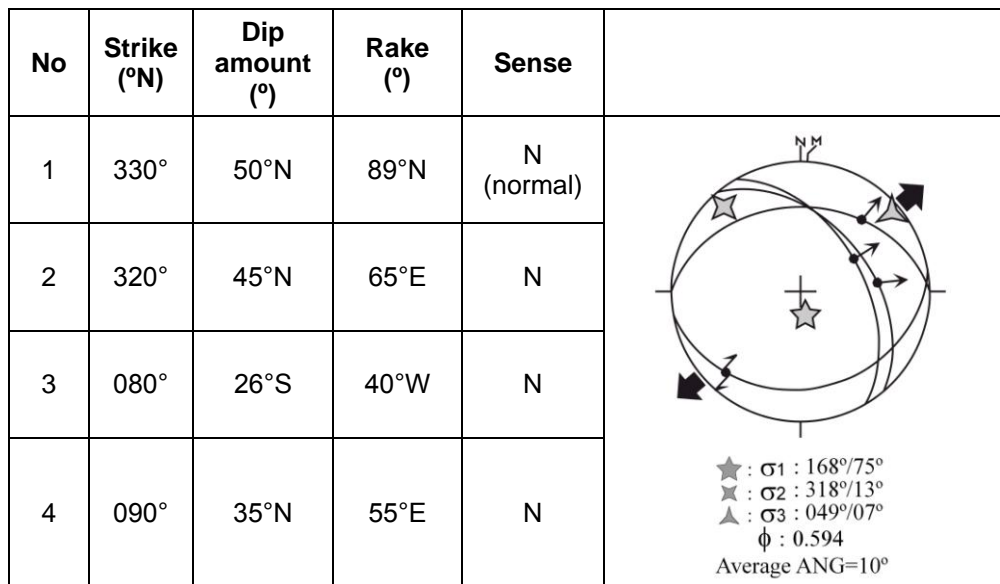


Figure 4.29. Stereographic plot of slip-plane data on the Schmidt's lower hemisphere net, S.3 in Appendix – A.

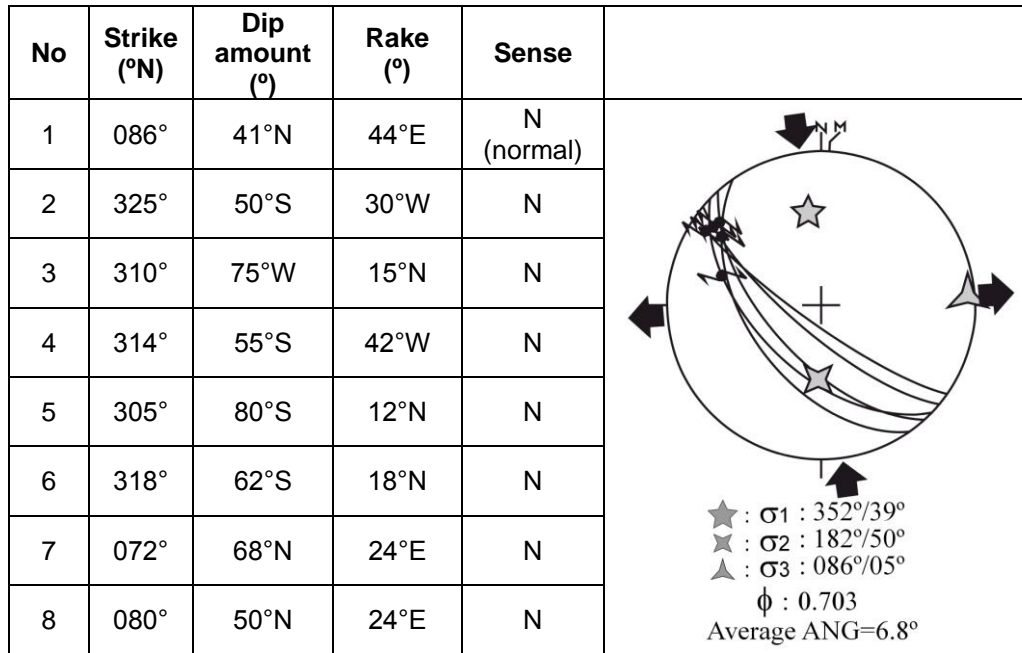


Figure 4.30. Stereographic plot of slip-plane data on the Schmidt's lower hemisphere net, S.4 in Appendix – A.

4.3.2.2.1.4. Kızılcayer Fault

The Kızılcayer fault is named in this study. It is an about 3 km long, approximately E-W-trending, and north-dipping normal fault located along the Muratdağı valley floor (Appendix – A) and cut across the alluvial deposits. It fault was moved by 1970.03.28 Gediz earthquake. So, it is interpreted an active fault, even though it does not display any topographic expression, such as sudden break in slope, steep fault scarp, etc.

4.3.2.2.1.5. Canbulat Fault

The Canbulat fault is named here. It is an about 8.5 km long and approximately NW-SE-trending zone of deformation where dominant oblique-slip normal faulting is accomplished with left-lateral strike-slip component (Figure 4.31). It cuts and displaces vertically the pre-modern

graben infill of Late Miocene-Early Pliocene age (Figure 4.32), and juxtaposes the unit tectonically with the Plio-Quaternary modern graben infill (Appendix – A).

Owing to the dense vegetation and the Gümele dam site, the fault plane has not been observed. Sudden change in the slope, the tectonic juxtaposition of lithofacies of dissimilar age and origin along straight and sharp traces, and the offset drainage system are used to support the existence of the Canbulat fault.

Although there is no fault plane and slip-plane data on it, some slip measurements have been taken from the Arica formation deformed by the Canbulat fault. Based on the stereographic plot of these slip-plane data, this fault is in the nature of oblique-slip normal fault, along which Erdoğmuş-Yenigediz graben in being extended in NE-SW direction (Figure 4.33).



Figure 4.31. General view of the Canbulat fault (location: 5 km south of Gümele village; view to NW). Vertical white arrows point to trace of the fault.



Figure 4.32. Field photograph indicating the Arica formation (near west of Gümele dam site).

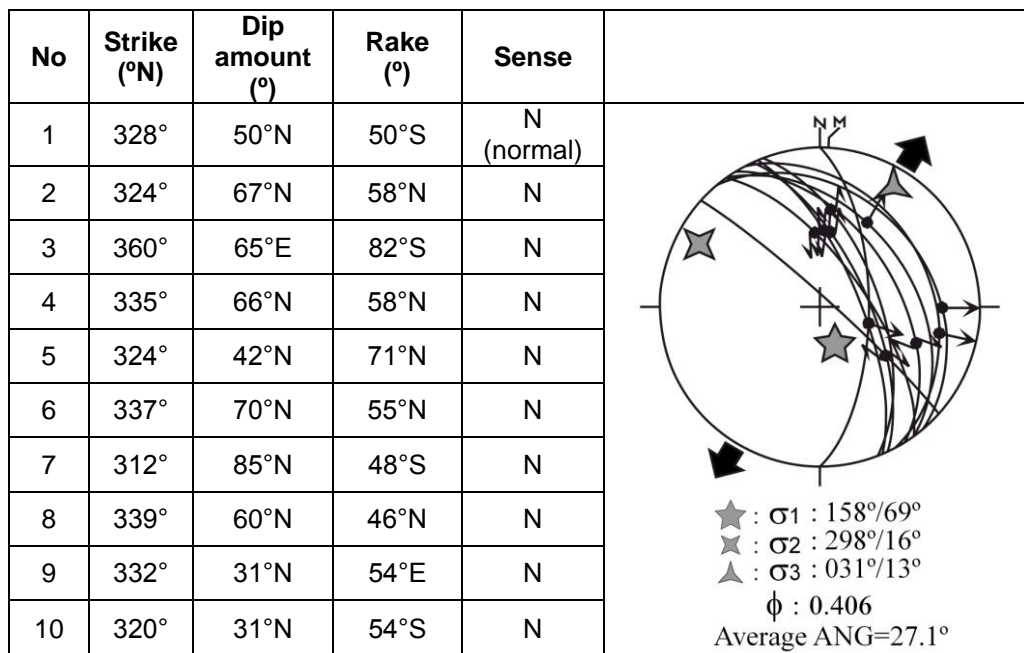


Figure 4.33. Stereographic plot of slip-plane data from Canbulat fault on the Schmidt's lower hemisphere net, S.5 in Appendix – A.

4.3.2.2.1.6. Gümele Fault

The Gümele fault is named in this study. It is a 6.5 km long, approximately NW-SE-trending and southwesterly dipping deformation zone in the nature of oblique-slip normal faulting with left-lateral strike-slip component (Figure 4.34). It cuts and displaces the pre-modern graben infill (the Arica formation and metamorphic rocks) and tectonically juxtaposes them with the Plio-Quaternary modern graben infill (Appendix – A).

The Gümele fault displays well-preserved slickenside in places (S.6 in Appendix – A). Slip-plane data (station S.6) indicates an oblique-slip normal fault and NE-SW directed tension (Figure 4.35).

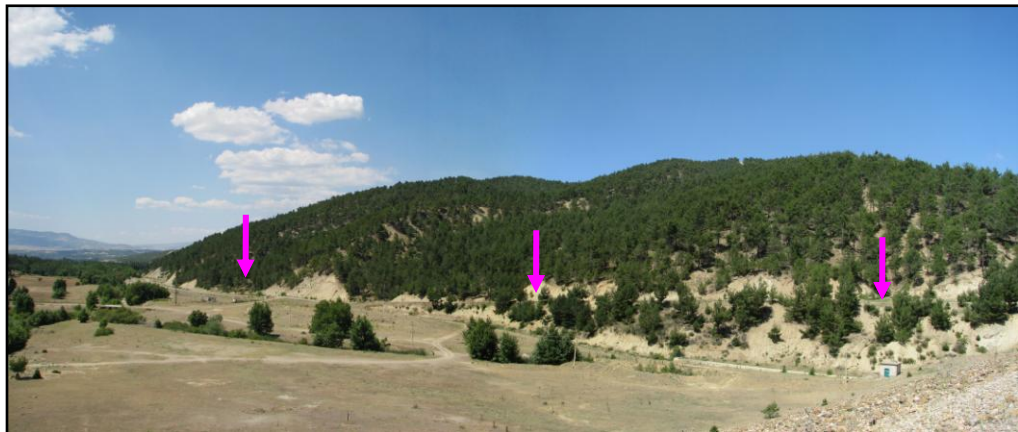


Figure 4.34. General view of the Gümele fault (location: 4 km SE of Gümele village; view to NW). Vertical purple arrows show trace of the fault.

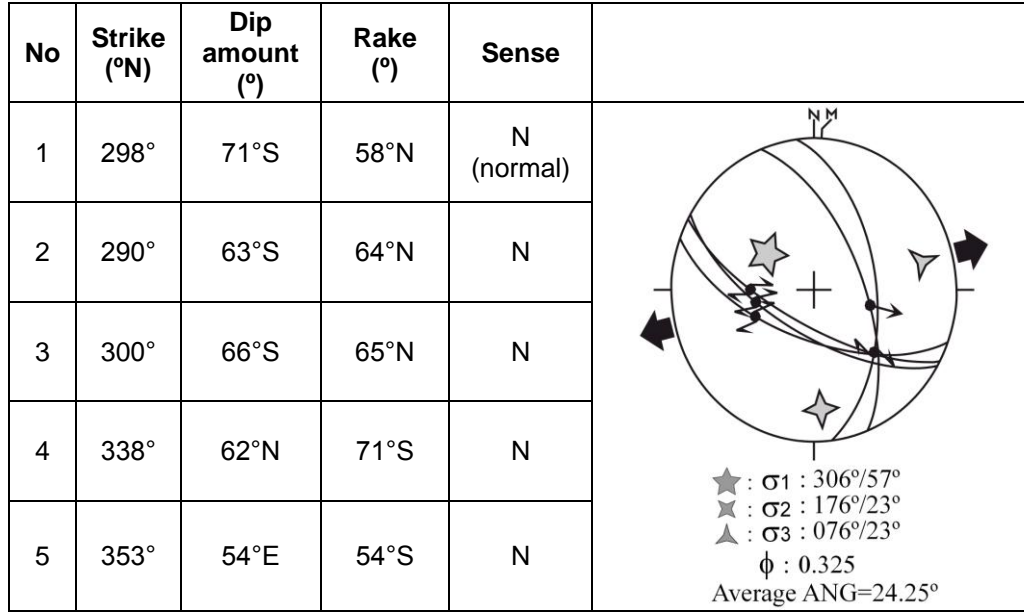


Figure 4.35. Stereographic plot of slip-plane data from Gümele fault on the Schmidt's lower hemisphere net, S.6 in Appendix – A.

4.3.2.2.1.7. Çomaklar Fault

The Çomaklar fault is named here. It is a 4.5 km long, approximately NNE-SSW-trending and northwesterly dipping oblique-slip normal fault with minor amount of right-lateral strike-slip component (Figure 4.36). It is located along the Binbatçayırı stream valley between Çomaklar village in the NNE and Gümüşlü village in the SSW (Appendix – A). The Çomaklar fault occurs along the NNE-trending anticline. It cuts and displaces the pre-modern graben infill and tectonically juxtaposes it with the Quaternary graben infill.



Figure 4.36. General view of the Çomaklar fault (location: 3 km SSW of Gümüşlü village; view to ENE). Vertical white arrows point to trace of the Çomaklar fault.

On the other hand, some slip-plane data representing the 1st phase of extension have been measured in the pre-modern graben infill (S.7 in Appendix –A). According to their stereographic plot, the existence of approximately NW-SE-trending palaeotectonic extension can be observed (Figure 4.37). So, this slip-plane data also indicated that the Çomaklar fault is an originally older structure, but it has been reactivated during the Plio-Quaternary neotectonic period.

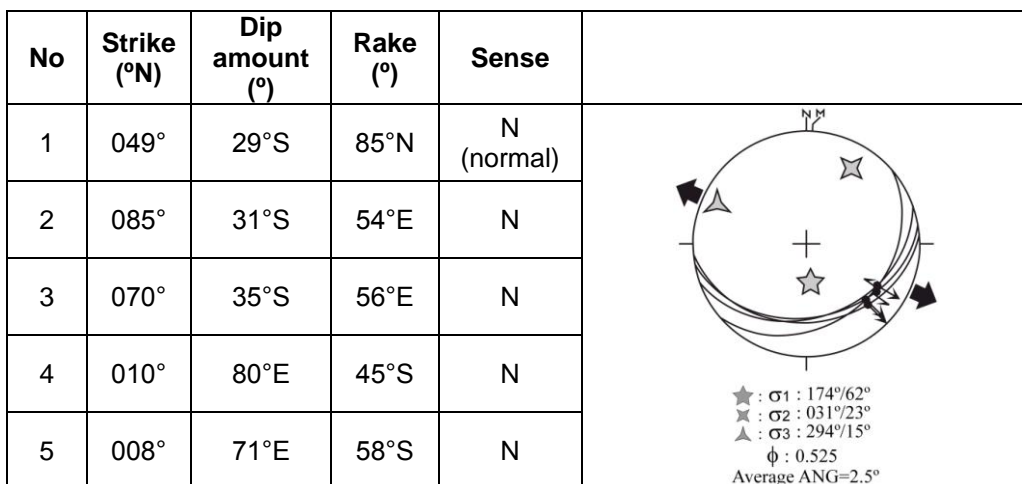


Figure 4.37. Stereographic plot of slip-plane data on the Schmidt's lower hemisphere net, S.7 in Appendix – A.

4.3.2.2.1.8. Binbatçayırı Fault

The Binbatçayırı fault is named in this study. It is an approximately 5 km long, approximately NNE-SSW-trending and southeasterly dipping oblique-slip normal fault with right-lateral strike-slip component (Figure 4.38). It is located along the western side of the the Binbatçayırı stream valley between near east of Çomaklar village in the north and Gümüşlü village in the south-southwest (Appendix – A). The Binbatçayırı fault displays well-preserved slickensides in places (S.8 in Appendix –A). Stereographic plots of slip-plane data (Figure 4.39) indicate an oblique-slip normal fault and in NE-SW directed tension (Figure 4.40).



Figure 4.38. General view of the Binbatçayırı fault (view to NNW). Vertical white arrows point to trace of the fault.



Figure 4.39. Close up view of a slickenside in Arica formation deformed by the Binbatçayırı fault.

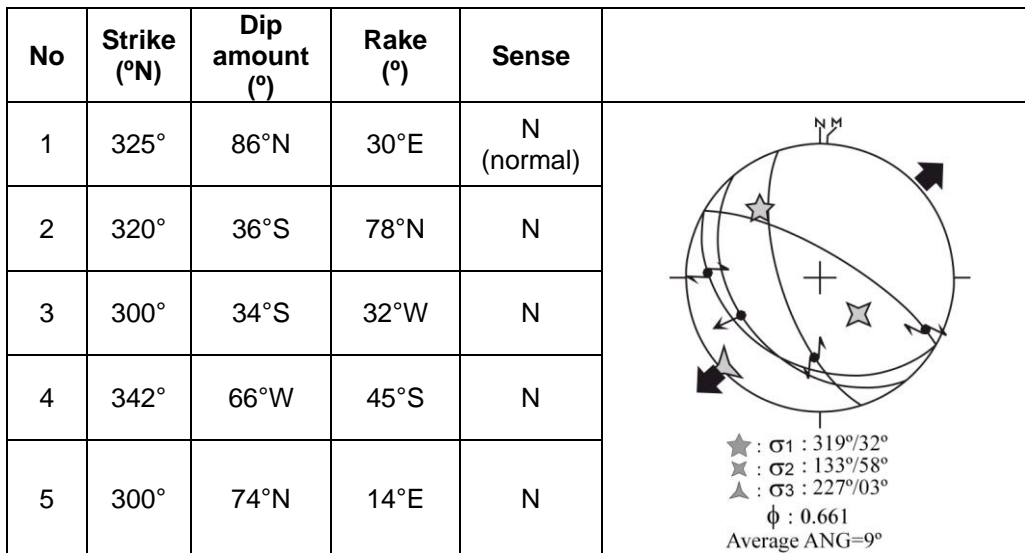


Figure 4.40. Stereographic plot of slip-plane data from Binbatçayırı fault on the Schmidt's lower hemisphere net, S.8 in Appendix – A.

4.3.2.2.1.9. Koç Fault

The Koç fault is named in this study. It is an approximately 6.5 km long, nearly NNE-SSW-trending and northwesterly dipping oblique-slip normal fault (Figure 4.41). It is located along the eastern side of the Koç stream valley developed on an anticline with the NE-trending axis. The Koç fault cuts and displaces the pre-modern graben infill and juxtaposes it tectonically with the Erdoğan graben (Appendix – A).



Figure 4.41. General view of the Koç fault (view to NE). Vertical white arrows show trace of the fault.

4.3.2.2.1.10. Altıntaş Fault

The Altıntaş fault is named in this study. It is an approximately 5 km long, nearly NNE-SSW-trending and southwesterly dipping oblique-slip normal fault (Figure 4.42), located along the western side of the Koç stream valley. It deforms the pre-modern graben infill (Appendix – A).

Sudden change in the slope (sudden break in slope), tectonic juxtaposition of the Arica formation and alluvial deposits (recent

deposits) and strips of intensely deformed, crushed and sheared rock packages form the evidence for the Arica fault.

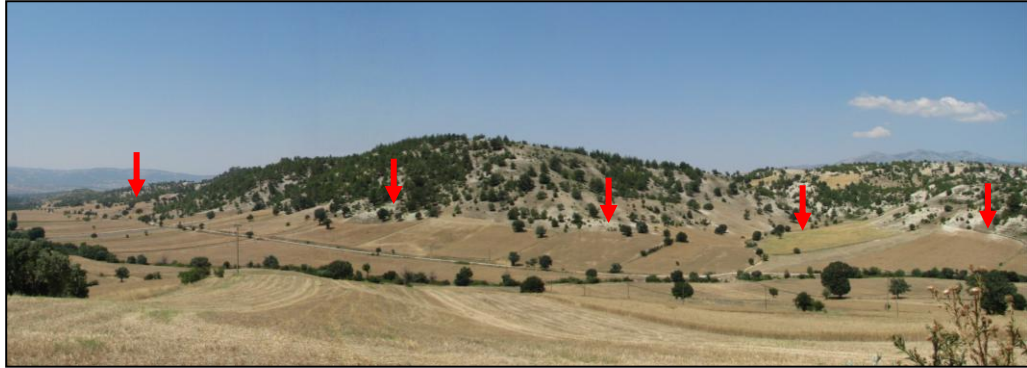


Figure 4.42. General view of the Altıntaş fault (view to NW). Vertical red arrows indicate trace of the fault.

The Çomaklar, Binbatçayırı, Koç, and Altıntaş faults determine and control newly-developing secondary grabens and horsts, namely the Koç and Binbatçayırı secondary grabens. Cross-section in Figure 4.43 indicates the relationship between faults and Arica and Erdoğanlı formations.

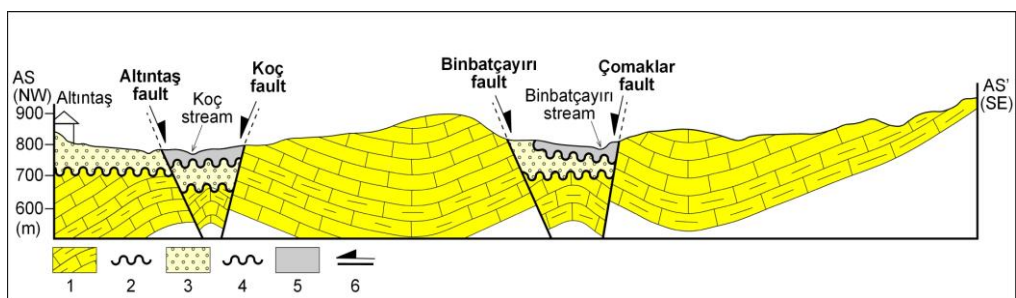


Figure 4.43. Geological cross-section along the line AS-AS'. 1. Miocene-Middle Pliocene pre-modern graben infill, 2. angular unconformity, 3. terrace conglomerate, 4. angular unconformity, 5. Quaternary deposits, and 6. normal fault (see AS-AS' in Appendix – A for location).

4.3.2.2.1.11. Kuyucak Fault

The Kuyucak fault is named in this study. It is an approximately 3.5 km long, nearly NW-SE-trending and southwesterly dipping oblique-slip normal fault (Figure 4.44) and cuts the Kuyucak stream valley (Appendix – A). The existence and activeness of the Kuyucak fault is indicated by the sudden change in the slope (break in slope), tectonic juxtaposition of the older Arica formation with the Plio-Quaternary terrace conglomerates and alluvial deposits.

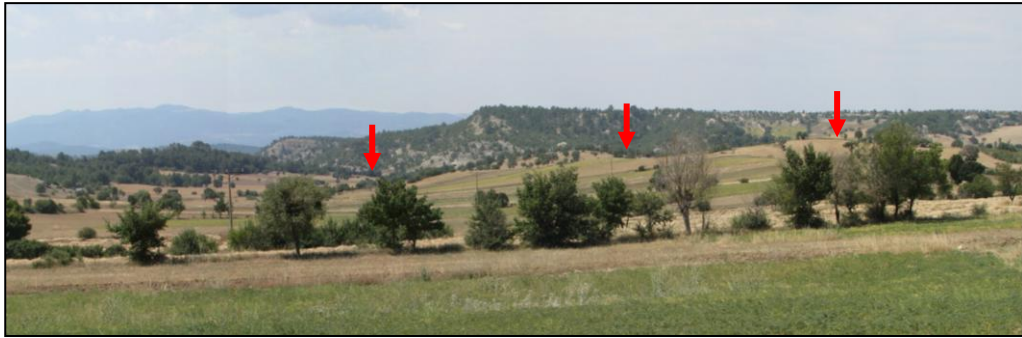


Figure 4.44. General view of the Kuyucak fault (view to NE). Vertical red arrows point to trace of the fault.

4.3.2.2.1.12. Gediz Fault

The Gediz fault is named here. It is a 7.5 km long, approximately NNE-SSW-trending and northwesterly dipping oblique-slip normal fault with right-lateral strike-slip component (Figure 4.45). It is located along the eastern side of the Gediz Çayı valley between Hacıbaba village in NNE and near west of Dörtdeğirmen village in SSW. Its southern half morphologically is more obvious than the northern half. The fault displays well-developed fault scarps, but no slickensides. The Gediz fault cuts across the pre-modern graben infill and juxtaposes

tectonically it with the Quaternary alluvial deposits of the Gediz Çayı (Appendix – A).



Figure 4.45. General view of the Gediz fault (view to SE). Vertical yellow arrows point to trace of the fault.

4.3.2.2.1.13. Yenigediz Fault

The Yenigediz fault is named here. It is an about 5 km long, approximately NNE-SSW-trending and southeasterly dipping oblique-slip normal fault with right-lateral strike-slip component (Figures 4.46 and 4.47). It is located along the western side of the Gediz Çayı. It cuts and displaces the pre-modern graben infill, displaces it in vertical direction and juxtaposes it tectonically with the Quaternary alluvial deposits (Appendix – A). The sudden break in slope, uplifted and fault-suspended terrace conglomerates, strips of crushed and sheared rocks are common morphotectonic criteria for the recognition of the Yenigediz fault. It also displays well-developed slickensides along the road cuts (S.9, 10 and 11 in Appendix – A) (Figure 4.48).

Along the road cut, a number of slip-plane data (Figure 4.49) have been collected and analyzed (Figures 4.50, 4.51 and 4.52) method. There are two different sets of slip-plane data. The first one (older) has the contractional motion (Figure 4.50) and the second one (younger) has

the extensional motion. The older and younger ages have been easily attained by using the cross cutting relationship between slip surfaces. Although the dominant extension direction is about NE-SW (Figure 4.51), different variances can be appeared in the range of NE-SW to E-W (Figure 4.52). It is not possibly true to give an only one extension direction for this area. Another to say a multidirectional extension is going on in the region.

The kinematic analysis of the slip-plane data indicates that the Yenigediz fault has experienced at least two different deformation phases (Figures 4.50 and 4.51).



Figure 4.46. Cross-sectional view of the Yenigediz fault (view to SSW). Dash line indicates to the Yenigediz fault.

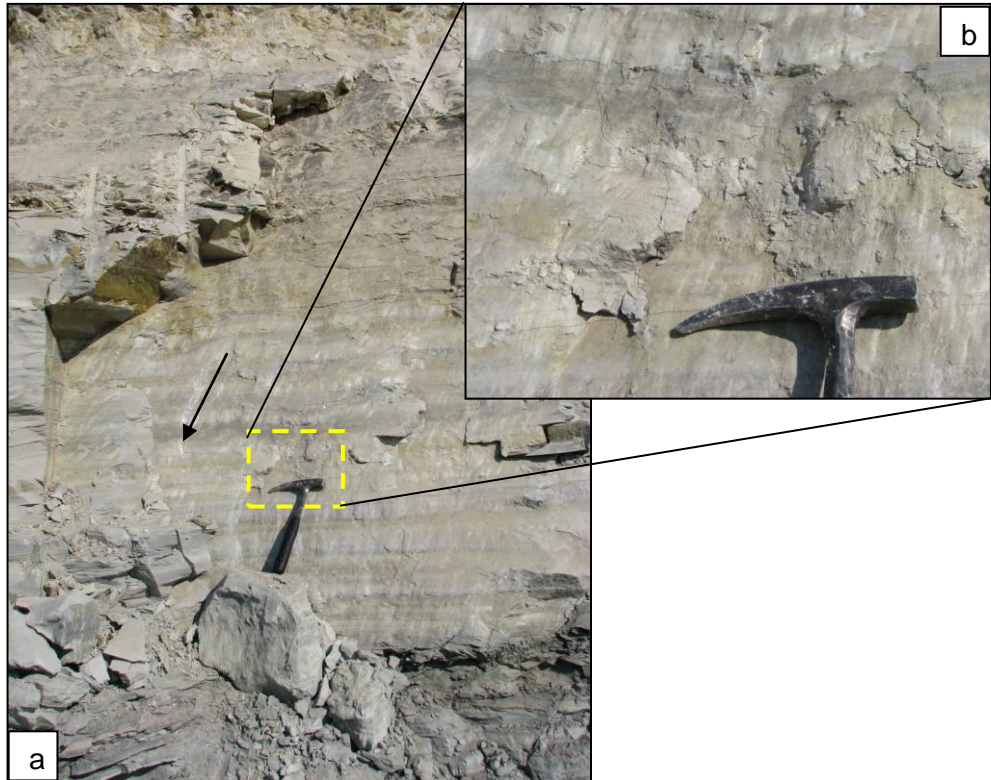


Figure 4.47. a. General view of the Yenigediz fault plane (view to NW), b. Close-up view of the slickenside. Black arrow points to the motion direction of hanging-wall block.

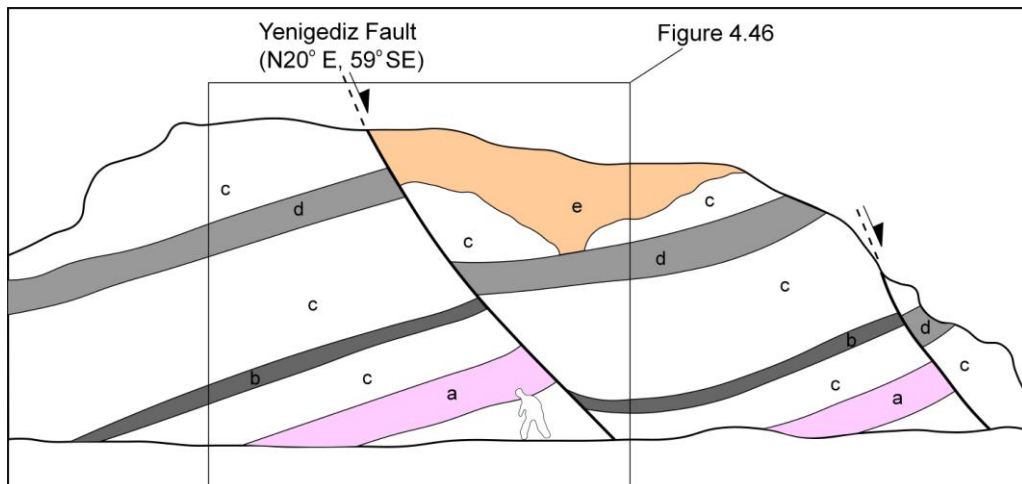


Figure 4.48. Sketched cross-section along the road cut in the near west of Hacibaba village. a. pinkish, highly crushed marl, b. dark black colored marl, c. highly crushed grey colored marl, d. highly crushed, dark grey colored marl, e. sandy channel fill.



Figure 4.49. Close-up view of the Yenigediz fault slickenside (see S.9 in Appendix – A for location).

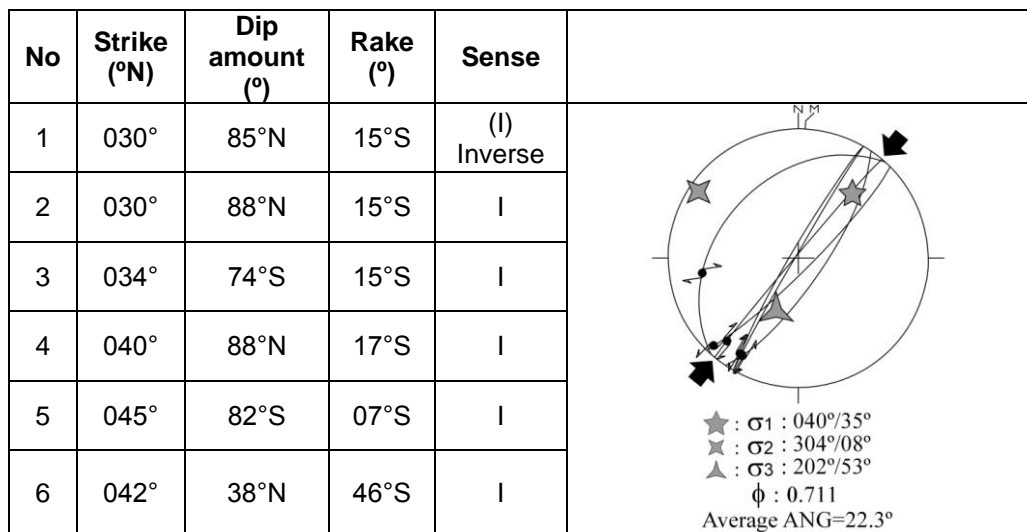


Figure 4.50. Stereographic plot of contractional slip-plane data, which was recorded during the last palaeotectonic period on the Schmidt's lower hemisphere net, S.9 in Appendix – A.

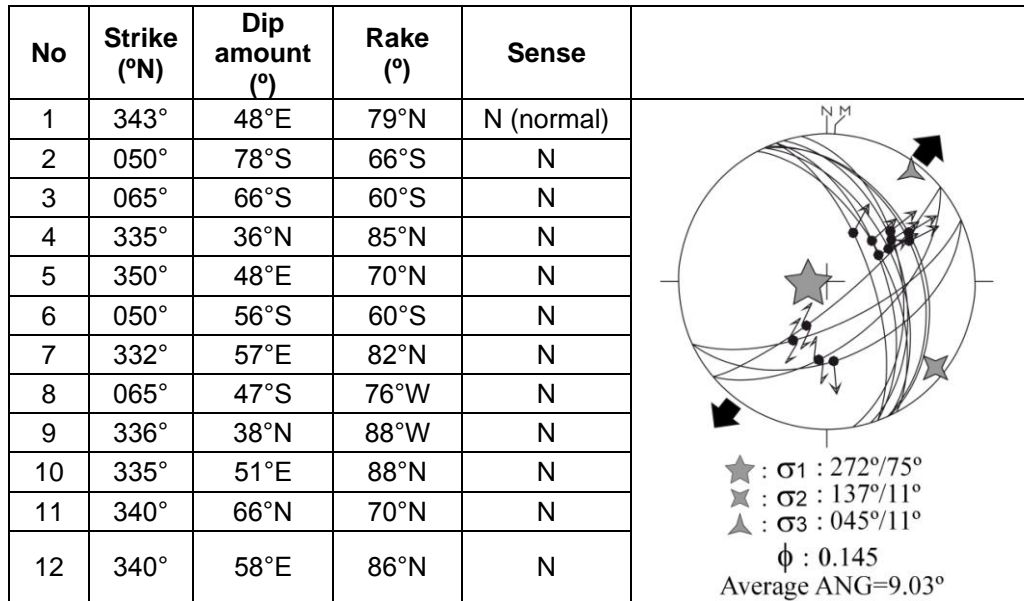


Figure 4.51. Stereographic plot of extensional slip-plane data from Yenigediz fault on the Schmidt's lower hemisphere net, S.10 in Appendix – A.

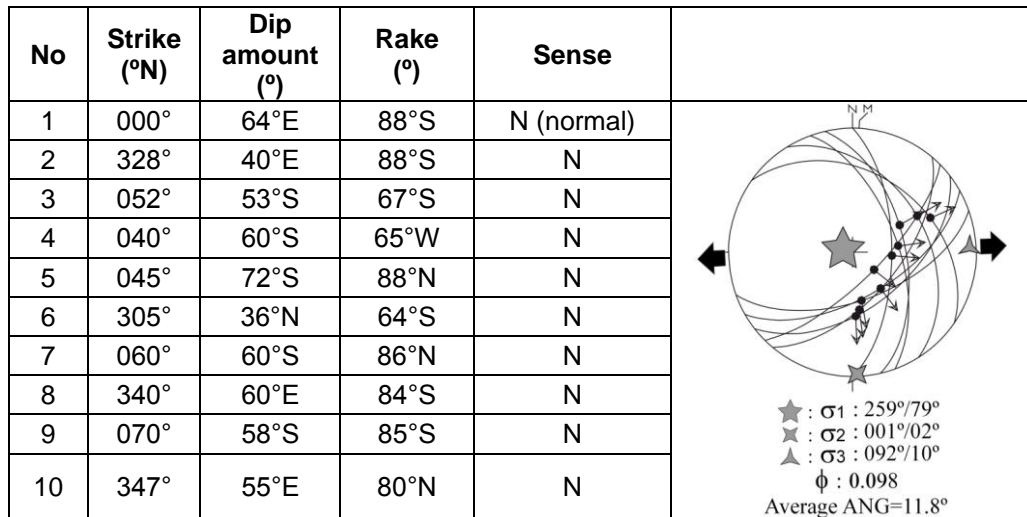


Figure 4.52. Stereographic plot of extensional slip-plane data on the Schmidt's lower hemisphere net, S.11 in Appendix – A.

4.3.2.2.1.14. Bahçeler Faults

Bahçeler faults are named here. They are 3 km long, approximately N-S-trending easterly to westerly dipping and closely-spaced oblique-slip normal fault with left-lateral strike-slip component (Figure 4.53). They are located on both sides of Gediz Çayı in the near north of Eskigediz county (Appendix – A). They cut and displace the pre-modern graben infill in vertical direction, and juxtapose them tectonically with Quaternary alluvial sediments. The deeply carved Gediz Canyon with nearly vertical walls is the diagnostic topographic expression of the Bahçeler faults.



Figure 4.53. General view of the Bahçeler fault (view to E). Vertical yellow arrows point to trace of the easterly dipping fault.

4.3.2.2.1.15. Dörtdeğirmen Fault

The Dörtdeğirmen fault is named in this study. It is an approximately 14 km long, approximately ENE-WSW-trending and southeasterly dipping normal fault with minor amount of right-lateral strike-slip component (Figure 4.54). It is located along the north-northwestern side of the

Gediz-Muratdağı valley in the area between Dedeköy in the east and Abide town in the west. It cuts and displaces vertically the pre-modern graben infill and tectonically juxtaposes them with the Quaternary alluvial sediments. Sudden break in slope, uplifted and fault-suspended terrace conglomerates, deflected to offset drainage system are common morphotectonic criteria used for recognition of the Dörtdeğirmen fault. The Dörtdeğirmen fault also displays well-preserved slickensides in places (Figure 4.55). The stereographic plots of slip-plane data (S.12 in Appendix – A) indicate that the Dörtdeğirmen fault is an oblique-slip normal fault, NE-SW directed tension (Figure 4.56).



Figure 4.54. General view of the Dörtdeğirmen fault (view to WSW). Vertical yellow arrows point to trace of the fault.



Figure 4.55. Close-up view of the Dörtdeğirmen fault slickenside. The slip-plane data have been recorded on the Plio-Quaternary deposits.

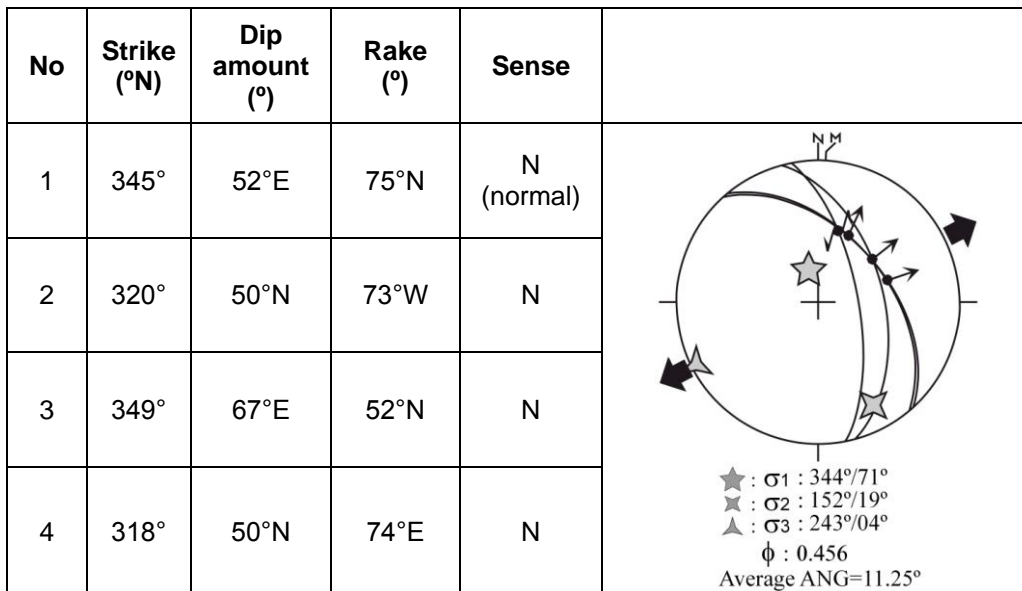


Figure 4.56. Stereographic plot of extensional slip-plane data from Dörtdeğirmen fault on the Schmidt's lower hemisphere net, S.12 in Appendix – A.

4.3.2.2.1.16. Gümüşlü Fault

The Gümüşlü fault is named here. In the study area, it is a 4.5 km long, approximately WNW-ESE-trending and southwesterly dipping normal fault with minor amount of right-lateral strike-slip component (Figure 4.57). It is located along the northern side of the Muratdağı valley floor between Gümüşlü village in the WNW and Çayyeri settlement in the east and outside the study area. The sudden break in slope, uplifted and fault-suspended terrace conglomerates, crushed and sheared rocks, sudden change in dip amount and strike of bedding are common criteria used for recognition of fault.



Figure 4.57. General view of the Gümüşlü fault in the Plio-Quaternary deposits (view to NW, location: near southwest of Gümüşlü village). Dash line shows the fault.

4.3.2.2.2. SIMAV FAULT ZONE

The Simav fault zone is an about 2-6 km wide, 160 km long and WNW-trending active zone of deformation characterized by normal faulting. It is located between Banaz County in the southeast and Gölcük Town (Sındırgı) in the northwest. Most of its southeastern and northwestern parts lie outside the study area (Appendix – A). In the study area, it is 32 km long. The Simav fault zone determines and controls the south-southwestern margin of the Erdoğmuş-Yenigediz graben (Figure 4.2). In the frame of this study, the Ilica-Sandıklı section of the Simav fault zone was studied, mapped and analyzed. This section consists of several parallel to sub-parallel and closely-spaced normal fault segments of dissimilar lengths (200 m - 15 km). Fault segments generally dip north-northeast and display steeply sloping fault scarps and step-like land shapes. They cut and displace (up to 600 m vertically) various rocks of dissimilar age and facies, such as metamorphic rocks, ophiolitic rocks, both the pre-modern to modern graben infill. Fault segments also tectonically juxtapose older rocks and the younger graben infill. The master fault in the study area is termed the Abide fault (Figure 4.58). It is located between the near northwest of the Ilica thermal bathhouses in the northwest and Arıca village in the southeast. Steeply-sloping scarp, triangular facets, linear distribution of hot to cold water springs, alluvial fans, uplifted-dissected and fault-suspended terrace conglomerates, deflected to offset drainage system, tectonic juxtaposition of older rocks with the Quaternary alluvial sediments and the slickensides are common criteria used for recognition of fault segments comprising the Simav fault zone.



Figure 4.58. General view of the Ilica-Abide section of the Simav Fault Zone (red arrows indicate trace of the master fault) (Abide town in foreground, view to SSE).

4.3.2.2.1. Abide Fault

The Abide fault is named here. In the study area, it is an about 5 km long, nearly WNW-ESE-trending and northerly dipping normal fault with minor amount of right-lateral strike-slip component. It starts around Abide town in the east and runs in WNW direction for about 5 km, then continuous outside the study area (Appendix – A).

The Abide fault cuts and displaces vertically the pre-modern graben infill and juxtaposes tectonically with the Plio-Quaternary modern graben infill. Sudden break in slope, steep fault scarp and triangular facets (Figures 4.59 and 4.60), fault-parallel alignment of cold and hot water springs (e.g. Ilıca and Abide thermals), crushed to sheared rocks are common morphotectonic criteria for recognition of the fault. The Abide fault also displays well-developed and preserved slickensides in places (S.13 in Appendix – A). Their stereographic plot on Schmidt's lower hemisphere net (Figure 4.61) indicates an oblique-slip normal fault. Additionally, the Abide fault was moved by the 1944.06.24 Abide earthquake of $M_s=6.0$ (Eyidoğan *et al.*, 1991; Eyidoğan and Jackson, 1985), indicating the seismicity of the Abide fault.



Figure 4.59. General view of the Abide fault (view to SE). Vertical black arrows point to trace of the fault.



Figure 4.60. General view of the Abide fault scarp (view to SE). Vertical yellow arrows indicate trace of the fault.

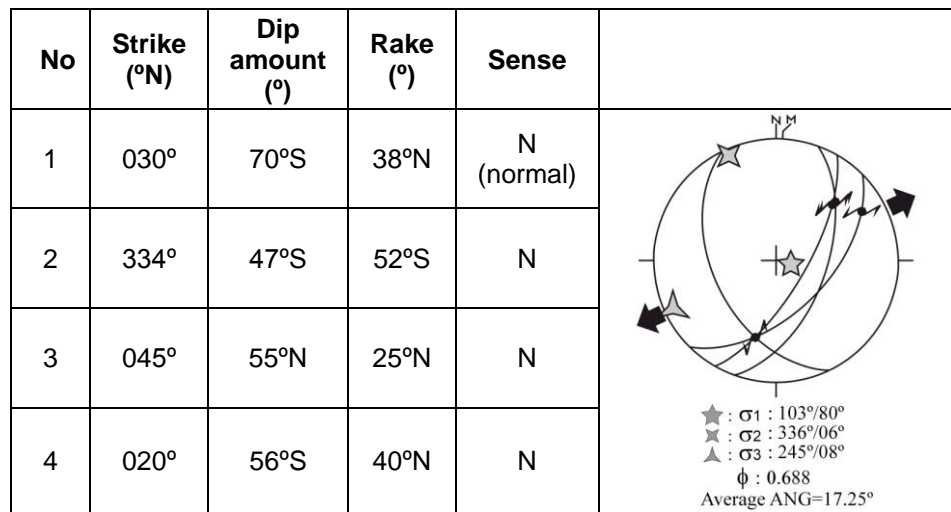


Figure 4.61. Stereographic plot of extensional slip-plane data from Abide fault on the Schmidt's lower hemisphere net, S.13 in Appendix – A.

4.3.2.2.2. Gedik Fault

The Gedik fault is named here. It is about 4 km long, approximately WNW-ESE-trending and northeasterly dipping normal fault with minor amount of right-lateral component (Figure 4.62). It is located to the south of the Abide fault, and shows step-like morphology (Figure 4.62).

It cuts and displaces vertically the Plio-Quaternary and pre-modern graben infill. Sudden break in slope, fault scarp and crushed rocks are common morphotectonic criteria used for recognition of fault.



Figure 4.62. General view of the Gedik fault (view to S). Vertical white arrows point to trace of the fault.

4.3.2.2.2.3. Kagnı Fault

The Kagnı fault is named here. It is about 4 km long, E-W-trending and northerly dipping normal fault (Figure 4.63). The Kagnı fault is located on the east-southeastern side of the Gediz Çayı valley, and displays step-like morphology (Figure 4.63). The Kagnı fault cuts across the pre-modern graben infill and determines the boundary between, and juxtaposes pre-modern graben infill and Plio-Quaternary modern graben infill (Appendix – A).

The sudden break in slope, steeply sloping fault scarp and tectonic juxtaposition of older and younger graben infill are common morphotectonic criteria used for the recognition of Kagnı fault (Figure 4.63).



Figure 4.63. General view of the Kagnı fault (view to S). Vertical yellow arrows point to trace of the fault.

4.3.2.2.4. Aksaklar Fault

The Aksaklar fault is named here. It is about 4.5 km long, E-W-trending and northerly dipping normal fault (Figure 4.64). It splays off the Muratdağı fault in the W and then runs eastwards for about 4.5 km distance, and then terminates. The Aksaklar fault cuts and displaces vertically the pre- and modern graben infill juxtaposes tectonically with them (Appendix – A). Sudden break in slope, steeply-sloping fault scarp, crushed to sheared rocks and tectonic juxtaposition of older and younger graben infill are common morphotectonic criteria used to map the Aksaklar fault.



Figure 4.64. General view of the Aksaklar (yellow arrows), and Kagnı (white arrows) fault scarps (view to S).

3.3.2.2.2.5. Kurupinar Fault

The Kurupinar fault is named in this study. It is an approximately 3.5 km long, nearly NW-SE-trending and northeasterly dipping normal fault (Figure 4.65). It cuts and displaces both the pre- and modern graben infill, displace them in vertical direction, and juxtaposes tectonically with them (Appendix – A).

The existence and activeness of the Kurupinar fault are indicated by the sudden change in the slope, steeply-sloping scarp, deflected streams and tectonic juxtaposition of older and younger graben infill.

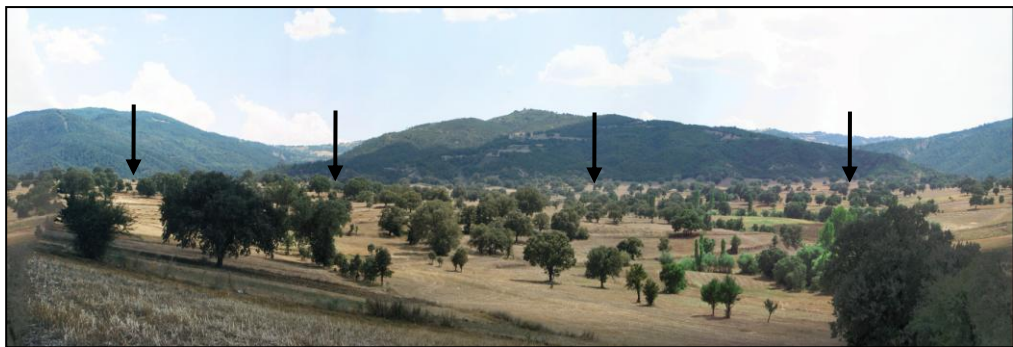


Figure 4.65. General view of the Kurupinar fault (view to S). Vertical black arrows point to trace of the fault.

4.3.2.2.2.6. Arica Fault

The Arica fault is named in this study. It is an approximately 4 km long, nearly E-W-trending, and northerly dipping normal fault (Figure 4.66). Sudden break in slope, steeply-sloping fault scarp, triangular facets, deflected stream beds, sudden change in both strike and dip amount of bedding, crushed-broken rocks and tectonic juxtaposition of older and

younger graben infill are common morphotectonic criteria observed along the Arica fault (Figure 4.66).



Figure 4.66. General view of the Arica fault (view to S). Vertical yellow arrows point to trace of the fault.

4.3.2.2.2.7. Tültepe Fault

The Tültepe fault is named in this study. It is the southeastern segment of the Simav Fault Zone in the study area. The Tültepe fault is an approximately 5.5 km long, nearly WNW-ESE-trending and northeasterly dipping normal fault. It cuts and displaces the pre- and modern graben infill in vertical direction and juxtaposes tectonically with them.

4.3.2.2.3. ŞAPHANE FAULT ZONE

The Şaphane fault zone is an about 1-4 km wide, 36 km long and E-W to NE-trending zone of deformation in the nature of normal faulting (Figure 4.67). It is located between Eskigediz County in the east and Yeşilköy town in the west. The E-W-trending western half of the fault zone runs westward across Şaphane County up to the eastern tip of the Simav graben and lies outside the study area. Its eastern half trends in NE direction and determines the northern margin of the Erdoğmuş-Yenigediz graben (Appendix – A). The Şaphane fault zone consists of 2-15 km long, closely-spaced fault segments. They display both the south-southeastward facing step-like land shape and steeply-sloping fault scarps (Figure 4.2). Fault segments cut and displace (up to 500 m) metamorphic rocks, ophiolitic mélangé and younger volcano-sedimentary sequence of the pre-modern graben infill. They also tectonically juxtapose both the older rocks to each other and to younger graben infill. The Şaphane fault zone has formed at the initial stage of the Erdoğmuş-Yenigediz graben and controlled sedimentation of the pre-modern graben infill. This is proved by a series of normal type of growth faults and overprinted sets of slip-lines. The master fault segments of the Şaphane fault zone are the Şaphane and the Eskigediz faults (Appendix – A). Both were reactivated during the 1970.03.28 $M_w=7.2$ Gediz earthquake (Ambraseys and Tchalenko, 1972). Detailed explanation of the fault segments comprising the Şaphane Fault Zone is presented below.



Figure 4.67. General view of the Şaphane Fault Zone and its scarp (view to NW).

4.3.2.2.3.1. Şaphane Fault

The Şaphane fault is named here. It is an about 6 km long, nearly E-W to ENE-WSW-trending and southerly dipping normal fault. It determines and controls north-northwestern margin of the Erdoğmuş-Yenigediz graben and forms the mountain front to Şaphane horst (Appendix – A). Steeply sloping fault scarp, sudden break in slope, intensely crushed and pulverized fault rocks, fault-parallel-aligned water springs, colluvial wedge accumulated along the mountain fronts, active landslides, tectonic juxtaposition of older rocks with younger, deflected to offset drainage system and well-developed to preserved slickensides (Figures 4.68 and 4.69) are common morphotectonic features used for the recognition of the Şaphane fault. The stereographic plot of slip-plane data (S.14 in Appendix – A) on the Schmidt's lower hemisphere net indicates a dip-slip normal fault (Figure 4.70). Kinematic analysis reveals that the Şaphane fault is a reactivated structure.



Figure 4.68. General view of the Şaphane fault slickenside (view to NW) (location: 1 km west of Gürlek village).

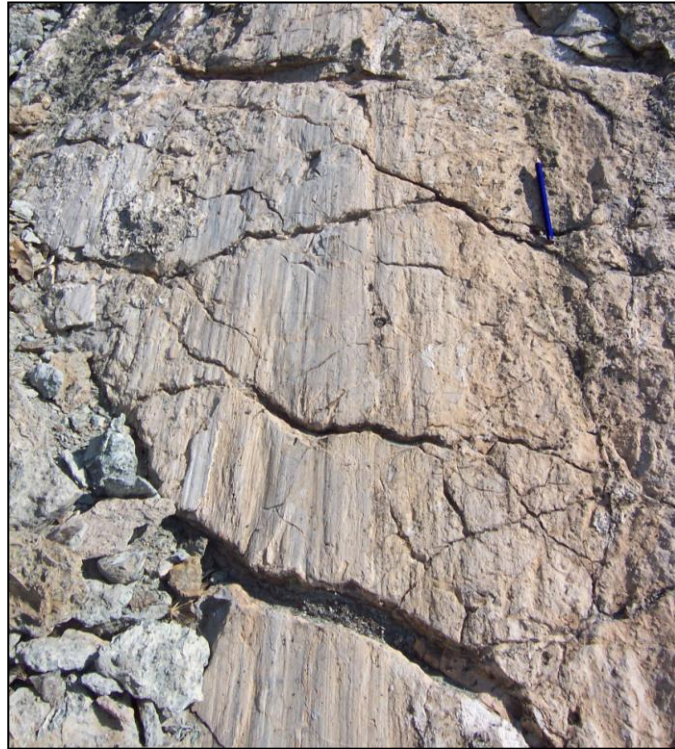


Figure 4.69. Close-up view of the Şaphane fault slickenside.

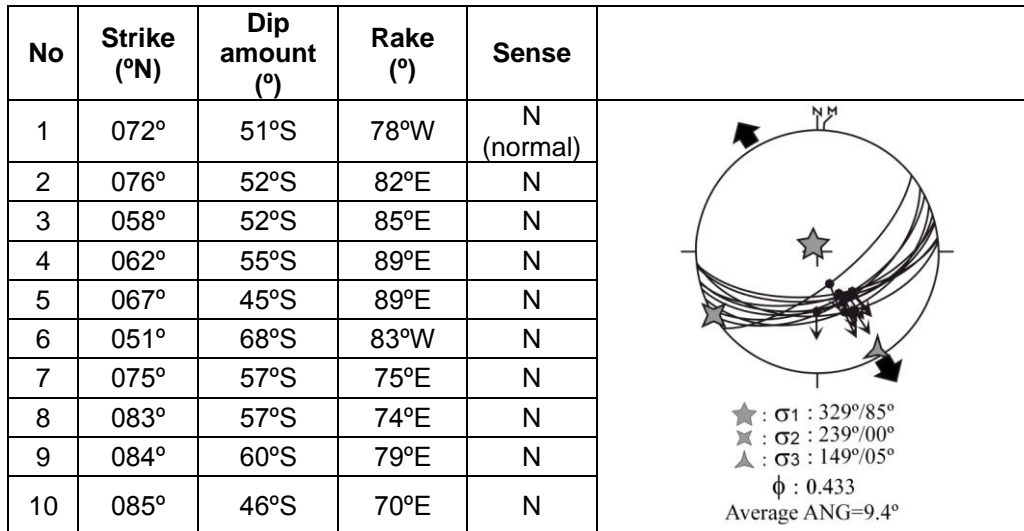


Figure 4.70. Stereographic plot of slip-plane data from Şaphane fault on the Schmidt's lower hemisphere net at, S.14 in Appendix – A.

4.3.2.2.3.2. Gürlek Fault

The Gürlek fault is named here. It is an about 3.5 km long, NE-SW-trending and southeasterly dipping normal fault with minor left-lateral strike-slip component (Figure 4.71). The Şaphane fault, the Gürlek fault and the Eskigediz fault are closely-spaced, parallel normal fault segment that marks a southerly-facing step-like morphology (Appendix – A). The Gürlek fault cuts and displaces basement rocks and juxtaposes them tectonically with the Erdoğan formation (Appendix – A). The Şaphane fault also displays well-preserved slip-lines (Figures 4.71 and 4.72). Their kinematic analyses are consistent with a reactivated structure; it is an oblique-slip normal fault, and suggests a NE-SW directed tension (Figure 4.73). Additionally, the Gürlek fault was moved by the 1970.03.28, $M_w=7.2$ Gediz earthquake.



Figure 4.71. General view of the Gürlek fault scarp and slickenside (view to NW) (S.15 in Appendix – A).



Figure 4.72. Close-up view of the Gürlek fault slickenside (S.15 in Appendix – A).

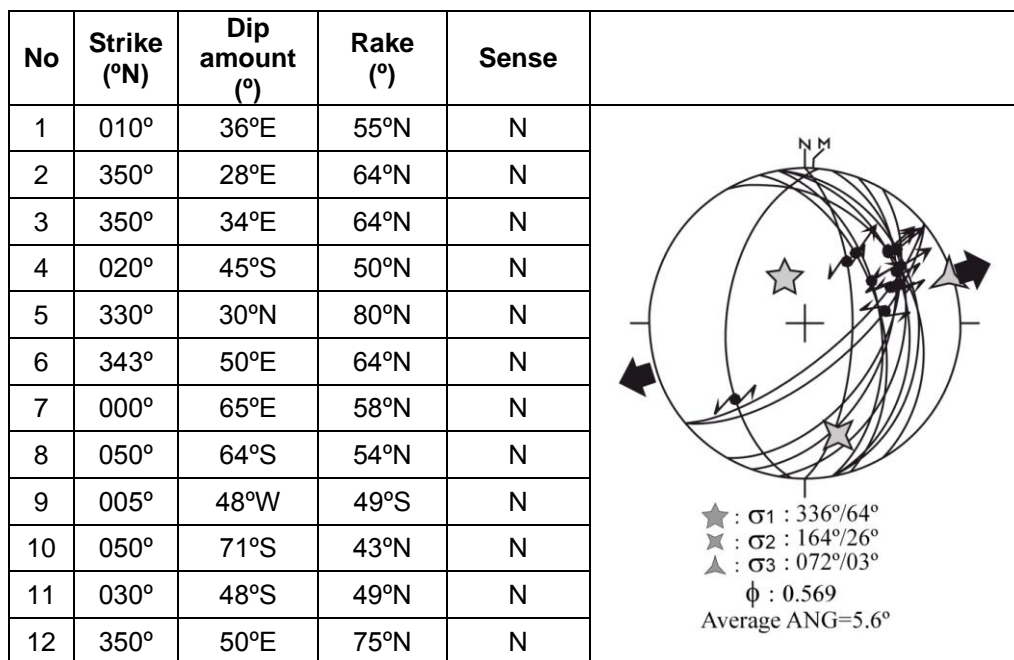


Figure 4.73. Stereographic plot of extensional slip-plane data from Gürlek fault on the Schmidt's lower hemisphere net, S.15 in Appendix – A.

4.3.2.2.3.3. Eskigediz Fault

The Eskigediz fault is named here. It is about 9 km long, NE-SW-trending and southeasterly dipping normal fault with minor amount of right-lateral strike-slip component (Figure 4.74). The Eskigediz fault is located in the area between Gürlek village in the SW and Eskigediz county in the NE (Appendix – A). The Eskigediz fault cuts and displaces basement rocks, pre- and modern graben infill and juxtaposes each other tectonically (Appendix – A). Sudden break in slope, steeply-sloping fault scarp, deflected stream beds, fault-parallel-aligned landslides and crushed-sheared rocks are common morphotectonic criteria used for recognition of the fault (Figures 4.74, 4.75 and 4.76). The Eskigediz fault also displays well-preserved slickenside (S.16 in Appendix – A). Stereographic plot of the slip-plane data on Schmidt's lower hemisphere net is consistent with an oblique-slip normal motion with minor amount of dextral strike-slip component and NNE-SSW directed extension (Figure 4.77). The Eskigediz fault is also seismically active as indicated by the 1970.03.28, Mw=7.2 Gediz earthquake.

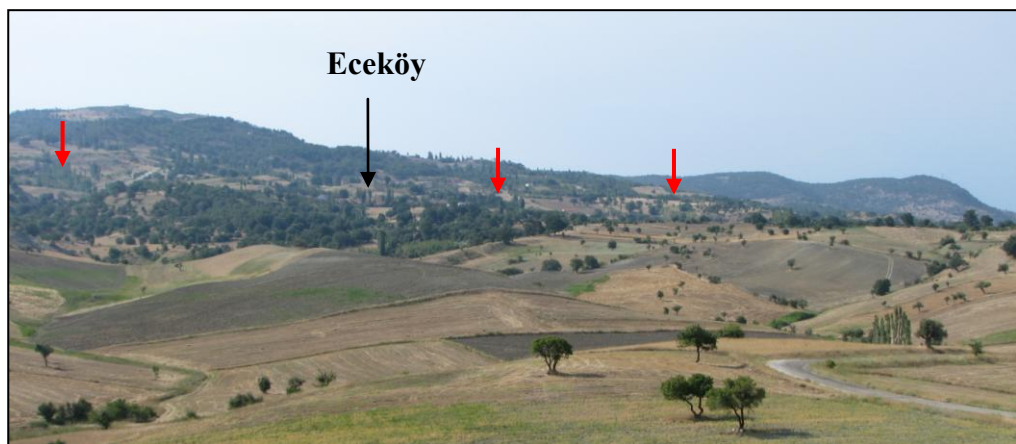


Figure 4.74. General view of the Eskigediz fault (view to NNW). Vertical red arrows show trace of the fault.

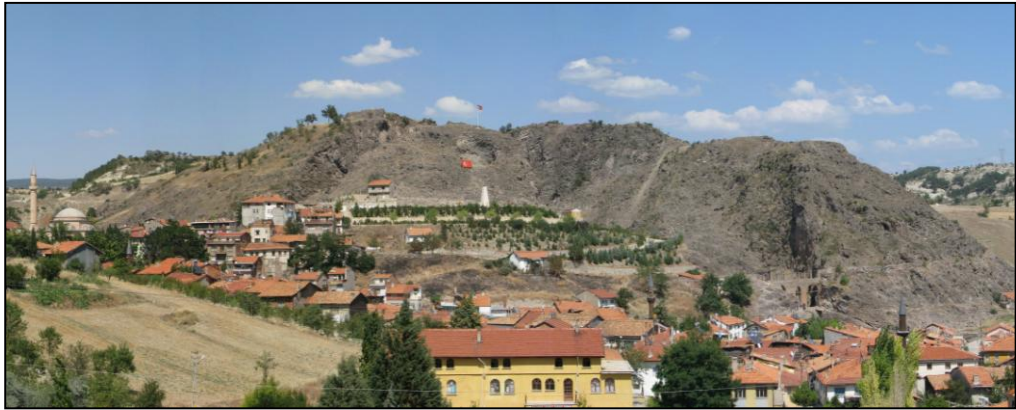


Figure 4.75. General view of the Eskigediz fault scarp cutting across the volcano-sedimentary sequence of Late Miocene age (settlement in foreground is Eskigediz county, view to NE).

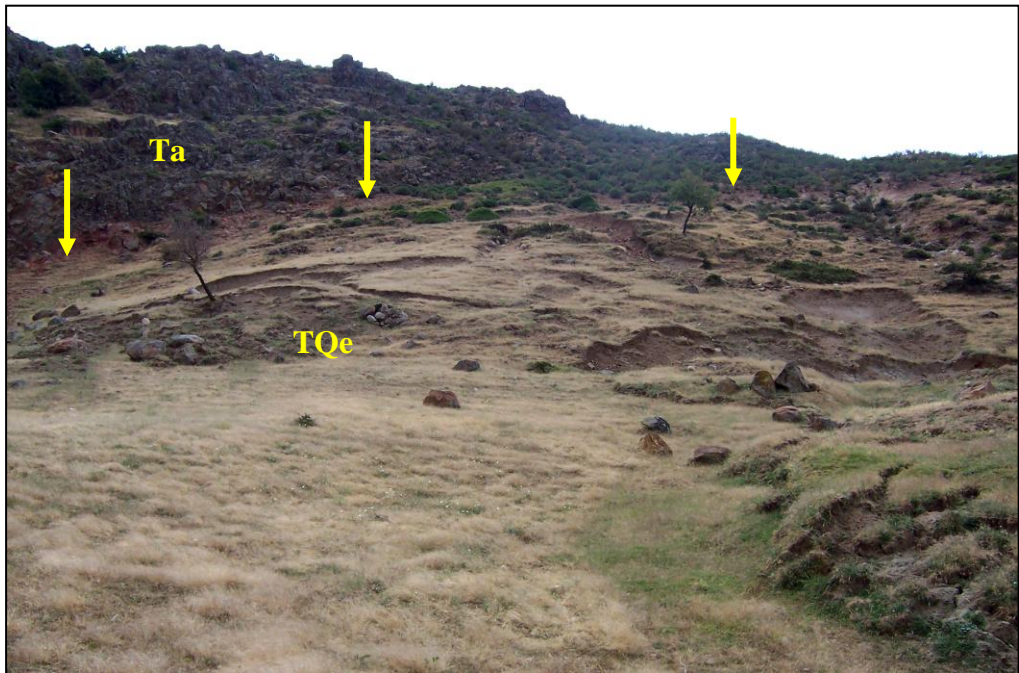


Figure 4.76. Landslides developed along the Eskigediz fault. In this locality, Eskigediz fault defines the boundary between volcano-sedimentary units (Ta) and Plio-Quaternary deposits (TQe) (yellow arrows indicate trace of the Eskigediz fault).

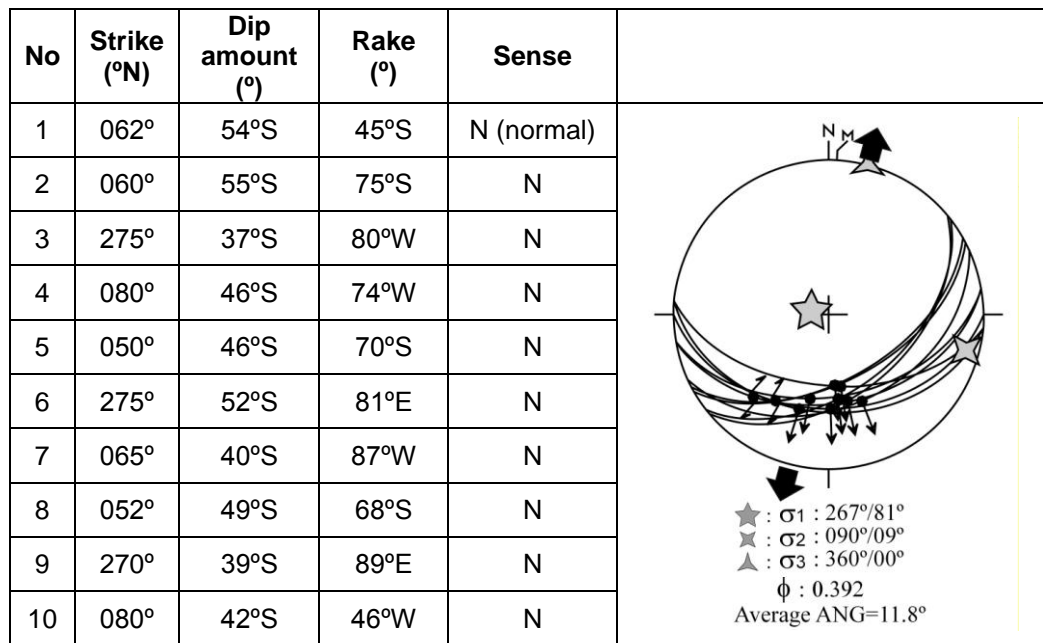


Figure 4.77. Stereographic plot of extensional slip-plane data from Eskigediz fault on the Schmidt's lower hemisphere, net S.16 in Appendix – A.

4.3.2.2.3.4. Çeltikçi Fault

The Çeltikçi fault is named here. It is about 6 km long, WNW-ESE-trending and southwesterly dipping normal fault with minor amount of right-lateral strike-slip component (Figure 4.78). It cuts and displaces the pre-modern and modern graben infill, displaces them in vertical direction, and juxtaposes tectonically (Appendix – A). Sudden break in slope, deflected stream beds, crushed and sheared rocks, steeply sloping fault scarp are common criteria used for recognition of the Çeltikçi fault. The Çeltikçi fault also displays well-preserved slickensides in places (S.17 and S.18 in Appendix – A). Two sets of slickenlines suggest that the Çeltikçi normal fault is a reactivated reverse fault. One of sets is the record of last palaeotectonic (contractional) phase, while the other set reveals the extensional neotectonic period. Stereographic

plots of both the first and second sets of slip-plane data (S.17 and S.18 in Appendix – A) indicates N-S compression, then NE-SW extension both the contractional palaeotectonic and extensional neotectonic configurations of the Çeltikçi fault, respectively (Figures 4.79 and 4.80).

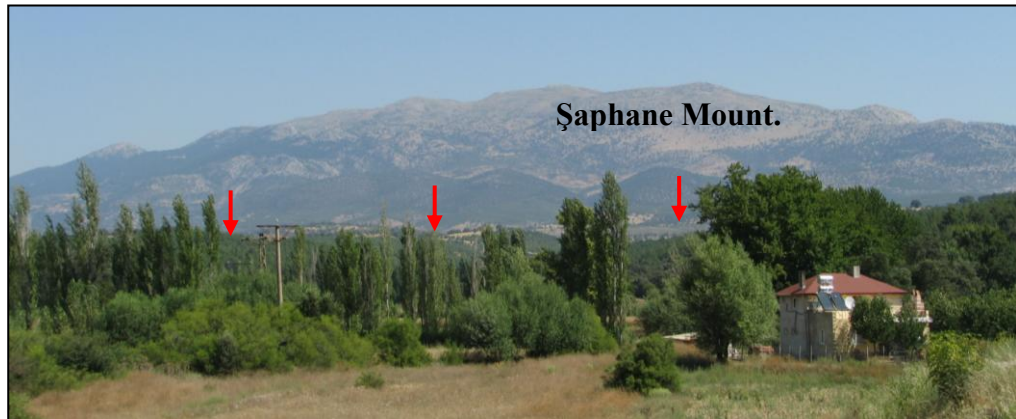


Figure 4.78. General view of the Çeltikçi fault scarp (view to N). Vertical red arrows point to fault trace.

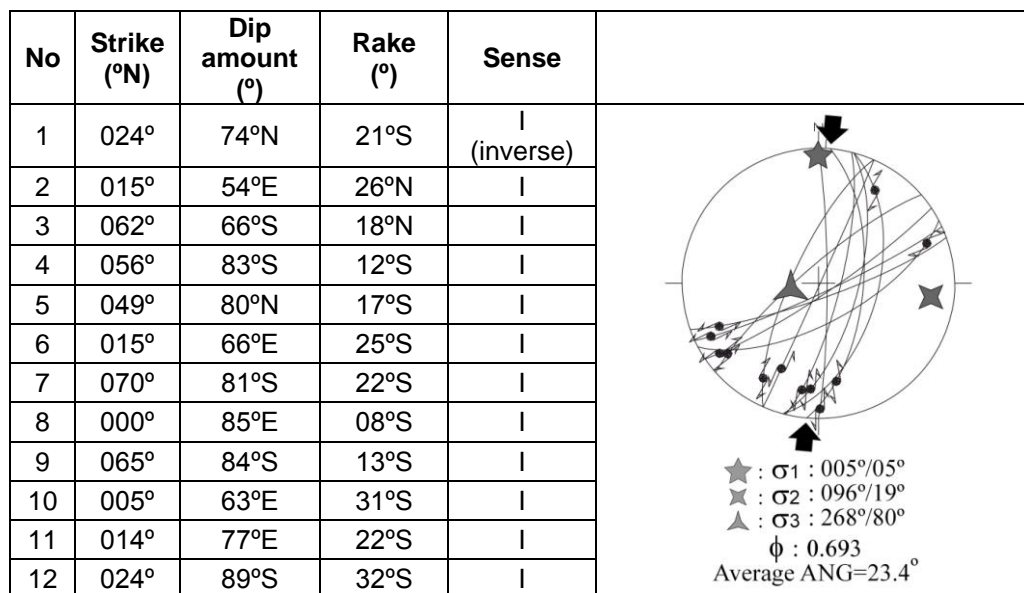


Figure 4.79. Stereographic plot of contractional slip-plane data from Çeltikçi fault on the Schmidt's lower hemisphere net S.17 in Appendix – A.

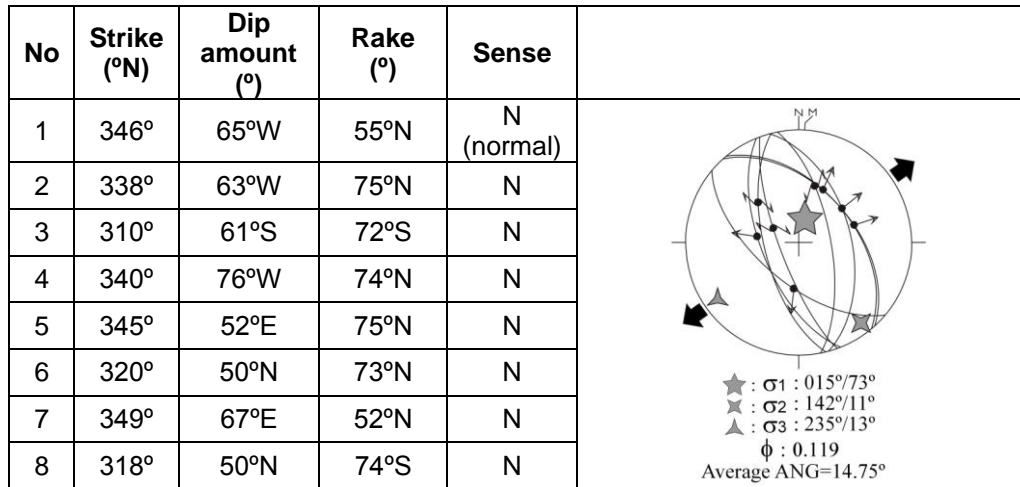


Figure 4.80. Stereographic plot of normal motion along Çeltikçi fault on the Schmidt's lower hemisphere net, S.18 in Appendix – A.

Furthermore, a relay ramp has though interaction of fault segments of the Şaphane fault zone. In the following lines, a summary of literature on relay ramp and their evolution will be given, and then a full description of new structure will form the subject of a new section.

4.3.2.2.3.5. Background on Relay Ramp

Relay ramp structure is defined that if two segments dip in the same direction, the transfer zone in between is called a relay ramp (Larsen, 1988; Peacock and Sanderson, 1991, 1994) or a synthetic transfer zone (Morley *et al.*1990) (Figure 4.81). Widths of relay ramps between overstepping normal faults follow a power-law (fractal) relation from millimetre scales to tens or hundreds of kilometers (e.g., Peacock and Sanderson, 1994; Schlische *et al.*, 1996; Peacock, 2003). Although Larsen (1988) explained relay ramps by means of listric faults with a common detachment, a relay structure can form between two separate

planar normal faults (Figure 4.81) (Peacock and Sanderson, 1991; Çiftçi and Bozkurt, 2007).

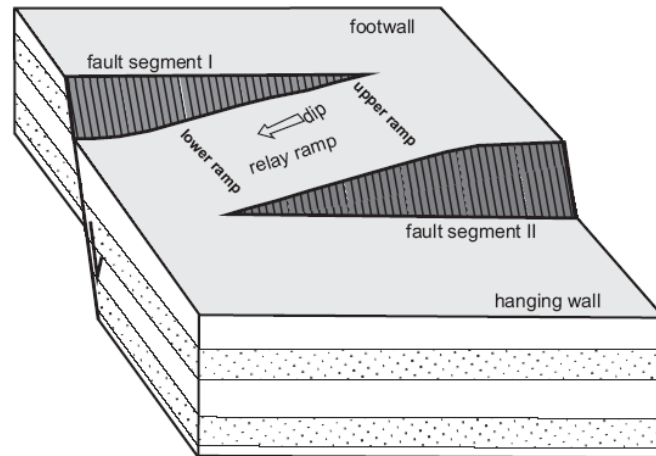


Figure 4.81. Block diagram of two overstepping normal fault segments dipping in the same direction. Displacement among the fault segments is transferred by formation of a relay ramp (Bozkurt and Çiftçi, 2007).

The terms '*soft-linked*' and '*hard-linked*' characterize the two different geometries at the end of the relay ramp formation (Gibbs, 1984; Walsh and Watterson, 1991). Soft-linked segments are characterized by a distributed deformation of a relay ramp without a breaching fault (Figures 4.81, 4.82A and B). However, hardlinked segments include a breaching fault that cuts through the relay ramp and links the individual segments (Figure 4.82D and E). Soft-linked segments may become hard-linked segments through time in an evolution of relay ramp (Peacock and Sanderson, 1994). Four different stages were described through soft-linked to hard-linked evolution (Figure 4.82; Peacock and Sanderson, 1991, 1994). The primary factors controlling the breaching of a relay ramp can be underlined as slip vectors and displacement gradients of overlapping faults that bound the ramp area (Ferrill and Morris, 2001). Depending on the stress conditions at the overlap area,

breaching may take place either at the upper ramp or at the lower ramp with abandonment of the other.

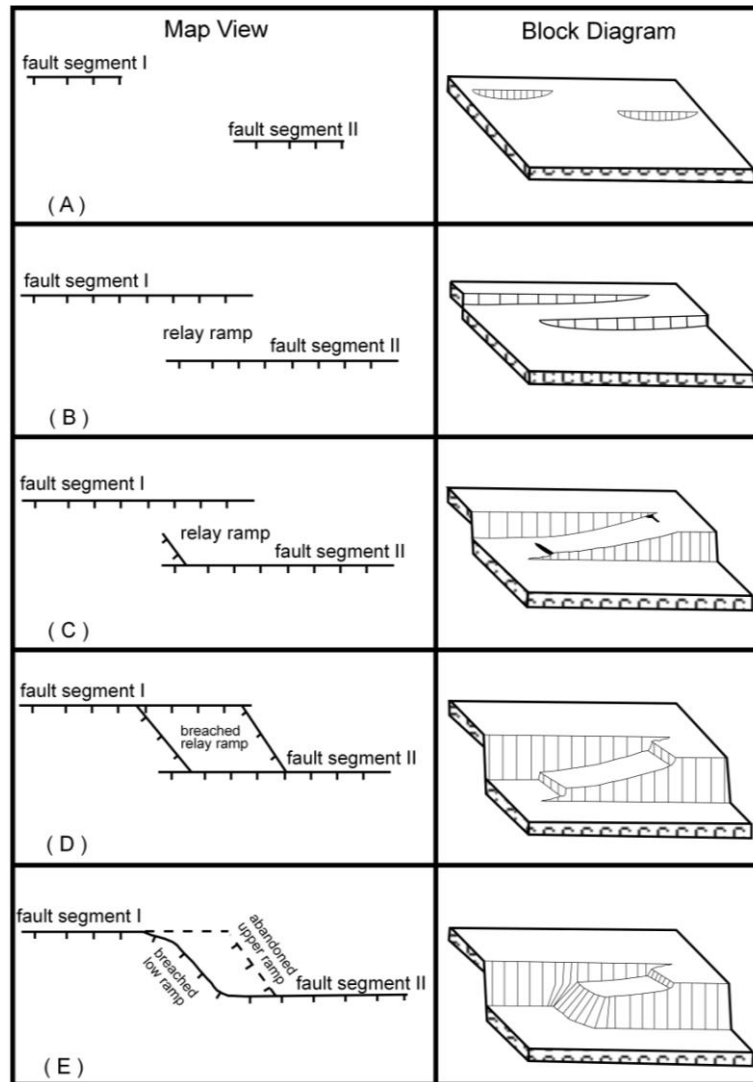


Figure 4.82. Schematic diagram to show the evolutionary stages of a relay ramp. (A) There is no interact between faults; (B) The faults have started to interact and a relay ramp developed to transfer the displacement among the segments; (C) The initiation of fracturing resulted from accumulated strain between faults; (D)The relay ramp is broken by a breaching fault to form a single fault zone with strike irregularity; (E) Upper bench is abandoned and two segments joined through breaching of lower ramp that form an along strike bend on the course of the main fault (Çiftçi and Bozkurt, 2007).

A new relay ramp structure is described between Şaphane and Gürlek faults. They are nearly parallel and dip in the same direction (~S).

4.3.2.2.3.6. Şaphane Relay Ramp

Knowledge of the geometry of fault segments is important to understand fault zone development (Peacock and Sanderson, 1991). This sentence is the best to describe the strange shape of the Şaphane fault zone. It is approximately SE-dipping and convex towards southeast direction (Appendix – A). Two parallel faults in Şaphane fault zone (Şaphane and Gürlek fault) bounds the relay structure (Figure 4.83). Another interesting observation is that there are two breaching fault to produce the convex Şaphane fault zone; the first one is between Şaphane and Gürlek faults, another one is Gürlek fault and Yumrutaş fault (Figure 4.83). During field study, first breaching fault (1 in Figure 4.83) surface has been observed in a quarry (Figure 4.84) but second one (2 in Figure 4.83) has been observed in a limited part (Figure 4.85). Hence, for the second breaching fault fracture measurements are used to identify it.

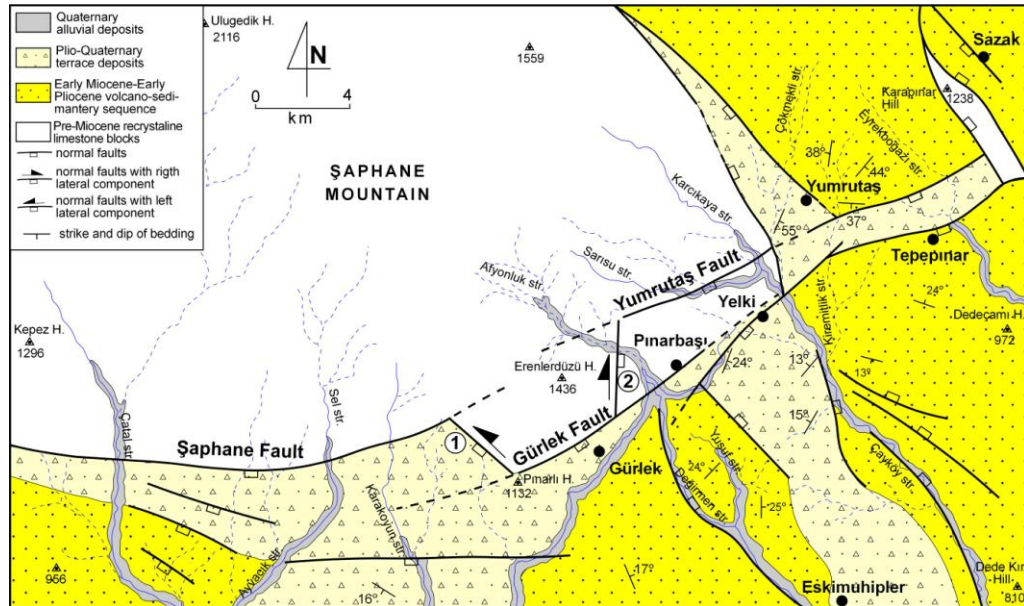


Figure 4.83. Geological map of the area around Şaphane relay ramp.



Figure 4.84. Field photograph showing the first breaching fault (view to N).

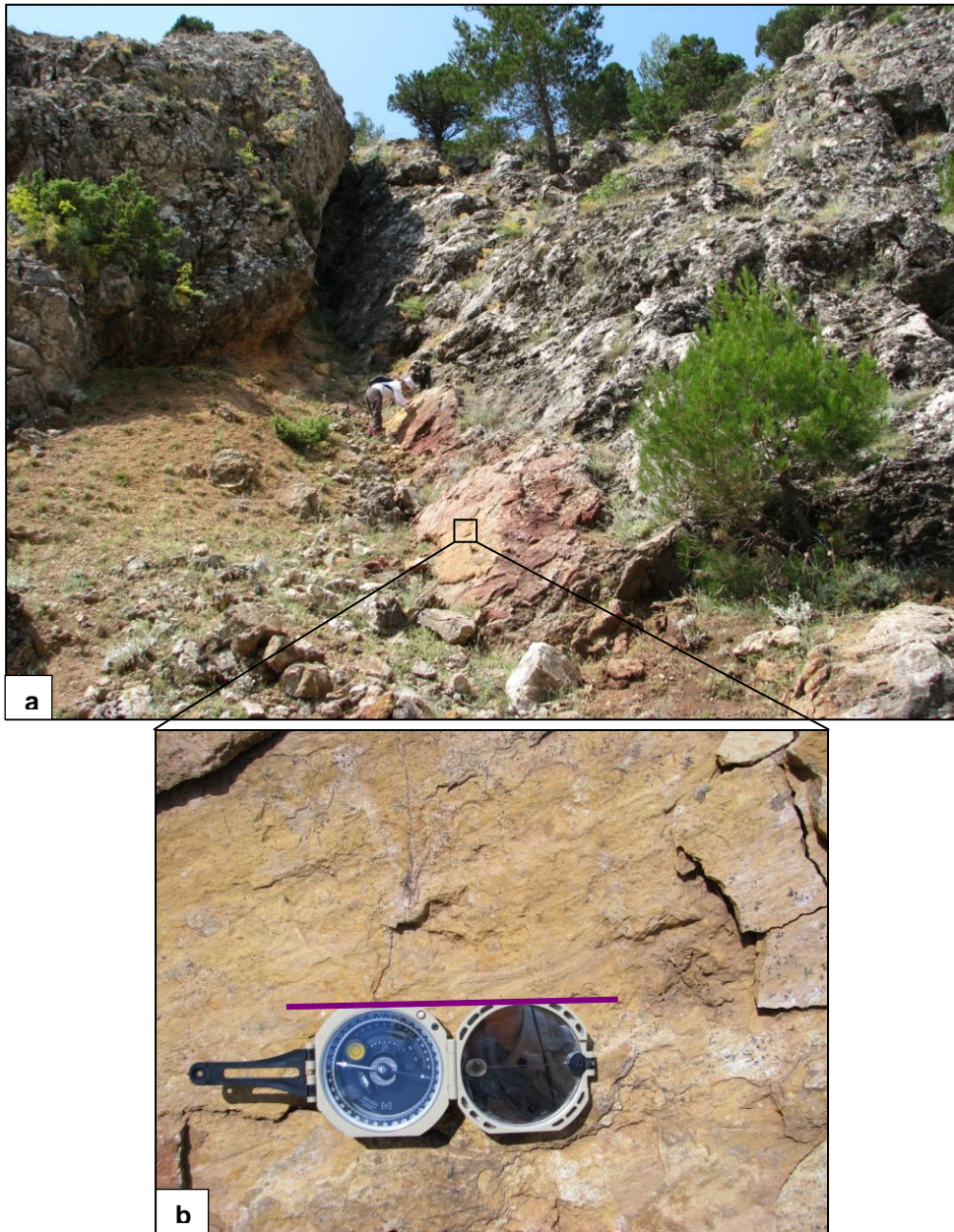


Figure 4.85. a) Field photograph showing the second breaching fault (view to S), b) Close-up view of the slickenside (purple line indicate the strike of fault plane).

For each breaching fault, two types of motion have been measured from the fault surfaces (slickensides). They are older normal and strike-slip motion based on their overprinting relationship. According to

stereoplot results, regional extension direction is NNE-SSW (Figure 4.86.a and b), but local stress anomalies indicate ENE-WSW directed orientation (Figure 4.87.a and b).

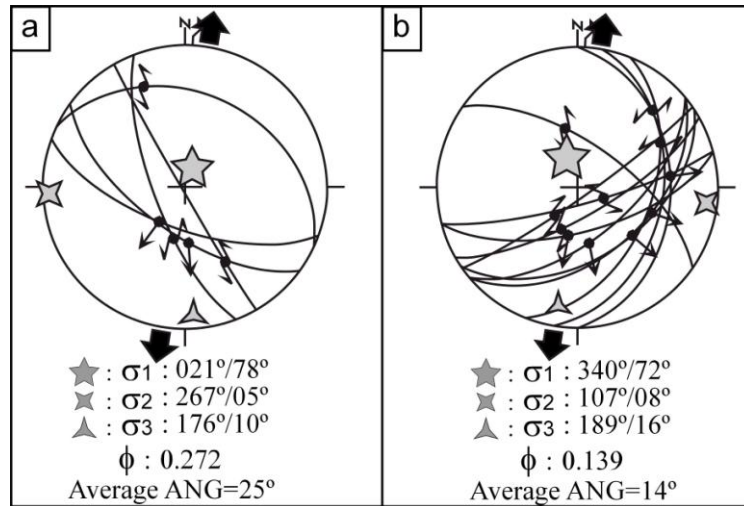


Figure 4.86. Stereoplots illustrating fault slip-data from Şaphane and Gürlek faults. Regional extension direction is NNE-SSW.

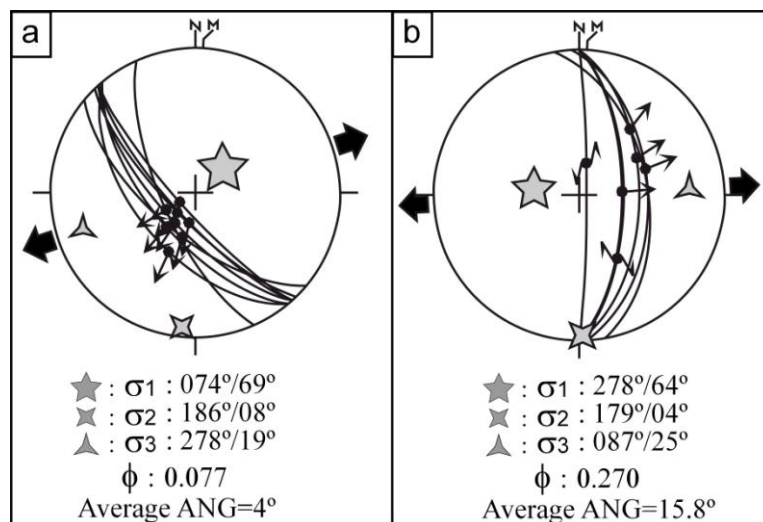


Figure 4.87. Stereoplots illustrating fault slip-data from breaching fault to show the local stress anomalies.

Şaphane relay ramp is characterized by two main breaching and ramp-related faults and fracture zones that exhibit significant orientation shifts from ~ E-W-trend of the bounding fault zone. Based on regional stress field, fault data (slickenlines) and fractures acquired from the breaching faults, roughly E-W-oriented structures conformable with the ~N-S- and NE-SW-oriented extension (4.86).

The recent configuration of the Şaphane relay ramp is the most diagnostic structure. The formation stages and distinct deformation styles at the ramp area have been summarized in Figure 4.88.

Northern margin boundary structure (Şaphane fault zone) of the Erdoğmuş-Yenigediz graben is significant for the formation of graben. The fault segments are dipping in the same direction and two main breaching faults are constructed in this fault zone. Various scaled faults and fractures are observed in the Şaphane relay ramp. Moreover, single faults for both breaching areas are observed. On both breaching fault surfaces, two different slip motions have been detected which are older normal (Figure 4.89a) and younger strike-slip motion (Figure 4.89b). Probably, progressive fracturing and faulting yielded this data. Even some variations on the stress field based on these slip-plane measurements are presented, approximately N-S extension along the ~ E-W-trending faults are obtained. Therefore, progressive evolution of stress field changes at the ramp area probably follows the ramp evolution stages as suggested by Peacock and Sanderson (1991, 1994). The observed field relations in the study area clearly show that the stress field at the relay ramp displays some variations. The differential displacement in relay ramp have been accommodated by the deformation. This is directly related to both local and regional strain change.

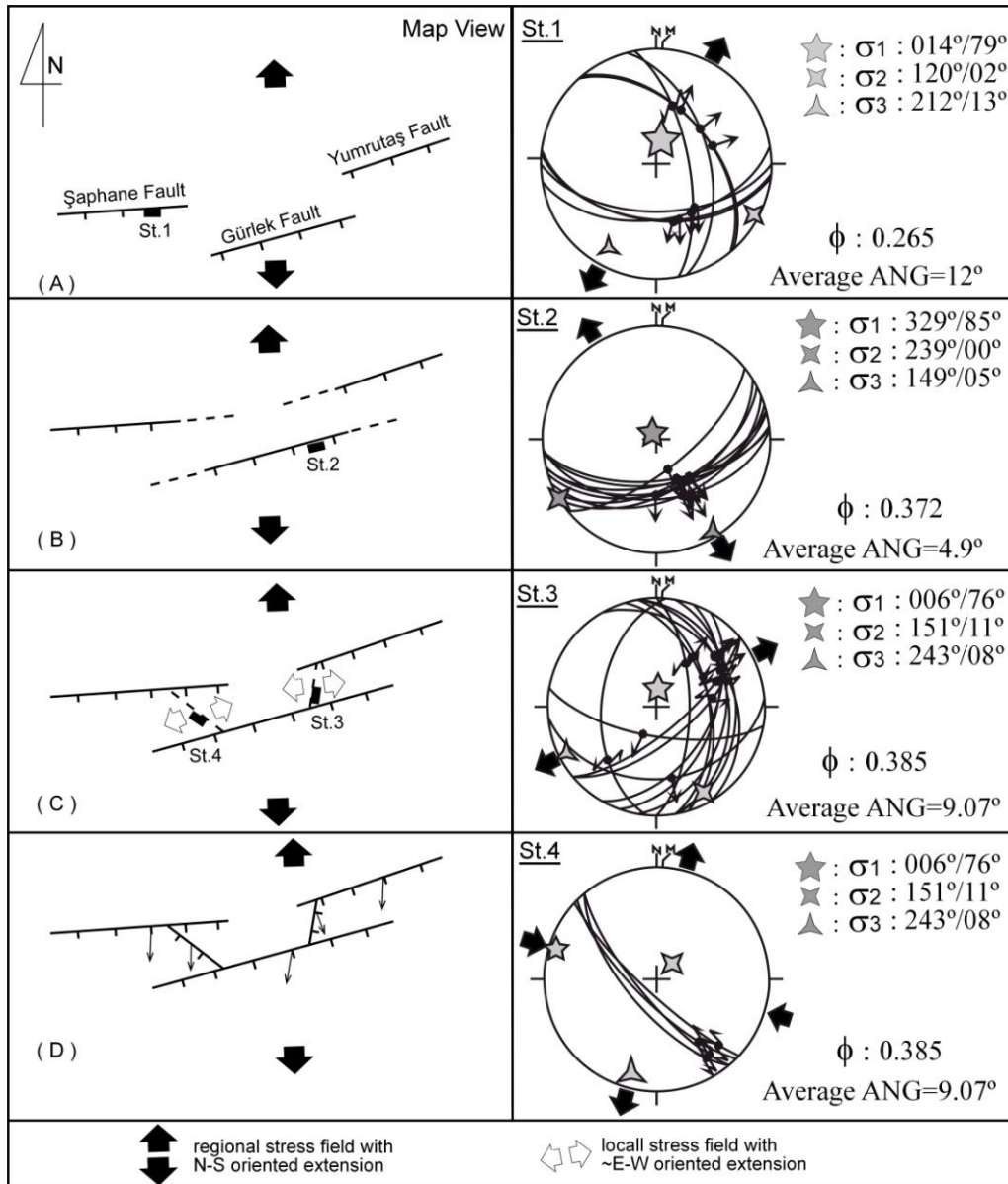


Figure 4.88. Formation stages of Şaphane relay ramp and related stress orientations. (A) There is no interaction between fault segments and stereographic plot of slip-plane data from Şaphane fault indicates regional stress direction at station 1 (St.1); (B) The faults have started to interact and two relay ramps developed to transfer the displacement among the segments and stereographic plot of slip-plane data from Gürlek fault indicates regional stress direction at station 2 (St.2); (C) The initiation of fracturing resulted from accumulated strain between fault segments; (D) The relay ramps are broken to form a single fault zone with strike irregularity.

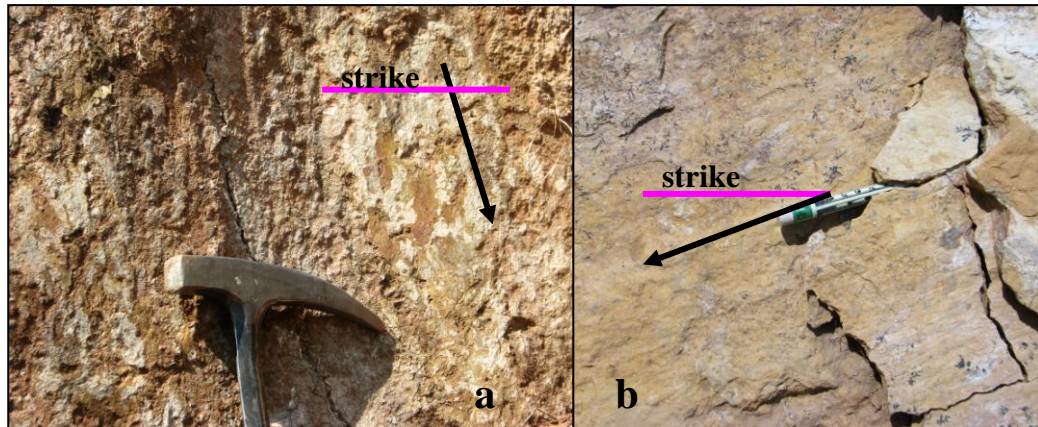


Figure 4. 89. Two different slip motion along the breaching fault; a) older extensional motion, and b) younger strike-slip motion at St. 4 in Figure 4.88 (C) and (D), respectively.

4.3.2.2.4. YEŞİLOVA FAULT ZONE

Yeşilova fault zone is an about 4 km wide, 44 km long and NW-trending zone of active deformation characterized by normal faulting. It is located between Göynük in the southeast and Hisarcık County in the northwest. The 20-km-long northwestern part of the fault zone lies outside the study area while its 24 km long northeastern part is included within the study area where controls the northeastern margin of the Erdoğan-Yenigediz graben (Figure 4.2). The fault zone mainly consists of closely-spaced (1-3 km), diverse-sized (2-18 km), NW-trending and southwesterly dipping *en-échélon* fault segments. They composed of longer and *en-échélon* fault segments is linked to each other by an intervening another fault set composed of numerous, closely-spaced (0.2-3 km), shorter (1.5-10 km), easterly and westerly dipping and NNE-trending fault segments. The Upper Paleozoic metamorphic rocks, Cretaceous ultramafic rocks and the Miocene-Quaternary graben infill are cut and displaced in vertical direction up to 0.5 km and tectonically juxtaposed by its segments. The linear to curvi-linear fault trace,

steeply-sloping fault scarp, triangular facets, sudden break in slope, graben-ward facing step-like land shape, diverted to offset stream courses, sheared and intensely crushed strips of fault rocks, tectonic juxtaposition of older rocks with the Plio-Quaternary travertine and alluvial sediments are common criteria used for the recognition of the Yeşilova fault zone (Figure 4.90). In addition, closely-spaced several fault segments comprising the Yeşilova-Hisarcık section of the fault zone were also reactivated during the 1970.03.28 $M_w=7.2$ Gediz earthquake (Ambraseys and Tchaleko 1972).

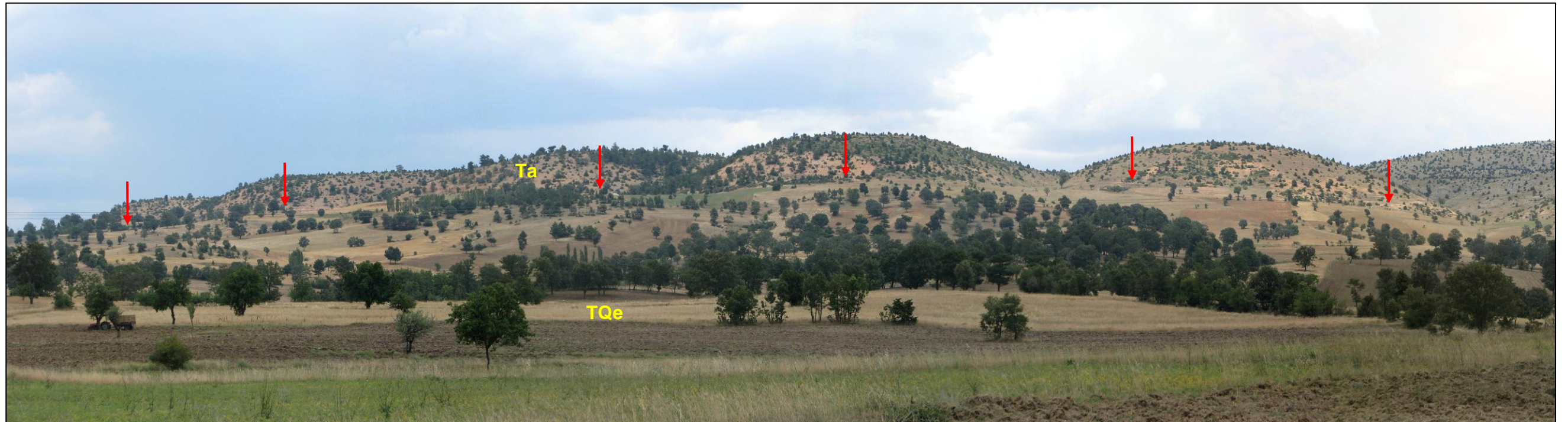


Figure 4.90. General view of the Yeşilova fault zone (view to N). Vertical red arrows point to trace of the master fault (Ta: Arıca formation; TQe: Erdoğanlı formation).

4.3.2.2.4.1. Yeşilova Fault

The Yeşilova fault is named here. It is about 6 km long, WNW-ESE-trending and southwesterly dipping normal fault (Figure 4.91). The fault determines the boundary between pre-modern and modern graben infill. It cuts across the travertine deposits. Sudden change in the slope, occurrence of young travertine deposits on hanging wall blocks of the fault and tectonic juxtaposition of units of dissimilar age and facies are common morphotectonic criteria used for recognition of the Yeşilova fault.

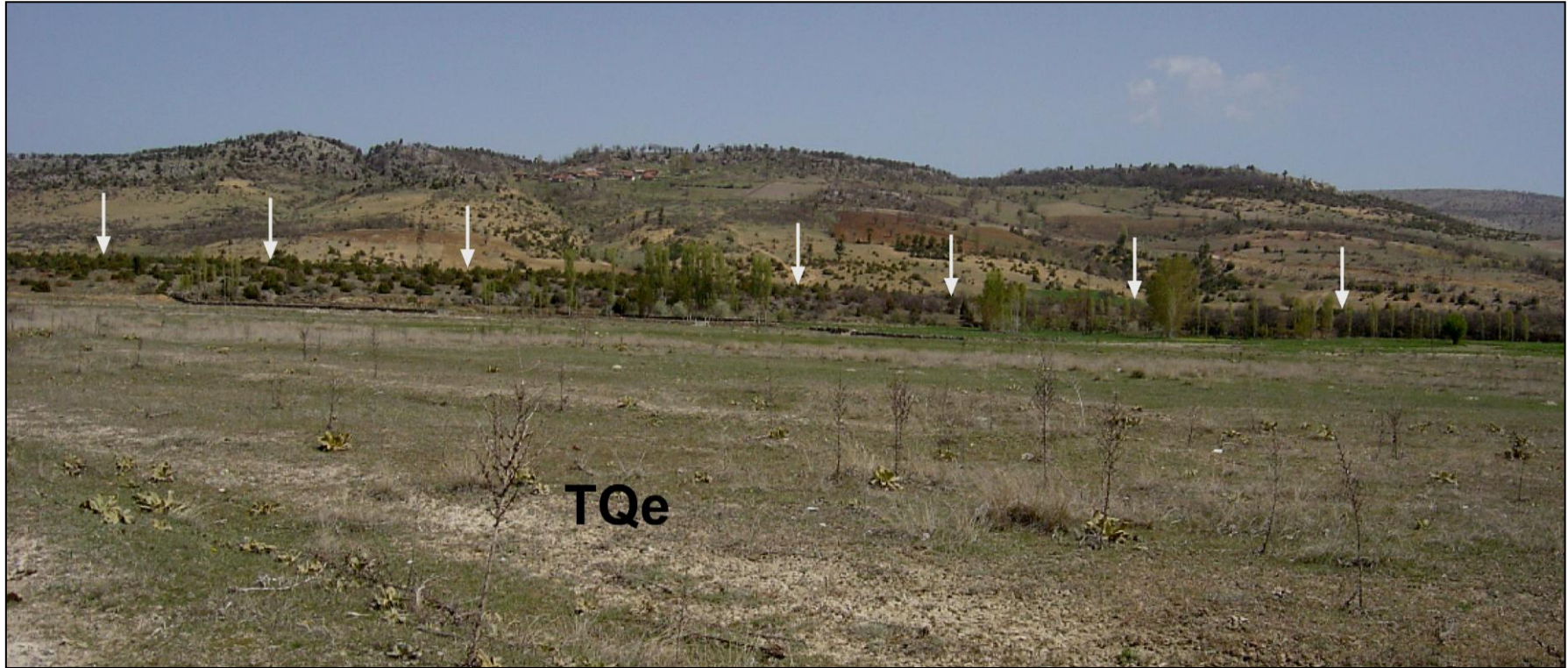


Figure 4.91. General view of the Yeşilova fault scarp. The vertical arrows indicate trace of master fault, along which older rocks were tectonically juxtaposed with the nearly flat-lying Plio-Quaternary travertine (TQe) (NNE of Yeşilova settlement, view to E).

4.3.2.2.4.2. Akkaya Fault

The Akkaya fault is named in the present study. It is an approximately 5 km long, NW-SE-trending and southwesterly dipping left-lateral strike-slip fault with normal component (Figure 4.92). The Akkaya fault cuts and displaces both pre- and modern graben infill, and juxtaposes them each other tectonically in places (Appendix – A). Sudden change in slope, steeply sloping fault scarp, deflected drainage system, triangular facets, crushed to sheared rocks, uplifted and fault-suspended terrace conglomerates are common morphotectonic criteria used for recognition of the Akkaya fault. The Akkaya fault also displays well-preserved slickenside in places (Figure 4.93, S.19 in Appendix – A). The slip-plane data are clearly showing that the Akkaya fault is a strike-slip fault, along which the Erdoğan-Yenigediz graben is being extended in NNE-SSW direction (Figure 4.94).



Figure 4.92. General view of the Akkaya fault zone (view to NE). Vertical red arrows point to trace of the fault.



Figure 4.93. Close-up view of the Akkaya fault slickenside (see S.19 in Appendix – A for location).

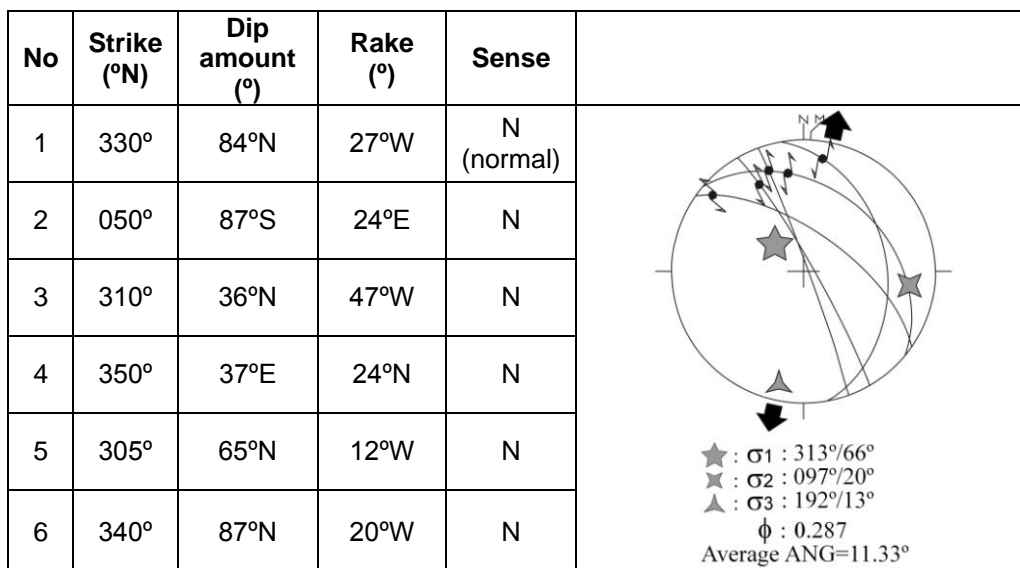


Figure 4.94. Stereographic plot of slip-plane data from Akkaya fault on the Schmidt's lower hemisphere net, S.19 in Appendix – A.

4.3.2.2.4.3. Güzüngülü Fault

The Güzüngülü fault is named in the present study. It is an approximately 6 km long, NW-SE-trending and southwesterly dipping left-lateral strike-slip with normal component (Figure 4.95). The Güzüngülü fault is located in the area between Hacivat Hill in the west and Güzüngülü village in the east (Appendix – A). It cuts and displaces the sedimentary and volcanic facies of the pre-modern graben (Figure 4.96) and juxtaposes them tectonically. The Güzüngülü fault displays well-developed slickenside in places (Figures 4.97, S.20 in Appendix – A). The slip-plane data indicate that it is a left-lateral strike-slip with normal component (Figure 4.98).



Figure 4.95. General view of the Güzüngülü fault zone (view to NE). Vertical yellow arrows point to trace of the fault.



Figure 4.96. The Güzüngülü fault forms the boundary between volcanics (basalt) and lacustrine (marl-limestone) deposits (location: ~1 km SW of Yaylaköy village on the Kütahya-Uşak highway). Yellow dash line indicates the site of Güzüngülü fault.



Figure 4.97. Close-up view of the Güzüngülü fault slickenside (see S.20 in Appendix – A for location).

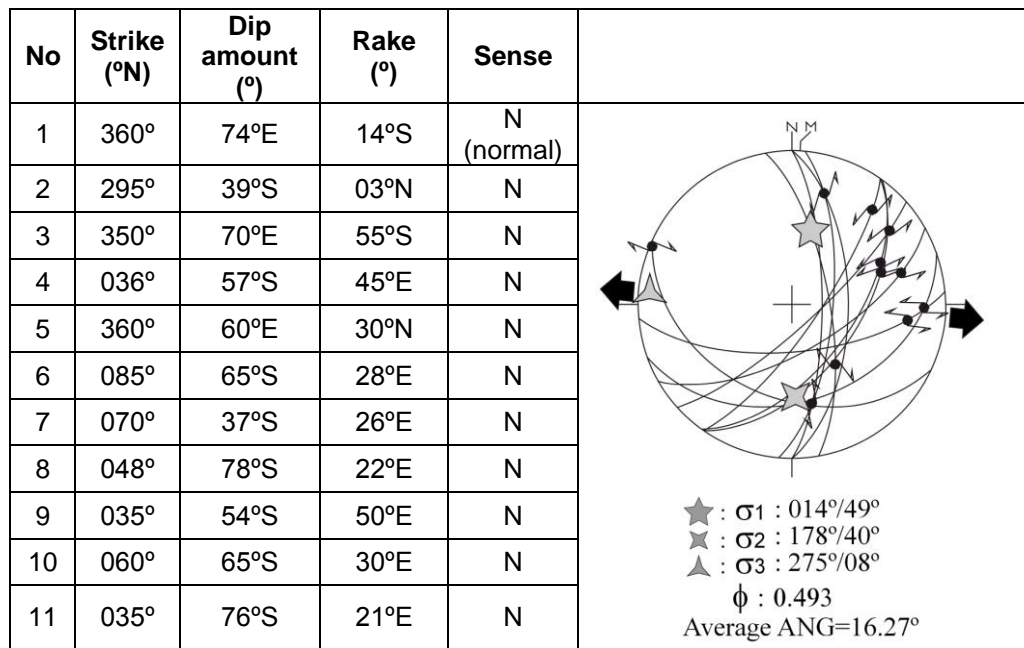


Figure 4.98. Stereographic plot of extensional slip-plane data from Güzüngülü fault on the Schmidt's lower hemisphere net, S.20 in Appendix – A.

4.3.2.2.4.4. Akçaalan Fault

The Akçaalan fault is named in the present study. It is an approximately 6 km long, NW-SE-trending and northeasterly dipping normal fault (Figure 4. 99). It is located in the area between Midilli Hill in the NW and the upstream side of Gediz Çayı in the SE (Appendix – A). The Akçaalan fault cuts and displaces both the pre- and modern graben infill. Sudden break in slope, fault-parallel-aligned landslides, steeply sloping fault scarp, deflected to offset stream beds, sudden change in strike and dip amount of bedding, uplifted and fault-suspended terrace conglomerates are common morphotectonic criteria used for recognition of this fault.

The Akçaalan fault displays well-preserved slickenside in places (S.21, S.22 and S.23 in Appendix – A). Three sets of overprinted slickenlines were observed on the Akçaalan slickenside. These sets are the 1st phase of extension (palaeotectonic extension), 1st phase of contraction (last palaeotectonic phase) and the 2nd phase of extension (neotectonic extension) respectively (Figures 4.100, 4.101, 4.102 and 4.103). The kinematic analyses of slip-plane data also indicated that the Akçaalan fault is an originally older normal fault but later on, it has experienced reverse and again normal faulting in time.

The Akçaalan fault was moved and caused heavy damage to the structures in and around Akçaalan village during the 1970.03.28 Gediz earthquake. It also caused ground surface ruptures with vertical displacements up to 2 m (Figure 4.104).

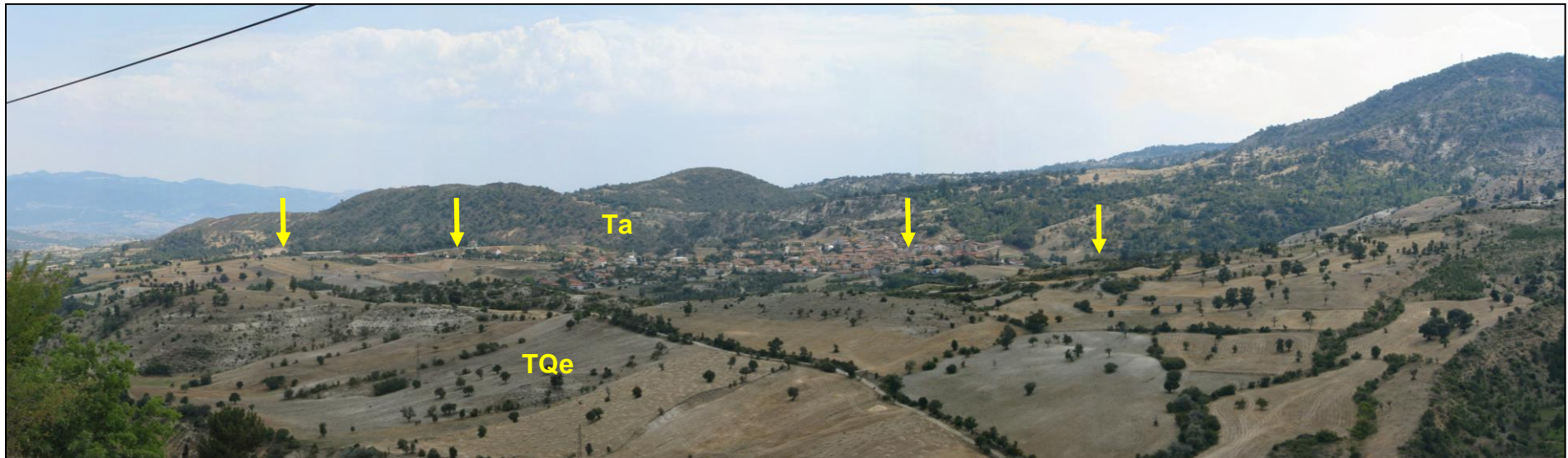


Figure 4.99. General view of the Akçaalan fault scarp and trace (view to SW). Vertical yellow arrows point to trace of the fault. The settlement in background is Akçaalan village. The Akçaalan fault defines the boundary between pre-modern (Ta) and modern graben infill (TQe).

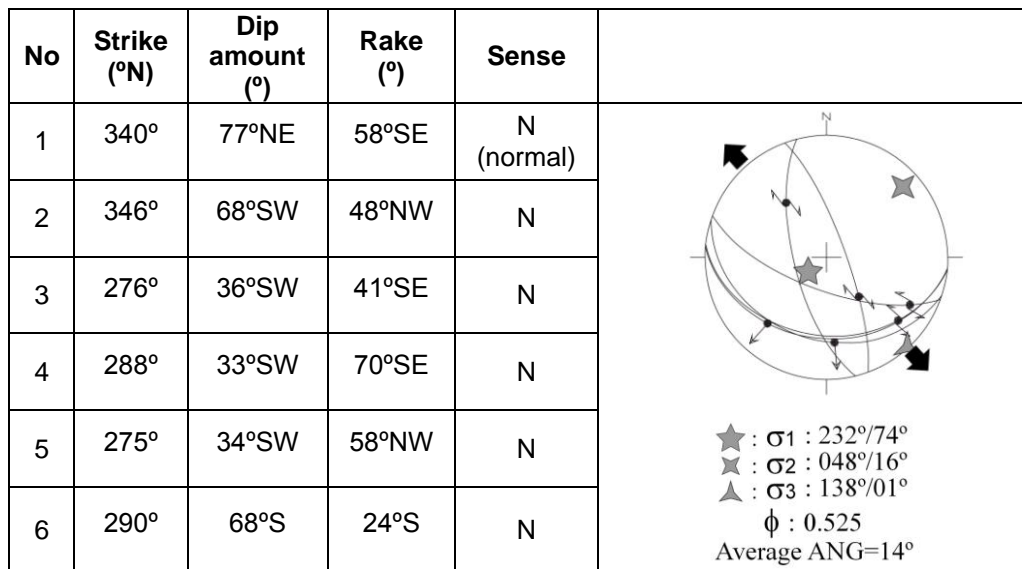


Figure 4.100. Stereographic plot of 1st phase of extensional slip-plane data on the Schmidt's lower hemisphere net, S.21 in Appendix – A.

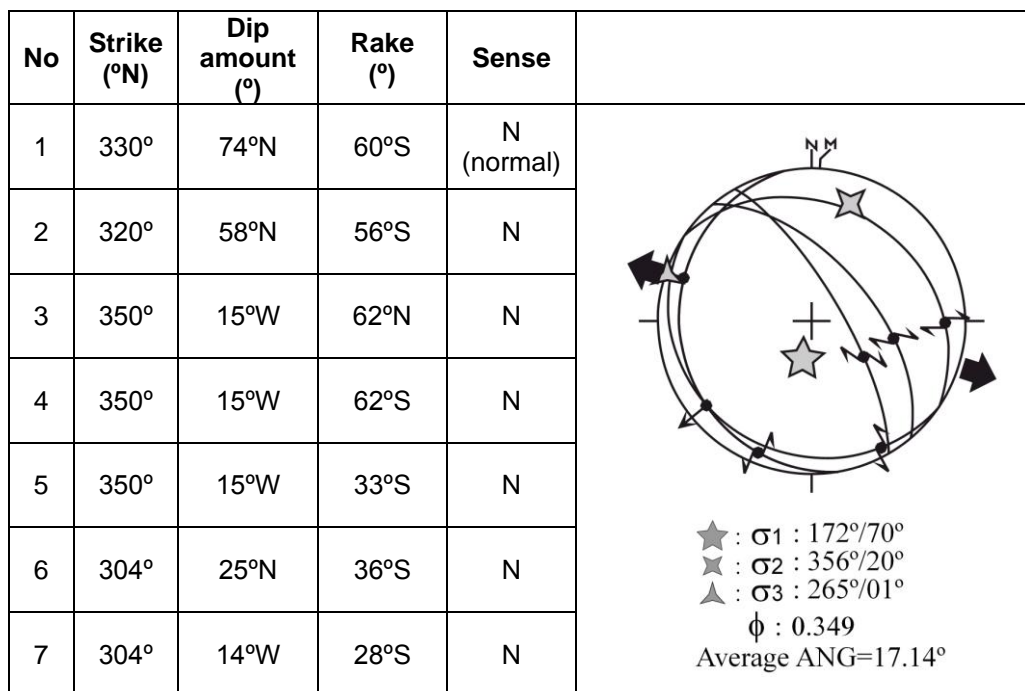


Figure 4.101. Stereographic plot of extensional slip-plane data on the Schmidt's lower hemisphere net, S.22 in Appendix – A.

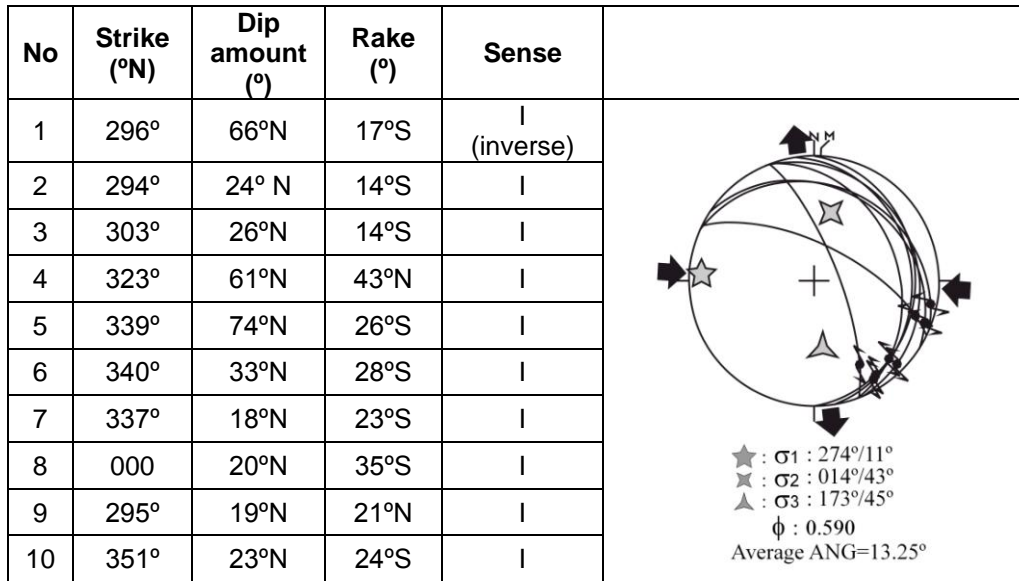


Figure 4.102. Stereographic plot of contractional slip-plane data on the Schmidt's lower hemisphere net, S.23 in Appendix – A. Large black arrows indicate palaeotectonic contraction direction along the Akçaalan fault.

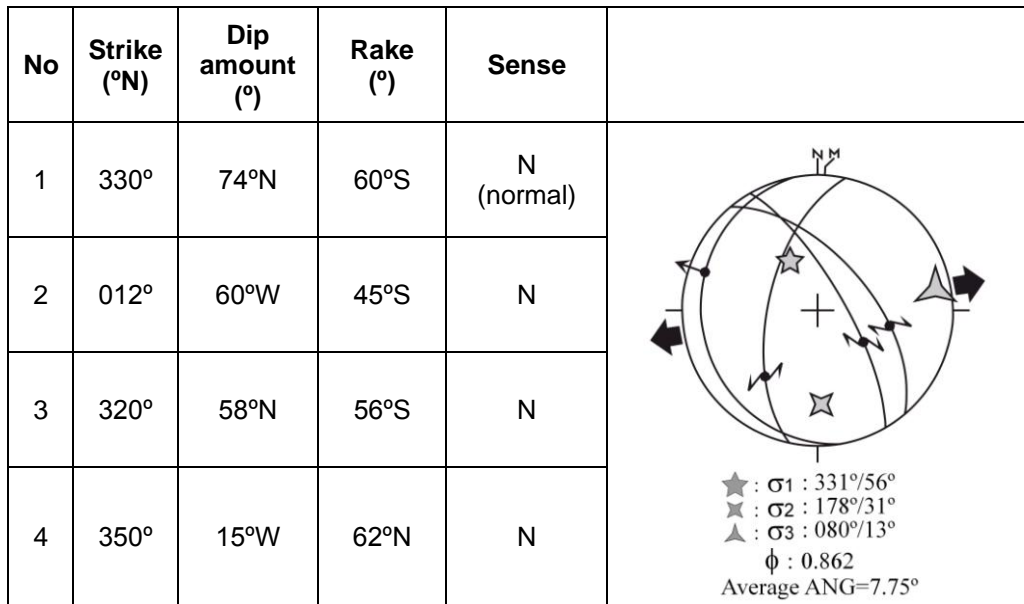


Figure 4.103. Stereographic plot of extensional (2nd phase) slip-plane data on the Schmidt's lower hemisphere net, S.24 in Appendix – A. Large black arrows indicate neotectonic extension (2nd phase of extension) direction along the Akçaalan fault.



Figure 4.104. Close-up view of ground surface rupture (~ 2 m vertical displacement) of the 1970.03.28, $M_w=7.2$ Gediz earthquake in the far northwest of Akçaalan village (courtesy of Prof. Dr. James Jackson).

4.3.2.2.4.5. Aşıkpaşa Fault

The Aşıkpaşa fault is named in the present study. It is an approximately 4 km long, NW-SE-trending and northeasterly dipping normal fault (Figure 4.105). The Aşıkpaşa fault is located between near west of Soğuksu village in the west and Kayayanı Hill in the SE (Appendix – A). It cuts both the Upper Cretaceous ophiolitic mélange and pre-modern graben infill and juxtaposes them with to each other. Sudden break in slope, deflected stream beds, steeply sloping fault scarp, crushed to pulverized rocks are common morphotectonic criteria used for recognition of the Akçaalan fault. It was moved and caused development of ground surface ruptures (Figure 4.106) by the

1970.03.28, $M_w=7.2$ Gediz earthquake, i.e. the Aşıkpaşa fault is also seismically active.



Figure 4.105. General view of the Aşıkpaşa fault scarp and trace (view to SW). Vertical yellow arrows point to trace of the fault.



Figure 4.106. Close-up view of the ground surface rupture along the Aşıkpaşa fault moved by the 1970.03.28, $M_w=7.2$ Gediz earthquake in the far west of Aşıkpaşa village (courtesy of Prof. Dr. James Jackson, 2010).

4.3.2.2.4.6. Sazak Fault

The Sazak fault is named in the present study. It is an approximately 7 km long, NNW-SSE-trending and northeasterly dipping normal fault (Figure 4.107). The Sazak fault is located in the area between Karasu stream in the NW and Eceköy in the SE (Appendix – A). It cuts and displaces the Upper Cretaceous ophiolitic mélangé, pre- and modern graben infill displaces them in vertical direction and juxtaposes tectonically with each other. The fault displays slickenside in places. The stereographic plot of slip-plane data on Schmidt's lower hemisphere net indicated that the Sazak fault is an oblique-slip normal fault, and E-W extension direction (Figure 4.108).

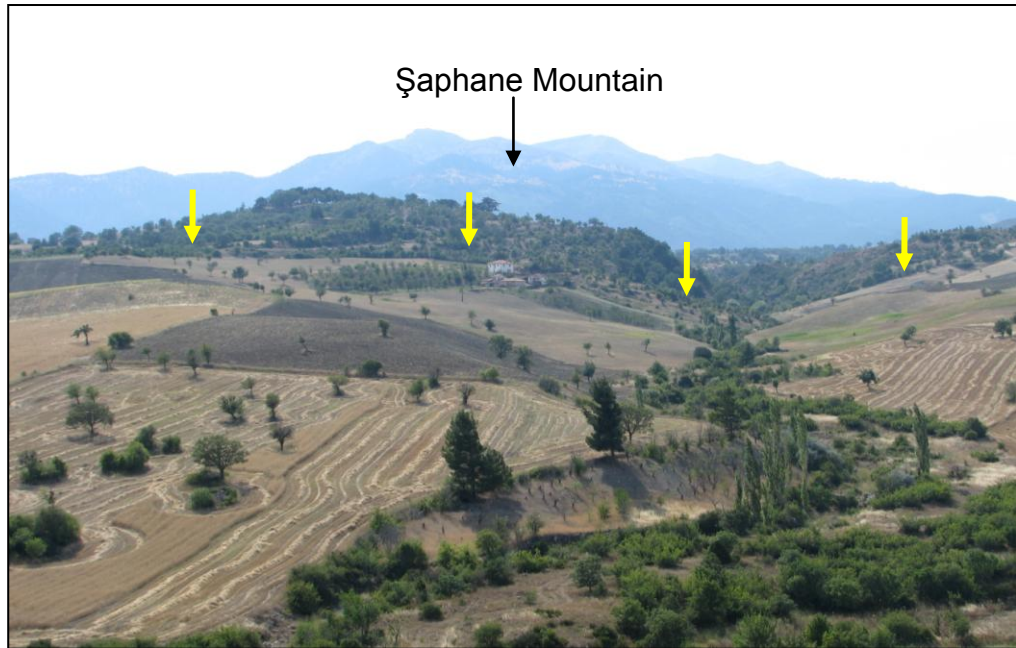


Figure 4.107. General view of the Sazak fault scarp and trace (view to SW). Vertical yellow arrows point to trace of the fault.

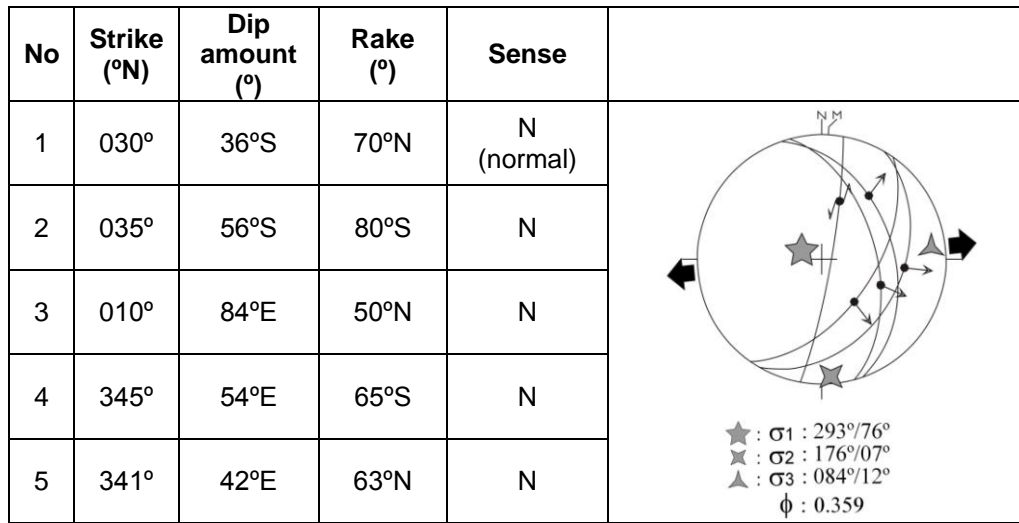


Figure 4.108. Stereographic plot of extensional slip-plane data on the Schmidt's lower hemisphere net, S.25 in Appendix – A. Large black arrows indicates neotectonic extension direction along the Sazak fault.

4.3.2.2.5. INDIVIDUAL FAULTS

In the study area, there are also single fault segments mapped. They are;

Muhipler and Eskimuhipler faults. These are 6 and 5 km long, approximately NNW-SSE-trending and easterly dipping normal fault segments which link both the ENE-trending Muratdağı and the Şaphane fault zones to each other (Appendix – A). They occur along the Değirmen and Çayköy stream beds and control them. Sudden break in slope, steeply sloping fault scarp (Figure 4.109), deflected and fault-controlled drainage system are common morphotectonic criteria used for recognition of these two faults. They are seismically active as indicated by the 1970.03.28 Gediz earthquake, during which they were moved resulting in ground surface ruptures (courtesy of local people).

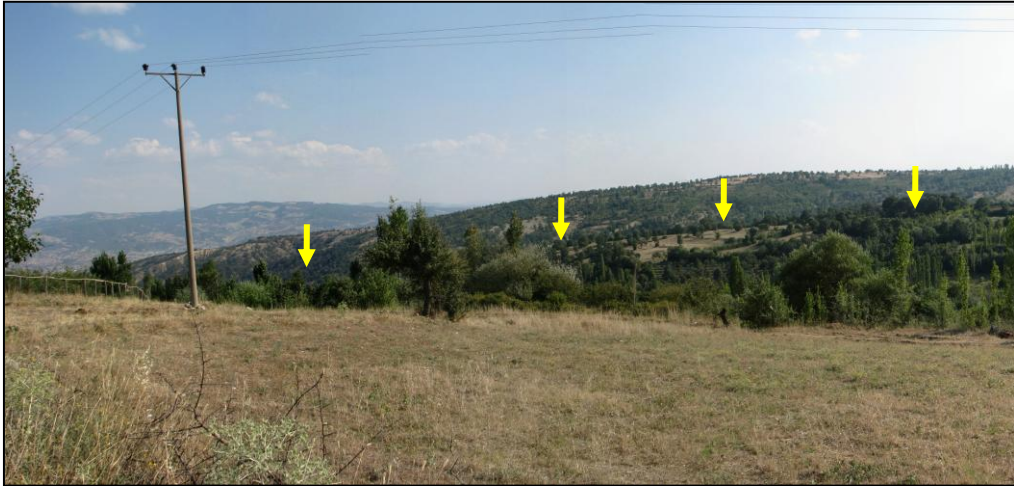


Figure 4.109. General view of the Eskimuhipler fault scarp and trace (view to SW). Vertical yellow arrows point to trace of the fault.

Çaltılık fault is an approximately 3 km long, N-S-trending and easterly dipping oblique-slip normal fault located along the western side of Değirmen streams (Appendix – A). It cuts and displaces both the pre- and modern graben infill, juxtaposes them tectonically. The Çaltılık fault was also moved by the 1970.03.28, Mw=7.2 Gediz earthquake resulting in ground surface rupture with 20 cm vertical displacement (courtesy of local people).

Üçbaş fault is an approximately 4 km long, N-S-trending and easterly dipping oblique-slip normal fault located along the western side of Çınarlı stream valleys (Appendix – A). The Üçbaş fault cuts and displaces both the pre- and modern graben infill, and juxtaposes them tectonically (Figure 4.110, Appendix – A).



Figure 4.110. General view of the Üçbaş fault cutting across the Plio-Quaternary terrace conglomerate (view to S, location: 1.3 km south of Üçbaş village).

Kışla fault is an approximately 4 km long, E-W-trending and southerly dipping normal fault located in the south-southeast of Çeltikçi village (Appendix – A, Figure 4.111). It cut and displaces the pre-modern and modern graben infill, and juxtaposes them tectonically. Sudden break in slope, sudden change in strike of bedding, uplifted and fault-suspended terrace conglomerate are common criteria for recognition of the Kışla fault.

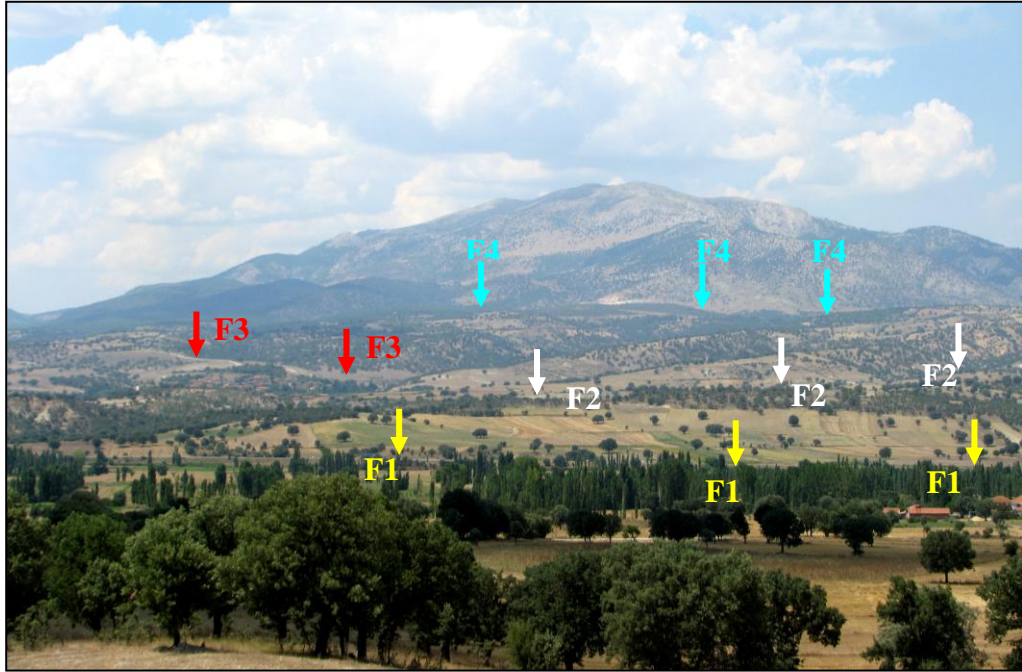


Figure 4.111. General view of the Dörtdeğirmen fault (F1), the Kışla fault (F2), the Çeltikçi fault (F3) and the Şaphane fault zone (F4) (view to N).

4.3.2.3. Fault Patterns of the Erdoğmuş-Yenigediz Graben

In the modern graben infill, there are a number of mesoscale normal faults with cm- to m-scale displacements. In general, the trend of mapable faults are E-W, NW and NE (Appendix – A), while their dip amounts range from 35° to 65°. The palaeostress analyses have also indicated that most of the faults are oblique-slip normal faults with minor amount of dextral to sinistral strike-slip components. The type of strike-slip component changes as the strike of the fault varies from one place to another place (Figure 4.112).

During the field study, observations were concentrated around relatively larger margin-boundary faults and others cutting across the graben infill (Figure 4.113). Additionally, numerous secondary faults were also

observed around master fault which have also added some extra deformational effects.

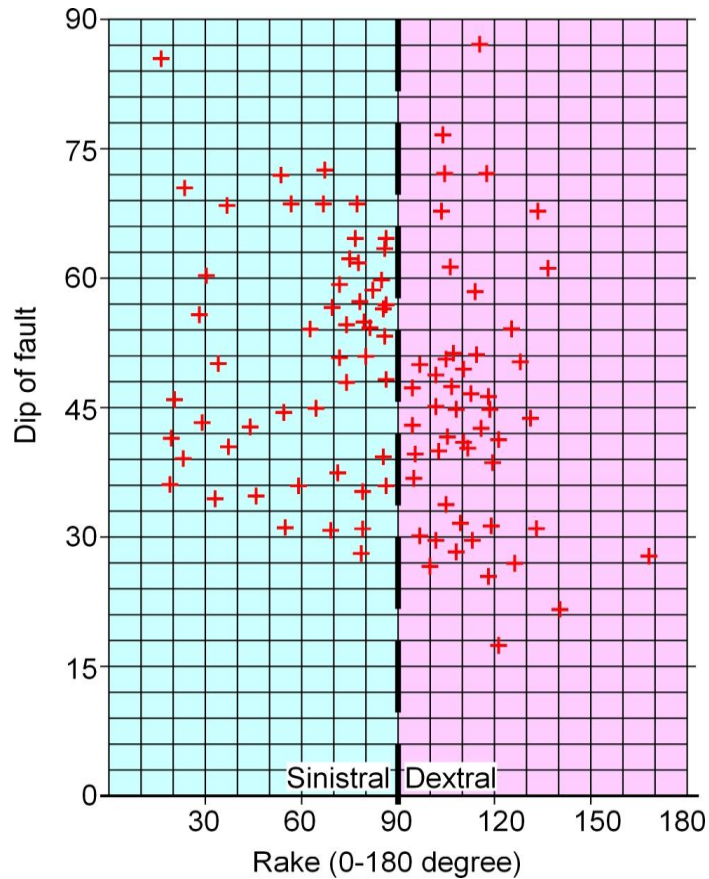


Figure 4.112. Fault data (N=50) of the near NE of Erdoğmuş village. Plot showing the fault dips versus rake of the slickenside lineations.

Diverse-sized faults have been deforming the modern graben infill accumulated on the hanging-wall blocks of the normal faults. The margin-boundary master faults of the graben are dipping in both north and south senses on both sites of graben margins. Master faults have numerous antithetic and synthetic secondary faults at different scale

(Figures 4.114). There are two general occurrences of the secondary faults. These are the ENE- and WNW-trending secondary faults with an interlimb angle of 60° , so they are conjugate faults in nature between the two sets, they can be named as conjugate faults (Anderson, 1951). The existence of intersecting normal faults (antithetic and synthetic faults) is an anticipated result in the extensional areas. Many researches have dealt with the relationships between tectonic regime and structures (Horsfield, 1980; Nicol *et al.*, 1995; Watterson *et al.*, 1998; Castagna, 1996; Ferrill *et al.*, 2000). Northern and southern margins of the Erdoğmuş-Yenigediz graben are the place where conjugate faults are concentrating. Analysis of slip-plane data gathered from these faults is also depicting this situation (Figure 4.115).

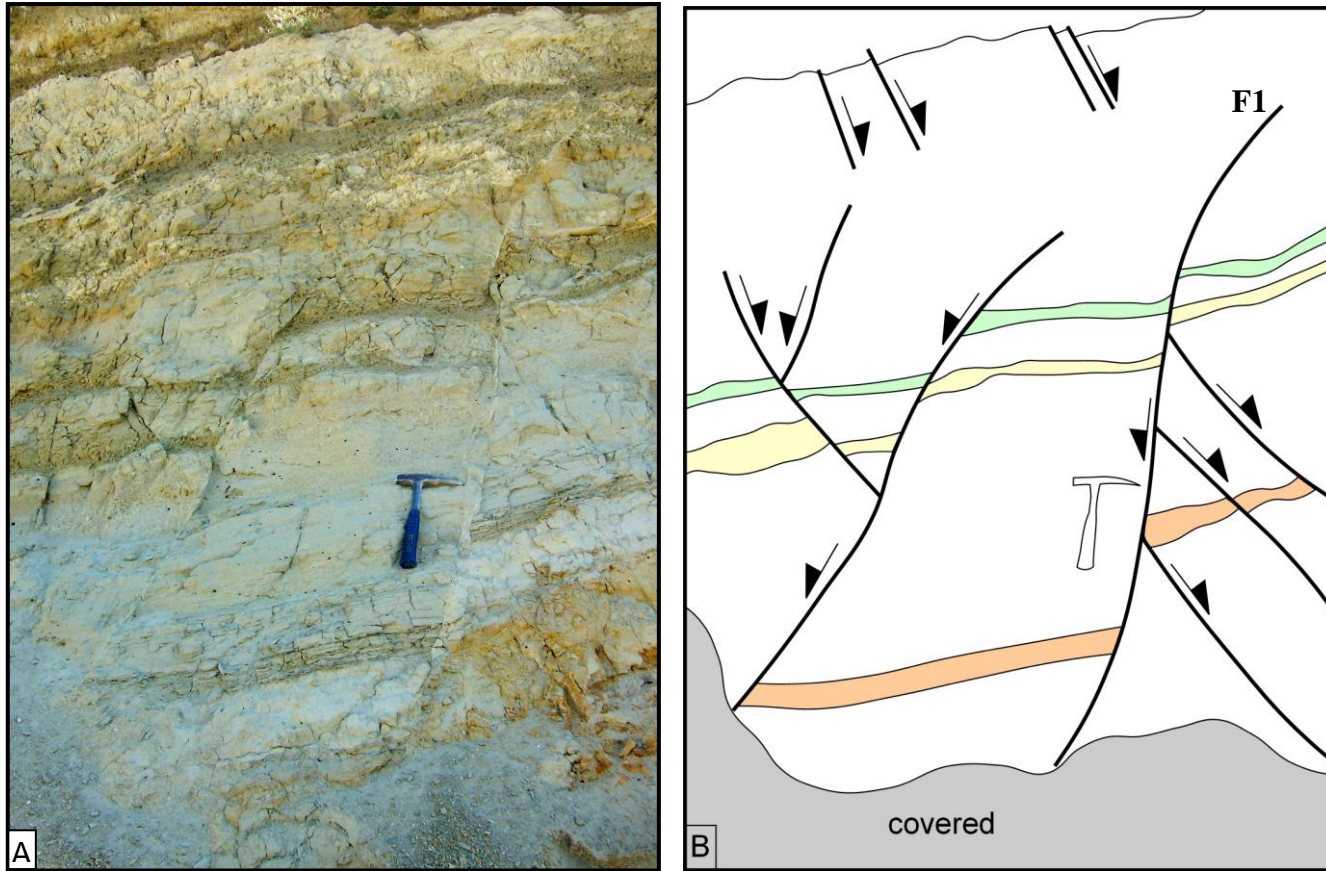


Figure 4.113. A field photograph (A) and its sketched pattern (B) in the near north of the Erdoğmuş village. Master fault (F1) cut and displaced the sedimentary deposits. A series of antithetic and synthetic faults have also deformed the modern graben infill.

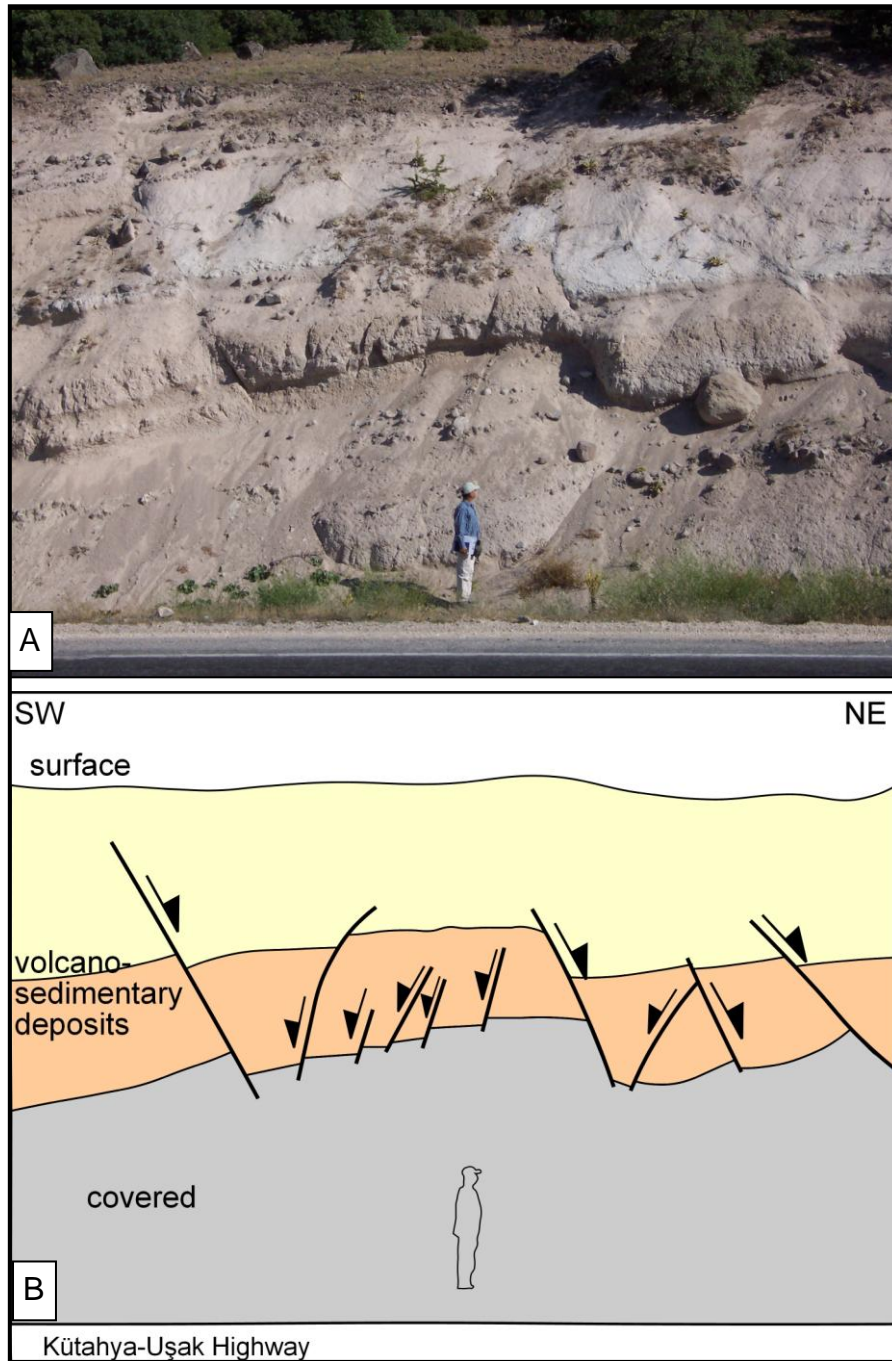


Figure 4.114. Field photograph (A) and its sketched (B), near NE of Eskigediz County. Antithetic and synthetic normal faults developed in the area between pre- and modern graben infill along the northern outline of the Erdoğan-Yenigediz graben.

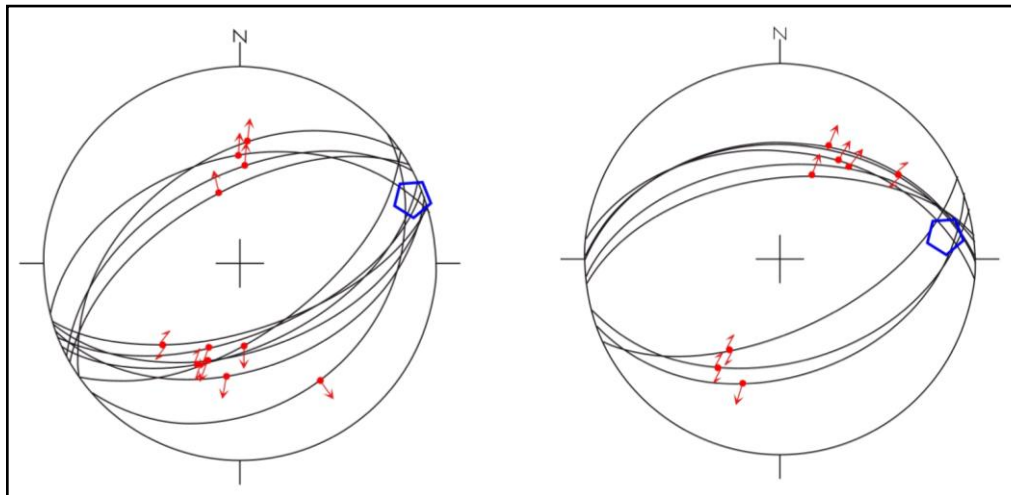


Figure 4.115. Two sets of conjugate faults measured near NE of Eskigediz County. Pentagon shows the average position of the line of intersection of the two sets (β -axis).

The fault pattern at any place can be used to identify the deformation mechanism by the help of kinematic analyses. To do so, depositional geometry and deformation patterns should be evaluated. In the Erdoğmuş-Yenigediz graben, there are two predominant sets of major faults which control the deformation pattern of the graben infill. Moreover, second order antithetic and synthetic faults are also used. To check the reliability between field observations and results of the slip-plane data by Angelier stress tensor programme, kinematic results are needed. At the end of the kinematic analyses, the recent and the palaeotectonic configurations of stress field can be obtained. Computed stress field in the palaeotectonic and neotectonic period can be used to identify geological evolution of the study area.

4.3.2.4. Deformation Patterns of Graben Infill

5 different cross-sections have been prepared to discuss deformation by means of pre-modern and modern graben infill (Figure 4.116). According to A-A', B-B', C-C', D-D' and E-E' sections, pre-modern and modern graben infill are separated from each other by an intervening angular unconformity up to the $\sim 45^\circ$. It can be observed in many places in the study area. This high angular difference between the graben infills is one of the most important evidence to prove occurrence of a differentiation took place in the tectonic regime. Because of the deformation and rock type differences in Erdoğmuş-Yenigediz graben, tectonic phases are separated as two periods; palaeotectonic and neotectonic (Figure 2.1). There are two motions (older extension and younger contraction) in palaeotectonic period, which is proved by the structural evidence. The existence of recent extensional neotectonic period is confirmed by the current earthquakes.

Firstly, pre-modern graben infill has been folded and reverse faulted. Because of the impact of the extensional neotectonic period, they have been swept out and these limited structures as an evidence of compression can only be observed. Even though the dominant extensional motion, many footprints still are there, for instance, in Figure 2.3, and in Chapter 4 (Figures 4.5 and 4.6 (stereographic analysis of slip-plane data), Figure 4.9b (approximately vertical beds) and Figure 4.28 (stereographic analysis of slip-plane data)).

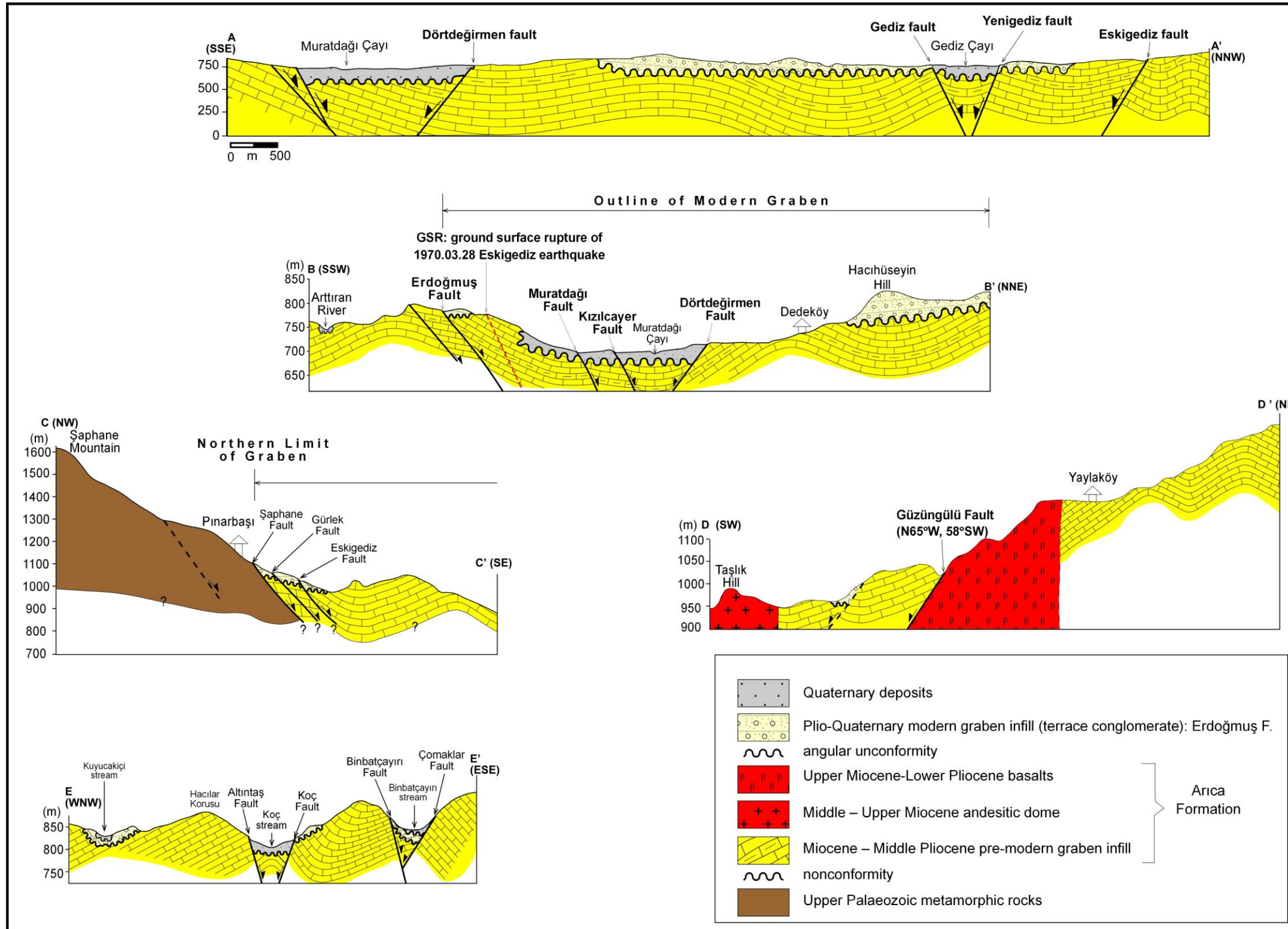


Figure 4.116. Cross-sections along the lines A-A', B-B', C-C', D-D' and E-E' in Appendix – A.

4.4. The Computed Stress Field

The oblique-slip normal faults are dominant in the Erdoğmuş-Yenigediz graben. Mainly, they are E-W, NE-SW and NW-SE-trending structures (Appendix – A). In aforementioned chapters, the kinematic analyses for each fault have already been presented. They clearly show that there is not a single stress direction in both the palaeotectonic and neotectonic periods over the study area. The kinematic analyses of deformation patterns recorded in both the pre-modern graben deposits (palaeotectonic period) and the modern graben deposits (neotectonic period) are summarized below.

Before, stress inversion and its meaning and limitation should be explained briefly. Slip-lines (slickenlines) measured on the fault slickenside in the field are used to identify the stress field, that controls the deformation mechanism in an area. Fault kinematic analysis methods (e.g., Carey and Brunier, 1974; Angelier, 1979, 1984; Etcheopar *et al.*, 1981; Gephart and Forsyth, 1984; Yamaji, 2000) are used frequently to analyse the brittle deformation. They commonly establish the reduced stress tensor, the directions of principal stresses ($\sigma_1 > \sigma_2 > \sigma_3$), and the stress ratio $R = \sigma_2 - \sigma_3 / \sigma_1 - \sigma_3$ at a station. The term “stress” is used to identify the fault kinematic analysis; furthermore, it should be kept in mind that the analysis essentially deals with strain. It means that principal stress axes are actually referring “kinematic axes”.

For the fault kinematic analysis, there are three basic assumptions. They have to be validated if fault kinematic data are interpreted in terms of stress:

- (1) The stress tensor is symmetric, i.e. deformation is coaxial, pure shear,
- (2) Deformation is homogeneous, and
- (3) Faulting is consistent

with the Mohr-Coulomb yield criterion (Coulomb, 1773), i.e. faults develop parallel to σ_2 and with a material-inherent fracture angle (the “angle of internal friction”) to σ_1 .

Truthfully, none of these assumptions mostly cannot be applied in nature. For example, if homogeneous deformation took place and its’ slip-plane data are present, it is an unproblematic case to establish the stress that was responsible for the faulting by means of the stress inversion method. As has been stated before, there are many stress tensor determination software. Some of them apply the homogeneous deformation assumption, but, others use heterogeneous deformation assumptions (Angelier, 1979, 1994; Reches, 1987; Arminjo et al., 1982; Huang, 1988; Angelier, 1994; Yamaji, 2000). In this work, Angelier (1990, 1994) stress inversion method has been used to get stress tensor based on the direction and sense of slip on the faults. Because, the stress inversion method gives a chance to analyse the multiphase deformation history. By using this method, the orientation of principal stress axes and their ratio Φ have been solved (Bishop, 1966; Angelier, 1984).

$$\Phi = (\sigma_2 - \sigma_3) / (\sigma_1 - \sigma_3) \quad 0 \leq \Phi \leq 1 \text{ (Bishop, 1966)}$$

Slip-plane data collected from the Erdoğmuş-Yenigediz graben have been analyzed with Angelier’s stress inversion method and they have been presented under the two separate titles as stress field of faulting in pre-modern and modern graben infill. It refers palaeotectonic and neotectonic period in the study area.

4.4.1. Stress Field of Faulting in pre-modern Graben Infill

Stress inversion method has been applied at 6 stations in pre-modern graben infill. They were collected from the polished fault surface

(slickenside) and others from deformed sedimentary packages. According to their inversion results, two different tectonic regimes have prevailed in the palaeotectonic period. They are the extensional tectonic regime and the compressional tectonic regime, respectively. Their effects were recorded as the two sets of overprinted slickenlines on both the margin-boundary faults and the infill of the Erdoğmuş-Yenigediz graben. The pre-modern graben infill was deposited under the control of extensional tectonic regime, but it was deformed by the compressional tectonic regime. The operation directions of principal stress axes during sedimentation are illustrated in Figure 4.117. For each analysis, not only the principal stress axes but also other two variables which are the Φ ratio and the quality estimator ANG values are also important to evaluate the stress ellipsoid. According to Angelier's (1994) limits, Φ ratio ranges between 0 which is uniaxial compression ($\sigma_2=\sigma_3$; $\Phi=0$) and 1 which is uniaxial extension ($\sigma_1=\sigma_2$; $\Phi=1$). In the palaeotectonic period, older extensional tectonic settings are characterized by relatively elevated values of about $\Phi = 0.5$. It shows the considerable difference between well-defined σ_3 and σ_1 - σ_2 values. On the other hand, lower Φ values show the small difference between σ_2 and σ_3 (Angelier, 1994).

Another variable to evaluate stress axes is the ANG value. It defines the angle between the sedimentary units deformed by the fault and the theoretical shear vector on the fault plane computed stress axes (Angelier, 1994). In general, values of ANG point out a well fit of the computed stress axes with the measured fault slip-plane. As a rule, ANG values smaller than 22.5° are regarded as good match and those between $22.5^\circ - 45^\circ$ characterize poor match. The larger value than 45° indicates a bad consistency between the measured slip and the computed stress tensor.

As a result, yielded ANG values smaller than 45° are acceptable (Angelier, 1984). As it is stated before, the analyses are indicating older extensional period and their Φ values are ranging between 0.218 – 0.674. Expected values for Φ in an extensional motion are around 0.5. Probably, local stress field anomalies yielded such deviations. When the results of ANG values have been examined, all are smaller than 22.5° and it shows a well-fit between computed stress axes and measured data from field (Angelier, 1984).

The results of the contractional palaeotectonic phase have been presented in Figure 4.118. Stations 2, 9, 17 and 21 have contractional slip-plane data as well. According to their stress axes analyses, a multidirectional contraction direction has been detected. This result is also related to composite fault pattern.

Even though the differences between computed Φ ratio for two palaeotectonic regimes (older tensional and younger compressional) in itself, they are still in the acceptable range.

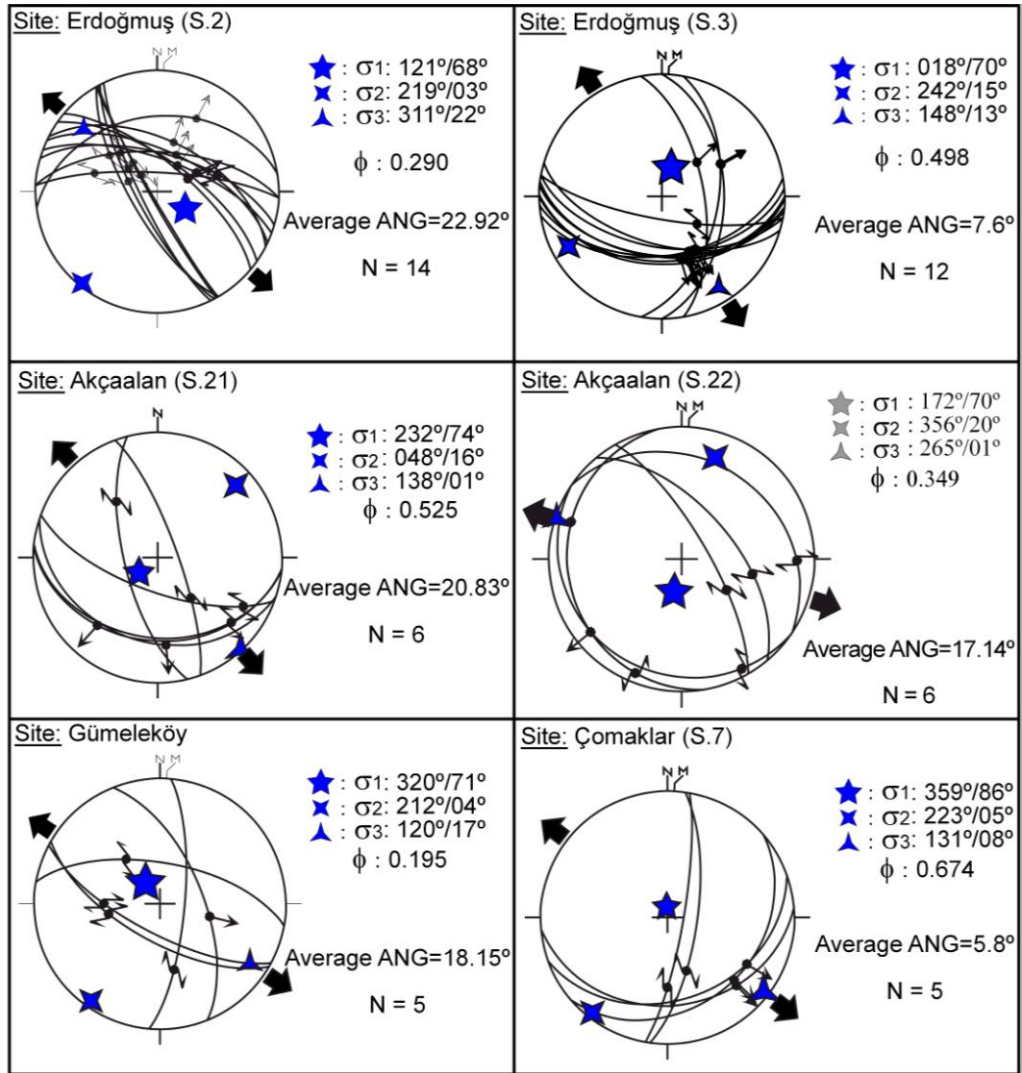


Figure 4.117. Stress analyses obtained the pre-modern graben infill. Stereographic plots illustrate slip-plane data measured on the fault slickenside and in the deformed sediments, and the operation direction of principle stress axes. All analyses have also Φ ratio and ANG value.

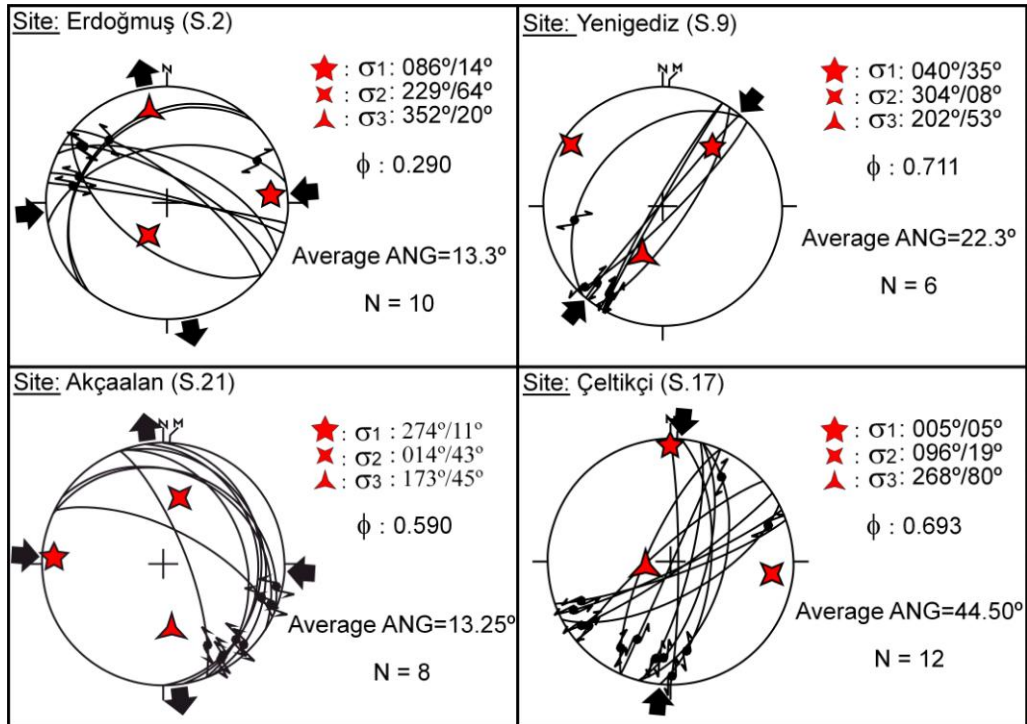


Figure 4.118. Stress analyses obtained from the pre-modern graben infill. Stereographic plots illustrate slip-plane data from fault slickenside to deformed sediments, and the positions of principle stress axes. All analyses have also Φ ratio and ANG value.

4.4.2. Stress Field of Faulting in Modern Graben Deposits

Stress inversion method was also applied for the recent slip-plane data measured at 18 stations. They were measured on the fault slickenside and in the deformed modern graben infill. The most representative 10 analyses have been presented in Figure 4.119.

The solution of the inverse problem implies that bulk of the fault data confirms the NNE–SSW- and NE-SW-orientated extension with subvertical σ_1 , WNW-ESE- and NW-SE-trending σ_2 and NNE–SSW- and NE-SW- trending σ_3 axes (Figure 4.119). Φ ratio is around 0.5.

Even though some of the average ANG value slightly higher than the good-fit threshold of 22.5° , generally they show good confirmation with the theoretical slip vector calculated by using the inversion method (Figure 4.119). But a few results are indicating small differences. Probably, they have been affected from the local stress field anomalies.

Additionally, focal mechanism solution diagram of the 1970.03.28, $M_w=7.2$ Gediz earthquake is the most recent data to check the operation direction of the principal stress axis gathered from the slip-plane data analyses. Consequently, they have consistent in operation direction of σ_1 (in Figure 4.119 and Figure 4.13d).

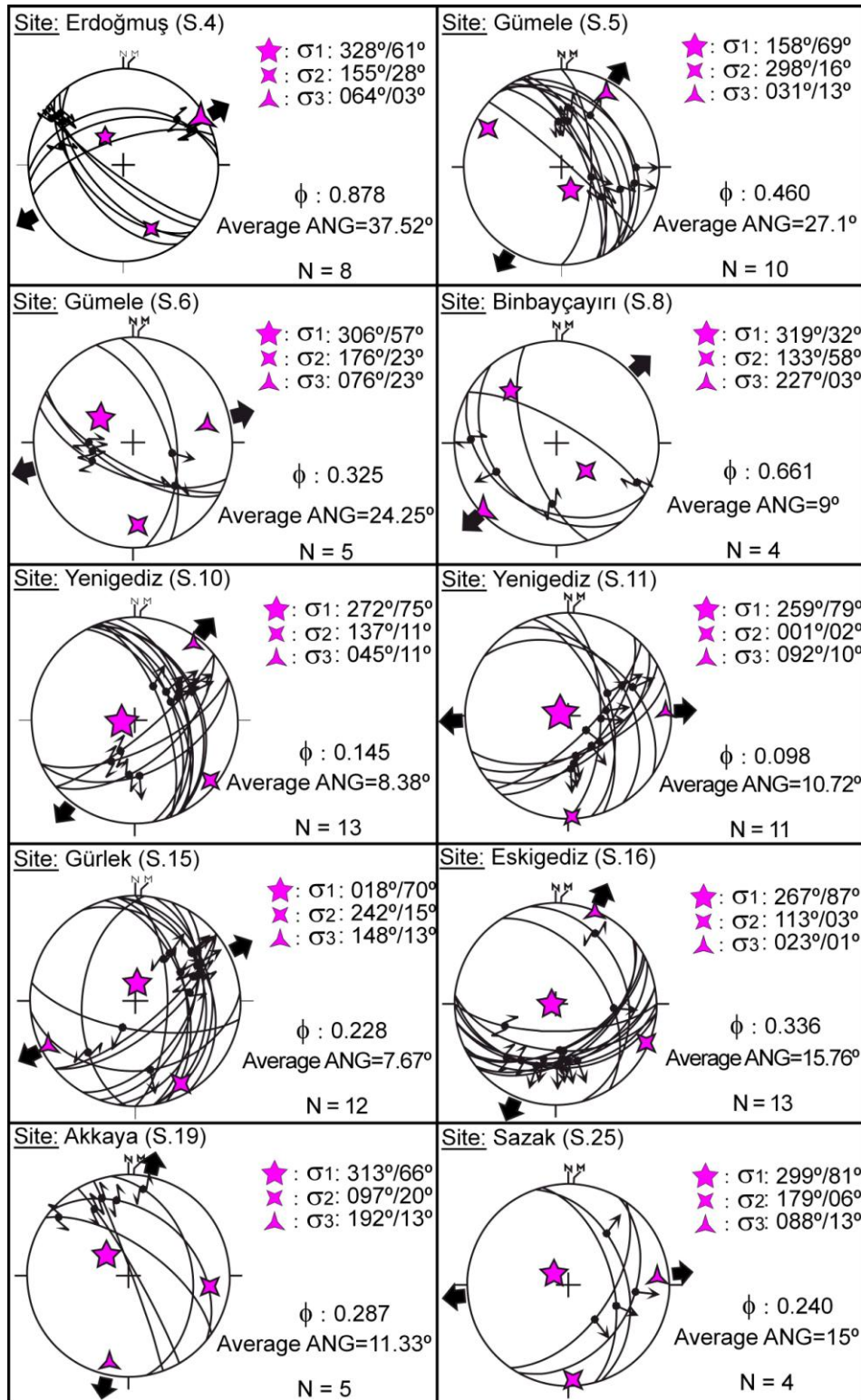


Figure 4.119. Stress analyses obtained from the modern graben infill. Stereographic plots illustrate slip-plane data from the slickenside and deformed sediments, and the position of principle stress axes.

4.5. Conclusion

As a first and the most significant is that the study area has experienced two tectonic regimes namely the tensional and compressional tectonic regimes. It is indicated by the deformation patterns of the pre-modern graben infill and the angular unconformity between it and the modern graben infill. This is also proved by different tensor populations collected from sediments and faults slickenside (slip-plane data). According to field observation, there are two basin infill; deformed older and non-deformed younger infill. They are separated from one another by an intervening angular unconformity. This is one of the most important clues implying to the compressional tectonic regime experienced by the pre-modern graben infill of the Erdoğmuş-Yenigediz graben. The earlier extensional and later contractional deformation phases are also indicated by tensor populations (Figures 4.117 and 4.118). They are also overprinted by the second phase of extension (neotectonic extension) (Figure 4.119). These three different tensor populations have been detected in terms of kinematic analyses of slip-plane data measured on fault slickenside and recorded in graben infill. Consequently, fault kinematic analyses are implying to the older extension (1st phase of extension) in ~NW-SE direction (Figure 4.117), the intervening contraction (contractional phase) in ~N-S, NE-SW, and ~E-W multidirectional contraction (Figure 4.118), and the Plio-Quaternary neotectonic extension in ~NE-SW, and NNE-SSW direction (Figure 4.119).

CHAPTER 5

PALAEOSEISMOLOGY

5.1. Introduction

Palaeoseismology is an interdisciplinary science between geology and seismology. It is deeply concerning with the identification of active faulting, amount of slip rate, rupture length, repeated time, slip per event and assessment of magnitude of future events. In palaeoseismology, the activation of the same fault with similar behavior and the last earthquake are critical to judge about the possible hazard to be caused by that fault. Although it is very difficult to get information about past events, pre-historical or historical events, palaeoseismological investigations have been, all over the world, very effective method for assessing the seismogenic potential of any given fault. In the past few decades, researchers dealing with the historical earthquakes often use palaeoseismological approach to describe the possible big seismic events in the future. Such studies are significant to characterize the size of future earthquakes along a fault or within a region if the event is characteristic (Schwartz and Coppersmith, 1984).

Palaeoseismological methods developed in the area within high seismic areas for the faults with high slip rates are increasingly used to improve the calculations of seismic hazard and seismogenic characteristics of the faults with very low slip rates. In fact, the recognition of the seismogenic characteristics of a fault, such as the evaluation of its slip rate, the size of the expected peak earthquake and the age of the

around surface rupture-forming earthquake can substantially change the perception of seismic hazard in regions traditionally considered to be stable or not very active.

This chapter presents the results of a palaeoseismological study carried out in the Erdoğmuş-Yenigediz graben. As stated, the study area is included in the seismic zone of 1970.03.28 $M_w=7.2$ Gediz earthquake occurred along the Erdoğmuş fault. The Erdoğmuş Fault is an approximately 11 km long, E-W-trending northerly dipping normal fault with minor amount of right-lateral strike-slip component. The seismic potential of the Erdoğmuş fault was previously recognized by the occurrence of both 1944.06.25 and 1970.03.20 Abide and Gediz earthquakes with magnitudes $M_s= 6.0$ and $M_s= 7.1$, respectively. For this reason, the Erdoğmuş fault was selected as a target palaeoseismic investigation.

5.2. Pre-trenching Survey

Before focusing on the trenching surveys on the Erdoğmuş Fault, potential trenching locations have been investigated and evaluated. Two possible sites were chosen. First one is on the Şaphane Fault which is the northwestern margin-boundary fault of the Erdoğmuş-Yenigediz graben. This fault has taken a critical role at the initial stage of the graben formation. During the 1944.06.25 Abide and 1970.03.28 Gediz earthquakes considerable amount of displacement were compensated by the Şaphane fault. In the northwestern part of Gürlek village, a lineament was identified the aerial photograph (Figure 5.1). The field mapping reveals that a scarp is evidently visible at the surface; and it displaces a change in the direction and a colluvial wedge (debris slope) is developed on its trace (Figure 5.2). Along the fault scarp, measured thickness of the colluvial wedge is 5.2 m. Depth more than

5.2 m is far thicker than a trench where a possible displacement of various units can not be observed.

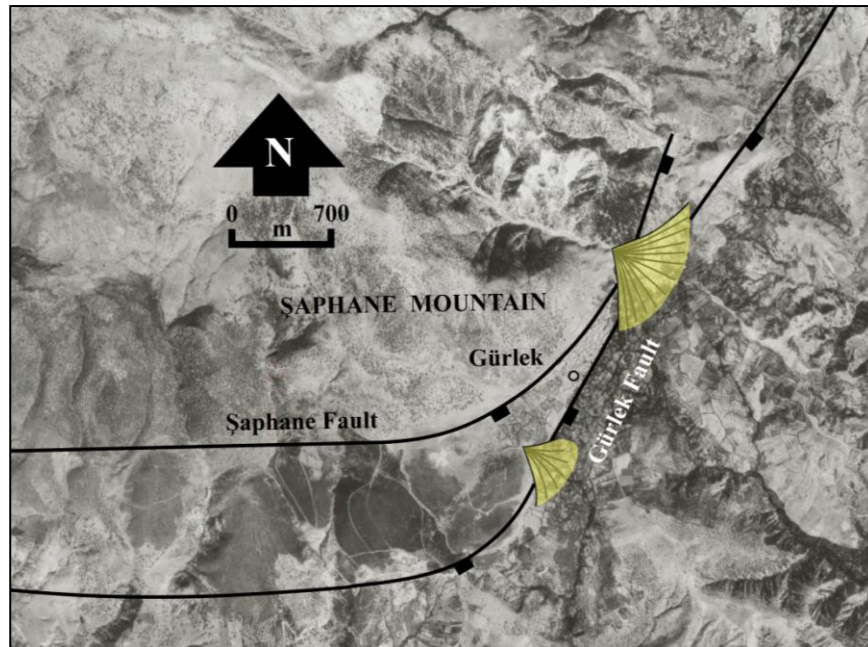


Figure 5.1. Aerial photograph of the Şaphane and Gürlek faults.

Second candidate for a trench is located on the Erdoğmuş Fault, which forms the southern margin-boundary fault of the Erdoğmuş-Yenigediz graben. This fault was possibly the source of the 1944.06.25 Abide earthquake but 1970.03.28 Gediz earthquake occurred on it. During the 1970 Gediz earthquake, considerable amount of vertical and lateral displacements occurred along the 11-km-long segment of the Erdoğmuş fault (Figure 5.3). Ground surface ruptures and consequent scarps are still present. Furthermore, geological and geomorphological studies carried out on and around the fault indicate that the fault cuts and displaces the recent graben infill, such as the flood plain and terrace deposits.

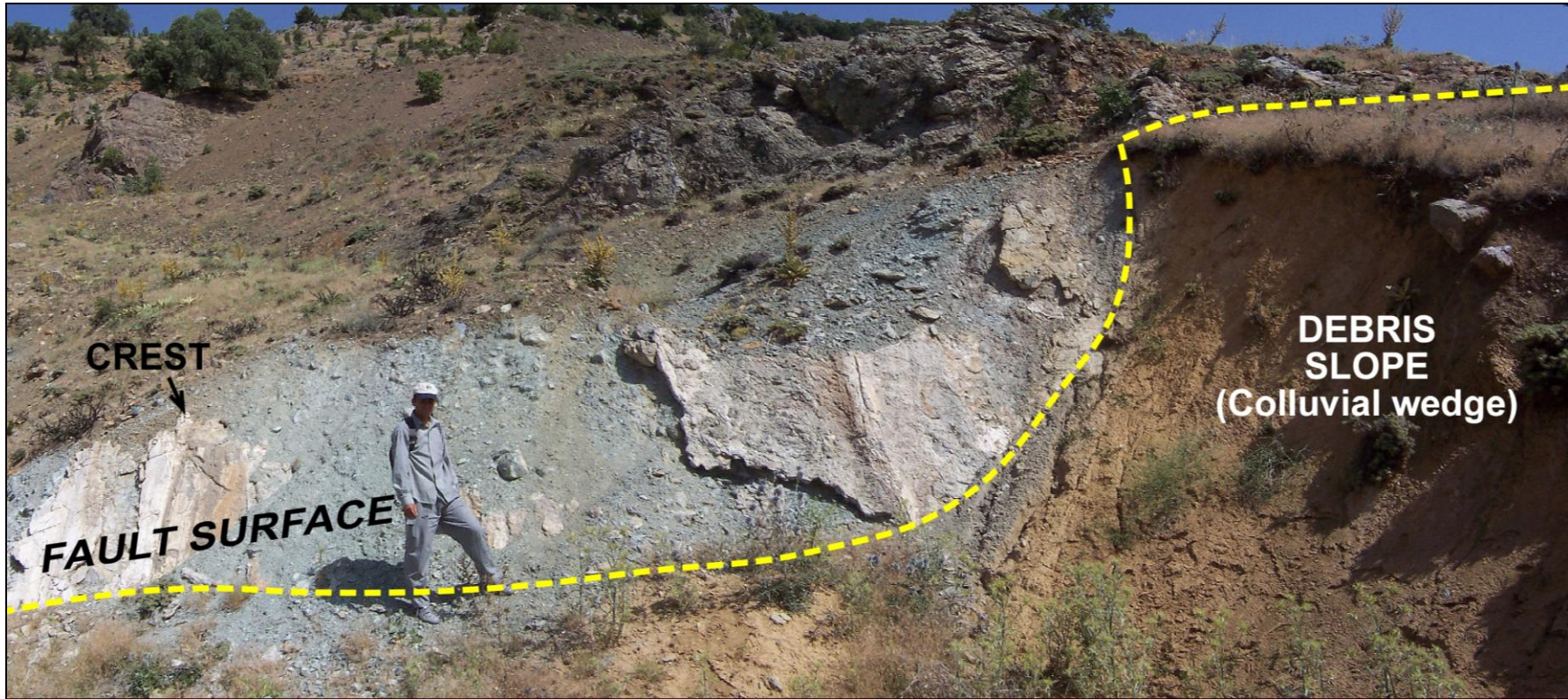


Figure 5.2. Close-up view of the Şaphane active fault slickenside and the colluvial wedge (debris slope) accumulated on the hanging block (view to NNW).



Figure 5.3. Field photograph showing the ground surface rupture of the 1970.03.28 Gediz earthquake on the western side of Erdoğmuş village (view to ESE).

5.3. Trench Site Selection

As a result of pre-trenching survey carried out by using the site selection, geological and geomorphologic investigations, the Erdoğmuş fault was selected for trenching. The fault is approximately 11 km long and it needs very detailed survey to find out the suitable trench sites. Additionally, location of ground surface rupture of Gediz earthquake is known and it is the most favorable situation for trenching.

The following criteria are used to define the target area for palaeoseismological research:

1. A visible step in the terrain to allow geomorphological modeling, and provide additional constraints for the interpretation.

2. Dating of Holocene events is crucial. So, a trench site should contain well-dated deposits.

3. The survey area should not locate under laws preventing trenching (nature reserve).

Based on above-mentioned criteria, two potential sites were selected across the Erdoğmuş fault, close to the Kör stream near-west of Erdoğmuş village (Figure 5.4). A detailed geological and geomorphological survey were carried out at two sites to determine the sub-surface configuration of the Erdoğmuş fault. A micro-topographic map (Figure 5.4) of the selected area and two topographic profiles (Figure 5.5. A-A') were prepared. This information is helpful to select the most suitable sites. The first site, close to the village, there is an obvious break in slope that correspond a fault scarp. The second as seen at the microtopographic map (Figure 5.4. B-B'), is marked by an obvious fault scarp but at depth. For this reason, it was decided to carry out an additional survey. These two selected areas are located on the ground surface rupture of 1970.03.28 Gediz earthquake. The distance between them is about 1 km and the ground surface display step-like landslide oblique to the ground surface rupture (profile in Figure 5.5).

Profile A-A' [for Trench-1 (EF-1)] is taken in SE-NW direction and cut obliquely the ground surface rupture of the 1970 Eskigediz earthquake. It is very near to the Çay and the ground water level is suitable for trenching owing to summer season. Profile B-B' [for Trench-2 (EF-2)] is located again on the ground surface rupture of the 1970 Gediz earthquake. For both cross-section directions, the exact location of the fault plane is probably estimated by using the geological criteria and the ground surface rupture of the 1970 earthquake.

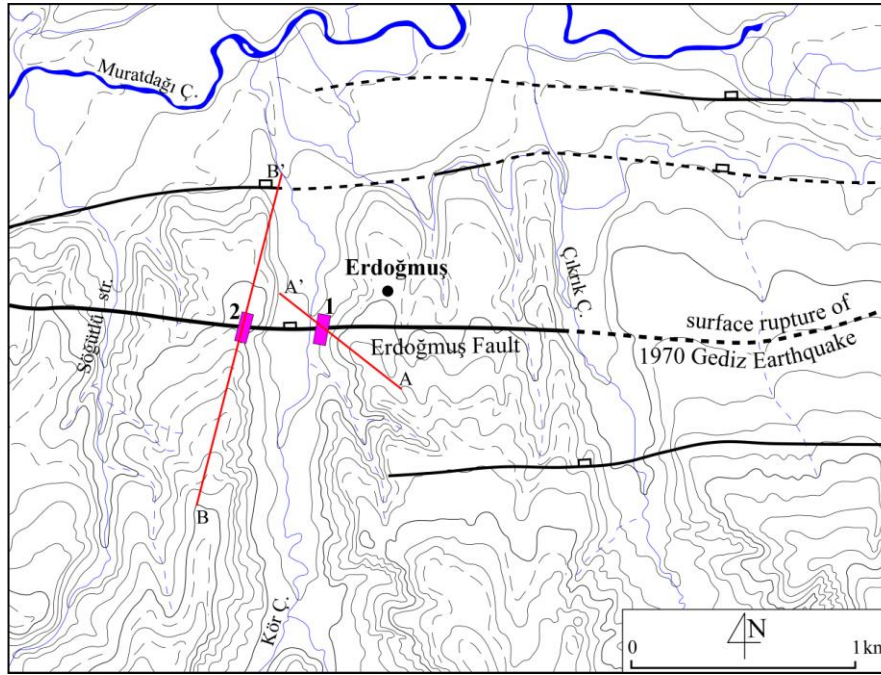


Figure 5.4. Microtopographic map of the target area showing the location of trenches (1 and 2), surface rupture of the 1970.03.28 Gediz earthquake and geologic cross-sections (A-A' and B-B') along the Erdoğan fault.

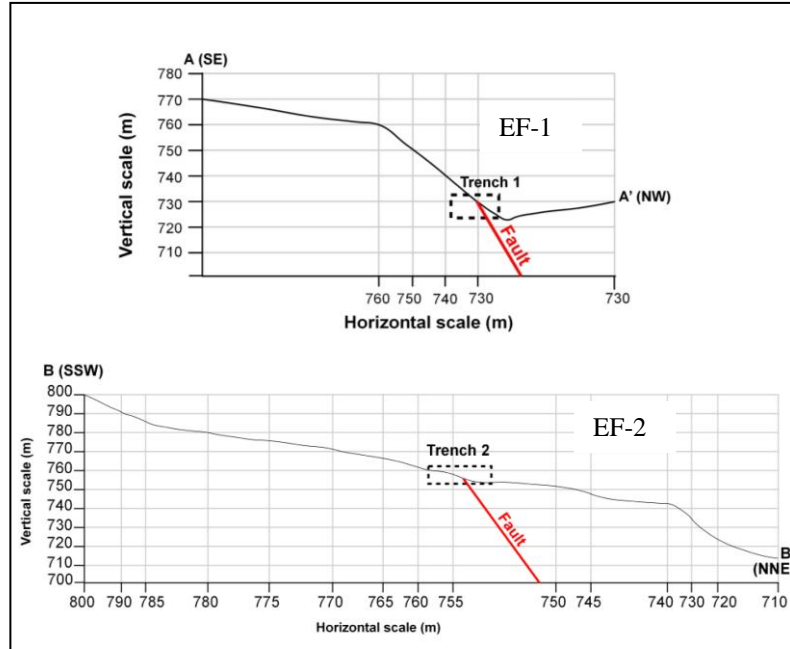


Figure 5.5. Geological cross-sections across the ground surface rupture of 1970.03.28 Gediz earthquake. A maximum and minimum displacement is plotted on each cross-section (see Figure 5.4. for location).

Digital elevation model (Figure 5.6.) and topographic map (Figure 5.7.) of the area were prepared (Figure 5.4) to select the trench site. Erdoğmuş village is a unique settlement where the ground surface rupture of the 1970 earthquake is evidently observed along the fault trace that is shown in Figures 5.4 and 5.8.

As previously stated, integration of all information obtained from the study area indicates that these two favorable places can be used for trenching (Figure 5.8).

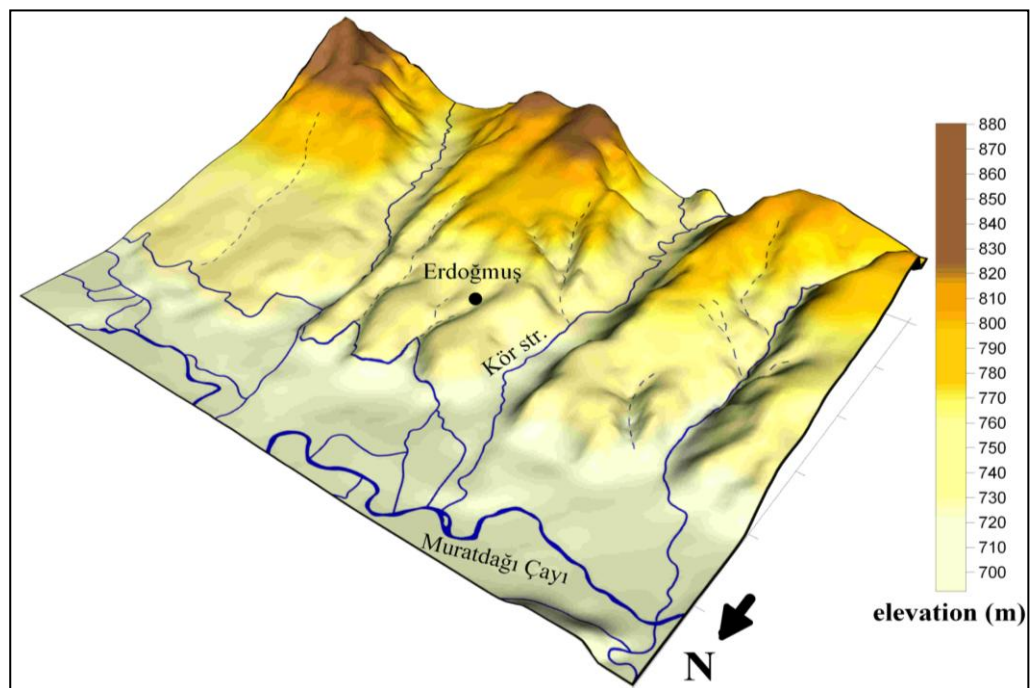


Figure 5.6. Digital elevation model of Erdoğmuş village and its vicinity based on elevations.

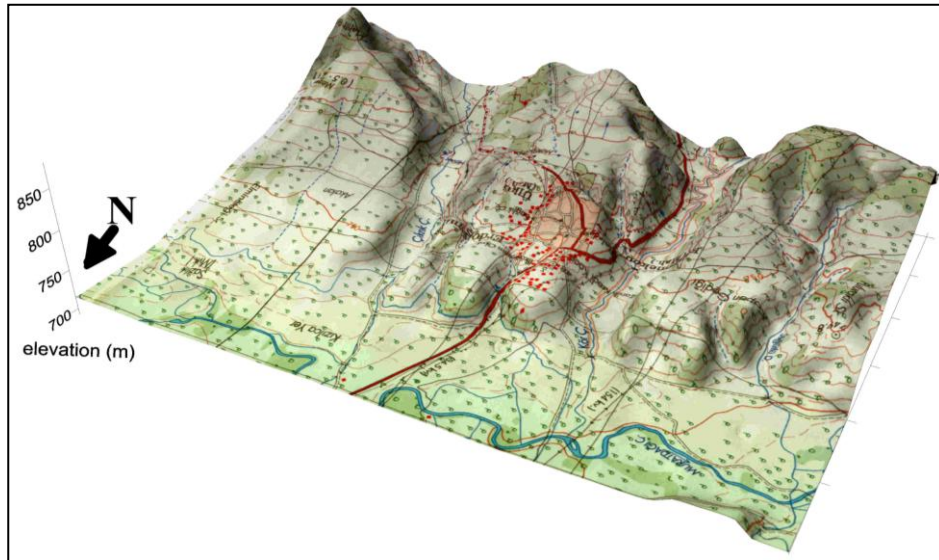


Figure 5.7. Digital elevation model of Erdoğmuş village and its vicinity based on topographic map.

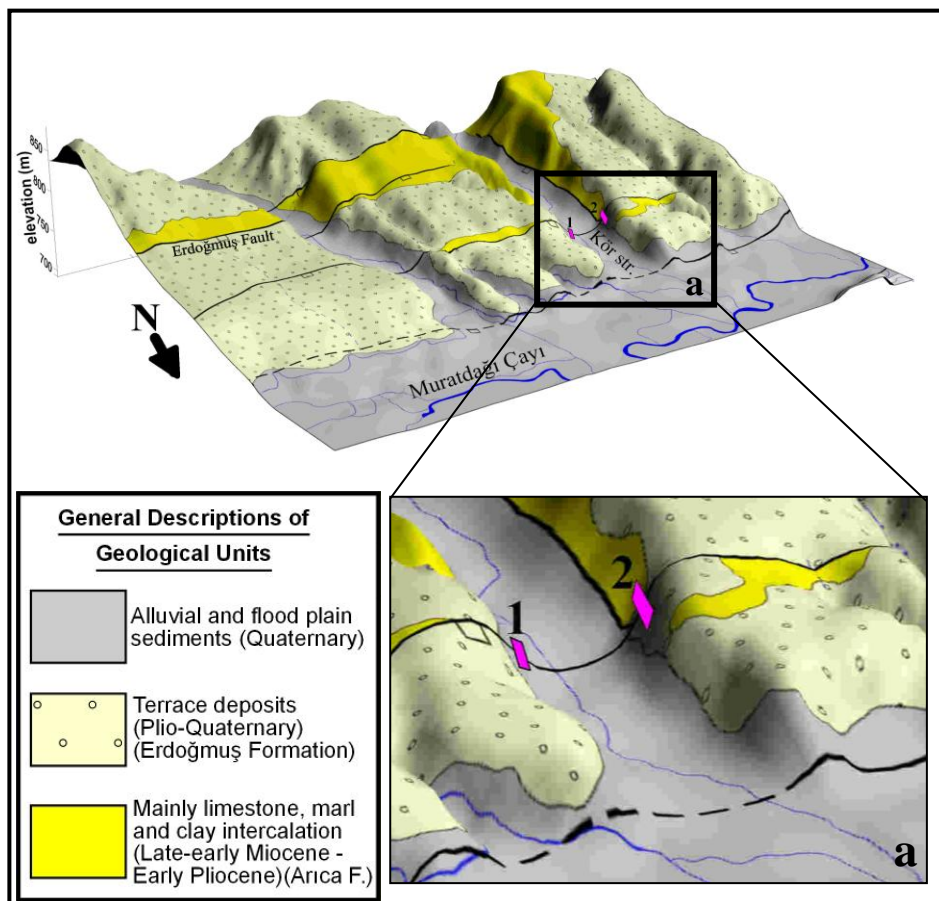


Figure 5.8. Digital elevation model of Erdoğmuş village and its close vicinity based on topographic map. a) close up view of trench sites.

5.4. Trench Descriptions

The stratigraphy in the trenches were determined by detailed mapping of the trench walls (1:50), absolute dating and lithostratigraphic correlation. Five stratigraphic units have been identified.

The most important part of trenching is to define suitable trench site so that the fault can be identified in a distance of a few metres. The people in Erdoğmuş village showed the location of the ground surface rupture of 1970 Gediz earthquake (Figure 5.9). This information was great help to locate suitable places, where the thickness of slope scree deposited just after the 1970 earthquake is minimum.

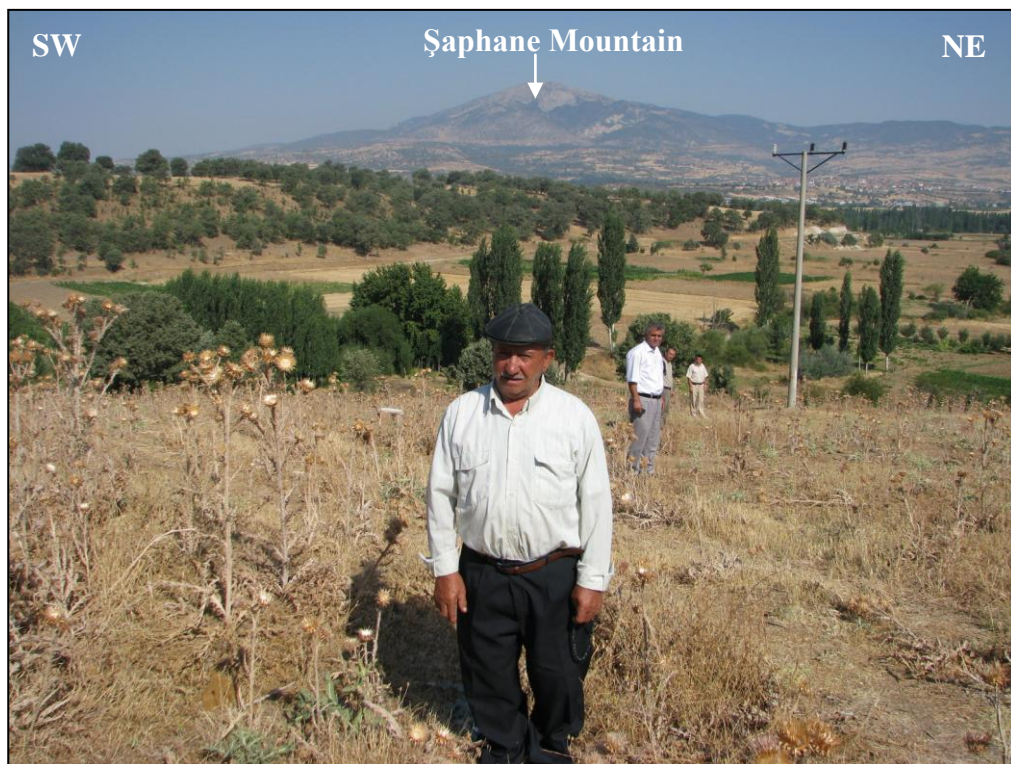


Figure 5.9. Field photograph showing the ground surface rupture of 1970.03.28 Gediz earthquake; where people are aligned on the rupture (view to NNW).

5.4.1. Trench – 1 (EF-1)

Trench – 1 (EF-1) is located at the near NW of Erdoğan village (Figure 5.4) where flood plain sediments of the Kör Çay are observed at the surface. The clear fault pattern and faulted units are well-exposed along the eastern wall of the trench (EF-1) (Figure 5.10). Five faulted lithofacies (units) were identified (Figure 5.11).

The lowest unit is a dark to light grey marl (a in Figure 5.11). It is observed at different elevations on both sides of the eastern wall of the EF-1. It is highly deformed, crushed and dissected by faults and fractures (Figure 5.12).

Above the marl (b in Figure 5.11) lies a dark brown sandstone and pebble-sized polygenetic, unsorted conglomerate. They display irregular contact relationship with the overlying light to dark yellow, fine- to coarse-grained sand and gravels (c2 in Figure 5.11), that contain light brown and uneven lenses of sand (c1) deformed by faults and fractures at different scales ranging from millimeter (Figure 5.13) to metre. These facies are succeeded by a moderately lithified unit made up of light brown-yellow sandy gravel, gravelly sand, and imbricated polygenetic pebble horizons. It is interpreted as fault breccia, originated from surface (alluvial) materials (d in Figure 5.11).

The most top unit is a brown to yellow-brown soil horizon composed of polygenetic, unsorted and angular to semi rounded pebble clasts set in a granular matrix (e2 in Figure 5.11). It is coarse-grained but monogenetic at lower level (e1 in Figure 5.11).

In EF-1, three different sets of faults were identified (Figure 5.11). The red set is the youngest reactivated during 1970 Gediz earthquake,

green set lies in between purple set is the oldest fault and. The purple set cuts only the marl (a), and it does not continue up to the unit e2 and c. Additionally, the oldest set is cut by green colored fault set. The units b and c are deformed by the green fault sets, but the fault does not deform the unit e2. The relative ages of the fault sets give an idea about the number of palaeoearthquakes sourced from the Erdoğmuş fault. According to the relative age of fault sets, at least three different seismic events have been originated from the Erdoğmuş fault.

Totally, 13 faults have been measured at the EF-1 and they have been listed in Table 5.1. Fault signed by number 9 is the surface rupture of the 1970 Gediz earthquake. A few slip-plane data have been obtained (Figure 5.14), but they are not enough for tensor analysis. These faults are both antithetic and synthetic in nature.



Figure 5.10. Panoramic view of the eastern wall of EF-1.

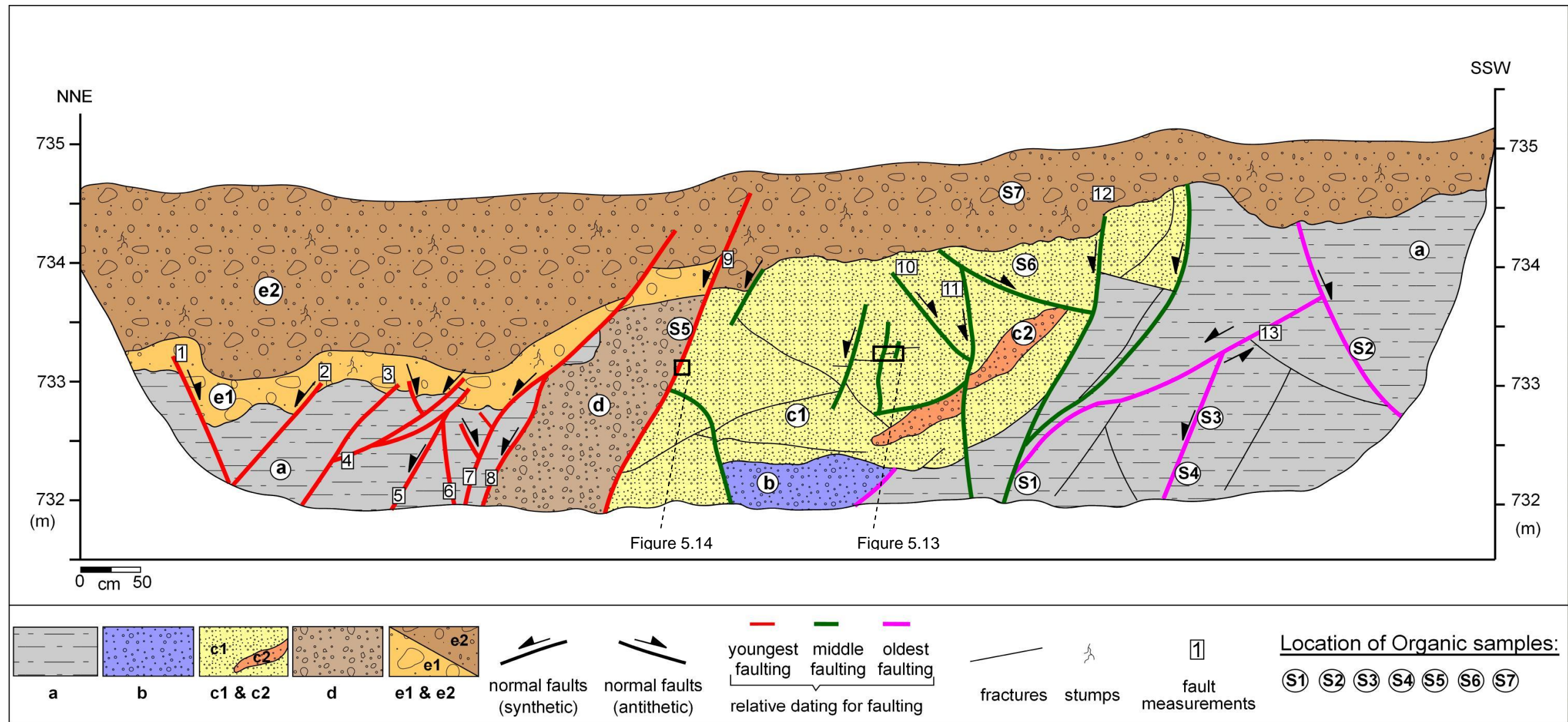


Figure 5.11. EF-1 trench log of eastern wall (see text for more explanation). a. Dark to light grey highly deformed marl. Dark brown sand to pebble size polygenetic unsorted conglomerates having irregular boundary between c1 unit, c1. Light brown colored, coarse grained sandy gravel lenses, c2. Light yellow to dark yellow, fine to coarse grained sandy gravels, massive containing uneven lenses with larger grain size of sand, highly deformed by faults and fractures, d. Light brown-yellow sandy gravel to gravelly sand imbricated pebbles massive layer polygenetic, unsorted well-rounded, moderately lithified, e1 and e2. Brown to yellow-brown soil level made up of boulder to pebble clasts polygenetic, unsorted and angular to semi rounded with granular matrix contains stumps abundantly (Horizon A).

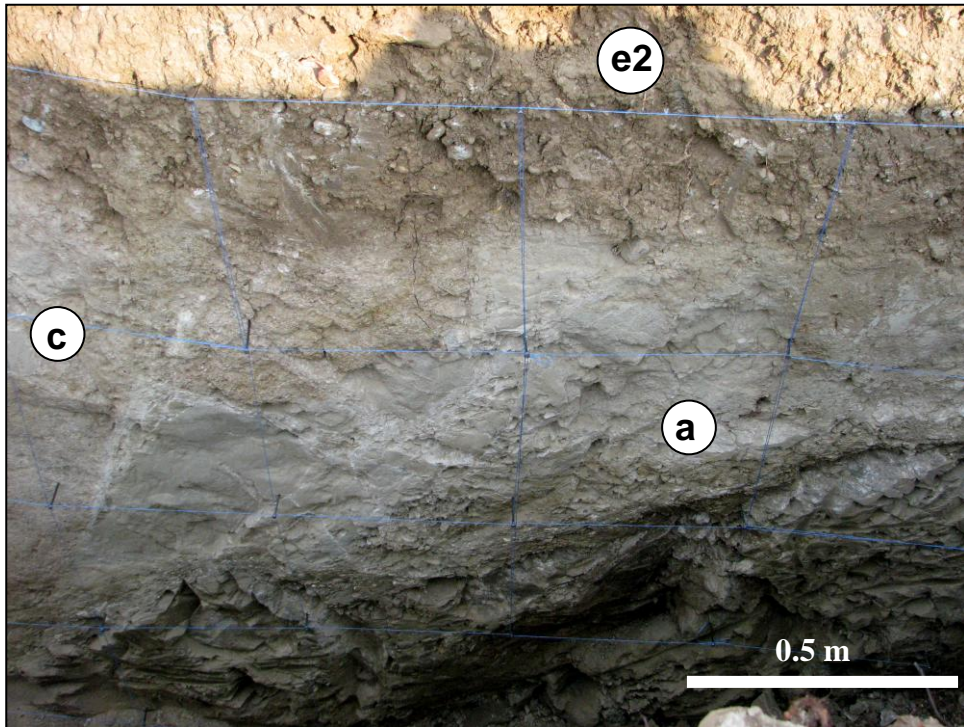


Figure 5.12. Close up view of the deformed marl (unit a) exposed on the eastern wall of EF-1.



Figure 5.13. Close up view of the faulted unit c1.

Table 5.1. Fault measurements on slickenside in EF-1.

Fault no:	Attitude
1	N30°W, 65°SW
2	N55°W, 45°NE
3	N60°W, 55°NE
4	N20°W, 20°NE
5	N48°W, 60°SW
6	N48°W, 82°SW
7	N40°W, 48°NE
8	N55°W, 56°NE
9	N60°W, 55°NE
10	N80°W, 54°SW
11	N87°W, 85°NE
12	N70°W, 60°NE
13	N46°W, 34°NE



Figure 5.14. Close-up view of the slickenside on the ground surface rupture of the 1970 earthquake (Fault no: 9 in Figure 5.11).

By using the cross-cutting relationship between faults and the faulted units, palaeoseismic events can be dated relatively. However, we also need to know the absolute ages of such seismic events. Thus, seven organic samples from different horizons of the EF-1 w collected for radiocarbon (C^{14}) dating. 6 of them (S1, S2, S4, S5, S6 and S7 in Figure 5.11) were dated at Beta Analytic Laboratory, Florida, USA (Table 5.2).

Four of the samples (S1, S2, S4, and S5) gave conventional ^{14}C age as pMC (percentage of modern carbon). The conventional ^{14}C age is the result after applying $^{13}C/^{12}C$ corrections to the measured age and is the most appropriate radiocarbon age. It means the $^{13}C/^{12}C$ was estimated rather than measured. Ages are reported as BP (before present). Present is defined as AD 1950 for the purpose of radiocarbon dating. Furthermore, results for samples containing more ^{14}C than the modern reference standard are reported as “percent modern carbon” (pMC). These results indicate the material was respiring carbon after the advent of thermo-nuclear weapons testing and is less than ~ 50 years old. Because of this reason, these 4 samples can not be used for past events. On the other hand, samples S6 and S7 gave the date as AD and BP. They indicate the timing of the last ground surface rupture-forming major earthquake on the Erdoğmuş fault occurred after cal AD 1020 (2 sigma calibration AD 980-1050/970-900) and before this event there was one more ground surface rupture-forming event which occurred after cal 990 AD (2 sigma calibration AD 890-1030). The results of these samples are very close to each and most probably, they are related to a single event occurred around AD 1060.

Table 5.2. Summary of radiocarbon dating results

Field sample number	Laboratory sample number	Trench	Material type	Measured ¹⁴ C age (years BP)	¹³ C/ ¹² C Ratio (‰)	Conventional ¹⁴ C age (years BP)	Calibrated age (years AD or BC and BP)
S1	Beta-271371	EF-1	Organic sediment	106.7 +/- 0.5 pMC	-25.9	106.9 +/- 0.5 pMC	-
S2	Beta-271372	EF-1	Organic sediment	114.8 +/- 0.6 pMC	-26.5	115.1 +/- 0.6 pMC	-
S4	Beta-271373	EF-1	Organic sediment	107.3 +/- 0.5 pMC	-25.7	107.5 +/- 0.5 pMC	-
S5	Beta-271374	EF-1	Organic sediment	113.1 +/- 0.5 pMC	-26.3	113.4 +/- 0.5 pMC	-
S6	Beta-271375	EF-1	Organic sediment	970 +/- 40 BP	-22.4	1010 +/- 40 BP	AD 1020 (930 BP)
S7	Beta-271376	EF-1	Organic sediment	1030 +/- 40 BP	-23.0	1060 +/- 40 BP	AD 990 (960 BP)

Briefly, by using the timing of the 1060 and 1970 events sourced from the Erdoğmuş Fault, it can be concluded that the recurrence interval of the ground surface rupture-forming large earthquake is an approximately 910 yrs. If it is compared with the slip-rate measured by TUTGA data (0.5 mm/yr), the result is reliable. During this time, 4.55 meter displacement might be occurred. In 1970, maximum 2 m displacement was measured (Ambraseys and Tchalenko, 1972). This is the value measured on ground surface. In the deeper part of the fault, the displacement should be more than 2 m.

5.4.2. Trench – 2 (EF-2)

Trench – 2 (EF-2) is located at the near NW of Erdoğmuş village (Figure 5.4), where terrace sediments of the Kör Çay are observed at the surface.

The western wall of the trench (EF-2. Figure 5.15) displays a very obvious fault pattern of the the 1970 Gediz earthquake (fault no: 1 in Figure 5.16) and various faulted lithofacies same as those in the EF-1 eastern wall (Figure 5.16). Unfortunately, there is no any organic materials can be obtained from EF-2 for radiocarbon dating. However, by using the cross-cutting relationships between faults, and two different events were interpreted.



Figure 5.15. Photo from western wall of the EF-2.

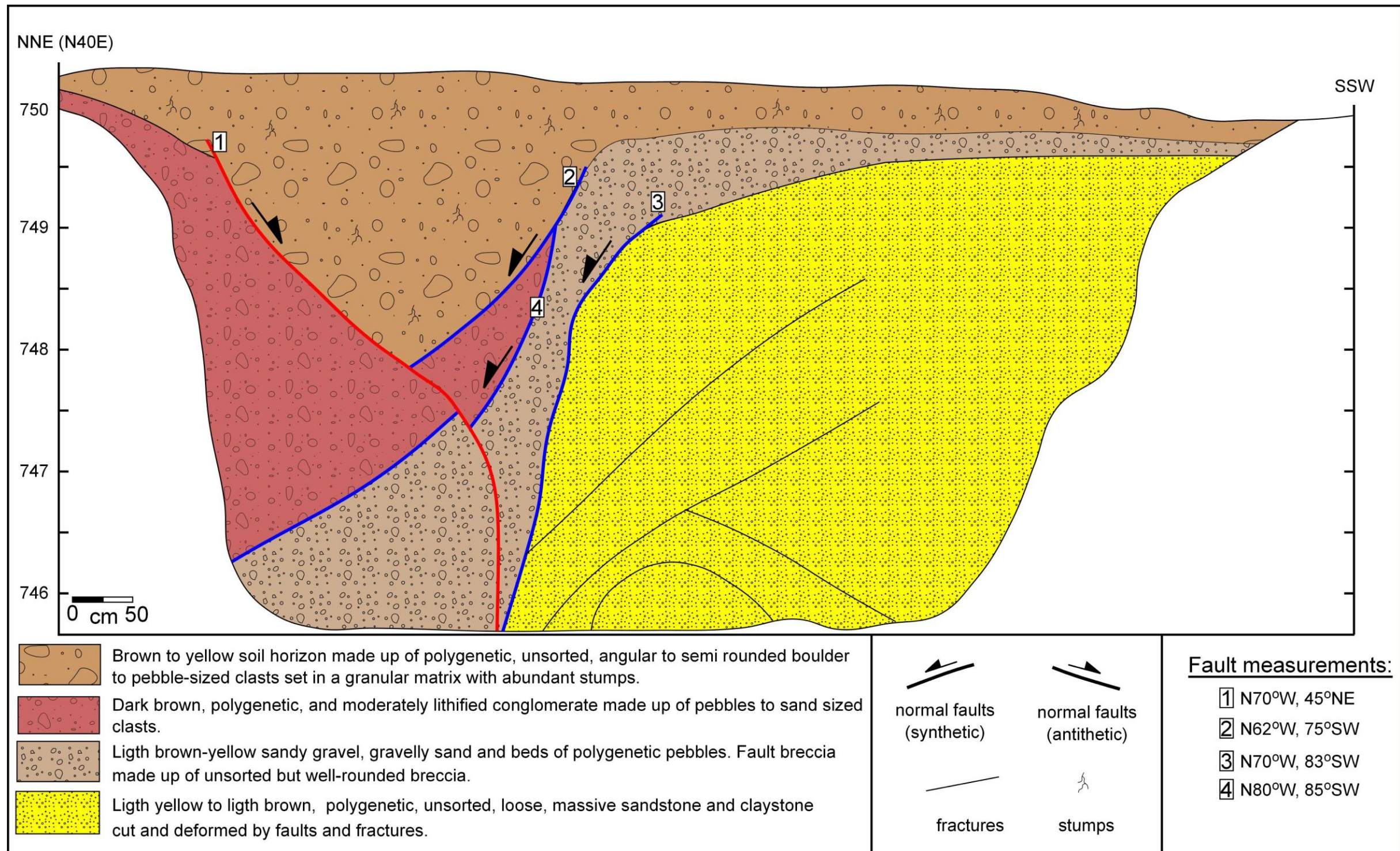


Figure 5.16. EF-2 trench log of western wall.

CHAPTER 6

DETERMINISTIC SEISMIC HAZARD ASSESSMENT

6.1. Introduction

Seismic hazard studies have become increasingly more important for earthquake engineering applications all around the world. It is possible to mitigate the damages by using engineering techniques. Seismic hazard assessment is commonly used to define and classify any susceptible areas and in the preparation of seismic zonation maps. The first map in Turkey was published in 1996 by the Ministry of Public Works and Settlements (Figure 6.1.). Turkey is categorized into five different seismic zones: I to V, each of which has specific PGA (peak ground acceleration) values of >0.4 g, $0.3-0.4$ g, $0.2-0.3$ g, $0.1-0.2$ g and <0.1 g, respectively. 43 % of cities are located in zone I., whereas 28 % of them in zone II. These settlements are highly populated and industrialized; therefore they play important roles in contry's economy.

The main use of the seismic hazard mapping is to obtain ground motion distribution in any place. The ground motion parameters include peak ground acceleration, peak velocity, peak displacement, and response spectral values or histories of acceleration, velocity and displacement gained from past earthquakes. There are two main approaches for the preparation of seismic hazard map: deterministic and probabilistic.

As it is previously stated, the study area is located on the ASFS that is one of the major extensional structures causing a series of destructive earthquakes in western Turkey. Due to the significant earthquake sources in and around the thesis area (rectangle in Figure 6.1) on the I. degree earthquake zone that has ground acceleration 0.4 g and more, this place is under big earthquake susceptibility. The possible sources of large magnitude earthquakes are Muratdağı Fault Zone, Şaphane Fault Zone, Simav Fault Zone and Yeşilova Fault Zone. Geological characteristics of these fault zones are given in Chapter 4 in detail.

In this Chapter, seismic hazard evaluation of the study area is discussed and analyzed by using parameters like attenuation relationship, peak ground acceleration (PGA), and peak magnitude values.

6.2. Approaches for the Preparation of Seismic Hazard Maps

Two basic approaches for the seismic hazard analysis: (i) deterministic seismic hazard analysis (DSHA) and (ii) probabilistic seismic hazard analysis (PSHA). Deterministic approach is based on scenario earthquake that occur (Reiter, 1990; Anderson, 1997; Anderson, et al., 2000) at any site. The PSHA considers all possible earthquake scenarios as well as possible ground motion probability levels along with their associated probabilities; and it computes the probability that any of the scenarios produce a ground motion greater than the specific test value. The deterministic approach leads to a single ground motion for each scenario considered, whereas, the probabilistic approach guide to a hazard curve, giving the probability of exceeding various ground motion values (Abrahamson, 2000).

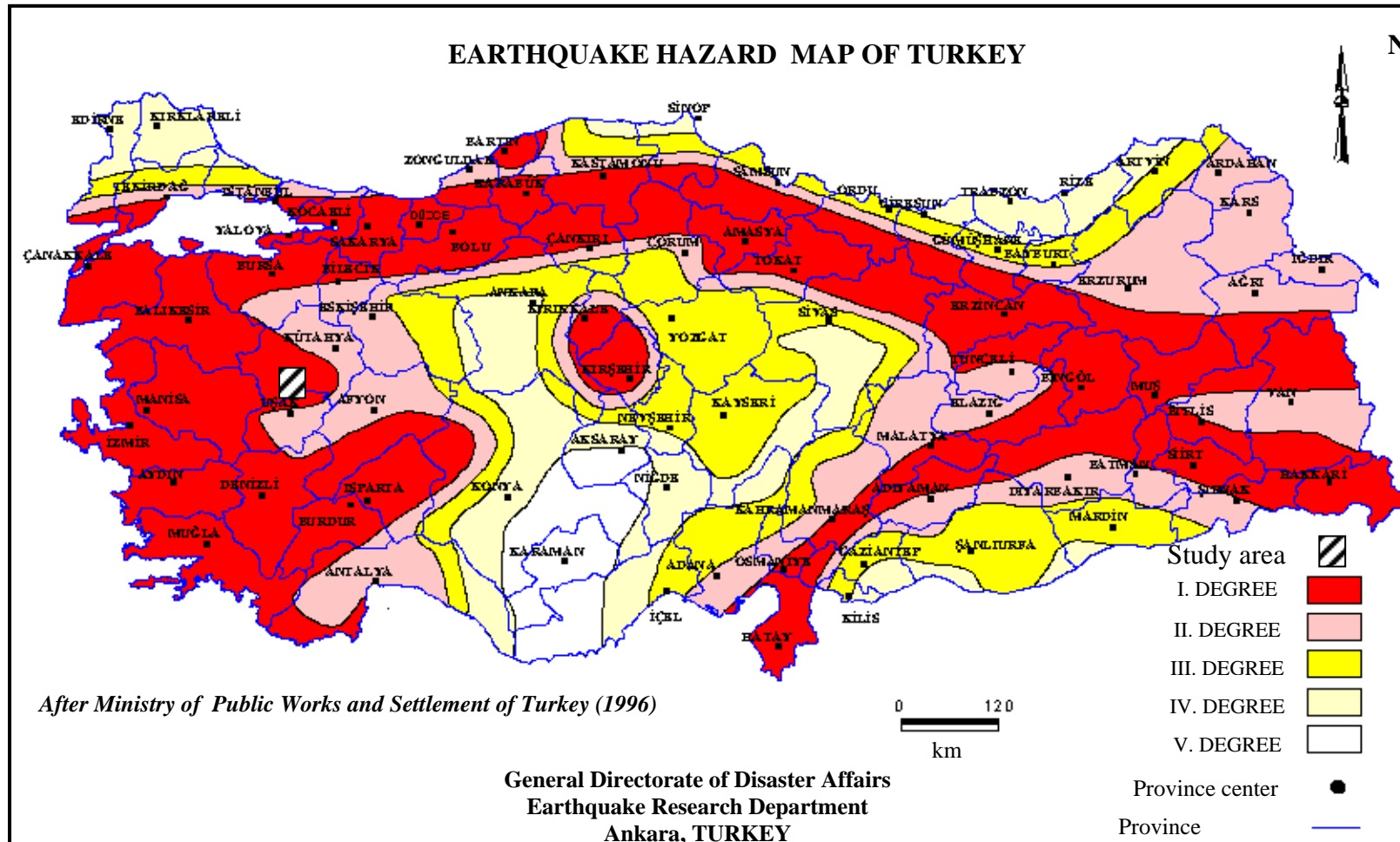


Figure 6.1. Earthquake hazard map of Turkey. Rectangle shows the study area (After Ministry of Public Works and Settlement of Turkey, 1996).

In the content of this research, deterministic approach is chosen to prepare seismic hazard assessment. In the following part, deterministic and probabilistic approaches have been explained and compared to each other.

6.2.1. Deterministic Seismic Hazard Analysis

In a deterministic seismic hazard analysis (DSHA), earthquake scenarios are evaluated separately and for each sources (single faults or fault zones), a scenario earthquake is defined by magnitude, distance between source and area, style of faulting and in some cases rupture direction. The ground motion for the scenario earthquake is usually estimated by using attenuation relationship, but is sometimes estimated using seismological simulations of the ground motion (Abrahamson, 2000). DSHA is based on geology and is attenuated to physical reality in nature. Deterministic approach therefore is useful and accurate method for seismic hazard assessment in the present study.

A typical DSHA can be described in four-step process (Reiter, 1990) :

1. Identification and characterization of all earthquake sources capable of producing significant ground motion at the site. Source characterization includes definition of each source's geometry and earthquake potential (Figure 6.2).

2. Selection of a source-to-site distance parameter for each source zone. In most DSHAs, the shortest distance between the source zone or point and the site of interest is selected. The distance may be expressed as an epicentral distance or hypocentral distance, depending on the measure of distance of the predictive relationship(s) used in the following step.

3. Selection of the controlling earthquake (i.e, the earthquake that is expected to produce the strongest level of shaking), generally expressed in terms of some ground motion parameter, at the site. The selection is made by comparing the level of shaking produced by earthquakes (identified in step 1) assumed to occur at the distances identified in step 2. The controlling earthquake is described in terms of its size (usually expressed as magnitude) and distance from the site (Figure 6.2).

4. The characteristics of hazard are usually described by one or more ground motion parameters obtained from predictive relationships. Peak ground acceleration, peak velocity and response spectrum ordinates are commonly used to characterize the seismic hazard (Figure 6.2).

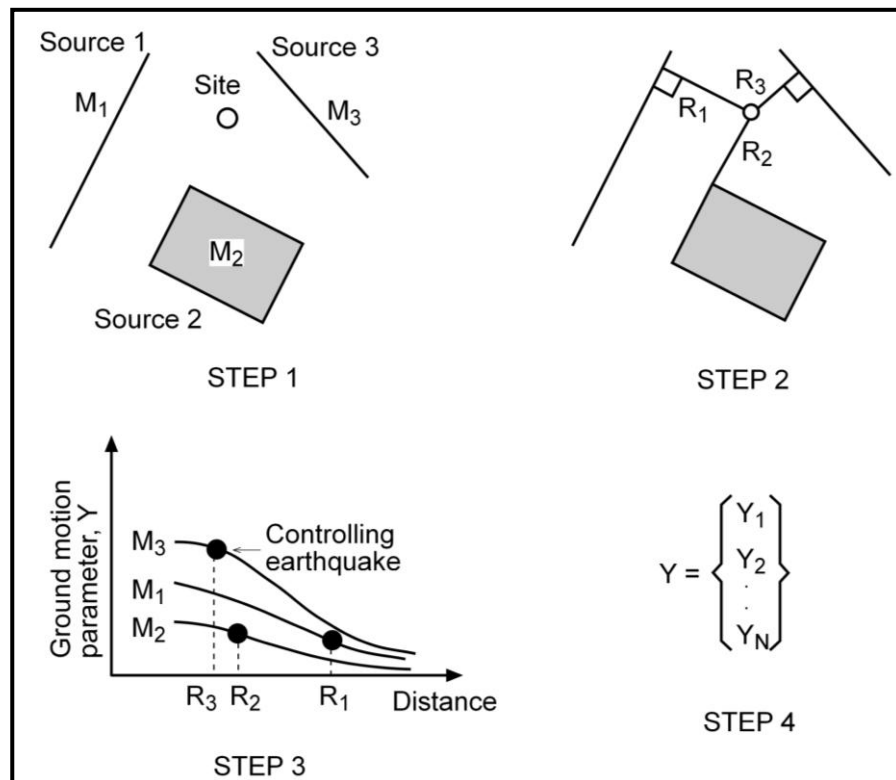


Figure 6.2. Four main steps of a deterministic seismic hazard analysis (Kramer 1996).

6.2.2. Probabilistic Seismic Hazard Analysis

Probabilistic seismic hazard analysis (PSHA) is more complicated than deterministic analysis and is often seen as a “black box” by practicing engineers. For this reason, PSHA seems to be less reliable than DSHA. In the past 20 to 30 years, the use of probabilistic concepts has allowed uncertainties in the size, location and rate of recurrence of earthquakes and in the variation of ground motion characteristics with earthquake size and location to be explicitly considered in the evaluation of seismic hazards. Probabilistic seismic hazard assessment (PSHA) provides a framework in which these uncertainties can be identified, quantified and combined in a rational manner to provide a more complete picture of the seismic hazard.

The PSHA can be described as a procedure of four steps (Reiter, 1990):

1. The first step, identification and characterization of earthquakes sources, is identical to the first step of DSHA, except that the probability distribution of potential rupture locations within the source must also be characterized (Figure 6.3).

2. Next, the seismicity or temporal distribution of earthquake recurrence must be characterized. A recurrence relationship, which specifies the average rate at which an earthquake of some size can be exceeded, is used to characterize the seismicity of each source zone. The recurrence relationship may accommodate the maximum size earthquake, but it does not limit consideration to that earthquake, as DSHA often do (Figure 6.3).

3. The ground motion produced at the site by earthquakes of any possible size occurring at any possible point in each source zone must

be determined with the use of predictive relationships. The uncertainty inherent in the predictive relationship is also considered in a PSHA (Figure 6.3).

4. Finally, the uncertainties in earthquake location, earthquake size, and ground motion parameter prediction are combined to obtain the probability that the ground motion parameter can be exceeded during a particular time period (Figure 6.3).

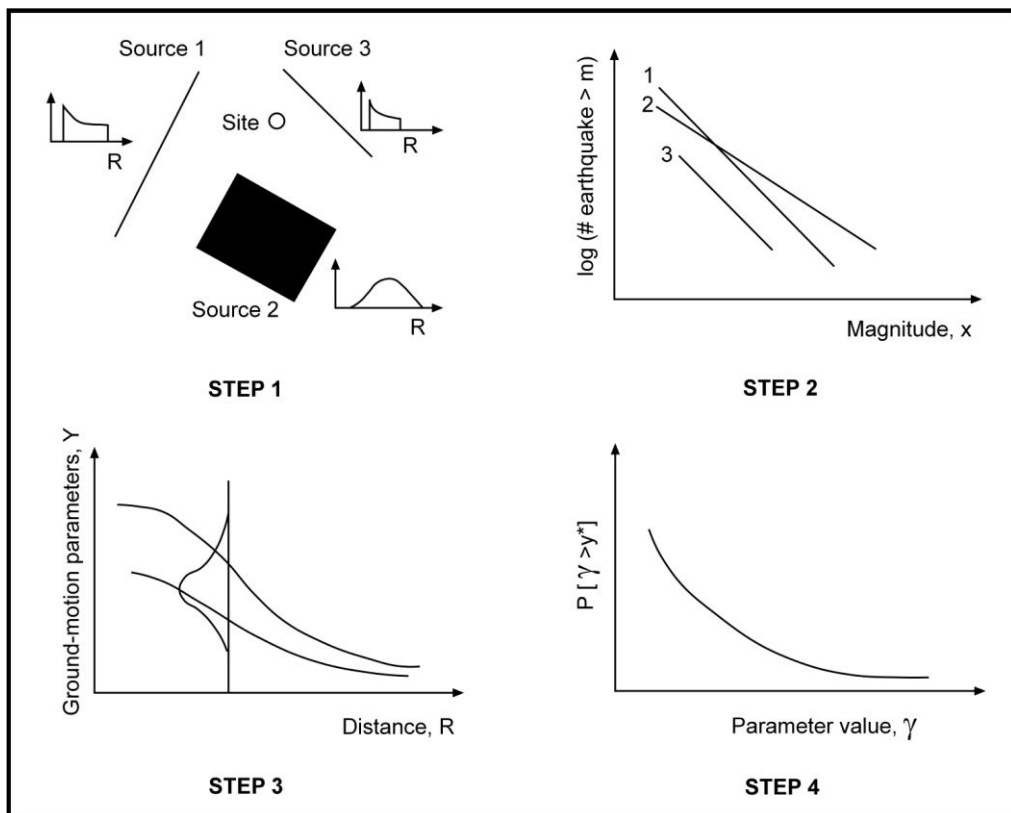


Figure 6.3. Four main steps of a deterministic seismic hazard analysis (Kramer, 1996).

The proper performance of a PSHA requires careful attention to the problems of source characterization and ground motion parameter

prediction and to the mechanics of the probability computations. But in the application of probabilistic approach, there are many uncertainties. So, probabilistic method should never be used for (1) multiple expert opinion, (2) logic tree, and (3) deaggregation. On the other hand, it can be used for (1) preliminary evaluation, (2) for an operating basis earthquake, (3) for risk analysis, and (4) for design of non-critical construction (Krinitzsky, 2003).

The advantages and disadvantages between deterministic and probabilistic approaches are compared below.

6.2.3. Comparison between DSHA and PSHA

In the 1960s and 1970s, the DSHA was used as the main type of seismic hazard analysis, but it has been gradually replaced by the PSHA. For the past two decades, the discussions are based mainly deciding which method can predict hazard of future earthquakes more accurately. The probabilities of occurrence for the “worst-case” in DSHA can be very low. This means that the construction of facilities designed for the worst hazard can be very expensive. On the other hand, the PSHA has been discussed in different aspects such as used algorithm and damage of historical earthquake. But they cannot succeed properly to imitate the earthquake generation, damage of historical earthquake and the accurate ground motion (McCalpin, 2009).

On the other hand, probabilistic approach needs more information; moreover, some assumptions have many inputs. In the case of many assumptions, the amounts of uncertainties might be increased. PSHA is just a large number of deterministic analyses with added feature such as recurrence interval, computer applications, standard deviation and definite attenuation relationship. Simpler decisions and well-understood seismicity and tectonics point to deterministic representations (McGuire,

2001). There are more discussions about the probabilistic and deterministic approaches, but they are beyond the scope of this thesis. Additionally, DSHA is based on the geological features of the site (Bommer, 2002; Krinitzsky, 2003), whereas PSHA is focused on earthquake statistics and numerical calculations (e.g., Cornell, 1968; Kijko and Öncel, 2000; Musson, Henni, 2001; Sokolov *et al.*, 2001). Because of the reasons and substantial input data, deterministic approach has been chosen to apply preparation of seismic hazard map. DSHA is more reliable than PSHA for this application, because it considers the actual geological features and is more obvious. DSHA evaluates earthquake hazards reliably based on geology regardless of time and has no need for time-based probability.

Deterministic approach is aimed to find maximum possible ground motion at the site of interest, and then the size of the largest possible earthquake is estimated for each of the previously defined seismic sources. The underlying philosophy behind, also termed as the "scenario" ground motions procedure (Anderson, 1997) is: (i) "scenario earthquake" is both scientifically reasonable and estimated to produce most severe strong ground motion at the site, (ii) the public can be informed about the possible earthquake hazards and (iii) a wide audience can fully be assured to the safety of important structures and critical facilities even for the largest possible seismic events (Bulajic and Manic, 2006).

The seismic hazard analysis in this study is assessed by using the deterministic approach for analyzing the seismic hazard probability. Before starting the detailed steps of analyses, data used for the preparation of seismic hazard map has to be clarified.

6.3. Input Data

The results of all analysis in the concept of deterministic seismic hazard analysis are extremely dependent on our knowledge about the source (faults) and other parameters. Data defining the structural models and seismic sources must be properly defined and assigned to the area (Parvez *et al.*, 2003).

In the first step of seismic hazard map preparation, earthquake sources have to be described based on their characteristics such as line, point and area and lengths. The main inputs for this application are the earthquake sources such as the fault zones namely Muratdağı, Simav, Şaphane and Yeşilova fault zones (as line sources), previous earthquake information (1970.03.28 Gediz earthquake) (as a point source), types of geologic units for the calculation of attenuation relationship and possible future events as “scenario earthquakes” sourced from the fault zones.

6.3.1. Fault Zones (as line sources)

To analyze the seismic vulnerability of the Yenigediz county and its vicinity, earthquake sources (fault zones) that may affect the area have been defined regarding the main tectonic structures. There are four main fault zones in this part of ASFs in the thesis area that may create big earthquakes and hit the study area sternly. These fault zones include a number of single faults; however, they are being represented and evaluated separately as a single line. The demonstration of fault zones has also very important variable for the estimation of magnitude. In this point of view, fault segmentation has to be done properly. For example, it was common to use 1/3 to 1/2 of the total fault length for the estimation of earthquake magnitude (Mark, 1977). Later on, fault segmentation studies on well-studied faults have replaced

(Abrahamsan, 2000). But in this study, all single faults in each fault zones were connected to get as single line. The main reason of this assumption is that the study area is not very large, so, in case of an earthquake they may move together within each fault zone at once. Briefly, these four fault zones can be drawn as a single line and should be analysed as a line source. This is very helpful for the estimation of earthquake magnitude.

6.3.1.1. Muratdağı, Simav, Şaphane and Yeşilova Fault Zones

Detailed explanations about the fault zones such as structural characteristics, displacements along them, affects of the fault zones on the evolution of study area and their length observed on the ground surface have already been presented in Chapter 4. The main data from the fault zones is the length of the faults that have been mapped at the surface. Their lengths are used to define the potential maximum magnitudes by using the logarithmic relationships derived by Aydan *et al.*, (2002) based on the data from Turkish earthquakes.

6.3.1.2. Estimation in Magnitudes of Scenario Earthquakes

Another significant step is to define the magnitude of the scenario earthquake. For these fault sources, estimated peak earthquakes so called scenario earthquake here are clarified by using the surface rupture length. Wells and Coppersmith (1994) proposed a relationship between rupture length and various magnitude values such as M_s , M_b , M_d , M_L and M_w . For the calculation of earthquake magnitudes for Turkish earthquakes, the relation proposed by Aydan (1997) was chosen. According to this research, fault rupture length versus M_s (Aydan, 1997) and fault rupture length in logarithmic scale versus M_s relations were described (Aydan *et al.*, 2002).

Before going to explain the determination of M_s and M_w by using the surface rupture length of the faults, the explanations and relationships of the various types of magnitudes are briefly clarified below:

There are different magnitude types to determine the size of an earthquake. They can be done by using the seismogram rather than on the amount of damage. To obtain different magnitudes of an earthquake, different parts of the radiation pattern of earthquake waves (body or surface waves) are used. The concept of earthquake magnitude, a relative size scale based on measurements of seismic phase amplitudes, was developed by K. Wadati and C. Richter in the 1930s, over 30 yrs before the first seismic moment was calculated in 1964 (Lay and Wallace, 1995). The general form of all magnitude scales is given by

$$M = \log (A/T) + f(\Delta, h) + C_s + C_r \quad (5.1)$$

where A is the ground displacement of the phase on which the amplitude scale is based, T is the period of the signal, f is a correction for epicentral distance (Δ) and focal depth (h), C_s is a correction for the siting of a station (e.g., variability in amplification due to rock type), and C_r is a source region correction. Magnitudes are obtained from multiple stations to overcome amplitude biases caused by radiation pattern, directivity, and anomalous path properties. Four basic magnitude scales are in use today: M_L , m_b , M_s and M_w . M_L local magnitude known as Richter magnitude was suggested by Richter (1935). Richter observed that the logarithm of maximum ground motion decayed with distance along parallel curves for many earthquakes.

$$M_L = \log A - 2.48 + 2.76 \log \Delta \quad (5.2)$$

where A is the displacement, and Δ is epicentral distance. M_L is also very useful scale for engineering applications. Many structures have natural periods close to Wood-Anderson that is a seismometer for the observation of seismic waves. Furthermore, this magnitude type can be used for an earthquake that has magnitude bigger than 6.0 and distance smaller than 700 km. m_b is the body wave magnitude which is based on the few first cycles of P-wave arrival and given by

$$m_b = \log (A/T) + Q (h, \Delta) \quad (5.3)$$

where A is the actual ground-motion amplitude in micrometers and T is the corresponding period in seconds, $Q (h, \Delta)$ is the correction for depth and distance. When m_b is measured, it is usually for the largest body wave (P, PP, etc.). M_s is surface-wave magnitude that is measured beyond the 600-km-long-period and used on $M > 6.0$ earthquakes. This is proper for the magnitudes of shallow earthquakes, because deep earthquakes cannot generate the surface-waves. The equation for surface-wave magnitude is given by

$$M_s = \log A_{20} + 1.66 \log \Delta + 2.0 \quad (5.4)$$

where A_{20} is the amplitude of the 20-s-period surface wave in micrometers.

M_w called as moment magnitude was derived by Kanamori (1977). The equation of moment magnitude is given by

$$M_w = (\log M_0 / 1.5) - 10.73 \quad (5.5)$$

where M_0 is seismic moment that is a better measure of the size of a large earthquake (Lay and Wallace, 1995). Moment magnitude (M_w) is

being increasingly used for moderate and large earthquakes all around the world. The reasons for this result are (1) it is very quick process to calculate the M_w by using the modern instruments and analytical techniques; (2) it is tied directly to physical parameters such as fault area, fault slip and energy, rather than to amplitudes of particular seismographic records in particular frequency bands; (3) geodetic, field-geology and seismographic methods are used to estimation of it; (4) this magnitude is adequately suitable for the estimation of size of large earthquakes (Yeats *et al.*, 1997). In addition, the best scale for scientific and engineering purposes is the moment magnitude (M_w) scale since it is related to the rupture parameters.

Because of the appropriate scientific and engineering usage for magnitudes, moment magnitude (M_w) was selected in this study for the construction of seismic hazard map. Moment magnitudes of scenario earthquakes sourced from different fault zones in an interested area can be calculated by using equations of Wells and Coppersmith (1994), Aydan (1997) and Ulusay *et al.* (2004). To provide a uniform and reliable scale for attenuation relationship, the database from the Turkish strong motion stations, developed by Ulusay *et al.* (2004) have been used to determine the M_w from M_s values for Turkish earthquakes. The relationship and conversion equations between $M_s - M_w$, $M_b - M_w$, $M_d - M_w$, and $M_L - M_w$, which were also derived by Ulusay *et al.* (2004) by considering the Turkish database, are given in Figure 6.4. Before defining the M_w , M_s values have to be found by using the probable surface rupture length of earthquake sources (Figure 6.5. from Aydan *et al.*, 2002). As it is mentioned before, there are four different fault zones. By using the surface length of these faults, possible rupture lengths are estimated and their relations given in Figure 6.5. are used to find the maximum magnitude (M_s) of an earthquake.

Finally, the reference point to determine the maximum magnitudes for each fault zone in the thesis area is their total lengths. The most important issue is to find out their actual lengths. In this study, all earthquake sources cut through of the study area. Although the parts of the faults that are outside of the study area are not considered in the topic of the thesis geologically, they have to be included in this chapter because of their affects in case of an earthquake. By means of the total lengths, probable M_s and then M_w values can be estimated. Later on, PGA values for interested area can be calculated.

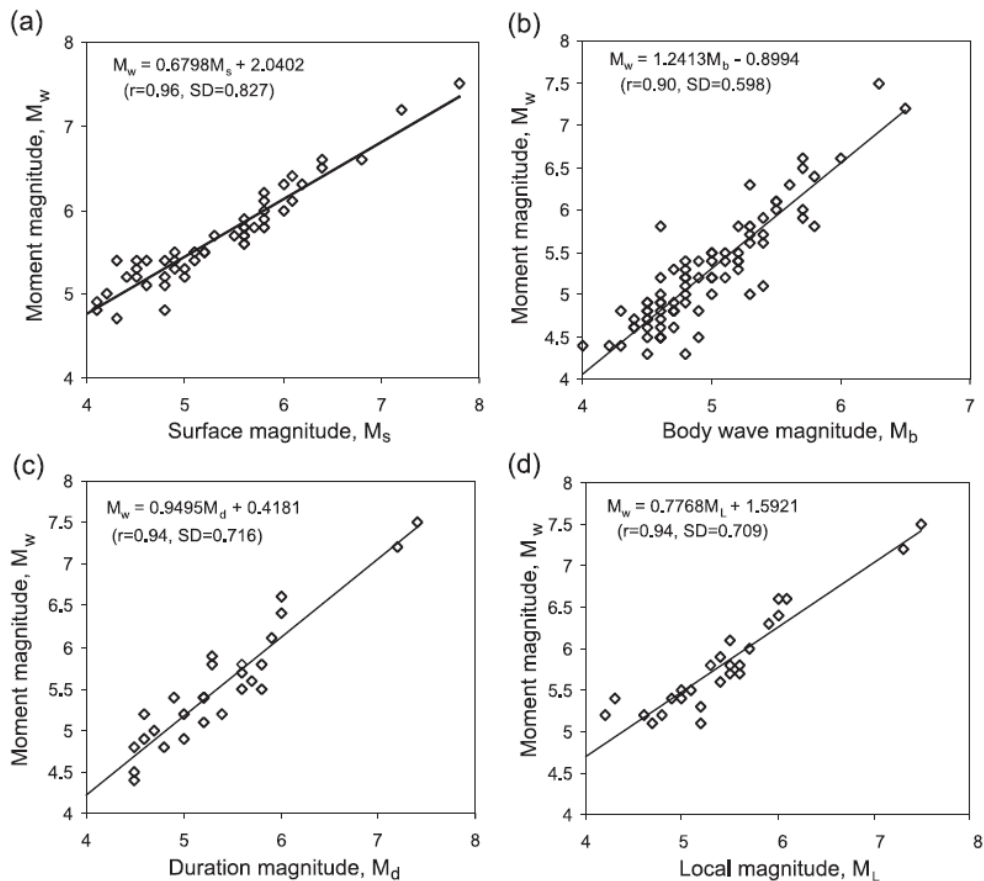


Figure 6.4. Correlations between M_w and M_s , M_b , M_d and M_L values for Turkish earthquakes (r : correlation coefficient; S.D: standart deviation) (Ulusay *et al.*, 2004).

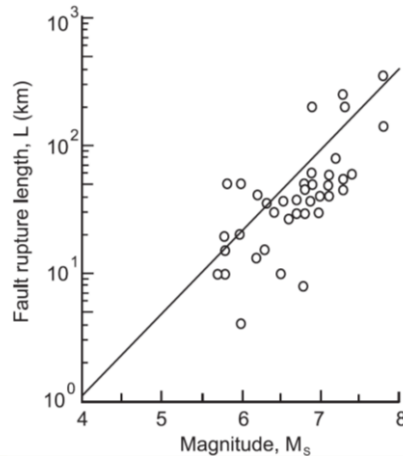


Figure 6.5. Relation between surface magnitude (M_s) and surface rupture length (L) based on the Turkish earthquakes (Aydan *et al.*, 2002).

6.3.1.3. Determination of PGA Values

The best way to estimate expected PGA is by investigating instrumental data of past strong earthquakes in a given area. This was not possible for this study, because, last strong earthquake took place in March 28, 1970 and at that time there was no strong motion station.

As a next step, PGA (peak ground acceleration) values can be calculated by using the M_w , distance between line for faults or epicenters for previous earthquakes and points assigned by the gridding on the map, and attenuation relationship equation. Attenuation relationship is a very controversial issue all around the world. Because of the dissimilar applications (PSHA or DSHA), special site conditions, different countries and authors, a number of attenuation relationships were proposed and each of them were used for different purposes. In this thesis, the equation suggested by Ulusay *et al.* (2004) was used, since, all data is from database of large Turkish earthquakes.

To analyze the faults, we need to know M_w for each fault zones by means of their total length, and S_A and S_B values. All these input data have been evaluated by ArcGIS 9.3 computer programme. The calculated values are $M_w= 6.7$ for Şaphane Fault Zone, $M_w= 6.6$ for Simav Fault Zone, $M_w= 6.6$ for Muratdağı Fault Zone and $M_w= 6.5$ for Yeşilova Fault Zone. Then, the study area was separated into equal intervals as vertical and horizontal lines (gridding). This grid system is composed of 2667 points. For each point, firstly, S_A and S_B site conditions were assigned. $S_A = S_B = 0$ for rock (basement and volcanic rocks) (Figure 6.6), $S_A = 1$ and $S_B = 0$ for soil (Miocene sediments) (Figure 6.7), and $S_A = 0$ and $S_B = 1$ for soft soil (Plio-Quaternary and alluvial deposits) (Figure 6.8) are used (Ulusay *et al.*, 2004). Secondly, attenuation relationship suggested for Turkish earthquakes by Ulusay *et al.*, (2004) was employed for this analysis.

$$PGA = 2.18 e^{0.0218(33.3M_w - R_e + 7.8427S_A + 18.9282S_B)} \quad (5.6)$$

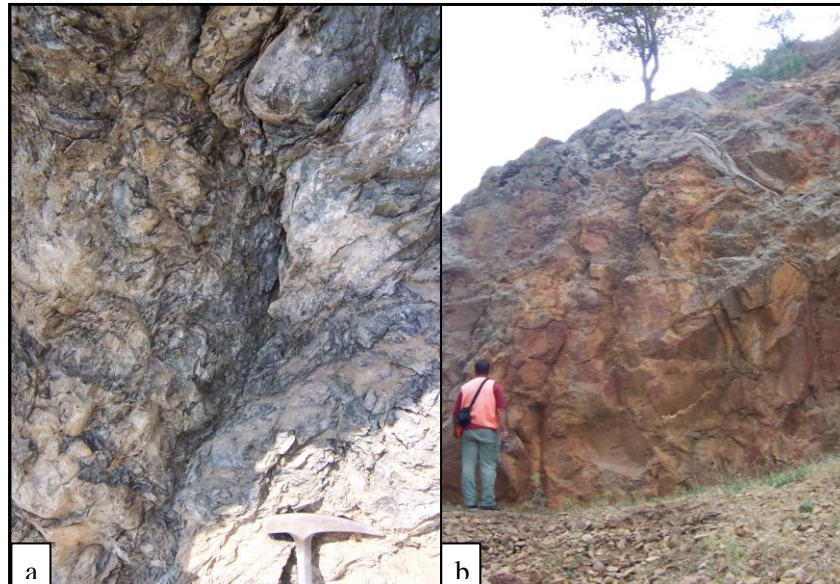


Figure 6.6. Close up view of the basement (a) and volcanic rocks (b) ($S_A = S_B = 0$).



Figure 6.7. General view of the tilted Miocene beds ($S_A = 1$ and $S_B = 0$).

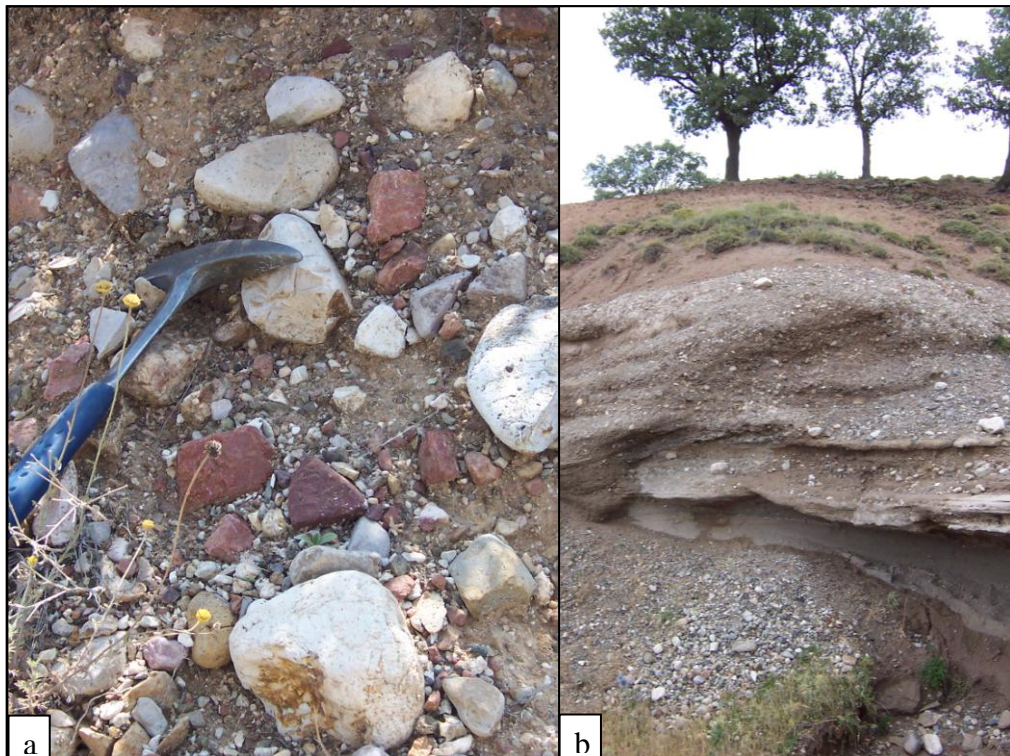


Figure 6.8. Close up view of the Plio-Quaternary (a) and alluvial deposits (b) ($S_A = 0$ and $S_B = 1$).

For the analysis of data, all unknown parameters have been determined such as total length of faults (earthquake sources) for maximum magnitude, gridding of the study area and the distance between center points of all gridding square and faults, site conditions (S_A and S_B), and attenuation relationship. Later on, the study area can be analyzed by using the computer program for each fault zone. It means that four different maps for four scenario earthquakes have been produced. Additionally, one more map has also been produced by using the epicenter of the 1970 Gediz earthquake as a point source. And then, these five maps have been compared to each other.

6.3.2. Previous Earthquake Information (as a point source)

Two types of DSHA have been performed in this study. They are the line sources (fault zones) and point source (1970 Gediz earthquake). Four maps have been produced. On the other hand, only one point (epicenter of the 1970 earthquake) source has been used to generate the hazard map. Although, in the thesis area, 2 large earthquakes occurred in the 1944 and 1970, there is no reliable epicentral information about the 1944 earthquake. Due to this restriction, the epicenter of the 1970 Gediz earthquake could only be used for hazard analysis.

6.4. Flow Chart of the Deterministic Seismic Hazard Mapping

As it was mentioned before, scenario-based deterministic approach is more appropriate for this study. It allows the user to a realistic definition of hazard in scenario-like format to be accompanied by the determination of advanced hazard indicators.

The steps which can be applied in the deterministic approach have been explained before. According to this flow chart, the geological map

of study area has been prepared (Appendix – A). Mapping is significant to determine the ground motion (shaking) in case of a scenario earthquake.

Two different scenario earthquakes have been arranged for the deterministic approach. First one is the reactivation of fault zones. Second is the previous events which gave huge damages on the study area, taken as a reference earthquake (28.03.1970 $M_w= 7.2$ Gediz earthquake) to create scenario earthquake. The source of this earthquake has been shown by red line in the Appendix – A. It gives approximately 9 km surface rupture length and can yield $\sim 6.6 M_w$ that is calculated by total length of the fault zone.

In this study, type of faulting is not considered in the usage of the attenuation relationship. In some recent studies (Douglas, 2003; Aydan and Hasgür, 1997), the attenuation models have different ground motion from reverse and strike-slip earthquakes.

In summary,

- 1) S_A and S_B values for each point have been assigned,
- 2) Shortest distance between fault line and assigned points have been calculated (R_e),
- 3) M_w values have been determined for each fault line and 1970 Gediz earthquake,
- 4) Lastly, by using the PGA formula suggested by Ulusay *et al.*, (2004) have been applied.

6.4.1. Results of the DSHA for Line Sources

According to 2667 point locations (Figure 6.9), results of the DSHA have been submitted. For each point, S_A and S_B values were described

by considering the rock types and the closest distance have been calculated. Based on the distance, zonation of PGA values has been performed.

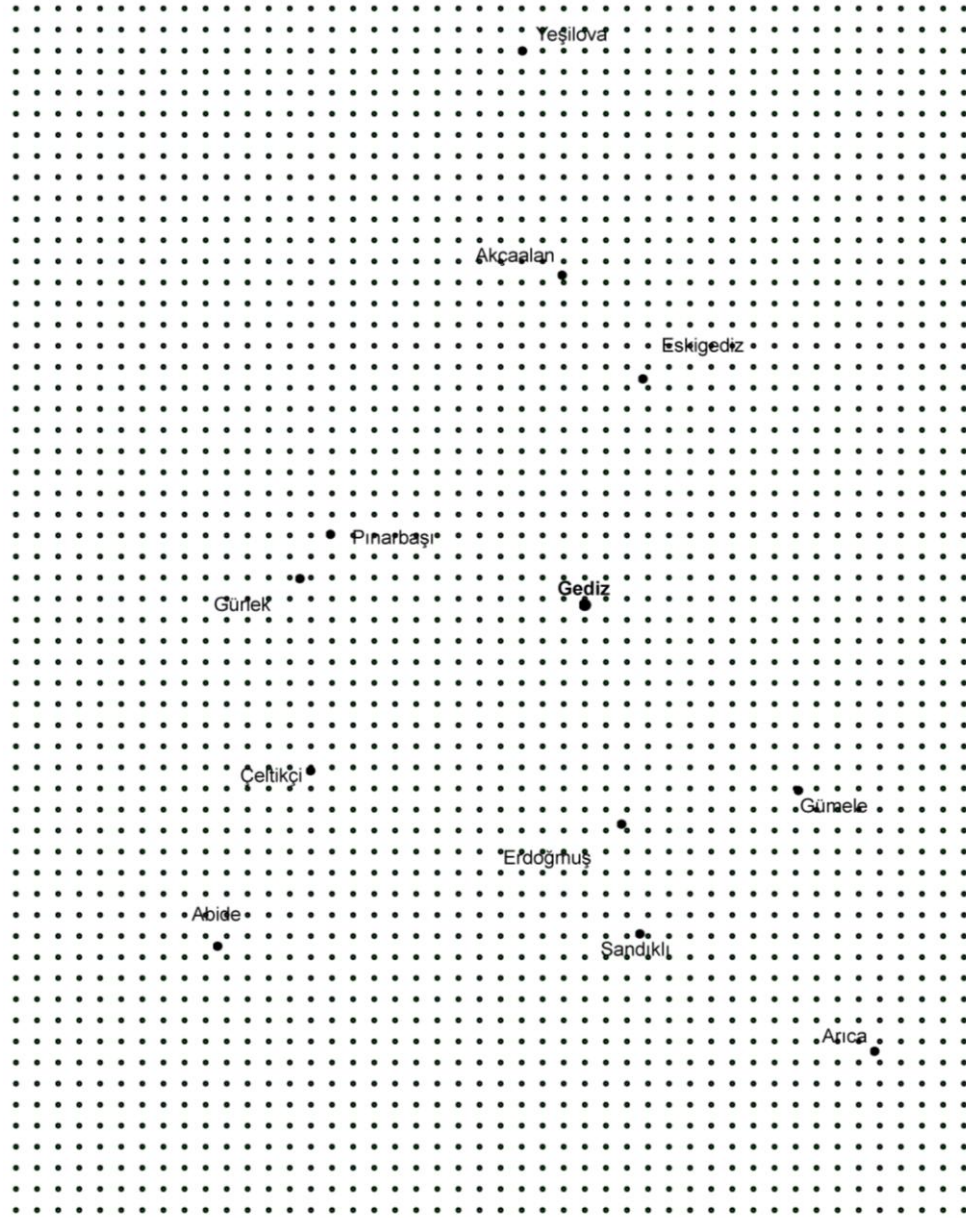


Figure 6.9. Assigned point locations of the study area as base map for deterministic hazard analysis.

The locations of the fault zones are shown in Figure 6.10 and for each fault, different calculation process were performed.

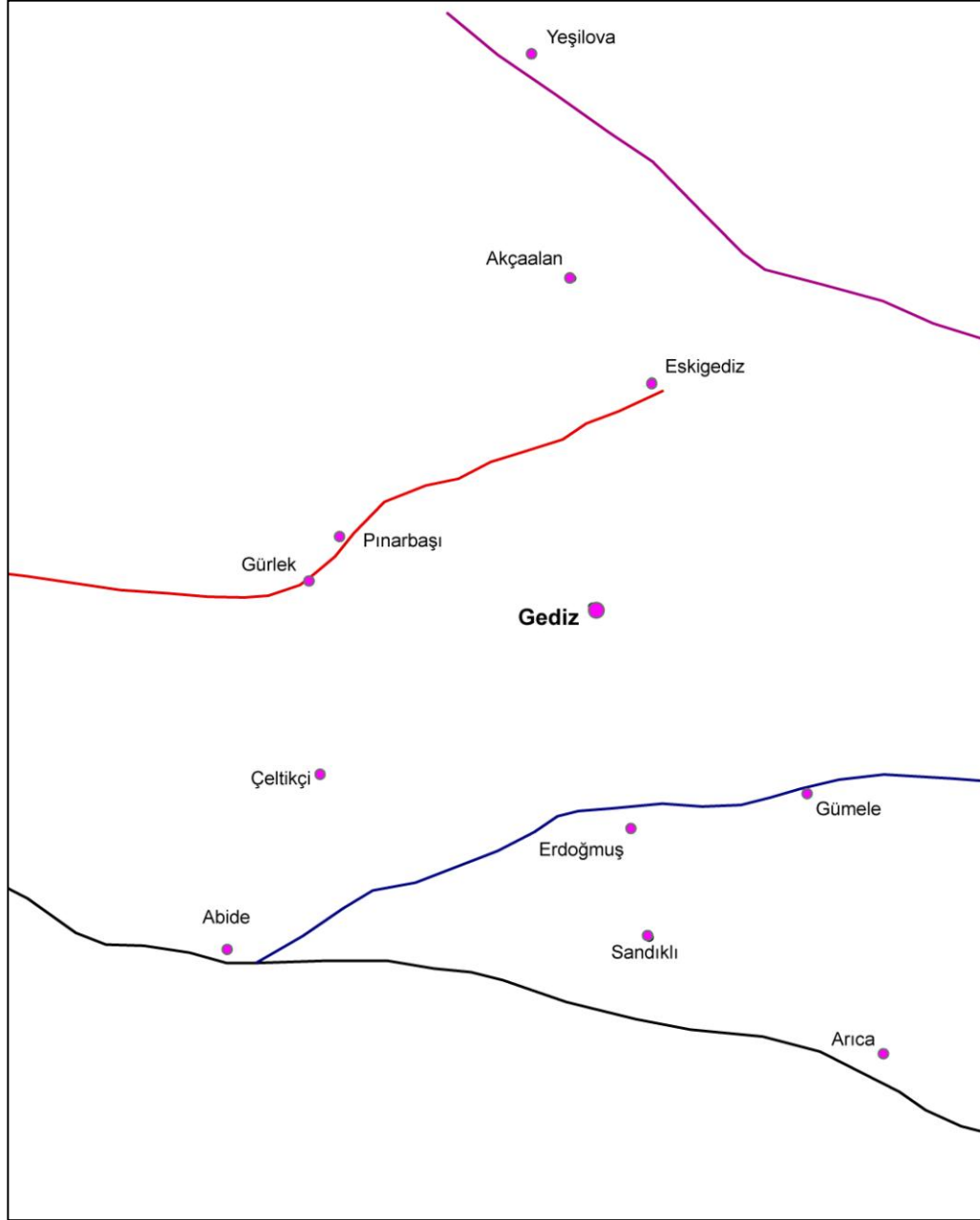


Figure 6.10. The locations of Muratdağı (blue line), Simav (black line), Şaphane (red line) and Yeşilova (purple line) fault zones (purple dots show the settlements).

In order to estimate the PGA values and prepare deterministic seismic hazard maps of the study area, four fault zones have been analyzed. The results of the zonation map of PGA values for Muratdağı (Figure 6.11), Simav, (Figure 6.12), Şaphane (Figure 6.13) and Yeşilova (Figure 6.14) fault zone have been presented.

The detailed examination of these results indicates that the PGA values changes in the range of 0.233 – 0.366 g. The peak values are observed in the places where major fault zone and alluvium exist. Oppositely, volcanic and metamorphic rocks yield very low PGA values.

Based on the main fault zones, the study area has been analyzed according to line source model. On the other hand, one more deterministic seismic hazard map has been produced based on point source as epicenter of 1970 Gediz earthquake (Figure 6.15). When it was examined in detail, the result is exactly the same as the result of Yeşilova Fault Zone. Because, the epicenter of this earthquake is very close to Yeşilova Fault Zone and their products are coincided.

Lastly, the comparison between computational result of the 1970 Gediz earthquake (Figure 6.15) and izoseist distribution (Figure 6.16) after the earthquake shows some differences because of the scale disparity. The most severe damage took place in Eskigediz county and Akçaalan village during the earthquake. The main reason was a fire in Eskigediz.

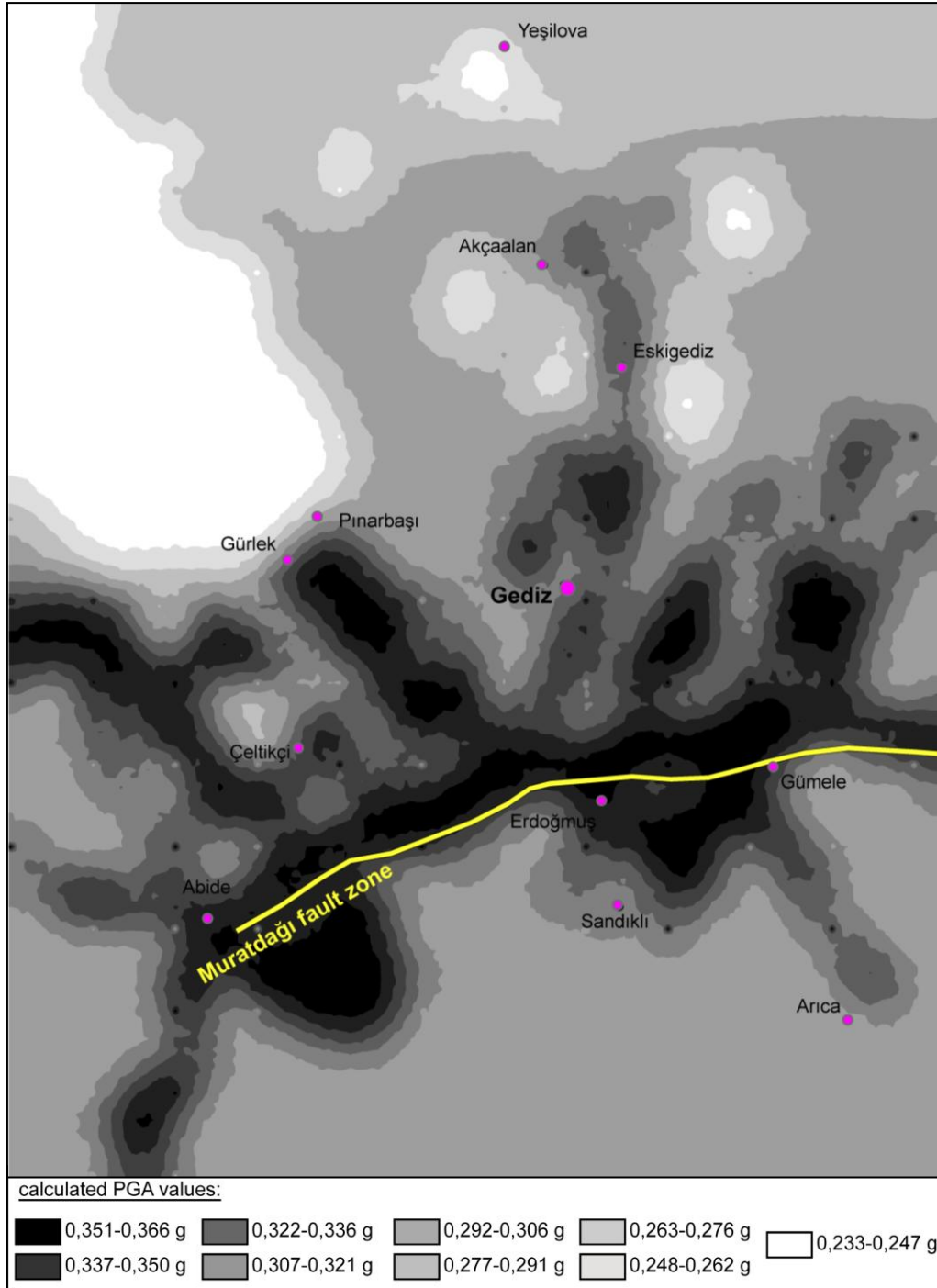


Figure 6.11. Deterministic seismic hazard map showing ground motions (PGA) expected from M_w 6.7 scenario earthquake sourced from Muratdağı fault zone.

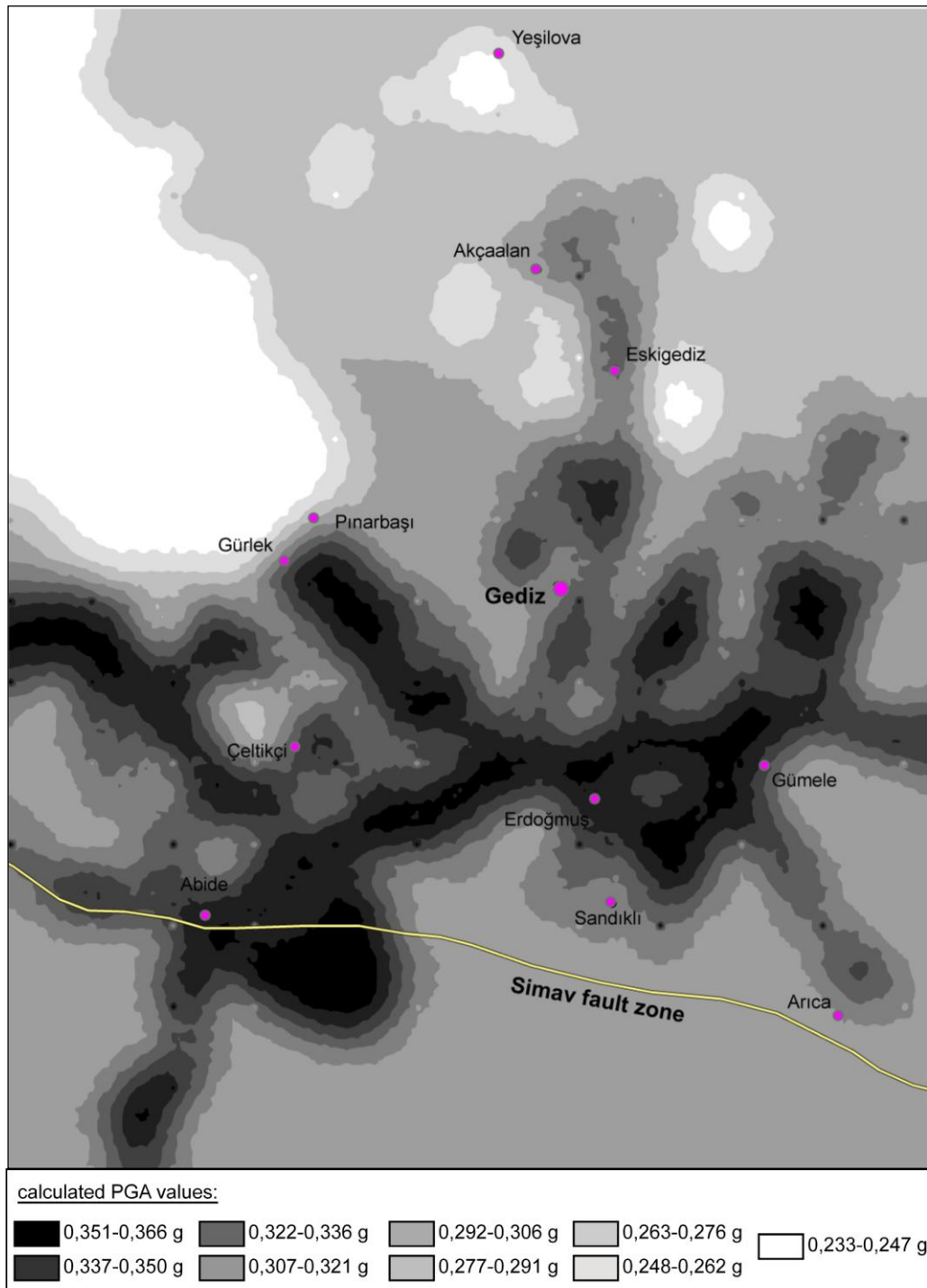


Figure 6.12. Deterministic seismic hazard map showing ground motions (PGA) expected from a M 6.6 scenario earthquake sourced from Simav fault zone.

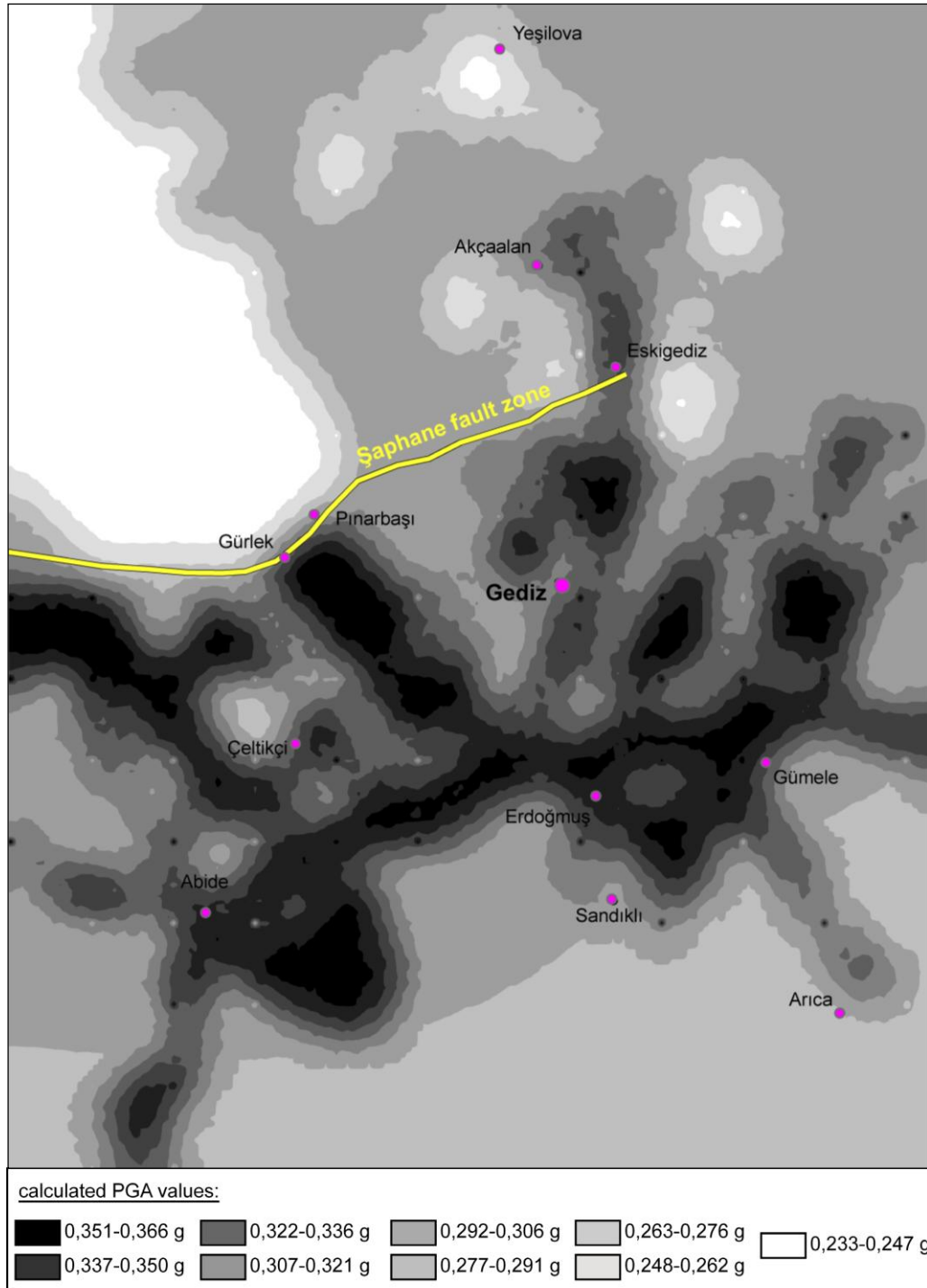


Figure 6.13. Deterministic seismic hazard map showing ground motions (PGA) expected from a M_w 6.6 scenario earthquake sourced from Şaphane fault zone.

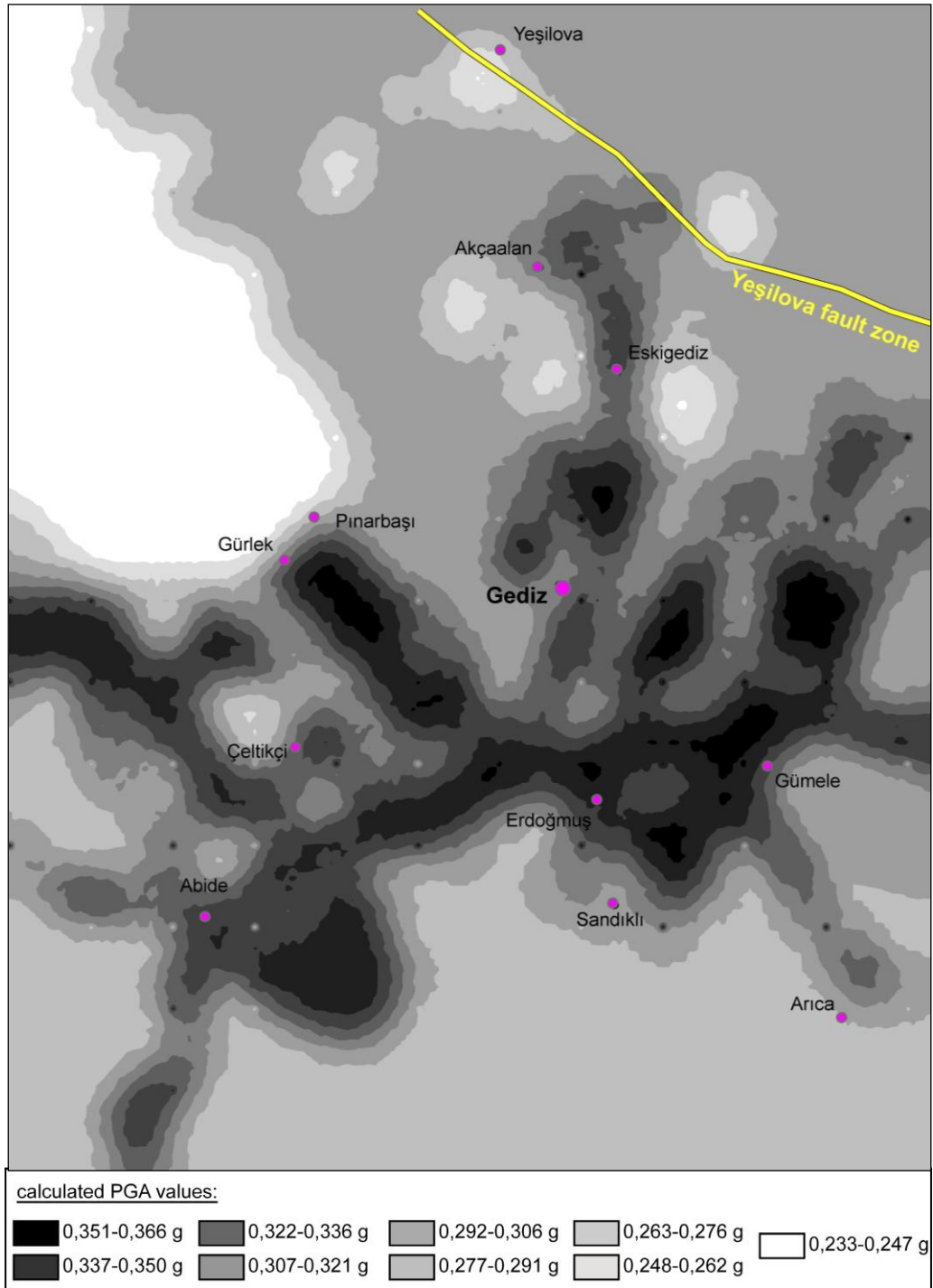


Figure 6.14. Deterministic seismic hazard map showing ground motions (PGA) expected from a M_w 6.5 scenario earthquake sourced from Yeşilova fault zone.

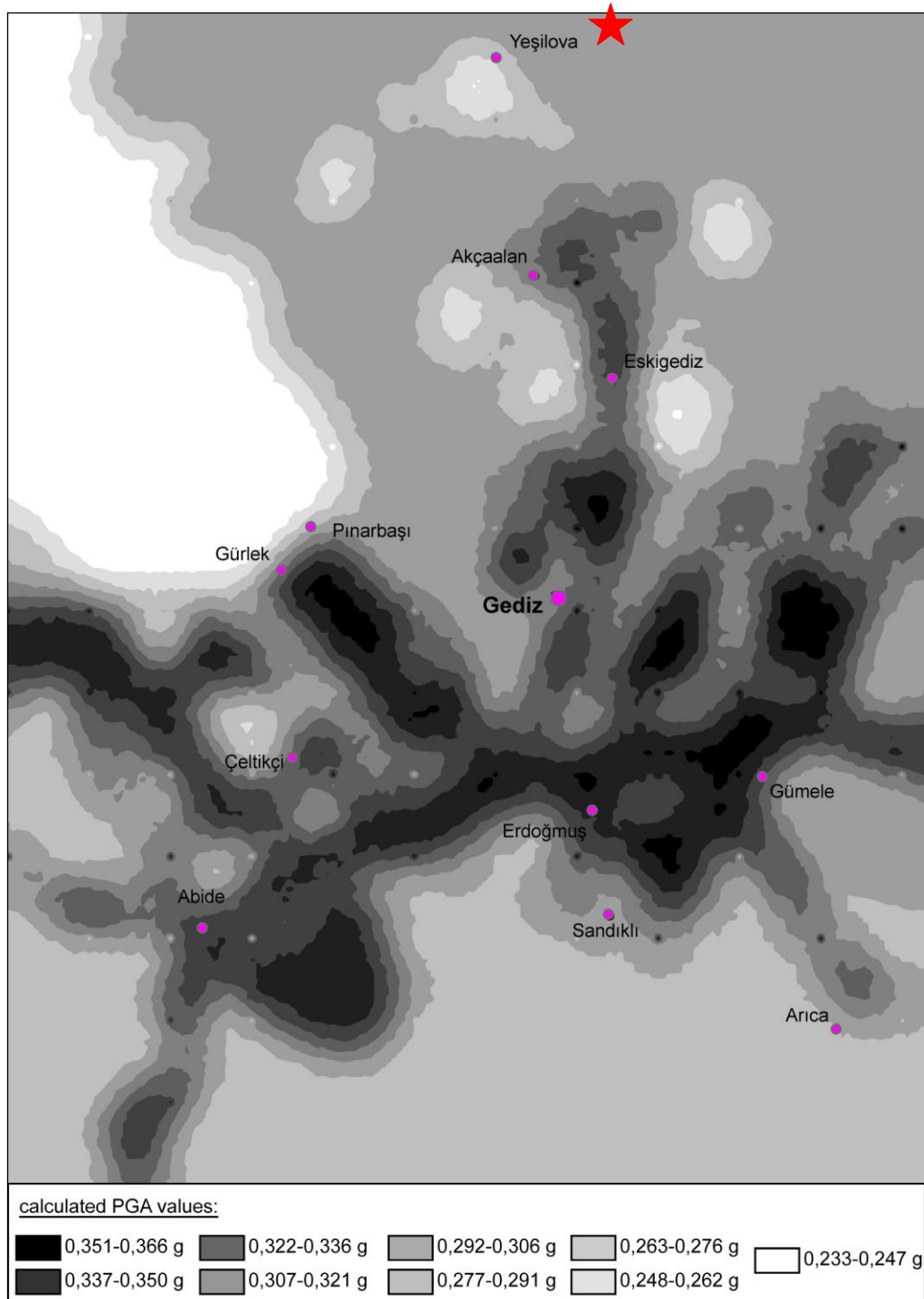


Figure 6.15. Deterministic seismic hazard map showing ground motions (PGA) expected from M_w 7.2 1970 Gediz earthquake (red star is the epicenter of the earthquake).

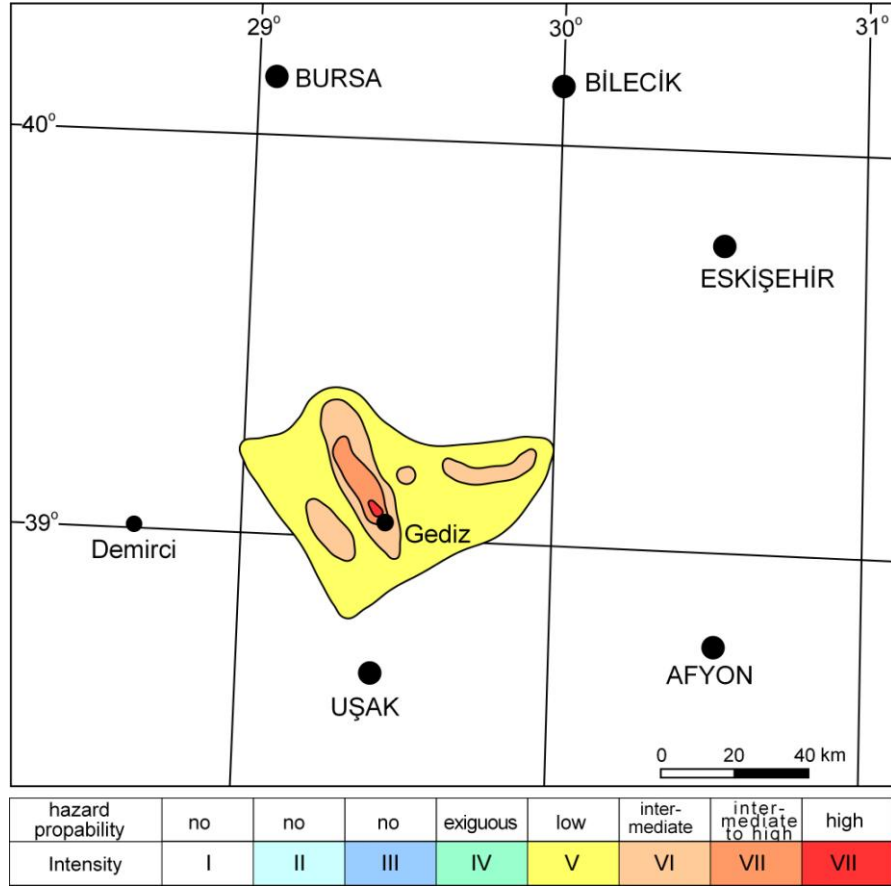


Figure 6.16. Izoseist map of the 1970 Gediz earthquake (Abdüsselamoğlu, 1970).

The deterministic approach gives a clear and trackable method of computing seismic hazard whose assumptions are easily discerned. In this study, site response analyses have not been carried out. Therefore, the users of these seismic hazard maps should be chary. Only the distance between points-point and points-line, maximum M_w and rock type are considered. In Figures 6.11, 6.12 6.13, 6.14 and 6.15, the highest PGA values are obtained around recent alluvial deposits.

CHAPTER 7

DISCUSSION AND EVOLUTIONARY HISTORY OF THE AREA

Recently, discussions about the intraplate extension and the formation of related graben-horst system in western Anatolia are focused on two points: (a) source and commencement age of tensional tectonic regime, (b) evolutionary style or models of the graben-horst system. Even if there are several ideas and numerous studies carried out in western Anatolia to solve these problems, there is still no a common agreement on particularly the evolutionary history of the Southwest Anatolian graben-horst system (SWAGHS). In general, there are two views on the evolutionary style or model for the SWAGHS: (1) Latest Oligocene to recent continuous evolutionary model (continuous extension) (Seyitoğlu and Scott 1991; Glodny and Hetzel 2007; Seyitoğlu and Işık 2009; Agostini *et al.* 2010), and (2) Episodic two-stage extensional model (episodic or discontinuous extension) (Koçyiğit *et al.* 1999; Koçyiğit *et al.* 2000; Ring *et al.* 1999; Yılmaz *et al.* 2000; Gürer *et al.* 2001; Kaya *et al.* 2004; Bozkurt and Sözbilir 2004; Purvis and Robertson, 2004, 2005; Koçyiğit, 2005; Bozkurt and Rojay 2005; Beccaletto and Steiner 2005; Emre and Sözbilir 2007).

Based on the first idea, the SWAGHS has been evolving without any interruption under the control of the N-S extension since latest Oligocene-Early Miocene (Seyitoğlu and Scott 1991; Glodny and Hetzel 2007; Seyitoğlu and Işık 2009; Agostini *et al.* 2010). According to the first idea, the back-arc spreading is the main driving mechanism for the evolution of SWAGHS. Across Aegean Sea and its onshore section, a

back-arc spreading phenomenon is adapted to the southwestern migration of the western Anatolia by means of subduction along the South Aegean-Cyprian arc, where the African plate is being consumed at a rate of approximately 1cm/yr beneath the Anatolia (McKenzie, 1978; Le Pichon and Angelier, 1979; Jackson and McKenzie, 1988; Kissel and Laj, 1989; Meulen Kamp *et al.* 1988, 1994; Thompson *et al.* 1998; Avigad *et al.* 1997; Jolivet *et al.* 1998). In addition, some studies carried out in the central Aegean suggested that the back-arc extension has begun at least in Early Miocene (Seyitoğlu and Scott 1991; Doglioni *et al.* 1999; Rojay *et al.* 2005; Glodny and Hetzel 2007; Seyitoğlu and Işık 2009; Agostini *et al.* 2010). However, some other studies report a long range of initiation time from 5 Ma to 60 Ma for the extension (McKenzie, 1978; Mercier, 1981; Le Pichon and Angelier, 1979; Thomson *et al.* 1998). According to the mechanism of the back-arc extension, the roll-back of subducting slab takes place, and then it is followed by the plate escapement. Based on the numerical model (Hassani *et al.* 1997), the sufficient slab length should be at least 300 km so that it can provide forces enough to manage the roll-back process and back-arc extension. Similar progressive processes are also suggested by Meulen Kamp *et al.* (1988) who suggested 26 Ma for the initiation of subduction and 12 Ma for the commencement age of extension in the region.

Another version of the continuous evolutionary model for the SWAGHS is the plate escapement suggested by Dewey and Şengör (1979). According to this model, the wedge-shaped Anatolian fragment or platelet moves westward between dextral NAFS on the north and sinistral EAFS on the south. In this model, Anatolia is being squeezed by northward motion of the African plate. For this reason, the Anatolian platelet moves westwards along the two main fault systems to compensate the force coming from the plate motions. Şengör *et al.*

(1985) also stated that the westward plate motion has caused to the E-W shortening in Aegean Sea and N-S extension in western Anatolia during Late Miocene, which is the commencement age for the graben-horst system development in western Anatolia. Whereas, recent studies carried out on the NAFS indicated that the emergence age of both the NAFS and EAFS is not older than Late Pliocene, i.e., the Anatolian platelet has not been formed yet during Miocene (Barka and Kadinsky-Cade, 1988; Koçyiğit, 1988, 1989; Westaway, 1994; Koçyiğit *et al.* 2000).

According to another recent model, the current extension in the Aegean province is driven by the differential rate of convergence between the northeastward directed subduction of the African plate and the hanging-wall disrupted Eurasian lithosphere. Considering the African plate is fixed, the faster southwestward motion of Greece relative to Cyprus-Anatolia is the main cause of the Aegean extension (Doglioni *et al.* 2002). This model depends on the paleomagnetic studies (Gürsoy *et al.* 2003; Kissel *et al.* 2003).

Gürer *et al.* (2009) have also suggested a new evolutionary style for the development of the E-W trending Büyük Menderes graben, which is one of the well-development members of the SWAGHS. This evolutionary style supports the idea of episodic evolutionary model rather than continuous extension model. They have reported that the Büyük Menderes graben had recorded two successive and independent complex tectonic events. The first event is characterized by an E-W extension caused by the NE-SW contraction during Early-Middle Miocene. This is evidenced by an angular unconformity between the Lower-Middle Miocene basin infill and the Plio-Quaternary sequence. This unconformity implies to folding, uplift and severe erosion caused by NE-SW shortening. The second tectonic event is the change in the

sense of extension from E-W to N-S, which influenced the formation of the graben by a series of progressive pulses of deformation. These are the exhumation of Menderes Massif, rapid deposition of alluvial deposits, initiation and formation of approximately E-W-trending high-angle normal faults, which bound the graben, and in the last pulse, depocentre of the graben migrated into the present position by the diachronous activity of secondary steeper listric faults. The driving mechanism of the first tectonic event is the back-arc spreading or probably the roll-back of African slab below the south Aegean region. The cause of second and later event is the southwestward escape of the Anatolian block along its boundary faults that are the North Anatolian and the East Anatolian Fault Systems.

According to the second idea (Episodic two-stage evolutionary model), the SWAGHS has been evolving at two extensional phases interrupted by an intervening short-term contractional phase (Koçyiğit *et al.* 1999; Koçyiğit *et al.* 2000; Ring *et al.* 1999; Yılmaz *et al.* 2000; Gürer *et al.* 2001; Kaya *et al.* 2004; Bozkurt and Sözbilir 2004; Koçyiğit 2005; Bozkurt and Rojay 2005; Beccaletto and Steiner 2005; Emre and Sözbilir 2007). Episodic two-stage graben model or discontinuous extension model is based on detailed field data such as detailed field geological mapping, overprinted sets of slip-plane data and their tensor analysis, detailed stratigraphy of the basin infill and their deformation pattern. These data were obtained from a number of grabens and horsts in western Anatolia. Consequently, episodic two-stage evolutionary model argues that none of the above-mentioned models alone satisfactorily explains the age and origin of the multi-stage nature of crustal extension (Koçyiğit *et al.*, 1999), because the extension occurs in two distinct structural styles and episodes: (1) an Early-Middle Miocene phase of core-complex formation, and (2) a subsequent modern phase of Plio-Quaternary normal faulting and graben formation,

separated by an intervening N-S crustal shortening during a time slice between Late Miocene-Middle Pliocene times. They claim that the origin of first phase of extension is mostly readily attributed to orogenic collapse model along the İzmir-Ankara-Erzincan suture zone. Later on, it was replaced by a short phase of ~ N-S contraction in Late Miocene to Early Pliocene times. The intervening contractional phase is related to a change in the kinematics of the Eurasian and African plates. In the Late Early Pliocene time, sea-floor spreading started along Red Sea (Hempton, 1987), and then the main structures namely dextral NAFS and sinistral EAFS were formed; accordingly, the Anatolian platelet has started to move in south-southwestward direction (Koçyiğit *et al.* 1999, Koçyiğit *et al.* 2001). This model is being supported by numerous studies (Bozkurt, 2000, 2001, 2003; Yılmaz *et al.* 2000; Sözbilir, 2001, 2002; Cihan *et al.* 2003; Bozkurt and Sözbilir, 2004, 2006; Purvis and Robertson, 2004, 2005; Kaya *et al.* 2004; Bozkurt and Rojay, 2005; Beccaletto and Stenier, 2005; Westaway *et al.*, 2005; Koçyiğit and Deveci, 2007). Additionally, Yılmaz *et al.* (2000) also suggested another evolutionary process, which is slightly different than the episodic evolution model, but supports it. They concluded that the Early-Middle Miocene time is represented by N-S contraction phase related to the convergence along İzmir-Ankara suture zone. Subsequently, this phase was replaced by a N-S extension which has been caused by the orogenic collapse. The N–S extensional regime was interrupted by Late Miocene–Early Pliocene (?) quiescent period. Then, N–S extensional regime was rejuvenated again in Late Pliocene to establish the present day tensional neotectonic regime and related graben-horst formation. Consequently, the models suggested explaining the origin, initiation age of extension and evolutionary history of the SWAGHS are still under debate. However, mostly accepted model suggested for the driving mechanism of both extension and graben-horst development in western Anatolia is the orogenic collapse (gravitational collapse, extensional

collapse, etc.). It says that the continental extension over Aegean and western Anatolia is related to the spreading and thinning of over-thickened crust (Dewey, 1988). As a general description, orogenic or gravitational collapse refers to the gravity-driven flow that reduces lateral contrasts in gravitational potential energy (Rey *et al.*, 2001). It is a process that transfers gravitational potential energy from regions of high potential energy to regions of lower potential energy (Selverstone, 2005). The origin of this potential energy difference has been attributed either to an over-thickened crust only (Molnar and Tapponnier, 1978; Molnar and Lyon-Caen, 1988; Dewey, 1988) or to the over-thickened crust and convective removal of the lower lithospheric mantle (Fleitout and Froideveaux, 1982; England and Houseman, 1989; Platt and England, 1994; Houseman and Molnar, 1997). In this model, orogen starts to collapse under its own weight. For the occurrence of this process, a thick crust is needed. Şengör *et al.* (1985) suggested that following the Paleocene–Eocene collision across the northern branch of Neo-Tethys, a crustal thickness of 65–70 km was probably reached in western Turkey. This crustal configuration could be the potential cause of the extension in the region. Thus, post-orogenic collapse model, encouraged by field evidence in western Anatolia, supported by many researchers following the first proposal of Dewey (1988) (e.g., Seyitoğlu and Scott, 1991; Bozkurt and Park, 1994; Collins and Robertson, 1998; Ring *et al.*, 1999; Koçyiğit *et al.*, 1999a, b; Yılmaz *et al.*, 2000).

The combination of the back-arc spreading, the roll-back of subducting slab and the orogenic collapse model (Dewey 1988) seems to be the most attractive explanation for the emergence of the tensional tectonic regime and the incipient occurrence of the SWAGHS. In this frame, the final continent-continent collision of the northerly located Sakarya Block with the southerly located Menderes-Tauride platform, closure of the northern branch of the Neo-Tethys ocean floor (Şengör and Yılmaz

1981), southward tectonic transportation and emplacement of nappes onto the Menderes-Tauride carbonate platform (Okay 1986; Koçyiğit 1983, 2005), tectonic uplift and over-thickening of the crust may have triggered both the orogenic collapse (Seyitoğlu and Scott 1991) and the emergence of a tensional tectonic regime, which has led to the incipient occurrence of graben-horst system in southwestern Anatolia.

One of the incipient grabens starting to be developed in southwestern Anatolia in those days is the Erdoğan-Yenigediz pre-modern graben (Figure 7.1a). Formation of margin-boundary normal faults (Şaphane, Abide, Arica and Yeşilova faults) and the sedimentation of basal clastics of the Arica formation (pre-modern graben infill) have lasted in the graben under the control of these faults and fluvial conditions. Later on, the fluvial depositional setting was widened up to a fluviolacustrine setting in which an alternation of lacustrine limestone, blue marl, shale and andesitic to basaltic volcanic rocks were accumulated. This volcano-sedimentary sequence is full of syn-sedimentary features (slump folds, normal type of growth faults and broken formation etc.) which imply to a depositional setting controlled by both the tectonic and magmatic activities during late-Early Miocene-Middle Pliocene (Figure 7.1b). Particularly the marl facies of the pre-modern graben infill contains widespread slickenside indicating normal faulting during the sedimentation (Figure 4.11a). Stereographic plot of slickenside on the Schmidt's lower hemisphere net indicates that the pre-modern graben was widened under an extension in the direction of approximately NW-SE (Figure 4.11b and c). The graben has reached to its matured stage towards end of middle Pliocene, and then it started to be uplifted and closed. This is indicated by the deposition of a new clastic sedimentary package in the nature of coarsening-upward sequence (Figure 2.1). At the end of Middle Pliocene, the whole of pre-modern graben infill was deformed into a series of anticline and syncline by folding (Figures 4.7,

4.8 and 4.116), reverse faulting (Figure 4.9) and finally strike-slip faulting (Figure 7.1c). This style of deformation is the last contractional phase of the paleotectonic period in the Erdoğmuş-Yenigediz area. The strike-slip faulting was recorded as the strike-slip slickenside within the pre-modern graben infill (Figure 4.10a). Stereographic plot of strike-slip faulting-induced slip-plane data on the Schmidt's lower hemisphere net (Figures 4.10b and c) and the poles to bedding (Figure 4.8) reveal that the pre-modern graben infill was deformed by a stress system, in which the principal stress axis was operating in approximately NE-SW direction. This short-lived contractional event is regional. Because it was previously observed and reported from a number of grabens throughout Aegean and southwest to central Anatolia (Koçyiğit 1976; Akdeniz and Konak 1979; Dumont *et al.* 1979; Angelier *et al.* 1981; Koçyiğit 1983; Boray *et al.* 1985; Yağmurlu 1991; Inci 1991; Bozkuş 1996; Koçyiğit and Bozkurt 1997; Glover and Robertson 1998; Koçyiğit *et al.* 1999; Koçyiğit *et al.* 2000; Ring *et al.* 1999; Gürer *et al.* 2001; Sözbilir 2002; Kaya *et al.* 2004; Bozkurt and Sözbilir 2004; Bozkurt and Rojay 2005; Erkül *et al.* 2005; Koçyiğit 2005; Koçyiğit and Deveci 2007; Alçıçek *et al.* 2007; Emre and Sözbilir 2007; Çiçek, 2009; Gürer *et al.* 2009).

Starting from the latest Pliocene time onwards, the short-lived contractional tectonic regime was replaced by a new tensional tectonic regime and a new style of deformation (phase-II extension). This new regime is here termed as the Neotectonic regime, which has been lasting since Late Pliocene. Early formed margin-boundary normal faults reactivated and controlled the sedimentation in a new graben (modern graben) developed on the erosional surface of the deformed pre-modern graben (Figure 7.1d). This is indicated by the growth faults (Figure 2.6) and the younger sets of extensional slip-lines overprinted on the margin-boundary faults, and recorded in the graben infill.

Stereoplot of slip-plane data on the Schmidt's lower hemisphere net indicate that the modern graben continues to be widened in an approximately NE-SW direction (Figures 4.13a, b and c). This is also proved by the focal mechanism solution diagram (Figure 4.13d) of the March 28, 1970 Mw 7.2 Gediz earthquake (Eyidoğan and Jackson 1985). Evolution of the modern graben is still lasting under the control of a current tensional tectonic regime, which characterizes the neotectonic regime in southwestern Anatolia (Figure 7.1e).

Consequently, detailed field data obtained from numerous grabens in western Anatolia strongly support the episodic evolutionary model rather than the continuous model for the SWAGHS. For this reason, extensional phases recorded in graben infill and on the margin-boundary faults in western Anatolia have to be classified into two basic categories, namely the Peleotectonic phases and Neotectonic phases.

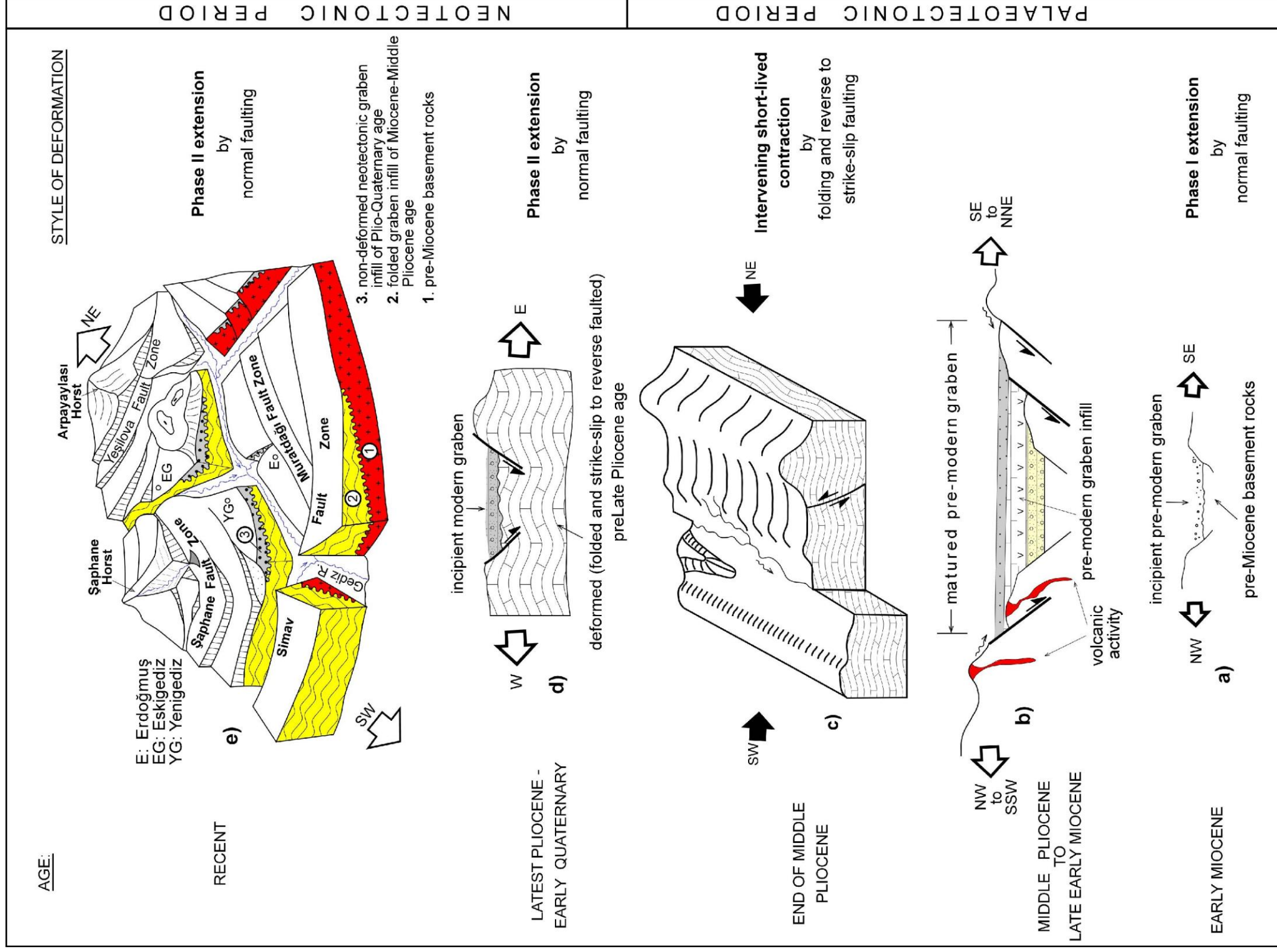


Figure 7. 1. Sketched cross-sections and block diagrams illustrating episodic two-stage evolution of the Erdoğmuş-Yenigediz graben.

CHAPTER 8

CONCLUSIONS

The main scope of the thesis is to enlighten neotectonic development of the Erdoğmuş-Yenigediz graben in the western Turkey. Newly obtained and presented data in the aforementioned chapters were analyzed, discussed and the formation of the Erdoğmuş-Yenigediz graben has been defined; Thus, some valuable contributions about commencement age of the neotectonic period, deformation phases, structural elements, seismic hazard capacity and the seismicity of the Erdoğmuş-Yenigediz graben was introduced for the solution of the regional neotectonic problems in western Turkey.

Both the field geochemical and geochronology dating studies of the rocks exposed in the study area are indicated that it has experienced at least three different phases of deformation during the palaeotectonic (older extensional and contractional deformations) and the neotectonic (younger extensional deformation) periods. First of all, slip-plane data have been obtained at 25 stations and then were analysed. Regional stratigraphic correlations, deformation patterns of graben infill, the field geological mapping, radiocarbon dating, fault geometries and motion altogether reveal that the Erdoğmuş-Yenigediz graben has an episodic evolutionary history accompanied by multiphase of deformation, namely the Early to Middle Miocene extension called 1st phase of extension, the Late Miocene–Early Pliocene contraction (intervening phase of contraction) and the Plio-Quaternary extension (2nd phase of extension). Slip-plane data representing the 1st phase of extension is seen in very

limited part of the study area (at 6 stations in Figure 4.117), because, it was overprinted and obliterated by two younger deformation phases such as the contraction and the 2nd phase of extension. Second phase of deformation is the intervening contractional phase that is proved by the mapable reverse faulting (Figure 4.9) and folding (Figure 4.8). Folds certainly take a part in the deformation pattern of the older graben infill. They are observable on the surface (Appendix – A). Folds of both contractional and extensional origin could be identified. Additionally, markers of this contractional phase are not limited in the present study area, they were reported from different grabens in southwestern Anatolia (Koçyiğit *et al.*, 1999; Bozkurt, 2000; Bozkurt and Rojay, 2005; Bozkurt and Sözbilir, 2006; Koçyiğit and Özacar, 2003; Bacceletto *et al.*, 2005; Kaya *et al.*, 2004, 2007; Rojay *et al.*, 2005; Westaway *et al.*, 2005; Koçyiğit and Deveci, 2007). Based on the field geological mapping, slip-plane data analyses, relative stratigraphic relationships between graben infill and their deformation patterns reveal that the Erdoğmuş-Yenigediz graben has experienced an episodic evolutionary history. Moreover, initiation age of the neotectonic period in western Turkey is another issue and here is still no agreement among researchers. Consequently, in terms of aforementioned field data and their evaluations, the followings are concluded:

(1) the faults in the study area were first identified, mapped, named and analysed by using the Angelier stress tensor. This is the first conclusion for the present study, because, the study area has not been studied before,

(2) two basin infill (deformed older and undeformed younger infill) separated from one another by an intervening angular unconformity were determined. Deformation patterns of these deposits were

determined, analysed and interpreted as a natural response to the compressive tectonic regime occurred in the study area,

(3) volcanic rocks comprising the central volcano-sedimentary package of the pre-modern graben infill are dated at 18.4 ± 0.1 Ma (late-Early Miocene). They were deformed by the contractional tectonic regime especially with reverse motion. Relative age order between volcanic rocks and modern graben infill evidently indicated that contractional deformation phase is older than Late Pliocene oppositely younger than 18.5 Ma (late-Early Miocene),

(4) along the margins and also within the infill of the Erdoğmuş-Yenigediz graben, slickensides (slip-plane data) of three groups of structures were identified, measured, mapped and evaluated. The first phase of extension and contraction (older) and the second phase of extension (younger) are the result of palaeotectonic and neotectonic regimes, respectively. In the Erdoğmuş-Yenigediz graben, ~N–S-oriented extension-related deformation pattern is documented by surface observations within the Arıca and Erdoğmuş formations and margin bounding structures, recently. Additionally, a contractional deformation is characterized by thrust/reverse faults and consistently folds that are conformable with ~NE–SW-oriented compressive stress field. The deformation obviously postdates the deposition of the Arıca formation and predates the deposition of Erdoğmuş formation. This relation evokes the episodic extension model in southwestern Anatolia,

(5) the source fault of the 1970.03.28 Gediz earthquake is the Erdoğmuş fault. According to Eyidoğan and Jackson (1985), there are two successive earthquake took place in the area, otherwise, it is not possible to occur the big earthquake with magnitude 7.2. Mainly, E-W and N-S-trending surface ruptures were created during this event. But,

the length of the Erdoğmuş fault (E-W-trending fault) is enough to produce this earthquake. The reason for the N-S-trending surface rupture is soil failure during the earthquake,

(6) based on studies carried out on the ground surface rupture of the 1970 Gediz earthquake caused by the Erdoğmuş fault, it was identified that at least two big earthquakes have originated from the same fault. They have been identified by using the relative displacement in the sedimentary packages in trenches. Only one of them could be dated which is 1060 and 1970 Gediz earthquake are known exactly. The 1060 destructive earthquake is a very important outcome but it is not enough to obtain a recurrence interval. It can be concluded by at least one more historical earthquake, and

(7) the seismic hazard study carried out in and around the Erdoğmuş-Yenigediz graben indicates that the main sources of seismic hazard in the present study area are the Şaphane, Muratdağı, Simav and Yeşilova fault zones. Seismic hazard study also designates that all of the scenario earthquakes can cause heavily damages to the facilities in the settlements located on the alluvial deposits where PGA values are larger than 0.337 g. The safest parts of the settlements are located on the recrystallized limestone and volcanic rocks based on the calculated PGA values (0.276 g). During the 1970 Gediz earthquake, the most of lost was reported from Eskigediz county and Akçaalan village. Indeed, the ground condition of the Eskigediz county is mostly volcanic rocks but the construction material in most of houses is wooden. So, the fire is the main reason for losses in 1970 event. After the earthquake, Gediz county was moved to it's new location. From the basement rock type point of view, new site of the county is less safe than the old site.

REFERENCES

Abdülselamođlu, Ő., 1970. Geology and Tectonic features of Gediz and its surroundings. Publication of Institute of earth Science of Hacettepe University 3, 1-2, 1-6.

Abrahamson, N.A., 2000. State of the practice of seismic hazard evaluation. GEOENG 2000 Conference Proceedings, Melbourne, Australia (on CD).

Agostini S., Doglioni C., Innocenti F., Manetti P. and Tonarini S., 2010. On the geodynamics of the Aegean rift. Tectonophysics doi:10.1016/j.tecto.2009.07.025.

Akdeniz, N. and Konak, N., 1979. Simav-Emet-TavŐanlı-Dursunbey-Demirci yrelerinin jeolojisi, MTA Gen. Mud., Report No 6547, Ankara (unpublished).

Akbulut, A., Aygn, A. and Dndar, A. 1984. Emet Yresi Bor Tuzu Sahalarının Jeolojisi ve kel Ortamları, 20-40.

AkkuŐ, M, F., 1962. Ktahya - Gediz arasındaki sahanın Jeolojisi. M.T.A, Dergisi s, 58f 21-30.

Akyz, H.S., Altunel, E., Karabacak, V. and Yalciner, C.., 2006. Historical earthquake activity of the northern part of the Dead Sea Fault Zone, southern Turkey. Tectonophysics 426, 281-293.

Alçıçek, M.C., 2007. Tectonic development of an orogen top rift Recorded by its terrestrial sedimentation pattern: The Neogene E en Basin of southwestern Anatolia, Turkey. *Sedimentary Geology* 200, 117-140.

Altunel, E., 1999. Geological and Geomorphological Observations In Relation To 20 September 1899 Menderes Earthquake, Western Turkey: *Journal of Geological Society London* 156, 241-246.

Ambraseys, N. and Tchalenko, J.S., 1972. Seismotectonic Aspect of the Gediz, Turkey, Earthquake of March 1972. *Geophysical Journal of the Royal Astronomical Society* 30, 229–252.

Ambraseys, N.N., 1988. *Engineering Seismology: Earthquake Engineering and Structural Dynamics* 17, 1–105.

Ambraseys, N., and Finkel, C., 1995. *The Seismicity of Turkey and Adjacent Areas*, Eren, Istanbul, 37–43.

Ambraseys, N. and Jackson, J., 1998. "Faulting Associated With Historical and Recent Earthquakes In The Eastern Mediterranean". *Geophysical Journal International* 133, 390-406.

Ambraseys, N., 2001. "A Note on the Far-Field Effects of Eastern Mediterranean Earthquakes in Lower Egypt". *Journal of Seismology* 5, 263-268.

Anderson, J.G., 1997. "Benefits of Scenario Ground Motion Maps", *Engineering Geology* 48, 43-57.

Anderson, J., Sucuoglu, H., Erberik, A., Yilmaz, T., Inan, E., Durukal, E., Erdik, M., Anooshehpour, R., Brune J. and Ni, S., 2000. Strong Ground Motions from the Kocaeli and Düzce, Turkey, Earthquakes and Possible Implications for Seismic Hazard Analysis, Earthquake Spectra, Supplement A 16, 113-137.

Angelier, J., 1979. Determination of mean principal direction of stress for a given fault population: Tectonophysics 56, T17-T26.

Angelier, J., Dumontj, F., Karamandefesi, H., Poissona, Şimşek, Ş. and Uysal, S., 1981. Analyses of fault mechanisms and expansion of southwestern Anatolia since the late Miocene. Tectonophysics 75, T1-9.

Angelier, J., 1984. Tectonic analysis of fault slip data sets: Journal of Geophysical Research 89, 5835-5848.

Angelier, J., 1989. Data Base for Tectonic Orientations "Tector" Version 5.42, Aug87-Oct88-Dec88-Aou89 Copyright 1987, 1988 and 1989.

Angelier, J., 1990. Inversion of field data in fault tectonics to obtain the regional stress. III. A new rapid direct inversion method by analytical means: Geophysical Journal International 103, 363–376.

Angelier, J., 1994. Fault slip analysis and paleostress reconstruction, in P.L. Hancock, ed., Continental Deformation: Pergamon Press, Oxford, p. 53–100.

Arminjo, R., Carey, E., and Cisternas, A., 1982. The inverse problem in microtectonics and the separation of tectonic phases: Tectonophysics 82, 145-160.

Arpat, E., and Bingöl, E., 1969. The rift system of western Turkey: thoughts on its development. General Directorate of Mineral Research and Exploration Bulletin 73, 1-9.

Arpat, E., and Özgül, N.F., 1970. 28 Mart 1970 Gediz depremi (ön rapor): M.T.A. Report No. 4250 (unpublished).

Avigad, D., Garfunkel, Z., Jolivet, L., and Azanon, H. M., 1997. Back-arc extension and denudation of Mediterranean eclogites. *Tectonics* 16, 924–941.

Aydan, Ö., 1997. The seismic characteristics and the occurrence pattern of Turkish earthquakes. Turkish Earthquake Foundation Report No.TDV/TR 97-007, 41 pp.

Aydan, Ö. and Hasgür, Z., 1997. The characteristics of acceleration waves of Turkish earthquakes. 4. Ulusal Deprem Mühendisliği Kongresi, Ankara, Deprem Mühendisliği Türk Milli Komitesi, pp. 30– 37, (in Turkish).

Aydan, Ö., Kumsar, H. and Ulusay, R., 2002. How to infer the possible mechanism and characteristics of earthquakes from the striations and ground surface traces of existing faults. *JSCE, Earthquake Structural Engineering Div.* 19 (2), 199–208.

Barka, A. A. and Hancock, P. L., 1984. Neotectonic deformation patterns in the convex-northwards arc of the North Anatolian fault zone. In" *The Geological Evolution of the Eastern Mediterranean region*", edited by J.E. Dixon and A.H.F. Robertson. Special Publication Geological Society of London 763-773.

Barka, A. A. and Kadinsky-Cade, K., 1988. Strike-slip fault geometry in Turkey and its influence on earthquake activity. *Tectonics* 7, 663-684.

Basokur, A., Ergun, G., Seyitoglu, G., Varol, G., Ulugergerli, B., Isık, V., Candansayar, E. and Tokgoz, E., 2002. Report on the Mechanism of 03.02.2002 Çay (Afyon) Earthquake, Causes of Damages and Sesimic Activity of the Affected Region Based on Geological and Geophysical Investigations, Publication of Ankara University, Ankara, 56 pp., in Turkish.

Beccaletto, L. and Steiner, C., 2005. Evidence of Two-Stage Extensional Tectonics from the Northern Edge of the Edremit Graben (NW Turkey). *Geodinamica Acta* 18, 283–97.

Bingöl, E., 1974. Muratdağı merkezi kesiminin jeolojisi, magmatik ve metamorfik kayaçların petrolojisi ve jeokronolojisi. Thesis, 105 p., (unpublished)

Bingöl, E., 1977. Muratdağı Jeolojisi ve ana kayaç birimlerinin petrolojisi Türkiye Jeoloji Kurultayı Bülteni 2, 13-67.

Bishop, A.W., 1966. The strength of solids as engineering materials: *Geotechnique*, 16, 91-130.

Bommer J. J., 2002. Deterministic versus probabilistic seismic hazard assessment: an exaggerated and obstructive dichotomy. *Journal of Earthquake Engineering* 6 (Special Issue 1), 43–73.

Boray J. H., Şaroğlu, F. and Emre, Ö., 1985. Isparta büklümünün kuzey kesiminde D-B daralma için bazı veriler. *Jeoloji Mühendisliği* 23, 9–20.

Bozkurt, E. and Park, R. G., 1994. Southern Menderes Massif: an incipient metamorphic core complex in western Anatolia, Turkey. *Journal of the Geological Society, London* 151, 213-216.

Bozkurt, E., 2000. Timing of Extension on the Büyük Menderes Graben, Western Turkey and its Tectonic Implications. In: Bozkurt, E., Winchester, J.A. and Piper, J.D.A. (Eds), *Tectonics and Magmatism in Turkey and the Surrounding Area*. Geological Society, London, Special Publications 173, 385–403.

Bozkurt, E., 2001. Neotectonics of Turkey. *Geodinamica Acta* 14, 3-30.

Bozkurt, E., 2003. Origin of NNE-trending basins in Western Turkey. *Geodinamica Acta* 16, 61-81.

Bozkurt, E. and Sözbilir, H., 2004. Tectonic Evolution of the Gediz Graben: Field Evidence for an Episodic, Two-Stage Extension in Western Turkey. *Geological Magazine* 141, 63–79.

Bozkurt, E. and Sözbilir, H., 2004. Geology of the Gediz Graben: new field evidence and its tectonic significance. *Geological Magazine* 141, 63–79.

Bozkurt, E. and Sözbilir, H., 2006. Evolution of the Large-Scale Active Manisa Fault, Southwest Turkey: Implications On Fault Development and Regional Tectonics: *Geodinamica Acta*, 19, 427-453.

Bozkurt, E. and Rojay, B., 2005. Episodic, Two-Stage Neogene Extension and Short-Term Intervening Compression in Western Anatolia: Field Evidence from the Kiraz Basin and Bozdağ Horst. *Geodinamica Acta* 18, 299-312.

Bozkuş, C., 1996. Kavacık (Dursunbey-Balıkesir) Neojen grabeninin stratigrafisi ve tektoniği, Turkish Journal of Earth Sciences, 5, 161-170 [in Turkish with English abstract].

Bulajić, B. and Manić, M., 2006. Selection of the Appropriate Methodology For The Deterministic Seismic Hazard Assessment on The Territory of The Republic of Serbiaarchitecture and Civil Engineering 4, No 1, 41 – 50.

Carey, E. and Brunier, B., 1974. Analyse théorique et numérique d'une modèle mécanique élémentaire appliqué a l'étude d'une population des failles: Comptes Rendus de l'Académie des Sciences, Paris, Serie D 279, 891–894.

Castagna, J., 1996. Exploration questions: the sequel: The Leading Edge, 15, no. 1, 43–46.

Cihan, M., Saraç, G. and Gökçe, O., 2003. Insights into biaxial extensional tectonics: an example form the Sandıklı Graben, West Anatolia, Turkey. Geological Journal 38, 47–56.

Collins, A. S. and Robertson, A. H. F., 1998. Processes of Late Cretaceous to late Miocene episodic thrustsheet translation in the Lycian Taurides, SW Turkey, Journal of Geological Society 155, 759–772, doi:10.1144/gsjgs. 155.5.0759.

Cohen, H. A., Dart, C. J., Akyüz, H. S. and Barka, A., 1995. Syn-rift sedimentation and structural development of Gediz and Büyük Menderes Graben, western Turkey. Journal of the Geological Society, London 152, 629-638.

Coulomb, C. A., 1773. Sur une application des règles de maximis et minimis k quelques problèmes de statique relatifs hl'Architecture, Acad. R. Sci. Mere. Math. Phys. Divers Sarans 7, 343-382, 1773.

Cornell, C. A., 1968. Engineering seismic risk analysis. Bulletin of Seismological Society of America 58(5), 1583–1606.

Çiçek, A., 2009. Neotectonics of the Karamık Graben (Isparta Angle), Turkey. Msc Thesis, 96pp, Middle East Technical University, (unpublished).

Çiftçi, N.B. and Bozkurt, E. 2007. Anomalous Stress Field and Active Breaching at Relay Ramps: A Field Example from Gediz Graben, SW Turkey. Geological Magazine 144, 687–699.

Demirsu, A. and Kutlu, R., 1955. Balıkesir, Soma Havalisinin Jeolojisi Hakkında Rapor. M. T. A. Report No. 2376 (unpublished).

Dewey, J. F., and Şengör, A. M. C., 1979. Aegean and surrounding regions: complex multiple and continuum tectonics in a convergent zone. Geological Society of American Bulletin 90, 84-92.

Dewey, J.F., 1988. Extensional Collapse of Orogens: Tectonics 7, 1123-1139.

Dinç, A. N., 2003. Determination of 3-D P-wave velocity structure beneath Sultandağı region by local earthquake tomography. MSc thesis (in Turkish), 77pp, Istanbul Technical University, Turkey.

Dirik, K., 2002. Akarçay (Afyon) Havzası'nın tektoniği ve Çay-Afyon (03.02.2002) depremi'nin önemi. ATAG6, Bildiri Özleri, 32.

Dogliani, C., Harabaglia, P., Merlini, S., Mongelli, F., Peccerillo, A. and Piromallo, C., 1999, Orogens and slabs vs their direction of subduction: *Earth Science Reviews*, 45, 167–208, doi: 10.1016/S0012-8252(98)00045-2.

Dogliani, C., Agostini, S., Crespi, M., Innocenti, F., Manetti, P., Riguzzi, F. and Savascin, Y., 2002. On the extension in western Anatolia and the Aegean sea: *Journal of the Virtual Explorer* 7, 117–131.

Douglas, J., 2003. Earthquake ground motion estimation using strong-motion records: a review of equations for the estimation of peak ground acceleration and response spectral ordinates. *Earth-Science Review* 61 (1–2), 43– 104.

Dumont. J.F., Uysal, Ş., Şimşek, Ş., Karamanderesi, İ.H. and Letouzey, F., 1979. Güneybatı Anadolu'daki Grabenlerin Oluşumu [Graben formation in Southwest Anatolia]. *Bulletin of Mineral Research and Exploration of Turkey* 92, 7–17.

Emre, Ö., Duman, T. Y., Doğan, A., Özalp, S., Tokay, F. and Kuşçu, İ. 2003. Surface Faulting Associated with the Sultandağı Earthquake (Mw=6.5) of 3 February 2002, Southwestern Turkey. *Seismological Research Letters* 74, 382-392.

Emre, T. and Sözbilir, H. 2007. Tectonic Evolution of the Kiraz Basin, Kucuk Menderes Graben: Evidence for Compression/Uplift-Related Basin Formation Overprinted By Extensional Tectonics in West Anatolia. *Turkish Journal of Earth Sciences* 16 (4), 441-470.

England, P.C. and Houseman, G.A., 1989. Extension during continental convergence, with application to the Tibetan Plateau, *Journal of Geophysical Research* 94, 17,561-17,579.

Ercan, T., Günay, E. and Savaşçın, Y., 1984. Simav ve çevresindeki Senozoyik yaşlı volkanizmanın bölgesel yorumlanması: *Bulletin of Mineral Research and Exploration of Turkey* 97/98, 86-101.

Ercan, T., Dinçel, A. and Günay, E., 1979. Uşak volkanitlerinin petrolojisi ve plaka tektoniği açısından Ege bölgesindeki yeri: *Türkiye Jeoloji Kurumu Bülteni* 22/2, 185-198.

Ergin, M., Aktar, M., Özalaybey, S., Tapırdamaz, M.C., Selvi, O. and Tarancıoğlu, A., 2009. A high resolution aftershock seismicity image of the 2002 Sultandağı-Çay earthquake (Mw=6.2), Turkey. *Journal of Seismology* doi:10.1007/s10950-009- 9155-1.

Erinç, S., Bilgin, T., Bener, M., Sungur, K., Erer, S., and Göçmen, K., 1970. 28 Mart 1970 Gediz depremi tatbiki jeomorfolojik etüdü, İstanbul Üniversitesi, Coğrafya Enstitüsü yayınları, No:60.

Erkül, F., Helvacı, C. and Sözbilir, H., 2005. Stratigraphy and Geochronology of the Early Miocene Units in the Bigadiç Basin, Western Turkey. *Turkish Journal of Earth Sciences* 14, 227-253.

Eyidoğan, H., Güçlü, U., Utku, Z. and Değirmenci, E., 1991. Türkiye Büyük Depremleri Makrosismik Rehberi (1900–1988) [A Macroseismic Guide for the Earthquakes of Turkey]. Istanbul Technical University [In Turkish].

Eyidoğan, H. and Jackson, J., 1985. A Seismological Study of Normal Faulting in Demirci, Alaşehir and Gediz Earthquakes of 1969-70 in Western Turkey: Implication for the Nature and Geometry of Deformation in the Continental Crust. *Geophysical Journal of the Royal Astronomical Society* 81, 569–607.

Etchecopar, A., Vasseur, G. and Daignieres, M., 1981. An inverse problem in microtectonics for the determination of stress tensors from fault striation analysis: *Journal of Structural Geology* 3, 51–65.

Ferrill, D. A., Morris, A. P. and McGinnis, N., 2000. Crossing conjugate normal faults in field exposures and seismic data. *American Association of Petroleum Geologists (AAPG)* 84, no. 10, 1543–1559.

Fleitout L., Froideveaux C., 1982. Tectonics and topography for a lithosphere containing density heterogeneities, *Tectonics* 1, 21-57.

Gephart, J.W., and Forsyth, D.W., 1984. An improved method for determining the regional stress tensor using earthquake focal mechanism data: an application to San Fernando earthquake sequence: *Journal of Geophysical Research* B89, 9305-9320.

Gibbs, A.D., 1984. Structural evolution of extensional basin margins: *Journal of the Geological Society London*, 141, 609–620.

Glodny, J. and Hetzel, R., 2007. Precise U-Pb Ages of Syn-Extensional Miocene Intrusions in the Central Menderes Massif, Western Turkey. *Geological Magazine* 144, 02, 235-246.

Glover, C. and Robertson, A., 1998. Neotectonic intersection of the Aegean and Cyprus Tectonic arcs: extensional and strike-slip faulting in the Isparta Angle, SW Turkey. *Tectonophysics* 298, 103-132.

Gökalp, E., 1970. Gazlıgöl (Afyon) sıcak sulan etüd raporu: M. T. A. Report No. 4366 (unpublished).

Gökten, E., Seyitoğlu, G., Varol, B. and Işık, V. 2003. 03.02.2002 Çay (Afyon) depreminin mekanizması: bölgenin deprem etkinliği [Çay (Afyon) Earthquake of Mechanisms: the region's seismic activity]. Kocaeli 2003 Earthquake Symposium, Kocaeli, Turkey, p. 24 [in Turkish with English abstract].

Gün, E., 1975. Gediz İlçesi (Kütahya İli) Neojen Havzası Ve Güneyinin Jeolojisi. M. T. A. Report No. 6276 (Unpublished).

Gün, H., Akdeniz, N. and Günay, E., 1979. Gediz ve Emet güneyi Neojen havzalarının jeolojisi ve yaş sorunları: Jeoloji Mühendisliği Dergisi, 8.

Gürer, A., Gürer, Ö.F., Pinçe, A. and İlkışık, O.M., 2001. Conductivity Structure along the Gediz Graben, West Anatolia, Turkey: Tectonic Implications. International Geology Review 43, 1129– 1144.

Gürsoy, H., Piper, J. D. A. and Tatar, O., 2003. Neotectonic deformation in the western sector of tectonic escape in Anatolia: Palaeomagnetic study of the Afyon region, central Turkey. Tectonophysics 374, 57–79, doi:10.1016/S0040-1951(03)00346-9.

Gürer, Ö. F., Sarıca, N-F., Özburun, M., Sangu, E. and Doğan, B., 2009. Progressive development of the Büyük Menderes graben based on new data, western Turkey. Geological Magazine 146 (5), 652-673.

Hassani, R., Jongmans, D., and Chéry, J., 1997. Study of plate deformation and stress in subduction processes using two-dimensional models. *Journal of Geophysical Research* 102, 17951–17965.

Helvacı, C., 1986. Stratigraphic and structural evolution of the Emet borate deposits, Western Anatolia. Dokuz Eylül University, Faculty of Engineering and Architecture, Research Papers, No: MM/JEO-86 AR 008, 28.

Hempton, M.R., 1987. Constraints on Arabian plate motion and extensional history of the Red Sea. *Tectonics* 6, 687-705.

Hetzel, R., Ring, U., Akal, C. and Troesch, M., 1995. Miocene NNE-directed extensional unroofing in the Menderes Massif, southwestern Turkey, *Journal of Geological Society* 152, 639–654, doi:10.1144/gsjgs.152.4.0639.

Horsfield, W. T., 1980. Contemporaneous movement along crossing conjugate normal faults: *Journal of Structural Geology* 2, 305–310.

Houseman G. and Molnar P., 1997. Gravitational (Rayleigh-Taylor) instability of a layer with non-linear viscosity and convective thinning of continental lithosphere, *Geophysical Journal International* 128, 125-150.

Huang, Q., 1988. Computer based method to separate heterogeneous sets of fault slip data into subsets: *Journal of Structural Geology* 10, 297–299.

İnci, U., 1991. Torbalı (İzmir) kuzeyindeki Miyosen tortul istifinin fasiyes ve çökeltme ortamları [Facies and depositional environment of Miocene sedimentary sequence in the north of Torbalı (İzmir)]. *General*

Directorate of Mineral research and Exploration (MTA) Bulletin 112, 13-26 [in Turkish with English abstract].

Jackson, J.A. and Mckenzie, D.P., 1984. Active Tectonics of the Alpine-Himalayan Belt between Western Turkey and Pakistan: Geophysical Journal of Royal Astronomy Society 7, 185-264.

Jackson, J. A., McKenzie, D. P., 1988. Rates of active deformation in the Aegean Sea and surrounding regions. Basin Research 1, 121-128.

Jolivet, L., Faccena, C., Goffe', B., Mattei, M., Rossetti, F., Brunet, C., Storti, F., Funiciello, R., Cadet, J.P., D'Agostino, N., and Parra, T., 1998. Midcrustal shear zones in postorogenic extension: example from the northern Tyrrhenian Sea. Journal of Geophysical Research 103, 12123–12160.

Kalafat, D., Kara, M., Öz, G., Kekovalı, K., Güneş, Y., Özel, N., Öğütçü, Z., Kılıç, K., Püskülcü, S., Horasan, G., Güngör, A., Yılmaz, M., Köseoğlu, A., Görgün, E., Kılıçer, F. B., Gümüş, H., Ölmez, Y., Çomoğlu, M., Berberoğlu, A., Deniz, P., Kafadar, N. and Suvarıklı, M. 2002. 3 Şubat 2002 Sultandağı (Afyon) depremi raporu [2002.02.03 Sultandağı (Afyon) earthquake report] KOERI, 51s.

Kanamori, H., 1977. The energy release of great earthquakes, Journal of Geophysical Research 82, 2981-2987.

Kaya O., Ünay E., Saraç, G., Eichhorn S., Hassenrück, S., Knappe, A., Pekdeğer, A. and Mayda, S., 2004. Halitpaşa Transpressive Zone: Implications for an Early Pliocene Compressional Phase in Central Western Anatolia, Turkey. Turkish Journal of Earth Sciences 13, 1–13.

Kaya, O., Ünay, E., Göktaş, F. and Saraç, G., 2007. Early Miocene Stratigraphy of Central West Anatolia, Turkey: Implications for the Tectonic Evolution of the Eastern Aegean Area. *Geological Journal* 42, 85–109.

Ketin, İ., 1969. Kuzey Anadolu Fayı hakkında, General Directorate of Mineral Research and Exploration Bulletin 72, 1-27.

Kissel, C., Laj, C., Poisson, A. and Simeakis, K., 1989. A pattern of block rotations in central Aegean, in *Paleomagnetic Rotations and Continental Deformation*, NATO ASI Ser., Ser. C, vol. 254, edited by C. Kissel and C. Laj, pp. 115–129, Kluwer Acad., Dordrecht, Netherlands.

Kissel, C., Laj, C. and Clemens, S., 2003. Magnetic signature of environmental changes in the last 1.2 Ma at ODP Site 1146, South China Sea. *Marine Geology* 201, 119–132.

Kijko A., and Öncel, A. O., 2000. Probabilistic seismic hazard maps for the Japanese islands. *Soil Dynamics and Earthquake Engineering* 20, 485–491.

Koçyiğit, A., 1976. Karaman-Ermenek (Konya) bölgesinde ofiyolitli mélange ve diğer oluşuklar [ophiolitic mélange and other occurrences in Karaman-Ermenek (Konya) area]. *Geological Society of Turkey Bulletin* 19, 103-116 [in Turkish with English abstract].

Koçyiğit, A., 1980. Hoyran gölü yöresinin (Afyon-Isparta) stratigrafik ve tektonik özellikleri [Stratigraphic and tectonic characteristics of the Hoyran Lake district (Afyon-Isparta)]. Associate Professors thesis, 177pp, Ankara University.

Koçyiğit, A., 1983. The Seismicity of the Eastern Anatolia Region and Required Studies. *The Earth and Human* 8, 25-29.

Koçyiğit, A., 1984. Güneybatı Türkiye Ve Yakın Dolayında Levha İçi Yeni Tektonik Gelişim, *Geological Society of Turkey Bulletin* 27, 1-16.

Koçyiğit, A., 1988. Tectonic Setting of The Geyve Basin: Age And Total Displacement Of The Geyve Fault Zone. *Metu, Journal of Pure and Applied Science* 21, 81-104.

Koçyiğit, A. 1989. Suşehri Basin: An Active Fault-Wedge Basin On The North Anatolian Fault Zone, Turkey. *Tectonophysics* 167, 13-29.

Koçyiğit, A. 1996. Superimposed Basins and Their Relations To The Recent Strike-Slip Fault Zone: A Case Study of The Refahiye Superimposed Basin Adjacent to the North Anatolian Transform Fault, Northeastern Turkey. *International Geology Review* 39, 701-713.

Koçyiğit, A. and Bozkurt, E., 1997. Kütahya-Tavşanlı çöküntü alanının neotektonik özellikleri. Proje No. TÜBİTAK-YDABÇAG-126, Final Raporu, 78 s.

Koçyiğit, A., Yusufoglu, H. and Bozkurt, E., 1999. Evidence from the Gediz Graben for Episodic Two-Stage Extension in Western Turkey. *Journal of the Geological Society, London* 156, 605–616.

Koçyiğit, A., Ünay, E. and Saraç, G., 2000. Episodic Graben Formation and Extensional Neotectonic Regime in West Central Anatolia and the Isparta Angle: A Key Study in the Akşehir-Afyon Graben, Turkey. In: Bozkurt, E., Winchester, J.A. and Piper, J.D.A. (Eds), *Tectonics and*

Magmatism in Turkey and the Surrounding Area. Geological Society, London, Special Publications 173, 405–421.

Koçyiğit, A. and Özacar, A., 2003. Extensional Neotectonic Regime through the NE Edge of the Outer Isparta Angle, Sw Turkey: New Field and Seismic Data. Turkish Journal of Earth Sciences 12, 67–90.

Koçyiğit, A., 2005. Denizli Graben-Horst System and the Eastern Limit of the West Anatolian Continental Extension: Basin Fill, Structure, Deformational Mode, Throw Amount and Episodic Evolutionary History, Sw Turkey. Geodinamica Acta 18, 167–208.

Koçyiğit, A. and Deveci, Ş., 2005. Akşehir-Simav fay sistemi: güneybatı Türkiye’de neotektonik rejimin başlama yaşı ve depremsellik [Akşehir-Simav fault system: initiation age of the neotectonic regime and seismicity in the southwestern Turkey. Deprem Sempozyumu Kocaeli 2005. Özler kitabı s.26 [In Turkish].

Koçyiğit, A. and Deveci, Ş., 2007. A N–S-Trending Active Extensional Structure, the Şuhut (Afyon) Graben: Commencement Age of the Extensional Neotectonic Period in the Isparta Angle, SW Turkey. Turkish Journal of Earth Science 16, P. 391-416.

Krinitzsky, E. L., 2003. How to combine deterministic and probabilistic methods for assessing earthquake hazards. Engineering Geology 70, 157–163.

Kramer, S.L., 1996. Geotechnical Earthquake Engineering. New Jersey: Prentice Hall.

Larsen, P.H., 1988, Relay structures in a Lower Permian basement involved extension system, East Greenland: *Journal of Structural Geology* 10, 3–8.

Lay, T. and Wallace, T. C., 1995. Modern global seismology, Volume 58 of International geophysics series. San Diego: Academic Press.

Lattman, L., H. and Ray, L., 1965. Aerial Photographs in Field Geology. Holt, Rinehart and Winston, Inc, New York.

Lebküchner, R. F., 1965. Bericht Über Die Detail Geologischen Und Lagerstättenundlichen Untersuchungen Im Braunkohlengebiet Von, Kütahya/Gediz/Sazköy-Gökler Kö. (Kütahya/Gediz/Sazköy-Gökler Kö. Linyit Sahasında Yataklarla İlgili Olarak Yapılan Detay Jeolojik Etüdlere Hakkında Rapor). M.T.A. Report No. 4635 (Unpublished).

Le Pichon, X., Chamot-Rooke, C., Lallemand, S., Noomen, R., and Veis, G., 1995. Geodetic Determination of The Kinematics of Central Greece With Respect To Europe: Implications For Eastern Mediterranean Tectonics: *Journal of Geophysical Research*, 100, 12675-12690.

Le Pichon, X. and Angelier, J., 1979. The Hellenic arc and trench system: a key to the neotectonic evolution of the Eastern Mediterranean area. *Tectonophysics* 60, 1-42.

Lueder, D., R., 1959. Aerial Photographic Interpretation: Principles and Applications. McGraw-Hill Book Company, Inc., New York.

Mariko, T., 1970, Muratdağı bölgesindeki Banaz_Uşak civa cevheri yatakları ve jeolojisi: M.T.A. Report No. 4572, (unpublished).

Mark, R.K., 1977. Application of linear statistical model of earthquake magnitude versus fault length in estimating maximum expectable earthquakes. *Geology* 5, 464–466.

Marrett, R. and Peacock, D.C.P., 1999. Strain and stress: *Journal of Structural Geology* 21, 1061-1067.

McCalpin, J. P., 2009. *Paleoseismology*, 564 pp. San Diego, New York, Boston, London, Sydney, Tokyo, Toronto: Academic Press.

McClusky, S., Bassalanian, S., Barka, A., Demir, C., Ergintav, S., Georgiev, I., Gurkan, O., Hamburger, M., Hurst, K., Hans-Gert, H.-G., Karstens, K., Kekelidze, G., King, R., Kotzev, V., Lenk, O., Mahmoud, S., Mishin, A., Nadariya, M., Ouzounis, A., Paradissis, D., Peter, Y., Prilepin, M., Relinger, R., Sanli, I., Seeger, H., Tealeb, A., Toksaz, M. N. and Veis, G., 2000. Global Positioning System Constraints on Plate Kinematics and Dynamics in the Eastern Mediterranean and Caucasus, *Journal of Geophysical Research* 105 (B3), 5695-5719.

McDonough, W. F. and Sun, S. S., 1995. The composition of the Earth. *Chemical Geology* 120,223– 253.

McGuire R.K., 2001. Deterministic vs. probabilistic earthquake hazards and risks, *Soil Dynamics and Earthquake Engineering* 21(5), 377-384.

McKenzie, D. P., 1978. Active tectonics of the Alpine-Himalayan belt: the Aegean and surrounding regions. *Geophysical Journal of the Royal Astronomical Society* 55, 217-254.

McKenzie, D. P., 1972. Active tectonics of the Mediterranean region, *Geophysical Journal of Royal Astronomical Society* 30 (2), 109–185.

Mercier J. L., 1981. Extensional-compressional tectonics associated with the Aegean arc: comparison with the Andean Cordillera of south Peru-north Bolivia, *Phil. Trans. Royal Society, London A* 300, 337-355.

Meulenkamp, J., Wortel, M.J.R., Van Wamel, W.A., Spakman, W. and Hoogerduyn Strating, E., 1988. On the Hellenic subduction zone and the geodynamic evolution of Crete since the Late Middle Miocene. *Tectonophysics* 146. 203-215.

Meulenkamp, J.E., van der Zwaan, G. J. and van Wamel, W.A., 1994. On late Miocene to recent vertical motions in the Cretan segment of the Hellenic arc. *Tectonophysics* 234, 53–72.

Molnar, P., and Tapponnier, P., 1978, Active tectonics of Tibet: *Journal of Geophysical Research B: Solid Earth* 83, 5361-5375.

Molnar, P. and H. Lyon-Caen, 1989. Fault plane solutions of Earthquakes and active tectonics of the Tibetan Plateau and its margins, *Geophysical Journal International* 99(1), 123-153;

Musson R. M. W. and Henni P. H. O., 2001. Methodological considerations of probabilistic seismic hazard mapping. *Soil Dynamics and Earthquake Engineering* 21, 385–403.

Nicol, A., Walsh, J.J., Watterson, J. and Bretan, P.G., 1995, Three dimensional geometry and growth of conjugate normal faults: *Journal of Structural Geology* 17, 847-862.

Okay, A., 1986. High-Pressure/Low-Temperature Metamorphic Rocks of Turkey. *Geological Society of America, Memoir* 164, 333-347.

Okay, A. I. and Tüysüz, O. 1999. Tethyan sutures of northern Turkey. In: Durand, B., Jolivet, L., Horvath, F. Serrane, M (ed). The Mediterranean Basins: Tertiary Extension within the Alpine Orogen. Geological Society, London, Special Publications 156, 475-515.

Oral, M.B., Reilinger, R.E., Toksöz, M.N., Kong, R.W., Barka, A.A., Kinik, I. and Lenk, O., 1995. Global Positioning System offers Evidence of Plate Motions in Eastern Mediterranean: Eos Transac., N.76 (9).

Özden, S., Över, S. and Ünlügenç, U.C., 2002. Quaternary Stress Regime Change Along The Eastern North Anatolian Fault Zone, Turkey. International Geology Review 44, 1037-1052.

Özmen, G., Pala, S., Orakdöğen, E. and Gülay, G., 1997. Investigation of structural irregularities in earthquake-resistant design of multi-story structures. Final report of the research supported by Turkish Technical and Scientific Research Council, Ankara (in Turkish), pp. 9-27.

Özpeker, L., 1969. Batı Anadolu borat yataklarının mukayeseli jenetik etüdü: İstanbul Teknik Üniv., Doktora tezi, İstanbul.

Parvez, I.A., Vaccari, F. and Panza, G.F., 2003. A deterministic seismic hazard map of India and adjacent areas, Geophysical Journal International 155, pp. 489–508.

Paton, S., 1992. Active normal faulting, drainage patterns and sedimentation in southwestern Turkey. Journal of the Geological Society, London 149, 1031-1044.

Peacock, D.C.P. and Sanderson, D.J., 1991. Displacements, segment linkage and relay ramps in normal fault zones: Journal of Structural Geology, 13, 721-733.

Peacock, D.C.P. and Sanderson, D.J., 1994. Geometry and development of relay ramps in normal fault systems: *American Association of Petroleum Geologists Bulletin*, 78, 147–165.

Pearce, J.A. and Norry, M., 1979. Petrogenetic implications of Ti, Zr, Y and Nb variations in volcanic rocks. *Contributions to Mineralogy and Petrology*, 69, 33-47.

Platt J. P. and England P. C., 1994. Convective removal of lithosphere beneath mountain belts: thermal and mechanical consequences. *American Journal of Science* 294, 307-336.

Price, S.P. and Scott, B., 1994. Fault-block rotations at the edge of a zone of continental extension, southwest Turkey. *Journal of Structural Geology* 16, 381–392.

Purvis, M. and Robertson, A.H.F., 2004. A pulsed extension model for the Neogene–Recent E–W trending AlaYehir Graben and the NE–SW trending Selendi and Gördes Basins, western Turkey. *Tectonophysics* 391, 171– 201.

Purvis, M. and Robertson, A.H.F., 2005. Miocene sedimentary evolution of the NE-SW-trending Selendi and Gördes Basins, Western Turkey: implications for extensional processes. *Sedimentary Geology* 174, 31-62.

Reches, Z., 1987. Determination of the tectonic stress tensor from slip along faults that obey the Coulomb criterion: *Tectonics* 6, 849-861.

Reches, Z., 1987, Determination of the tectonic stress tensor from slip along faults with Coulomb yield condition, *Tectonics*, 6, 849-861.

Reilinger, R.E., McClusky, S.C., Oral, M.B., King, W. and Toksöz, M.N., 1997. Gps Measurements of Present Day Crustal Movements in the Arabian-Africa-Eurasia Plate Collision Zone: *Journal of Geophysical Research* 102, P. 9983-9999.

Reiter, L., 1990. "Earthquake Hazard Analysis", Columbia University Press.

Renne, P. R., Swisher, C. C., Deino, A. L., Karner, D. B., Owens, T. L. and DePaolo, D. J., 1998. Intercalibration of standards, absolute ages and uncertainties in $^{40}\text{Ar}/^{39}\text{Ar}$ dating. *Chemical Geology* 145, 117-152.

Rey, P., Vanderhaeghe, O. and Teyssier, C., 2001. Gravitational collapse of the continental crust: definition, regimes and modes. *Tectonophysics* 342, 435– 449.

Ring, U., Brandon, M. T., Willett, S. D., and Lister, G. S., 1999. Exhumation Processes. Geological Society, London, Special Publications 154, 1-27.

Richter, C. F., 1935. An instrumental earthquake magnitude scale, *Bulletin of Seismological Society of America* 25, 1-32.

Rojay, B., Toprak, V., Demirci, C. and Süzen, L., 2005. Plio-Quaternary Evolution of the Küçük Menderes Graben, Southwestern Anatolia, Turkey. *Geodinamica Acta* 18, 317–331.

Ruffet, G., Féraud, G., Balèvre, M. and Kiénast, J.-R., 1995. Plateau ages and excess argon in phengites: an ^{40}Ar - ^{39}Ar laser probe study of Alpine micas (Sesia Zone, Western Alps, northern Italy). *Chemical Geology (Isotopic Geoscience Section)* 121, 327-343.

Ruffet, G., Gruau, G., Ballèvre, M., Féraud, G. and Philippot, P., 1997. Rb-Sr and ^{40}Ar - ^{39}Ar laser probe dating of high-pressure phengites from the Sesia zone (western Alps): underscoring of excess argon and new age constraints on the high-pressure metamorphism. *Chemical Geology* 141, 1-18.

Schlische, R. W., and M. H. Anders, 1996, Stratigraphic effects and tectonic implications of the growth of normal faults and extensional basins, in K. K. Beratan, ed., *Reconstructing the structural history of Basin and Range extension using sedimentology and stratigraphy: Geological Society of America Special Paper 303*.

Schwartz, D. P. and Coppersmith, K. J. 1984. "Fault Behavior and Characteristic Earthquakes from the Wasatch and San Andreas Faults," *Journal of Geophysical Research*, 89, 5681-5698.

Seyitoğlu, G. and Scott, B., 1991. Late Cenozoic Crustal Extension and Basin Formation in West Turkey. *Geological Magazine* 128, 155-166.

Seyitoğlu, G., Scott, B.C. and Rundle, C.C. 1992. Timing of Cenozoic extensional tectonics in west Turkey. *Journal of the Geological Society, London* 149, 533–538.

Seyitoğlu, G. and Işık, V., 2009. Meaning of the Küçük Menderes Graben in the Tectonic Framework of the Central Menderes Metamorphic Core Complex (Western Turkey). *Geologica Acta* 7, 323-331.

Selverstone, J., 2005. Preferential embrittlement of graphitic schists during extensional unroofing in the Alps: The effect of fluid composition on rheology in low-permeability rocks. *Journal of Metamorphic Geology* 23, 461– 470.

Seyitođlu, G., Scott, B.C. and Rundle, C.C., 1992. Timing of Cenozoic extensional tectonics in west Turkey. *Journal of Geological Society*, London 149, 533-538.

Sokolov, V., Loha, C.-H. and Wen, K.-L., 2001. Site-dependent design input ground motion estimations for the Taipei area: a probabilistic approach. *Probabilistic Engineering Mechanics*. 16, 177–191.

Soysal, H., Sipahiođlu, S., Kolçak, D. and Altinok, Y., 1981. Türkiye Ve Çevresinin Tarihsel Deprem Katalođu. Tbag 341 (In Turkish), 124 Pp.

Sözbilir, H., 2002. Geometry and origin of folding in the Neogene sediments of the Gediz Graben, western Anatolia, Turkey. *Geodinamica Acta* 15, 277-288.

Steiger, R.H. and Jäger, E., 1977. Subcommittee on geochronology: convention on the use of decay constants in geo- and cosmochronology. *Earth Planetary Science Letter* 36: 359-362.

Şengör, A.M.C., 1979. On some 50% extension in the Aegean area and its implications for orogenic reconstructions in the Taurides, *Rapp. Comm. Int. Mer. Mediterr.* 25/26 (2a) (1979) pp. 41–42.

Şengör, A.M.C. and Yilmaz, Y., 1981. Tethyan Evolution of Turkey: A Plate Tectonic Approach. *Tectonophysics* 75, 181–224.

Şengör, A.M.C., 1987. Cross faults and differential stretching of hanging wall in the regions of low-angle normal faulting: examples from western Turkey. In: COWARD, M. P., DEWEY, J. F., HANCOCK, P.L. (eds), *Continental Extension Tectonics*. Geological Society, London, Special Publications 28, 575–589.

Şengör, A. M. C., Görür, N. and Şaroğlu, F., 1985. Strike-slip faulting and related basin formation in zones of tectonic escape: Turkey as a case study, Strike-slip Deformation, Basin Formation, and Sedimentation, Soc. Econ. Paleont. Min. Spec. Pub. 37 (in honor of J.C. Crowell), 227- 264.

Sözbilir, H., 2001. Extensional tectonics and geometry of related macroscopic structures: field evidence from the Gediz detachment, western Turkey. Turkish Journal Earth Science 10, 51-67.

Tapırdamaz, M. C., Tarancıoğlu, A., Özalaybey, S., Ergin, M., Selvi, O., Yörük, A., Biçmen, F. and Aktar, M., 2002. Sultandağı (Afyon) Depremi (03 Şubat 2002, Mw = 6.2) Artçı Deprem Çalışması. Aktif Tektonik Araştırma Grubu Altıncı Toplantısı (ATAG-6), Ankara, pp 34–41 (in Turkish)

Taymaz, T., 1993. The Source Parameters of the Çubukdağ (W Turkey) Earthquake of 1986 October 11: Geophysical Journal International 113, 260-267.

Taymaz, T., Jackson, J.A. and Mckenzie, D.P., 1991. Active Tectonics of North and Central Aegean Sea: Geophysical Journal International 113, 433-490.

Taymaz, T. and Price, S., 1992. The 1971 May 12 Burdur Earthquake Sequence, SW Turkey: A Synthesis of Seismological and Geological Observations. Geophysical Journal International-Oxford 108, 589-603.

Taymaz, T., Westaway, R. and Reilinger, R., 2002. Active Faulting and Crustal Deformation in The Eastern Mediterranean Region. Special Issue of Tectonophysics 391, 1-4, 1-9 (Editorial Article).

Thomson, S.N., Stöckhert, B. and Brix, M.R., 1998. Thermochronology of the high-pressure metamorphic rocks on Crete, Greece: implications for the speed of tectonic processes. *Geology* 26, 259–262.

Ulusay, R., Kasapoğlu, E., Dirik, K. and Gökçeoğlu, C. 2002. 3 Şubat 2002 Sultandağı (Afyon) depremi ve saha inceleme raporu [2002.02.03 Sultandağı (Afyon) earthquake and field study report]. Hacettepe Üniv. Mühendislik Fak., Jeoloji Müh. Bölümü, Ankara, 44 s.

Ulusay, R., Tuncay, E., Sönmez, H. and Gökçeoğlu, C., 2004. An attenuation relationship based on Turkish strong motion data and iso-acceleration map of Turkey. *Engineering Geology*, 74(3-4), 265-291.

Walsh, J.J., and Watterson, J., 1991. Geometric and kinematic coherence and scale effects in normal fault systems, in A.M. Roberts, G. Yielding, and B. Freeman, eds., *The Geometry of Normal Faults: Geological Society, London, Special Publications*, 56, 193–203.

Watterson, J.A., Nicol, A., Walsh, J.J., and Meier, D., 1998, Strains at the intersections of synchronous conjugate normal faults: *Journal of Structural Geology* 20, 363-370.

Wells, D.L. and Coppersmith, K.J., 1994. New empirical relationships among magnitude, rupture length, rupture width, rupture area, and surface displacement. *Bulletin of Seismological Society of America* 4 (84), 975– 1002.

Westaway, R., 1990. Seismicity and tectonic deformation rate in Soviet Armenia: implications for local earthquake hazard and evolution of adjacent regions, *Tectonics* 9, 477-503.

Westaway, R., 1994. Evidence for Dynamic Coupling of Surface Processes with Isostatic Compensation In The Lower Crust During Active Extension of Western Turkey: *Journal of Geophysical Research* 99, 20203–20223.

Westaway, R., Guillou, H., Yurtmen, S., Demir, T., Scaillet, S. and Rowbotham, G., 2005. Constraints on The Timing and Regional Conditions At The Start of The Present Phase of Crustal Extension In Western Turkey, From Observations In and Around The Denizli Region: *Geodinamica Acta* 18, 209–238.

Winchester, J. A. and Floyd, P.A., 1977. Geochemical discrimination of different magma series and their differentiations products using immobile elements. *Chemical Geology* 20, 325-343.

www.es.ucl.ac.uk (last access date: 02.05.2011).

Yağmurlu, F., 1981. Bornova (İzmir) güneyi filiş topluluklarının jeolojisi: *Türkiye Jeoloji Kurumu Bülteni* 23(2), 141-152, Ankara.

Yalçın, H., 1984. Emet Neojen gölsel baseninin jeolojik ve mineralojik-petrografik incelenmesi. *Yük. Müh. Tezi*, H.Ü. Fen Bil. Enst., Beytepe, Ankara, 269s (unpublished).

Yalçınlar, I., 1946. Eşme civarında Miyosen'e ait bir omurgalılar faunası: *İ-Ü-FF. Mec- B XI*, 2, 124-129.

Yamaji, A., 2000. The multiple inverse method: a new technique to separate stresses from heterogeneous fault-slip data: *Journal of Structural geology* 22, 441-452.

Yeats, R.S., Sieh, K., and Allen, C.R., 1997. The geology of earthquakes: Oxford University Press, NY, 568 pages.

Yilmaz, Y., Genç, Ş.C., Gürer, F., Bozcu, M., Yilmaz, K., Karacik, Z., Altunkaynak, Fi. and Elmas, A., 2000. When Did The Western Anatolian Grabens Begin To Develop? In: Bozkurt, E., Winchester, J.A. and Piper, J.D.A. (Eds), Tectonics and Magmatism In Turkey and The Surrounding Area. Geological Society, London, Special Publications 173, 353–384.

Yusufoğlu, H., 1998. Palaeo-and Neo-Tectonic Characteristics of Gediz and Küçük Menderes Grabens in West Anatolia, Turkey. Phd Thesis, 251p., Middle East TechnicalUniversity (unpublished).

Zanchi, A. and Angelier, J., 1993. Seismotectonic of western Anatolia: regional stress orientation from geophysical and geological data. Tectonophysics 222, 259-274.

APPENDIX

A. GEOLOGICAL MAP OF THE STUDY AREA

(Appendix – A is attached inside the back cover with an envelope)

CURRICULUM VITAE

PERSONAL INFORMATION

Surname, Name: Gürboğa, Şule

Nationality: Turkish (TC)

Date and Place of Birth: 14 February 1979, Kayseri

Marital Status: Married

Phone: +90 312 210 57 38

Fax: +90 312 210 57 50

email: sdeveci@metu.edu.tr, sule.deveci@gmail.com

EDUCATION

Degree	Institution	Year of Graduation
BS	Ankara University, Department of Geological Engineering	2000
High School	Kalaba High School, Ankara	1996

WORK EXPERIENCE

Year	Place	Enrollment
2003- Present	METU, Department of Geological Engineering	Teaching and Research Assistant
June-July- August- 2008	AIST (The National Institute of Advanced Industrial Science and Technology), Active Fault and Earthquake Research Center Tsukuba, Japan	Invited Senior Researcher
2007-2008	The Group Training Course in Seismology, Earthquake Engineering and Disaster Mitigation "2007-2008", JICA, Japan.	Research Scholar

FOREIGN LANGUAGES

Advanced English

PUBLICATIONS

Refreed Journals

Koçyiğit, A., and Deveci, Ş., 2007. A N-S-trending active extensional structure, the Şuhut (Afyon) graben: Commencement age of the extensional neotectonic period in Isparta Angle, SW Turkey. Turkish Journal of Earth Sciences, volume 16, pp. 391-416.

Koçyiğit, A., and Deveci, Ş., 2008. Ankara Orogenic Phase, its age and Transition From Thrusting-dominated Paleotectonic Period to the Strike-slip Neotectonic Period Ankara-Turkey. Turkish Journal of Earth Sciences, volume 17, pp. 433-459.

Gürboğa, Ş., 2009. Geological Indicators Associated with Paleoearthquakes: Focusing on the Geomorphological Evidences. Bulletin of the International Institute of Seismology and Earthquake Engineering 43, 49-54.

National and International Conference Presentations

Koçyiğit, A., and Deveci, Ş., 2005. Akşehir-Simav Fault System: commencement age of neotectonic regime and seismicity, SW Turkey. Deprem Sempozyumu Kocaeli 2005, Özler Kitabı, s.26.

Koçyiğit, A., and Deveci, Ş., 2005. 31 Temmuz 2005, Mw = 5.2 Afşar (Bala-Ankara) Depremi ve Kaynağı. Aktif Tektonik Araştırma Grubu 9. Toplantısı, Özler kitabı, s. 3.

Koçyiğit, A., and Deveci, Ş., 2006. K-G-gidişli aktif bir genişleme yapısı, Şuhut (Afyon) grabeni: Isparta Açısı'nda genişlemeli neotektonik dönemin başlama yaşı, GB Türkiye. Aktif Tektonik Araştırma Grubu 10. Toplantısı, Özler kitabı, s. 59.

Koçyiğit, A., Bozkurt, E. and Deveci, Ş. 2006. The Transition zone between the Extensional and Strike-slip neotectonic regimes in southern Marmara region: Bursa Graben. "International Workshop on Comparative studies of the NAF (NW Turkey) and the SAF (Southern California) 1, 18-19.

Gurboga (Deveci), Ş., and Koçyiğit, A. 2007. Commencement Age Of Neotectonic regime And Seismicity In Southwest Turkey: Akşehir-Simav fault system. Poster presentation in Summer Schools in Integrated Solid Earth Sciences (ISES), July 27 – August 3, 2007, Colorado College, Colorado, USA.

Gurboga (Deveci), Ş., and Koçyiğit, A. 2009. Neotectonics of Gediz - Erdoğmuş (Kütahya) Graben, SW Turkey. Oral presentation. 13-17 April, 2009. 62. Geological Kurultai of Turkey, MTA, Ankara/Turkey.

Gurboga (Deveci), Ş., and Koçyiğit, A. 2009. A new extensional structure: Akgöl (Afyon-Burdur) modern graben and its neotectonic to seismic characteristics. Aktif Tektonik Araştırma Grubu 13. Toplantısı, Bildiri Özleri kitabı, s. 24.

Gurboga, Ş., and Koçyiğit, A. 2010. Palaeoseismological Results on the Source of 1970.03.28 Gediz Earthquake. the Tectonic Crossroads: Evolving Orogens of Eurasia-Africa-Arabia Conference being held in Ankara, Turkey, on 4-8 October 2010. The Geological Society of America.

PROJECTS and TECHNICAL REPORTS

Koçyiğit, A., Ayhan, E., Demir, C., Lenk, O., Kılıçoğlu, A., Aktuğ, Çetin, H., Aytun, A., Günaydın, O., Deveci, Ş., Arca, S., Biryol, B., Aktürk, Ö., 2005. Kuzey Anadolu Fay Sisteminin (KAFS) İsmetpaşa-Gerede ve Mengen Arasındaki kesiminin Depremselliği. TÜBİTAK-YDABAG-102Y053 kod nolu proje, 184 s.

Koçyiğit, A., Deveci, Ş., 2006. Çukurören– Çobanlar (Afyon) arasındaki deprem kaynaklarının (aktif fayların) belirlenmesi. TÜBİTAK-YDABAG-106Y209 kod nolu proje.

Karpuz, C., Koçyiğit, A., Tutluoğlu L., Koçal, A., Erdem, E., Alkılıçgil, Ç., Deveci, Ş., 2006. Tki Genel Müdürlüğü Çan İşletmesi Açık Ocaklarında Kocaçay Çayı İle Ocak Arası Ve Batı Panolarının Şev Tasarımı. Bölüm I: Çan Kömür Havzasının Jeolojik Yapısı Yapısal Analizi ve Fayların Kömür Kazılarına Etkisi. TÜBİTAK Proje Kod No: 2006-03-05-2-00-10.

Koçyiğit, A., Gürboğa (Deveci), Ş., 2009. Akgöl (Burdur) grabeninin neotektonik özellikleri ve kenar faylarının depremselliği (Neotectonic characteristics of the Akgöl (Burdur) graben and seismicity of its margin-boundary faults) TÜBİTAK Proje Kod No: 109Y168.

TECHNICAL FIELD EXCURSIONS

1) Koçyiğit, A., Aksoy, E., İmamoğlu, Ş., and Deveci (Gürboğa), Ş., 2010. Doğu Anadolu Fay Sistemi'nin Gölbaşı Kesimindeki Saha Gözlemleri ve Teknik İnceleme. ATAG (Active Tectonic Research Group). Adıyaman University.

COURSES and SUMMER SCHOOLS ATTENDED

1) “Application of geo-mechanics to the interpretation of tectonic structures in space and time (03-14 May 2004)” short course about tectonic structures in Department of Geological Engineering, METU.

2) “Satellite Radar Interferometry (04-08 July 2005)” short course in Department of Geological Engineering, METU.

3) “Tectonic Exhumation” Summer Schools in Integrated Solid Earth Sciences (ISES), the Colorado College, Colorado Springs, CO. USA (27 July – 3 August 2007).

